The superconductor-metal quantum phase transition in ultra-narrow wires

A dissertation presented

by

Adrian Giuseppe Del Maestro

to

The Department of Physics

in partial fulfillment of the requirements

for the degree of

Doctor of Philosophy

in the subject of

Physics

Harvard University

Cambridge, Massachusetts

May 2008

Thesis advisor
Subir Sachdev

Author
Adrian Giuseppe Del Maestro

The superconductor-metal quantum phase transition in ultra-narrow wires

Abstract

We present a complete description of a zero temperature phase transition between superconducting and diffusive metallic states in very thin wires due to a Cooper pair breaking mechanism originating from a number of possible sources. These include impurities localized to the surface of the wire, a magnetic field orientated parallel to the wire or, disorder in an unconventional superconductor. The order parameter describing pairing is strongly overdamped by its coupling to an effectively infinite bath of unpaired electrons imagined to reside in the transverse conduction channels of the wire. The dissipative critical theory thus contains current reducing fluctuations in the guise of both quantum and thermally activated phase slips. A full cross-over phase diagram is computed via an expansion in the inverse number of complex components of the superconducting order parameter (equal to one in the physical case). The fluctuation corrections to the electrical and thermal conductivities are determined, and we find that the zero frequency electrical transport has a non-monotonic temperature dependence when moving from the quantum critical to low temperature metallic phase, which may be consistent with recent experimental results on ultra-narrow MoGe wires. Near criticality, the ratio of the thermal to electrical conductivity displays a linear temperature dependence and thus the Wiedemann-Franz law is obeyed. We compute the constant of proportionality in a systematic expansion and find a universal and experimentally verifiable fluctuation correction to the Lorenz number.

In the presence of quenched disorder, a novel algorithm is developed to solve the self-consistency condition arising when the number of complex order parameter components is taken to be large. In this limit, we find striking evidence for the flow to infinite randomness, and observe dynamically activated scaling consistent with predictions from the strong disorder renormalization group. Moreover, the infinite randomness fixed point of the pair-breaking superconductor-metal quantum phase transition is found to be in the same universality class as the onset of ferromagnetism in the one dimensional quantum Ising model in a random transverse field. This discovery may lead to the first calculations of real electrical transport in an experimentally relevant system exhibiting infinite randomness.

Contents

Citations to Previously Published Work

Chapters 2 to 4 describe the calculation of thermal and electrical transport near the quantum superconductor-metal transition in ultra narrow wires, and a brief account was published in a short paper that appeared in Physical Review B.

> "Universal thermal and electrical transport near the superconductor-metal quantum phase transition in nanowires"
> Adrian Del Maestro, Bernd Rosenow, Nayana Shah and Subir Sachdev,
> Physical Review B **77**, 180501(R) (2008), `arXiv:0708.0687`.

The addition of disorder to the aforementioned model led to a study of infinite randomness and activated scaling with details given in Chapter 5. A summary of the important results have been submitted for publication in Physical Review Letters.

> "Infinite randomness fixed point of the superconductor-metal quantum phase transition"
> Adrian Del Maestro, Bernd Rosenow, Markus Mueller and Subir Sachdev,
> Submitted to Physical Review Letters, (2008), `arXiv:0802.3900`.

During the last five years I have had the pleasure of working on a number of extremely interesting projects on various topics that have not been included in this thesis for the aesthetic purpose of producing a self-contained document. The first includes studies of charge density wave ordering in both clean and disordered square lattices with application to the cuprate superconductors,

> "Thermal melting of density waves on the square lattice"
> Adrian Del Maestro and Subir Sachdev,
> Physical Review B **71**, 184511 (2005), `arXiv:cond-mat/0412498`;

> "From stripe to checkerboard order on the square lattice in the presence of quenched disorder"
> Adrian Del Maestro, Bernd Rosenow, Subir Sachdev,
> Physical Review B **74**, 024520 (2006), `arXiv:cond-mat/0603029`.

Large scale numerical studies of supersolids on the triangular lattice with nearest and next-nearest neighbor interactions were performed

> "A striped supersolid phase and the search for deconfined quantum criticality in hard-core bosons on the triangular lattice"
> Roger G. Melko, Adrian Del Maestro and Anton A. Burkov,
> Physical Review B **74**, 214517 (2006), `arXiv:cond-mat/0607501`,

and finally, I considered spin fluctuations and low temperature thermodynamic properties in the geometrically frustrated pyrochlore gadolinium stanate, which lead to a prediction that was ultimately confirmed by experimental results

> "Low temperature specific heat and possible gap to magnetic excitations in the Heisenberg pyrochlore antiferromagnet $Gd_2Sn_20_7$"
> Adrian Del Maestro and Michel J.P. Gingras,
> Physical Review B **76**, 064418 (2007), `arXiv:cond-mat/0702661`;

> "Evidence for gapped spin-wave excitations in the frustrated Gd2Sn2O7 pyrochlore antiferromagnet from low-temperature specific heat measurements"
> J.A. Quilliam, K.A. Ross, A. Del Maestro, M.J.P. Gingras, L.R. Corruccini and J.B. Kycia,
> Physical Review Letters **99**, 097201 (2007), `arXiv:0707.2072`.

Electronic preprints (shown in `typewriter font`) can be found online at

> `http://arXiv.org`

Acknowledgments

When choosing a path towards academia I had no idea of the importance of serendipity, but feel that I have been extraordinarily lucky in this regard. Through determination, obstinance, and possibly prowess, I was taken on as student by Subir Sachdev. The scope and depth of his knowledge of condensed matter physics, as well as his analytical accuracy and passion for formalism and technique are awe inspiring. Under his mentorship I was afforded remarkable freedom and independence and have worked on a number of challenging and fascinating problems that have greatly enhanced my understanding and shaped my perspective of the field. There were times when my approach towards physics tested his patience and his seemingly atmospheric standards tested mine, but in the end our collaboration has been both fruitful and productive and I look forward to working together as peers in the future.

My move from Yale to Harvard University provided a number of obstacles, none insurmountable, and resulted in my meeting Bernd Rosenow, who has played a crucial role in all of the work included in this thesis. He has made himself remarkably available to me, always carefully listening to my ideas and providing both knowledge and direction whenever I required. I can only hope that Bernd never kept a list of all the basic questions I asked him that I probably should have learned the answers to years before. He has been instrumental in helping me with the specific and tedious details of calculations as well as providing insights crucial to my understanding of the larger picture. I again hope my graduation will not mark the end of our collaboration and friendship.

I would like to thank the following scientists, with whom I have had the exceedingly good fortune of working with at various stages of my career. My high school physics teacher Ian Martin, convinced me that it can be both worthwhile and enjoyable to solve interesting and difficult problems. He was a major factor in my decision to study physics at the University of Waterloo. My undergraduate and masters supervisor Michel Gingras, picked me out of a crowd, and guided me with great expertise through the early stages of my career. While I was an undergraduate, I met Roger Melko, who I still count as a dear friend and mentor. We have had various adventures together over the last eight years and he is probably the only person I will ever write a paper with while driving forty hours to pick up a dog or boating in Tennessee. Jean-Yves Delannoy and I wrote a code together over several months without any version control, managing to not only finish it, but have a great time doing so. Although he has left academia, he continues to make great contributions to science. At various times I shared an office with Lorenz Bartosch and Predrag Nikolić, two postdocs of Subir's who always had time for my questions and absolutely exude class. More recently, Cenke Xu moved into the desk next to mine and has treated me as an equal, even in the presence of his bewildering grasp of field theory. Anton Burkov acted as a foil for my (often terrible) ideas, providing me with knowledge and perspective, and Markus Mueller taught me a great deal about disordered systems and how to really think deeply about a problem. Ribhu Kaul helped me evade various snares when performing calculations and provided thoughtful advice during my search for a postdoctoral position.

I thank Eugene Demler for agreeing to be on my committee and providing me with both contrasting and compatible viewpoints on my nanowires work. In addition to teaching me everything I know about scanning tunneling microscopy, I feel that Jenny Hoffman really cared about my success and state of mind, and our meetings to touch base provided me with a large dose of positivity when I needed it most.

Sometimes just explaining yourself can lead to forward progress and I am grateful to Matt Enjalran, Ying-Jer Kao, Nate Gilfoy, Jay Gambetta, Jacob Krich, Stephen Powell, Michael Levin, Alexandre Blais, Lars Fritz, Ivan Gonzalez and David Louapre for many stimulating and informative discussions.

I have received excellent administrative support throughout my tenure from Sheila Ferguson who Harvard is fortunate to have, and financial support from NSERC of Canada through grant PGS D2-316308-2005.

My friends in various places around the world have been essential to my sanity and well-being. There are far too many too mention, and a horribly incomplete list includes Ben Playford, Lori Woolner, Dave MacPhie, Colleen Stuart, Doug MacGregor, Brad Goddard, Esther Choi, Julius Lucks, Sera Young and Elliot White.

The core of my support structure, and the driving force behind my success is my family. My parents have provided me with canonical examples of how to be a good citizen as well as a good scientist and their seemingly exhaustive support over the years has never wavered. My brother and sister are my best friends, and they are the first people I contact for advice, direction or encouragement.

Finally I thank the city of Boston and specifically Nick at Sullivan's Tap where a portion of this thesis was written. I have enjoyed my time here a great deal and will always love that dirty water.

Dedicated to my sister Lana, for holding my passport, and my brother Christian, for the occasional mulligan.

Chapter 1

Introduction

Richard Feynman's 1959 lecture entitled "There is plenty of room at the bottom" [1] discussed the possibility and ramifications of manipulating matter at the atomic scale. He presented a number of microfabrication challenges including fitting the Encyclopedia Britannica on the head of a pin. In 1985, Tom Newman, a graduate student at Stanford University met this challenge by reducing the first page of Charles Dickens' *A Tale of Two Cities* by 25 000 times and writing it on a metallic surface using electron beam lithography [2].

As physicists working in this field, now known as nanoscience or nanotechnology, continue to stride towards the "bottom", a striking phenomena, originally envisioned by Feynman is apparent. The advances needed to build the ingenious tools and techniques required for the passive observation of nanoscale phenomena can often lead to a concomitant increase in our ability to actively sculpt and interact with matter on increasingly diminutive length scales. The fabrication and ultimate measurement of spin excitations in linear chains of less then ten manganese atoms using a scanning tunneling microscope in inelastic tunneling mode is an elegant example of this dual-purpose utility [3].

At the nanoscale, the basic mechanical, electrical and optical properties of materials that are well understood at macroscopic length scales can change in interesting and sometimes unexpected ways as quantization and fluctuation effects manifest themselves. An intriguing question thus arises regarding the implications of reducing the scale or effective dimensionality of materials, that even in the bulk, are known to already display interesting quantum mechanical behavior. Superconductors, or materials that exhibit dissipationless electrical currents due to the existence of macroscopic quantum phase coherence are natural physical systems to consider in this context. Conventional or low temperature superconductors are well understood in the bulk, unlike their high temperature cousins whose full description still remains elusive after more than twenty years of intensive research. A major obstacle to the study of high temperature superconducting materials is that they are plagued by their proximity to competing states with both *order* and *disorder* at the atomic scale. Through a

better understanding of the ways in which normal superconductivity is suppressed or destroyed in different confining geometries and effective dimensions, perhaps we can make progress towards a mastery of this fascinating emergent phenomena at all length and temperature scales.

In this chapter, we begin with a brief introduction to the physical properties of superconductors and some details of the pairing theory. Next, the confusion surrounding early transport measurements in narrow tin whiskers will lead us to an eventual theory of resistance fluctuations in narrow superconducting wires below their bulk transition temperature. The current state of the art fabrication processes for manufacturing wires with diameters less then 10 nm will be introduced along with modern experiments measuring their electrical transport properties. Many details of these experiments are well understood, but open questions remain regarding the destruction of superconductivity at low temperatures. Such a transition would necessarily fall in the pair-breaking class and we highlight the salient features of their description. If the source of pair-breaking is strong enough, superconductivity can be destroyed even at zero temperature, at a quantum critical point. We will thus briefly discuss the theory of quantum phase transitions, where quantum and not thermal fluctuations are the dominant driving force. A discussion of the modifications to critical phenomena in the presence of quenched disorder follows and we conclude with an outline of the organization of this thesis.

1.1 Superconductivity

Superconductivity was discovered nearly one hundred years ago in 1911 when H. Kamerlingh Onnes observed that if solid mercury was cooled below 4.2 K, its direct current (dc) electrical resistance dropped to zero [4]. Similar behavior was promptly observed in various other metals and alloys, albeit at different values of the critical temperature T_c. The next important discovery came in 1933 when Meissner and Ochsenfeld noticed that a material in the superconducting state is a perfect diamagnet; all magnetic fields are expelled from its bulk [5]. This is essentially an energetic effect, as dissipationless screening currents at the surface of the sample can reduce the total electromagnetic energy of the superconductor by exactly canceling any external field in its bulk. The superconductor attains an equilibrium state where the combination of its kinetic and magnetic energy is minimum. This implies that as the field is increased, there will eventually be some critical strength, H_c where the balance can no longer be sustained and superconductivity will be destroyed. The critical field is therefore directly related to the condensation energy, or the difference in free energy per unit volume of the superconducting and normal state

$$f_N(T) - f_{SC}(T) = \frac{H_c^2(T)}{8\pi}. \tag{1.1}$$

The presence of these two properties, zero resistance and perfect diamagnetism, which essentially define the superconducting state from an observational point of view, have profound and immediate technological implications. The absence of dc resistance implies that electricity could be transmitted without any power losses due to resistive heating. A current set up in a ring of superconducting material has been observed to last for times up to a year, and will last *much* longer under ideal conditions [6]. The perfect diamagnetism of a bulk superconductor due to the Meissner effect tells us that if we set a piece superconducting material on top of a permanent magnet, the expulsion of field lines will generate a repulsive force that could counteract the force of gravity. In a track geometry, this has been exploited to achieve mechanical motion with extremely low resistance. The main limiting factor in the technological use of superconducting materials is the low temperatures, below 20 K, to which they must be cooled before their special properties arise. In 1986, Bednorz and Müller [7] discovered superconductivity in $LaBaCuO_4$ near 35 K and spawned the study of a new class of materials known as the high temperature or cuprate superconductors, due to their ubiquitous CuO_2 planes. A host of new materials with higher and higher transition temperatures were rapidly discovered, but it appears a ceiling has been reached for the cuprates, with the current maximum at ambient pressure being just under 140 K for $HgBa_2Ca_2Cu_3O_{8+\delta}$ [8], still far below room temperature. To make matters worse, the cuprates have the mechanical properties of ceramics, and are ill suited for many technological applications. Although a huge amount of theoretical and experimental resources have been directed towards their understanding, a comprehensive description does not yet exists for these materials, unlike, as we are about to find out, conventional superconductors such as tin or lead.

The first major step towards a microscopic understanding of superconductivity was the experimental measurement of specific heat [9] which was observed to have an exponential or activated form at low temperatures. This is a significant departure from the linear temperature dependence predicted by the free electron theory of metals. The condensation energy per electron can also be determined from these results, and it was found to be *not* on the order of $k_{\mathrm{B}}T$ per electron, but much smaller, near $(k_{\mathrm{B}}T)^2/\varepsilon_{\mathrm{F}}$, where ε_{F} is the Fermi energy. These two observations lead to the following conclusions, (i) only a small fraction of the total number of electrons are involved in the condensation process at the critical temperature and (ii) their is a gap to electronic excitations at the Fermi level.

In a normal metal, the presence of a Fermi sea leads to excitations at arbitrarily low energies, as we can always form a particle-hole pair just around ε_{F}. The existence of a gap immediately evinces the presence of some sort of bound state; pairing is occurring near the Fermi energy. Cooper solidified this picture by deriving the existence of a pairing instability at the Fermi surface [10]. It was already known that the critical temperature of an elemental material depended upon the specific isotope studied; the so-called isotope effect [11, 12]. The well understood relationship between nuclear mass and the frequency of lattice vibrations or *phonons* was enough to implicate

their role as the "glue" which provided pairing.

The stage was set for a complete microscopic understanding of conventional superconductivity and it was provided in the Nobel prize winning work of Bardeen, Cooper and Schriefer (BCS), aptly titled *The Theory of Superconductivity* [13].

With the benefit of over fifty years of hindsight there are a plethora of methods one could use to derive the main features of BCS theory, in particular, the superconducting gap equation. A system of interacting electrons in the neighborhood of a rotationally invariant (s-wave) pairing instability could be analyzed within the framework of a finite temperature continuum quantum theory of anti-commuting Grassmann fields. A Hubbard-Stratonvich decoupling leads to the natural appearance of a gap function, and a self-consistent equation for its value follows directly from the saddle point approximation [14]. In order to preclude an immediate plunge into the methods of quantum field theory and the renormalization group, we present the salient points of the pairing theory of superconductivity in terms of the original variational approach of BCS.

1.1.1 BCS theory

In the superconducting state, a finite fraction of the total number of electrons in the system have condensed into a superfluidic state that can be described by a macroscopic wavefunction with phase coherence. It is the coherence of the condensate, which is complete at zero temperature, that allows for the conduction of electricity without resistance. The constituent charge carriers of the superfluid are paired electrons (known as Cooper pairs) with opposite momentum and spin which have undergone Bose condensation. The pairing instability of the Fermi sea ground state occurs for an arbitrarily weak interaction (as we shall see) and the second order electron-phonon interaction is enough to do the job. The key prediction of BCS theory, which has been fully verified by experimental measurements, is the relationship between the size of the superconducting energy gap (the energy required to break a Cooper pair) and the transition temperature. In addition to Ref. [13] the maturity of the field of superconductivity means that there are a wide variety of excellent references available. The approach taken here is most consistent with the presentation of Ref. [15].

Zero temperature

We begin by writing down the reduced BCS Hamiltonian for a finite size system

$$\mathcal{H} = \sum_{\boldsymbol{k},\sigma} \xi_{\boldsymbol{k}} \psi^{\dagger}_{\boldsymbol{k}\sigma} \psi_{\boldsymbol{k}\sigma} + \sum_{\boldsymbol{k},\boldsymbol{k}'} V_{\boldsymbol{k}\boldsymbol{k}'} \psi^{\dagger}_{\boldsymbol{k}\uparrow} \psi^{\dagger}_{-\boldsymbol{k}\downarrow} \psi_{-\boldsymbol{k}'\downarrow} \psi_{\boldsymbol{k}'\uparrow} \tag{1.2}$$

where all irrelevant and marginal interactions have been neglected and the kinetic energy is measured with respect to the Fermi energy

$$\xi_{\boldsymbol{k}} = \frac{\hbar^2 k^2}{2m} - \varepsilon_{\mathrm{F}}. \tag{1.3}$$

$\psi^\dagger_{\boldsymbol{k}\sigma}$ creates an electron with momentum $\boldsymbol{k}$ and spin σ and we have already exploited the existence of the Cooper instability by choosing a particular s-wave form for our pairing interaction which couples electrons with opposite spin on either side of the Fermi surface. BCS introduced the variational wavefunction

$$|\Psi_{\mathrm{BCS}}\rangle = \sum_{\boldsymbol{k}} \left(u_{\boldsymbol{k}} + v_{\boldsymbol{k}} \psi^\dagger_{\boldsymbol{k}\uparrow} \psi^\dagger_{-\boldsymbol{k}\downarrow} \right) |0\rangle \tag{1.4}$$

where $|0\rangle$ is the vacuum state, and $u_{\boldsymbol{k}}$ and $v_{\boldsymbol{k}}$ are parameters with respect to which $\langle \Psi_{\mathrm{BCS}} | \mathcal{H} | \Psi_{\mathrm{BCS}} \rangle$ can be minimized subject to the normalization condition

$$u^2_{\boldsymbol{k}} + v^2_{\boldsymbol{k}} = 1. \tag{1.5}$$

The expectation value of the Hamiltonian can be calculated to be

$$\langle \Psi_{\mathrm{BCS}} | \mathcal{H} | \Psi_{\mathrm{BCS}} \rangle = 2 \sum_{\boldsymbol{k}} v^2_{\boldsymbol{k}} \xi_{\boldsymbol{k}} - \sum_{\boldsymbol{k},\boldsymbol{k}'} V_{\boldsymbol{k},\boldsymbol{k}'} u_{\boldsymbol{k}} v_{\boldsymbol{k}} u_{\boldsymbol{k}'} v_{\boldsymbol{k}'} \tag{1.6}$$

and upon varying with respect to $v_{\boldsymbol{k}}$ we arrive at the variational minimum condition

$$2 \xi_{\boldsymbol{k}} u_{\boldsymbol{k}} v_{\boldsymbol{k}} = \sum_{\boldsymbol{k}'} V_{\boldsymbol{k}\boldsymbol{k}'} (u^2_{\boldsymbol{k}} - v^2_{\boldsymbol{k}}) u_{\boldsymbol{k}'} v_{\boldsymbol{k}'}. \tag{1.7}$$

We now make a change of variables from $(u_{\boldsymbol{k}}, v_{\boldsymbol{k}})$ to $(E_{\boldsymbol{k}}, \Delta_{\boldsymbol{k}})$ via

$$u_{\boldsymbol{k}} = \frac{1}{\sqrt{2}} \sqrt{1 + \frac{\xi_{\boldsymbol{k}}}{E_{\boldsymbol{k}}}} \tag{1.8a}$$

$$v_{\boldsymbol{k}} = \frac{1}{\sqrt{2}} \sqrt{1 - \frac{\xi_{\boldsymbol{k}}}{E_{\boldsymbol{k}}}} \tag{1.8b}$$

where

$$E_{\boldsymbol{k}} = \sqrt{\xi^2_{\boldsymbol{k}} + \Delta^2_{\boldsymbol{k}}}. \tag{1.9}$$

Substituting Eqs. (1.8a), (1.8b) and (1.9) into Eq. (1.7) leads to a self-consistent expression for $\Delta_{\boldsymbol{k}}$

$$\Delta_{\boldsymbol{k}} = -\frac{1}{2} \sum_{\boldsymbol{k}'} \frac{V_{\boldsymbol{k}\boldsymbol{k}'} \Delta_{\boldsymbol{k}'}}{\sqrt{\xi^2_{\boldsymbol{k}'} + \Delta^2_{\boldsymbol{k}'}}}, \tag{1.10}$$

which is known as the BCS gap equation. Eq. (1.9) certainly gives the impression that Δ_k should be associated with an energy gap, but before we present a solution to Eq. (1.10) we will confirm that this is indeed the case.

Let us return to our original reduced BCS Hamiltonian, and define new fermion operators

$$\psi^\dagger_{-\boldsymbol{k}\downarrow} = -v^\dagger_{\boldsymbol{k}}\gamma_{\boldsymbol{k}0} + u_{\boldsymbol{k}}\gamma^\dagger_{\boldsymbol{k}1} \tag{1.11a}$$

$$\psi_{\boldsymbol{k}\uparrow} = u^\dagger_{\boldsymbol{k}}\gamma_{\boldsymbol{k}0} + v_{\boldsymbol{k}}\gamma^\dagger_{\boldsymbol{k}1} \tag{1.11b}$$

with $u_{\boldsymbol{k}}$ and $v_{\boldsymbol{k}}$ taking the values in Eq. (1.8a) and (1.8b). We have changed from the spin indices $(\uparrow, \downarrow)$ to the generic labels $(0, 1)$ to indicate that $\gamma_{\boldsymbol{k},0}$ can either destroy an electron with momentum $\boldsymbol{k}$ and spin $\uparrow$ or create one with momentum $-\boldsymbol{k}$ and spin $\downarrow$. The net result of such an operation is to decrease the total momentum by $\boldsymbol{k}$ and the total z-component of the spin by $\hbar/2$.

The values of $u_{\boldsymbol{k}}$ and $v_{\boldsymbol{k}}$ which lead to a minimum variational energy also diagonalize our Hamiltonian and we are left with

$$\mathcal{H} = \mathcal{E}_0 + \sum_{\boldsymbol{k}} E_{\boldsymbol{k}}(\gamma^\dagger_{\boldsymbol{k}0}\gamma_{\boldsymbol{k}0} + \gamma^\dagger_{\boldsymbol{k}1}\gamma_{\boldsymbol{k}1}) \tag{1.12}$$

where $\mathcal{E}_0$ is a constant equal to the energy of the normal state plus the condensation energy. In this form, it is readily apparent that the $\gamma_{\boldsymbol{k}j}$ describe the elementary quasiparticle excitations of the system with energy $E_{\boldsymbol{k}} = \sqrt{\xi^2_{\boldsymbol{k}} + \Delta^2_{\boldsymbol{k}}}$ and thus $\Delta_{\boldsymbol{k}}$ can be identified as the superconducting energy gap; the energy needed to break a single Cooper pair.

Now returning to Eq. (1.10) we take the simplest possible form for the pairing interaction

$$V_{\boldsymbol{k}\boldsymbol{k}'} = \begin{cases} -V & ; \quad |\xi_{\boldsymbol{k}}|, |\xi_{\boldsymbol{k}'}| \leq \hbar\omega_{\mathrm{D}} \\ 0 & ; \quad \text{otherwise} \end{cases} \tag{1.13}$$

where $V > 0$, immediately leading to

$$\Delta_{\boldsymbol{k}} = \begin{cases} 0 & ; \quad |\xi_{\boldsymbol{k}}| > \hbar\omega_{\mathrm{D}} \\ \Delta & ; \quad |\xi_{\boldsymbol{k}}| < \hbar\omega_{\mathrm{D}} \end{cases} \tag{1.14}$$

with ω_{D} the phonon Debye frequency and Δ a constant. This form leads to a much simplified gap equation given by

$$1 = \frac{V}{2}\sum_{\boldsymbol{k}} \frac{1}{\sqrt{\xi^2_{\boldsymbol{k}} + \Delta^2}}. \tag{1.15}$$

Converting the sum over $\boldsymbol{k}$ into an integral over energy using the normal density of

states $N(\xi)$ we find

$$\frac{1}{N(0)V} = \int_0^{\hbar\omega_{\rm D}} \frac{d\xi}{\sqrt{\xi^2+\Delta^2}} = \sinh^{-1}\left(\frac{\hbar\omega_{\rm D}}{\Delta}\right) \tag{1.16}$$

where we have replaced $N(\xi) \approx N(0)$, the density of states at the Fermi energy since we are only interested in a small interval of width $\hbar\omega_{\rm D} \ll \varepsilon_{\rm F}$. We find a solution only if $V > 0$ and in the weak coupling regime where $N(0)V \ll 1$ (which is almost always justified) we finally arrive at the solution

$$\Delta \simeq 2\hbar\omega_{\rm D} {\rm e}^{-1/N(0)V}. \tag{1.17}$$

This result, valid at $T = 0$ has two immediately striking properties. The first is that a solution exists for an arbitrarily small value of the attractive interaction $-V$; the Fermi liquid is always unstable to pairing. The second is that Δ is a non-analytic function of the strength of the coupling and thus no perturbative methods at weak coupling could ever reproduce Eq. (1.17).

Finite temperature

The method just presented for the derivation of the gap equation can be straightforwardly generalized to $T > 0$. The major modification is that at finite temperature, quasiparticles above the superconducting ground state will be thermally excited. However, it turns out that they can be approximated as a gas of non-interacting particles and the only modification will be that the gap Δ acquires a temperature dependence. The finite temperature self-consistency equation which corresponds to Eq. (1.16) is now given by

$$\frac{1}{N(0)V} = \int_0^{\hbar\omega_{\rm D}} \frac{d\xi}{\sqrt{\xi^2+\Delta^2}} \left[1 - 2f\left(\sqrt{\xi^2+\Delta^2}\right)\right] \tag{1.18}$$

where $f(x)$ is the Fermi function

$$f(x) = \frac{1}{{\rm e}^{x/k_{\rm B}T}+1}. \tag{1.19}$$

It is easy to see that in the limit $T \to 0$ this reduces to our previous result. The transition temperature T_c is defined as the temperature at which the gap identically vanishes and we have

$$1 = N(0)V \int_0^{\hbar\omega_{\rm D}} \frac{d\xi}{\xi} \tanh\frac{\xi}{2k_{\rm B}T_c}. \tag{1.20}$$

For $k_{\rm B}T_c \ll \hbar\omega_{\rm D}$ we find

$$1 = N(0)V \ln \frac{1.14\hbar\omega_{\rm D}}{k_{\rm B}T_c} \tag{1.21}$$

or

$$k_{\rm B}T_c = 1.14\hbar\omega_{\rm D} {\rm e}^{-1/N(0)V}. \tag{1.22}$$

Again we see that for any non-zero pairing interaction this equation has a solution and thus there will be a continuous phase transition to a superconducting state as the temperature is lowered through T_c.

The methods we have used can be extended to calculate various thermodynamic quantities which can be compared with experiments using the known value of the Debye frequency with appreciable success. In this way, the value of $N(0)V$ can be extracted and its value is always found to be small, justifying our weak coupling approximation. We will eventually return to Eqs. (1.18) and Eq. (1.21) in the context of the pair-breaking transition but for now we conclude this section with the comment that although BCS theory works remarkably well, its key assumption is the lack of any spatial dependence of the gap Δ. To address the theory of superconductors in constrained geometries or in the presence of additional perturbations we will have to appeal to macroscopic Ginzburg-Landau, theory which directly describes a slowly varying superconducting order parameter.

1.2 Fluctuations in low dimensional superconductors

In 1968, Webb and Warburton performed a remarkable transport experiment on thin whisker-crystal Sn wires [16] with the result shown in Fig. 1.1. The tin whiskers had diameters between 40 and 400 μm and they noticed that for the thinnest wires, resistive fluctuations leading to a finite voltage persisted below the bulk critical temperature for tin. This strongly departed from any mean field estimates using the maximum supercurrent [17].

The understanding of this behavior, which is specific to quasi-one dimensional superconductors followed rapidly thereafter and is composed of three parts. The first was Little's qualitative introduction of thermally activated phase slips [18]; a jump in the phase of the superconducting order parameter by $\pm 2\pi$, equivalent to a vortex tunneling across the system. Next came the Ginzburg-Landau (GL) theory of Langer and Ambegaokar [19] for the free energy barrier height of a phase slip event which qualitatively reproduced the most important features of Webb and Warburton's experiments. The story concludes with the time-dependent Ginzburg-Landau theory of McCumber and Halperin [20] who correctly computed the rate at which these resistive fluctuations occur, and led to full quantitative agreement. Little's initial is not prepended to the acronym *LAMH* which is used as the moniker for the theory

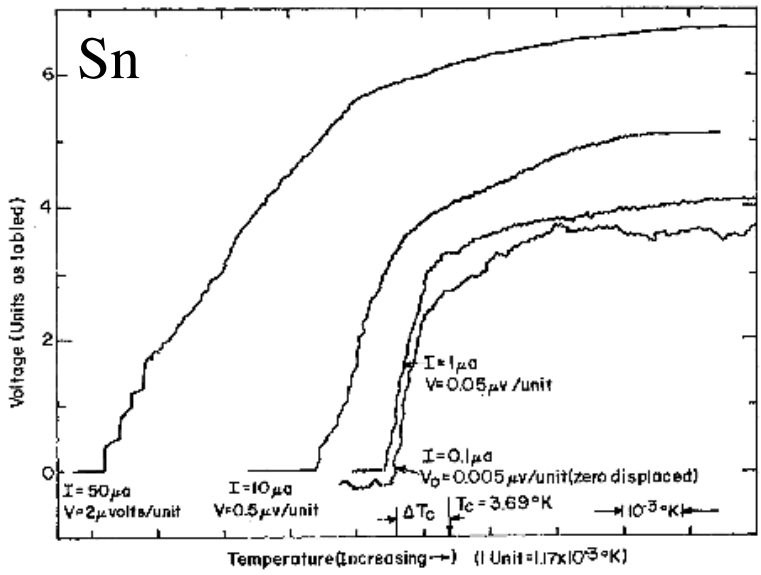

Figure 1.1: The main result from transport measurements on narrow tin whisker-crystals from Ref. [16] showing resistive fluctuations below the bulk Sn T_c that are not accounted for within the simple BCS theory. The different curves correspond to whiskers of varying diameters with the applied currents indicated.

of thermally activated phase slips proposed by Langer, Ambegaokar, McCumber and Halperin. It is not evident why this is the case, but one can speculate that due to the overwhelming success of the LAMH theory, it was considered ill advised to attach a name, that when confused with an adjective, infers a diminutive accomplishment.

1.2.1 LAMH theory

It is well known that the Mermin-Wagner-Hohenberg theory [21, 22] precludes the possibility of long range superconducting order at any non-zero temperature in one dimension. However, any real wire is three dimensional, and can be approximated as a cylinder with a finite radius R. In the Landauer picture [23] conduction occurs ballistically and is proportional to the number of channels in the wire, $N_\perp$, equal to the number of states that can be occupied for a given energy in all dimensions transverse to transport. Thus, if we imagine free electron states propagating down the wire, $N_\perp \propto A/\lambda_F^2$ where A is the cross-sectional area and λ_F is the Fermi wavelength. Any real wire will have $R \gg \lambda_F$ implying that $N_\perp \gg 1$ and we can imagine that it will undergo a phase transition to a superconducting state below some critical temperature. As the diameter of the wire decreases, or at suitably low temperatures, we will eventually enter a regime where the superconducting coherence length, ξ_0 equal to the average separation between Cooper pairs, is longer than the radius.

This condition defines the *quasi-one dimensional* limit, as paired electrons necessarily experience the finiteness of the transverse dimension while unpaired electrons do not.

The presence of resistive fluctuations in a narrow wire implies that there are spatial variations in the magnitude of the superconducting order parameter along its length. In the presence of such inhomogeneities, the BCS theory is not entirely appropriate and we instead appeal to the simple Ginzburg-Landau theory of the superconducting state [6]. In the quasi-one dimensional case, this phenomenological theory assumes that the free energy of a superconductor of length L and cross-sectional area $A = \pi R^2$ can be written in the form

$$\mathcal{F} = A \int_0^L dx \left[|\nabla \Psi|^2 + \alpha |\Psi(x)|^2 + \frac{\beta}{2} |\Psi(x)|^4 \right] \tag{1.23}$$

where α, β and are arbitrary parameters for the chosen normalization of the order parameter. $\Psi(x) = \Delta(x) \mathrm{e}^{i\varphi(x)}$ is the complex superconducting order parameter that is assumed to vary slowly along the x direction and be essentially constant in the transverse directions. The phenomenological theory can actually be rigorously derived as a limiting case of the microscopic theory in the spatially inhomogeneous regime [24].

The stationary condition $\delta\mathcal{F}/\delta\Psi^* = 0$ leads to the Ginzburg-Landau differential equation

$$-\nabla^2 \Psi + \alpha \Psi + \beta |\Psi|^2 \Psi = 0 \tag{1.24}$$

for suitable boundary conditions. Introducing the magnetic vector potential $\boldsymbol{A}$ through the standard replacement $\boldsymbol{\nabla} \rightarrow \boldsymbol{\nabla} - (ie^*/\hbar c)\boldsymbol{A}$ the constant current solution to Eq. (1.24) is a helix described by

$$\Psi(x) = \sqrt{\frac{\alpha - k^2}{\beta}} \mathrm{e}^{i\varphi(x)} \tag{1.25}$$

where $\varphi(x) = kx$ and the pitch is $2\pi/k$. The allowed wavevectors $k = (2\pi/L)n$ where n is an integer are fixed by requiring that the order parameter be single valued for periodic boundary conditions, $\varphi(x+L) = \varphi(x) + 2\pi n$. This is equivalent to taking our wire of radius R and length L and connecting it end-to-end to form a loop. Thus for each integer n there exists a helical solution given by Eq. (1.25) which is an isolated saddle-point of Eq. (1.23). A continuous path in function space connecting two such solutions must overcome a free energy barrier.

In this multiply connected geometry, the requirement for a dissipationless current is the familiar flux quantization condition

$$\oint \boldsymbol{\nabla} \varphi \cdot d\boldsymbol{\ell} = 2n\pi. \tag{1.26}$$

However, for a straight finite wire with an imposed current, the potential difference between the two ends is related to the rate of change in time of the total phase difference via the Josephson relation [25]

$$\frac{d\Delta\varphi}{dt} = \frac{2eV}{\hbar}, \tag{1.27}$$

where $\Delta\varphi = \varphi(L) - \varphi(0)$. In this configuration, a supercurrent, defined by $V = 0$ requires a constant value for the phase difference, or at least a fluctuating alternating current (ac) value which oscillates about some mean. The measurement of a finite voltage which is constant in time implies that the phase difference $\Delta\varphi$ must be increasing linearly with time. This can be understood by imagining that the helical solution described above is fixed at one end of the wire while it is continually wound at the other end around the x axis. Re-expressing this winding phase in terms of the superfluid velocity v_s, the Josephson relation, Eq. (1.27) can be written as

$$\frac{dv_s}{dt} = \frac{eE}{m}. \tag{1.28}$$

The tighter the order parameter is wound, the greater the cost in kinetic energy coming from an increasing superfluid velocity v_s contributing to Eq. (1.23). Thus, there is a critical velocity v_c related to the critical current J_c where the entire picture of a uniform solution breaks down.

Little [18] arrived at the solution to this problem by suggesting that the steady-state could be maintained in the presence of a finite voltage, provided that the order parameter was *unwound* by *phase slips* of 2π occurring at the exact rate needed to satisfy Josephson's relation. The important point is that since the order parameter must vary continuously, if its ends are held fixed, a phase slip event can only occur at a location along the x-axis where the magnitude of the order parameter is spontaneously suppressed to zero. As shown in Fig. 1.2 with $\Delta\varphi$ going from 12π to 10π, phase coherence is broken in some localized region along the wire, and a single loop is unwound before coherence is reestablished. Phase changes of more than 2π are a result of a sequence or cascade of single slips.

A single phase slip is thus a thermally induced activated resistive fluctuation that occurs at a random position in the wire. With this picture in mind, Langer and Ambegaokar (LA) [19] set out to determine the height of the minimum free energy barrier along the path in function space that connects two saddle point solutions of Eq. (1.23) corresponding to uniform solutions with different numbers of turns. They derived the physically appealing result that the free energy barrier is proportional to the condensation energy in one correlation length of the conductor

$$\Delta F = \frac{8\sqrt{2}}{3}\frac{H_c^2(T)}{8\pi}A\xi(T) \tag{1.29}$$

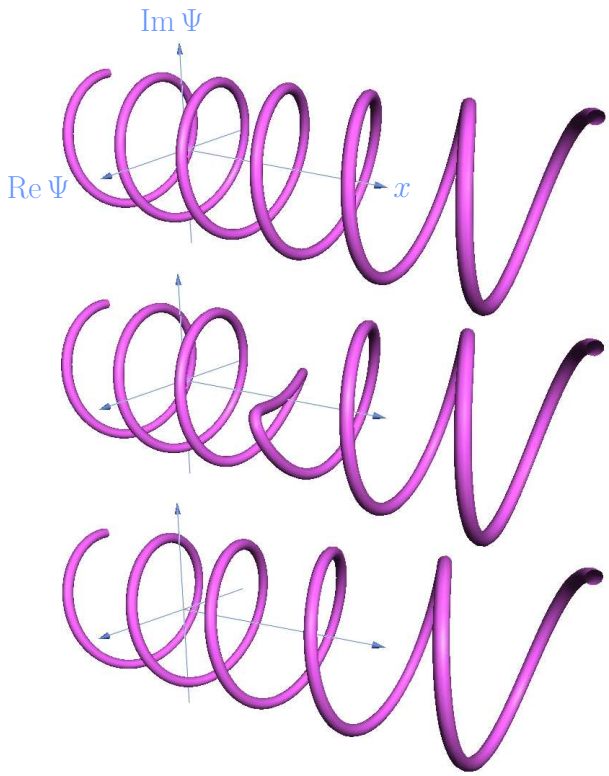

Figure 1.2: A schematic snapshot of the order parameter Ψ at some fixed time for a current carrying state at constant voltage. The total phase difference between the two ends changes from 12π in the top panel to 10π in the bottom panel as a result of a single phase slip event pictured at center.

where $H_c^2(T)/8\pi$ is the superconducting condensation energy per unit volume introduced previously, A is the cross-sectional area of the wire and $\xi(T)$ is the Ginzburg-Landau correlation length at temperature T. McCumber [26] showed that in the in the absence of an applied current, phase slips of $\pm 2\pi$ will occur with equal probability. In the presence of small current, the arguments above require that -2π phase slips occur at rate of $2eV/h$ per second greater than $+2\pi$ slips. This is related to the different electrical work corresponding to plus and minus jumps

$$\begin{aligned} \delta F &\equiv \Delta F^+ - \Delta F^- \\ &= \frac{h}{2e} I \end{aligned} \tag{1.30}$$

where I is the applied current. In order to determine the rate of change of the phase difference between the two ends, an attempt frequency Ω must also be calculated. Langer and Ambegaokar essentially guessed that this was the temperature indepen-

dent quantity

$$\Omega = \frac{NAL}{\tau_e} \tag{1.31}$$

where N is the density of conduction electrons in the wire and $\tau_e \approx 10^{-12}$ s is the typical elastic scattering time of electrons in the normal state. The time rate of phase change between the ends of the wire is thus given by

$$\begin{aligned}\frac{d\Delta\varphi}{dt} &= \Omega \mathrm{e}^{-\Delta F/k_\mathrm{B}T}\left(\mathrm{e}^{\delta F/2k_\mathrm{B}T} - \mathrm{e}^{-\delta F/2k_\mathrm{B}T}\right) \\ &= 2\Omega \mathrm{e}^{-\Delta F/k_\mathrm{B}T} \sinh\frac{\delta F}{2k_\mathrm{B}T}\end{aligned} \tag{1.32}$$

which when combined with Eq. (1.30) and inserted into the Josephson relation, Eq. (1.27) leads to the voltage

$$V_\mathrm{LAMH} = \frac{\hbar\Omega}{e}\mathrm{e}^{-\Delta F/k_\mathrm{B}T}\sinh\frac{hI}{4ek_\mathrm{B}T}. \tag{1.33}$$

In the limit of small currents we assume there is a linear resistance coming from Ohm's law and thus

$$R_\mathrm{LAMH} = \frac{\pi\hbar^2\Omega}{2e^2k_\mathrm{B}T}\mathrm{e}^{-\Delta F/k_\mathrm{B}T}. \tag{1.34}$$

McCumber and Halperin (MH) realized that although the LA result for the size of the free energy barrier was correct, they had drastically overestimated (by a factor of almost 10^{10}!) the rate at which phase slips occur. They reformulated the problem in terms of the time dependent Ginzburg-Landau theory and discovered that although the basic structure of the MH form for Ω is correct, when derived properly it is temperature dependent and equal to

$$\Omega(T) = \frac{L}{\xi(T)}\sqrt{\frac{\Delta F}{k_\mathrm{B}T}}\frac{1}{\tau_{\mathrm{GL}(T)}} \tag{1.35}$$

where

$$\tau_\mathrm{GL}(T) = \frac{\pi\hbar}{8k_\mathrm{B}(T_c - T)} \tag{1.36}$$

is the Ginzburg-Landau relaxation time. Instead of being equal to the number of electrons per unit electron relaxation time, it is equal to the number of statistically independent sub-regions of the wire where a phase slip process could occur per unit superconducting relaxation time.

Due to the use of the GL free energy, this result should work only arbitrarily close to T_c, but when adding a normal resistive channel (R_N) in parallel, such that the total resistance is given by

$$R = \left(\frac{1}{R_N} + \frac{1}{R_\mathrm{LAMH}}\right)^{-1}, \tag{1.37}$$

excellent agreement was found over six orders of magnitude for micron diameter Sn whiskers. It would be almost thirty years before technological advances in fabrication techniques had improved enough to reduce the diameters by a factor of one thousand, pushing the limit of the LAMH theory and entering a truly quantum regime.

1.3 Ultra narrow wires

The self grown Sn-whiskers of the original Webb and Warburton experiment had diameters between 40 and 400 μm and their resistive properties were well described by the LAMH theory introduced in the previous section. As the diameter of a wire is reduced, there are two important changes that need to be considered. The first is the well known volume to surface area ratio, and thus surface effects which are somewhat poorly understood will begin to affect bulk behavior. The second is more subtle and is related to the increased effects of coupling with an external environment. In the presence of such dissipation, a small system can undergo a quantum localization transition, as is observed in small Josephson junctions [27].

1.3.1 Evidence for quantum phase slips

In the early 1990s, step edge electron beam lithography techniques were used to create narrow indium strips with diameters between 40 and 100 nm. When transport measurements were performed, there appeared to be significant deviations from the LAMH resistance at low temperatures resulting in a persisting resistance manifest as a "foot" raised upwards from the expected exponentially decreasing behavior [28, 29]. It was proposed that this was due to the onset of quantum phase slips at low temperatures occurring via the macroscopic tunneling mechanism of Caldeira and Leggett [30]. These ideas were vigorously pursued [31, 32, 33, 34] leading to a host of theories which did not necessarily agree on the observability of quantum phase slips in experiments. One of the most interesting results was a *upper bound* on the wire diameter of approximately 10 nm above which quantum phase slips would be strongly suppressed [32] as their rate $\Omega_{QPS} \sim \exp(-N_\perp)$ where $N_\perp$ is the number of transverse channels in the wire discussed above. This upper bound of ten nanometers was far too narrow for step edge lithography techniques and it would take the invention of novel nanofabrication methods to fully address these issues.

1.3.2 Suspended molecular templating

Wires with truly nanoscale dimensions were not studied until the introduction of a novel and pioneering nanofabrication technique known as *suspended molecular templating* in early 2000 [35]. This remarkable process can be used to manufacture wires with lengths between 100 and 200 nm with diameters less than 10 nm. The key feature

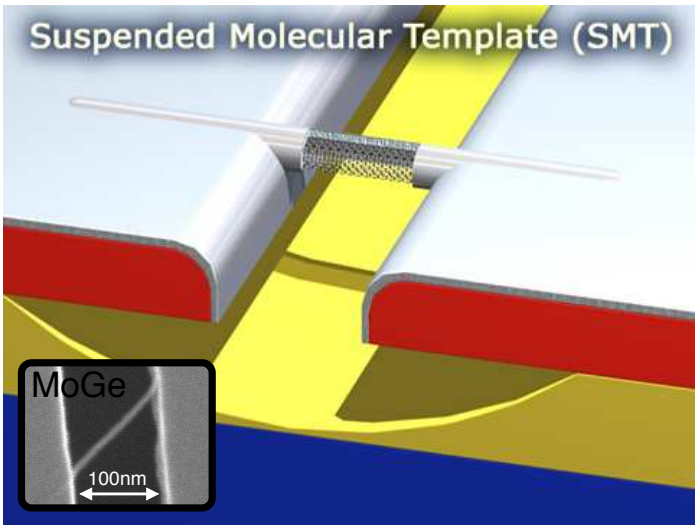

Figure 1.3: A diagram courtesy of Ref. [36] of an ultra-thin wire fabricated via suspended molecular templating which results in a single nanowire held up over a trench by a bridge consisting of a single carbon nanotube. The inset shows a scanning electron microscopy image of a MoGe nanowire with a diameter of approximately 10 nm.

is the top down approach that uses a long narrow molecule such as a carbon nanotube or DNA as a backbone on top of which the wire is deposited. The fabrication process begins by etching a trench in a substrate formed from a silicon wafer using electron beam lithography. The backbone molecules are then placed in solution and deposited over the substrate. They are allowed to settle, and at high concentrations some will end up resting over the trench. The entire surface of the substrate is then sputter coated with several nanometers of a metal like Nb or alloy such as MoGe. The result is that a thin uniform layer of the deposited material is suspended over the trench by the backbone molecule. It can be located via scanning electron microscopy (SEM) and then isolated with a mask that is also used to pattern electrodes that will be used for transport measurements. A schematic view of the final system is shown in Fig. 1.3 with an inset showing an actual SEM image of a MoGe nanowire. A huge advantage of the SMT technique, in addition to allowing for the fabrication of ultra narrow wires, is that it allows for a large number of wires with varying diameters to be quickly and easily made. Fig. 1.4 reproduces resistance versus temperature measurements from Ref. [37] for five wires ranging in diameter from 10.5 nm to 6.8 nm. The results show two exponential dips in the resistance for each wire. The first at high temperatures, corresponds to the large two dimensional leads going superconducting while the lower temperature drop is due to the actual wire undergoing a phase transition. The temperature at which the wire goes superconducting is strongly dependent on its diameter with thinner wires being pushed to lower temperatures. This is consistent with our

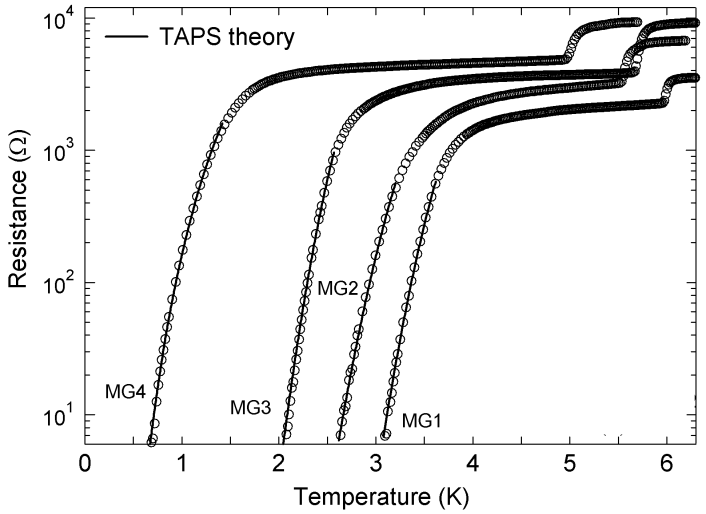

Figure 1.4: Experimental transport measurements on MoGe nanowires from Ref. [37] showing excellent agreement with the LAMH theory of thermally activated phase slips (TAPS) for resistances down to approximately 0.5 Ω. The diameters of wires MG1 to MG4 are 10.4, 10.0, 9.4 and 6.8 nm respectively.

expectations as discussed at the beginning of this section. Superb agreement with the LAMH theory is found for resistances down to 0.5 Ω using Eq. (1.34) with the bulk critical temperature T_c and the zero temperature coherence length $\xi(0)$ used as fitting parameters. At resistances below this value, or for thinner wires, there appears to be a growing experimental consensus that there is a non-monotonicity in the resistance and deviations from the theory of purely thermally activated phase slips. The wires seem to be entering a regime where resistive fluctuations coming from other effects, possibly including Coulomb blockade and quantum phase slips can either postpone or completely destroy the superconducting transition [35, 38, 39, 40]. This behavior can be seen by measuring the resistance of thinner and thinner wires as a function of temperature leading to a separation between superconducting and metallic transport all the way down to the lowest temperatures as seen in Fig. 1.5. If superconductivity is indeed being destroyed as the temperature is reduced to zero by quantum and not thermal fluctuations upon tuning some parameter related to the size of the transverse dimension, then such a transition is by definition a superconductor-metal *quantum phase transition* (SMT).

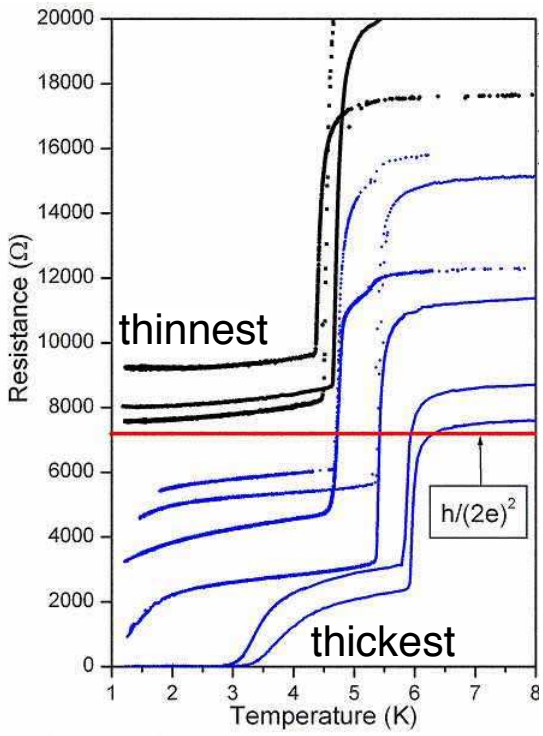

Figure 1.5: Experimental transport measurements on MoGe nanowires from Ref. [36] showing a distinct difference between thick superconducting and thin metallic or resistive wires as the temperature is reduced. At zero temperature, a quantum critical point would separate the superconducting and metallic phase, with the transition between them being described by a quantum superconductor-metal transition (SMT).

1.4 Pair-breaking theory

We have just seen a plot of the resistance versus temperature for a set of ultra-narrow MoGe wires with varying diameters (Fig. 1.5). As temperature was reduced the thicker wires all underwent a superconducting transition but it appeared that there was some critical wire diameter, below which no such transition occurred. Instead, the thinnest wires displayed metallic or resistive behavior down to the lowest temperatures measured and some even hinted at non-monotonic behavior in T. We proposed an explanation for these observations in terms of a quantum phase transition between a superconducting and metallic state, a SMT, that appeared to be tuned by the radius of the wire. The temperature-radius phase diagram would take the form of the schematic one depicted later in Fig. 1.10 where the choice of symbol for the tuning parameter seems particularly apt.

In our presentation of the BCS theory of conventional superconductivity we de-

rived an explicit equation for the transition temperature

$$k_{\mathrm{B}}T_c = 1.14\hbar\omega_{\mathrm{D}}\mathrm{e}^{-1/N(0)V} \tag{1.38}$$

where ω_{D} was the phonon Debye frequency, $N(0)$ the density of states at the Fermi energy and V the pairing strength. We argued that this expression *guarantees* that there will always be a superconducting state below some temperature for an arbitrarily small value of V. Our conclusions about the complete destruction of superconductivity in ultra-thin wires therefore seems to be at odds with a Nobel prize winning theory, an uncomfortable position to linger in. Luckily, this apparent contradiction was resolved some time ago by Abrikosov and Gor'kov (AG) [41] when they studied the suppression of T_c in superconducting alloys with paramagnetic impurities. They discovered that in the presence of a perturbation which makes it more difficult to form Cooper pairs, a *pair-breaking* interaction, Eq. (1.38) gets modified and some critical pairing strength is needed to form the superconducting state. The AG theory has since been generalized to many different sources of physical pair-breaking interactions and we will introduce the important features of their arguments as well as discuss some modern experimental realizations of the pair-breaking transition.

1.4.1 Magnetic fields and impurities

The most important observation that led to the pair-breaking theory was that the transition temperature of a clean superconductor is almost completely unchanged by the addition of a moderate concentration of non-magnetic impurities. This behavior is fully explained by Anderson's theorem [42] which states that although small concentrations of disorder will lead to some local impurity states, the system is still nearly homogeneous at lengths on the order of the BCS coherence length ξ_0, and thus Cooper pairs are not significantly affected. The Anderson theorem breaks down in the presence of magnetic impurities as a Cooper pair is composed of two electrons which are time reversed partners (opposite momentum and spin). Thus any perturbation which is odd under time reversal will act differently on the two paired electrons and lead to a finite probability of completely disassociating the pair. If the strength of the pair-breaking is large, ξ_0 can be reduced enough to completely destroy the phase coherent superconducting state.

The only restriction on a pair-breaking perturbation is that it must act oppositely on the two members of a Cooper pair. This condition is satisfied in a small or dirty superconductor placed in a suitably strong magnetic field. In addition, a restricted geometry leading to sufficient surface scattering or non-magnetic impurities providing body scattering and diffusive behavior are required to ensure that individual pair-breaking events are rapid and uncorrelated and that the electrons can explore their full phase space leading to so called *ergodic* behavior. A magnetic field can be incorporated into the single electron Hamiltonian in the usual way leading to a term of the form $\boldsymbol{p}\cdot\boldsymbol{A} + \boldsymbol{A}\cdot\boldsymbol{p}$ where $\boldsymbol{p}$ is the momentum and $\boldsymbol{A}$ is the magnetic

vector potential. This term is clearly odd under time reversal, changing sign when $\boldsymbol{p} \to -\boldsymbol{p}$. The contribution of a magnetic impurity as described by the AG theory is more complicated, and will couple to electrons via a super exchange mechanism

$$\mathcal{H}_{ex} = J(|\boldsymbol{x} - \boldsymbol{x}'|)\boldsymbol{S}(\boldsymbol{x}) \cdot \boldsymbol{\sigma}(\boldsymbol{x}') \tag{1.39}$$

where $\boldsymbol{S}(\boldsymbol{x})$ is the impurity spin located at position $\boldsymbol{x}$ and $\boldsymbol{\sigma}(\boldsymbol{x}')$ is the electron spin at $\boldsymbol{x}'$. Since a Cooper pair is made up of two paired electrons, one with spin $\boldsymbol{\sigma}$ and the other with spin $-\boldsymbol{\sigma}$ such an exchange term will cause spin flip scattering with an opposite orientation for each member.

Abrikosov and Gor'kov studied the latter case within the diagrammatic Green function formalism using the Born approximation for the scattering of an electron off an impurity atom. We will spare the reader from a presentation of their methods and instead quote some of the important results from de Genne's treatment [15] using the linearized Ginzburg-Landau equations in the presence of a constant pair potential which will be sufficient for our purposes. After some preliminary algebra and simplifications, the final discussion can be framed in terms of the time reversal Heisenberg operator $K(t)$ which acts on the single electron wave functions of the normal metal.

We begin with the usual local electron Hamiltonian

$$\mathcal{H}_e = \sum_\sigma \int d^d x \left\{ \psi_\sigma^\dagger(\boldsymbol{x}) \left[\frac{1}{2m} \left(\boldsymbol{p} - \frac{e}{c}\boldsymbol{A} \right)^2 - \varepsilon_{\mathrm{F}} \right] \psi_\sigma(\boldsymbol{x}) + \sum_{\sigma,\sigma'} \psi_\sigma^\dagger(\boldsymbol{x}) U_{\sigma\sigma'}(\boldsymbol{x}) \psi_{\sigma'}(\boldsymbol{x}) \right.$$
$$\left. - V \sum_{\sigma,\sigma'} \psi_\sigma^\dagger(\boldsymbol{x}) \psi_{\sigma'}^\dagger(\boldsymbol{x}) \psi_\sigma(\boldsymbol{x}) \psi_{\sigma'}(\boldsymbol{x}) \right\} \tag{1.40}$$

where $\psi_\sigma^\dagger(\boldsymbol{x})$ creates an electron at site $\boldsymbol{x}$ with spin σ and $U_{\sigma\sigma'}(\boldsymbol{x})$ is a static, local spin-dependent interaction. This Hamiltonian includes both types of pair-breaking interactions discussed above and the self-consistency equation for the superconducting gap Δ is given by

$$\Delta = \frac{V}{2} \sum_{\sigma,\sigma'} \epsilon_{\sigma\sigma'} \langle \psi_\sigma(\boldsymbol{x}) \psi_{\sigma'}(\boldsymbol{x}) \rangle \tag{1.41}$$

where $\langle \cdots \rangle$ indicates an average with respect to $\mathcal{H}_e$ and $\epsilon_{\sigma\sigma'}$ is a fully antisymmetric tensor.

The equations of motion for $\psi^\dagger$ and ψ can be linearized, and diagonalizing the Hamiltonian by introducing Bogoliubuv quasiparticles we arrive at a modified version of Eq. (1.41) (after some considerable algebra)

$$\Delta(\boldsymbol{x}) = \int d^d x' \Phi(\boldsymbol{x}, \boldsymbol{x}') \Delta(\boldsymbol{x}') \tag{1.42}$$

to lowest order where

$$\Phi(\boldsymbol{x},\boldsymbol{x}') = \sum_{\omega_n} \int d\xi \int d\xi' \frac{k_{\mathrm{B}} T V N(0) \mathcal{V}}{(\xi - i\hbar\omega_n)(\xi' + i\hbar\omega_n)} g(\boldsymbol{x},\boldsymbol{x}',\xi-\xi') \tag{1.43}$$

with $\mathcal{V}$ the volume of the system, V the BCS pairing interaction, $N(0)$ the density of states at the Fermi level and $\omega_n = (2n+1)\pi k_{\mathrm{B}} T/\hbar$ an odd electron Matsubara frequency. The function g is defined by

$$g(\boldsymbol{x},\boldsymbol{x'},\varepsilon) = \sum_m \langle \phi_n^*(\boldsymbol{x}) \phi_m^*(\boldsymbol{x}) \phi_m(\boldsymbol{x'}) \phi_n(\boldsymbol{x'}) \rangle \, \delta(\xi_m - \xi_n - \varepsilon) \tag{1.44}$$

where ϕ_m are the normal electron eigenstates of $\mathcal{H}_e$. Eq. (1.43) should remind the reader of Eq. (1.18) and a key simplification will come by recognizing that the time reversal operator has been essentially defined to lead to the conjugation of these states, i.e.

$$K\phi_m(\boldsymbol{x}) = \phi_m^*(\boldsymbol{x}). \tag{1.45}$$

Using this fact we can rewrite Eq. (1.43) in terms of $\widetilde{g}$, the power spectrum of the operator K

$$\frac{\hbar}{N(0)V} = \sum_{\omega_n} \int d\xi \int d\xi' \frac{k_{\mathrm{B}} T}{(\xi - i\hbar\omega_n)(\xi' + i\hbar\omega_n)} \widetilde{g}\left(\frac{\xi - \xi'}{\hbar}\right) \tag{1.46}$$

where

$$\widetilde{g}(\omega) = \int \frac{dt}{2\pi} \langle K^\dagger(0) K(t) \rangle \mathrm{e}^{-i\omega t}. \tag{1.47}$$

The first thing to note is that in the absence of any pair-breaking perturbations

$$\langle K^\dagger(0) K\ (t) \rangle = 1 \tag{1.48}$$

and $g(\omega) = \delta(\omega)$. Eq. (1.46) thus reduces exactly to Eq. (1.18) in BCS theory. In the presence of a pair-breaking interaction, the ergodicity condition discussed earlier is equivalent to requiring that

$$\langle K^\dagger(0) K\ (t) \rangle \sim \mathrm{e}^{-t/\tau_K} \tag{1.49}$$

as $t \to \infty$ where τ_K is the time required to sufficiently randomize the phase of the two electrons composing a single Cooper pair; the spin-flip scattering time. A corresponding energy scale,

$$\hbar\alpha = \frac{\hbar}{2\tau_K}, \tag{1.50}$$

can be interpreted as the depairing energy or splitting between the two time-reversed electrons of a Cooper pair, averaged over the time required to completely uncorrelated their phases. This interpretation allows one to generalize the pair-breaking

theory presented here to large variety of physical situations provided the destruction of superconductivity occurs via a second order phase transition [15].

Substituting Eq. (1.49) in Eq. (1.47) we find

$$\widetilde{g}(\omega) = \frac{1}{\pi}\frac{\tau_K}{1+\omega^2\tau_K^2} \tag{1.51}$$

which can be inserted into into Eq. (1.46), and performing the two energy integrals we arrive at

$$\frac{1}{N(0)V} = \frac{k_{\rm B}T}{\hbar}\sum_{\omega_n}\frac{2\pi}{2|\omega_n| + \tau_K^{-1}}. \tag{1.52}$$

The sum is divergent as a result of the fact that we have forgotten to enforce the BCS constraint in Eq. (1.13). Taking this into account, and adding and subtracting $\sum_{\omega_n}(2|\omega_n|)^{-1}$ the equation for the critical temperature is given by

$$\frac{1}{N(0)V} = \left[\ln\left(\frac{1.14\hbar\omega_{\rm D}}{k_{\rm B}T}\right) + \frac{2\pi k_{\rm B}T}{\hbar}\sum_{\omega_n}\left(\frac{1}{2|\omega_n| + \tau_K^{-1}} - \frac{1}{2|\omega_n|}\right)\right] \tag{1.53}$$

where we have used Eq. (1.38). The sum can now be performed and yields the final AG result for the mean field pair-breaking phase boundary

$$\ln\left(\frac{T}{T_{c0}}\right) = \psi\left(\frac{1}{2}\right) - \psi\left(\frac{1}{2} + \frac{\hbar\alpha}{2\pi k_{\rm B}T}\right) \tag{1.54}$$

where $\psi(x)$ is the polygamma function, $k_{\rm B}T_{c0} = 1.14\hbar\omega_{\rm D}{\rm e}^{-1/N(0)V}$ is the BCS transition temperature in the absence of any pair-breaking perturbations and α is the pair-breaking frequency defined in Eq. (1.50). Eq. (1.54) is the main result of this section and shows that by perturbing a conventional superconductor with a suitably strong interaction that breaks time reversal symmetry, it is possible to completely destroy the superconducting state at finite temperature as shown in Fig. 1.6. Mathematically, this is equivalent to the observation that for large enough α, Eq. (1.54) has no non-zero solution at finite temperature.

1.4.2 Experimental manifestations

We have presented a derivation of the relationship between the pair-breaking frequency α and the temperature at which superconductivity is destroyed for the particular case of a superconductor with paramagnetic impurities. However, we argued that the result is much more general and can be applied to any perturbation which breaks time reversal symmetry. We now introduce three experimentally tunable sources of pair-breaking which are of considerable interest.

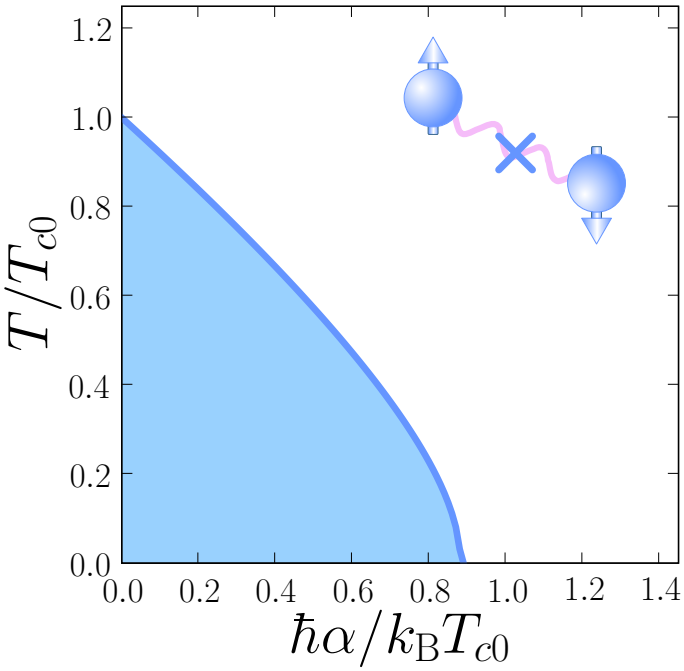

Figure 1.6: The Abrikosov-Gor'kov pair-breaking phase diagram [41] with the phase boundary given by Eq. (1.54). The superconducting phase is shaded, and for a suitably large α the ordered phase is completely destroyed for all finite temperatures.

Radius tuned nanowire

A possible superconductor-metal transition in ultra-narrow MoGe wires was discussed at the beginning of this section inferred from an examination of Fig. 1.5. At first glance, it would appear to be driven by a source of pair-breaking related to the diameter of the wire, however this could be an example of correlation not implying causation. Recent experiments have provided some evidence [37] that there may be magnetic impurities sitting on the surface of nanowires made using the SMT technique. Any impurity at the surface would be much less effectively screened, and one could imagine a BCS coupling $V(\rho)$ which depends on the radial coordinate of the wire. In this picture, $V(\rho)$ would change sign from negative (attractive) to positive (repulsive) as ρ changes from $\rho = 0$ to $\rho = R$ where R is the diameter of the wire. This behavior is schematically outlined in Fig. 1.7. For the thickest wires, $R > \xi_0$ and the mean field solution to the BCS equations will lead to the wire being described by a superconducting core surrounded by a cylindrical metallic envelope. A similar picture was recently put forward to describe the SMT in two dimensions by imagining superconducting grains embedded into a film with a pairing interaction which depended on the distance from the center of the islands [43]. In the nanowire case, as one reduces the transverse dimension, there will be a critical radius, $R \approx \xi_0$, where

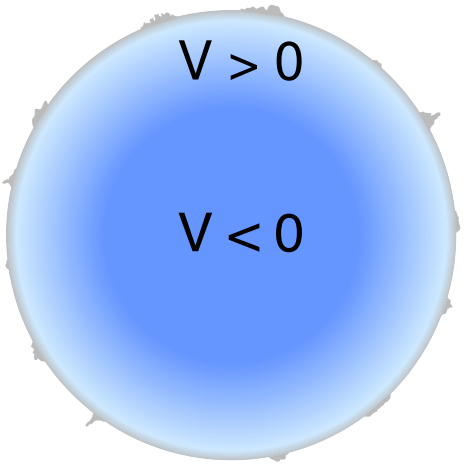

Figure 1.7: A schematic cross-section of a metallic wire where magnetic impurities on the surface are poorly screened leading to a change in sign of the BCS pairing interaction as one moves from the center, $|\Psi| \neq 0$ to the edge, $|\Psi| \simeq 0$ where $\Psi(\rho)$ is the superconducting order parameter. Below some temperature, the wire would be composed of a superconducting core with a normal resistive sheath.

the superconducting core will vanish and the wire will enter a metallic state. This is a rather physically appealing picture as it is suitable for the destruction of superconductivity in a wire that is only weakly disordered in the bulk and is well suited to theoretical models.

Magnetic field tuned nanowire

It is clearly impossible to systematically reduce the diameter of a single wire while measuring its transport properties and thus other more systematic examples of a SMT would be beneficial. The most obvious candidate is a transition that can be observed in a single wire by increasing the strength of a magnetic field oriented parallel to its long axis. This experiment has been performed by Rogachev, Bollinger and Bezryadin [44] on individual Nb nanowires with the most important result shown in Fig. 1.8. The rightmost curve is in zero magnetic field and shows a superconducting transition that is well described by LAMH theory (solid line). As the strength of the parallel magnetic field is increased, the transition appears at lower and lower temperatures with the expectation that for suitably strong fields it will vanish all together and the wire will exhibit metallic behavior; a quantum SMT. To completely destroy superconductivity, pair-breaking events must be uncorrelated over long time scales and a theoretical description would require diffusive electrons or suitably strong boundary scattering.

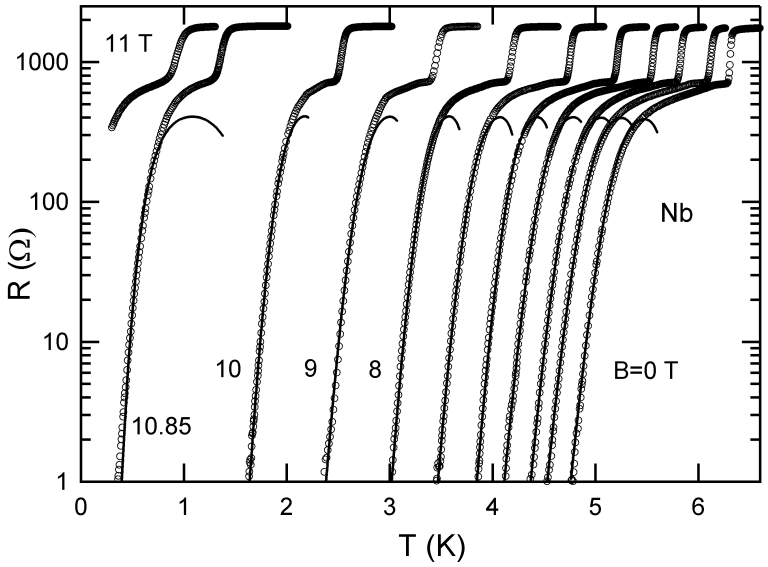

Figure 1.8: Resistance versus temperature for a Nb nanowire with a diameter of 8nm and length $L = 120$nm in a parallel magnetic field with strength ranging from 0 T (right curve) to 11 T (left curve). The symbols are data points while the lines are fits to LAMH theory using T_c and ξ_0 as free parameters.

Magnetic flux tuned cylinder

A final experimental example which is relatively well understood is the destruction of superconductivity in a multiply connected metallic cylinder with a nearly half-integer flux quantum trapped in its interior. Liu *et al.* have fabricated ultra-thin doubly connected metallic cylinders by coating quartz poles with aluminum [45]. The Al coating is thin enough to be considerably smaller than the penetration depth in the presence of a magnetic field oriented parallel to the long axis of the cylinder. Below some transition temperature the doubly connected cylinder will exhibit the well known phenomena of flux quantization in an external field as a result of global phase coherence and a circulating supercurrent around the cylinder. Because of the narrow walls, the superfluid velocity v_s should be constant in the aluminum and for a given value of the external magnetic flux $\Phi = \int \boldsymbol{H} \cdot d\boldsymbol{S}$ through the cylinder we find

$$v_s = \frac{\hbar}{m^* R}\left(n - \frac{\Phi}{\Phi_0}\right) \tag{1.55}$$

where R is the radius, $\Phi_0 = h/2e$ is the flux quantum and m^* is twice the electron mass. The integer n will adjust to minimize v_s for a given field strength and this is known to lead to Little-Parks oscillations in the critical temperature for large R [46]. However, if the radius of the wire is reduced until it is on the order of the

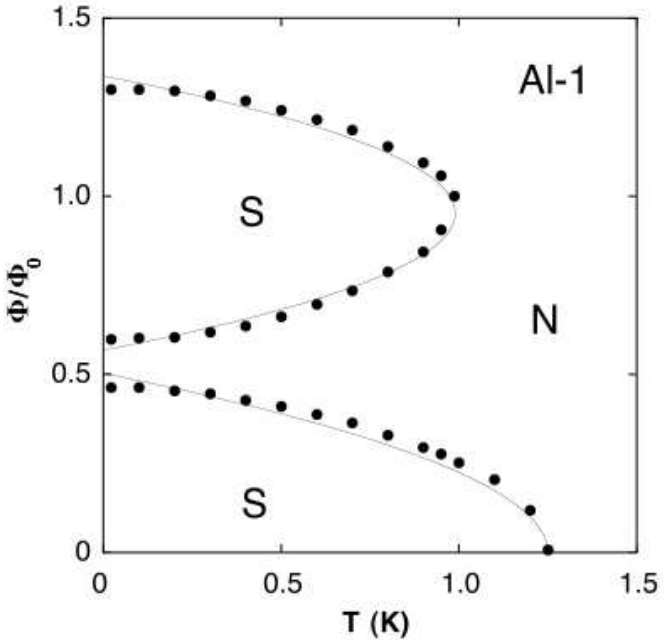

Figure 1.9: The superconductor-normal phase diagram for a 150 nm long ultra-thin walled aluminum cylinder as a function of the magnetic flux trapped inside, measured in units of the flux quantum $\Phi_0 = h/2e$ from Ref. [45].

superconducting coherence length, the ordered state can completely disappear. From Eq. (1.55), the superfluid velocity will reach a maximum whenever Φ/Φ_0 is equal to a half-integer. Due to the small sample volume, the condensation energy cannot overcome the drastic increase in kinetic energy due to v_s and superconductivity will no longer be energetically possible. This completely destructive quantum size effect was first observed in Ref. [45] and is highlighted in the phase diagram shown in Fig. 1.9. We observe a lobed structure showing finite temperature phase transitions between a superconducting and normal state, as well as indicating the presence of a series of quantum critical points at field strengths corresponding to a half integer trapped flux. The transition is crucially dependent on the specific topology of the system and is therefore not directly amenable to a microscopic pair-breaking description.

In this section we have presented three experimental examples of a quantum phase transition between a superconductor and a metallic state tuned by a non-thermal parameter. The quantum SMT is a single example of a broader class of transitions driven by quantum fluctuations at zero temperature. The complex interplay between thermal and quantum fluctuations will lead to a host of novel and interesting phase transitions and crossovers which we now address.

1.5 Quantum phase transitions

In the previous section we were led by an analysis of experimental results to the concept of a phase transition between a superconductor and a metal occurring at zero temperature, driven by *quantum* and not thermal fluctuations in a ultra-narrow wire or cylinder. This is just one example of a fascinating type of phase transition where the dynamic and static critical behavior are inexorably intertwined. The coupling between thermodynamics and dynamics at all length scales at $T = 0$ can have drastic and non-trivial effects throughout the finite temperature phase diagram and in this section we present the basic ingredients that will be necessary to motivate the results in the remainder of the thesis. The theory of quantum phase transitions and crossovers has been developing over the last thirty years with its official "coming out" party often attributed to Hertz [47]. As a result, many excellent books [48], lectures [49, 50] and colloquia [51] have been written on the subject; with the author having a conspicuous preference for Ref. [48].

We begin with a brief review of classical phase transitions and the scaling hypothesis which will be useful for mapping quantum phase transitions to their classical counterparts in one additional dimension. After highlighting the properties of the zero temperature quantum critical point, a generalization to finite temperatures is provided, where the finite size of the system in the imaginary time direction will lead to highly non-trivial crossover phenomena. We finally conclude with a discussion of the failings of the quantum to classical mapping and the necessity of taking a quantum field theoretic perspective from the outset.

1.5.1 Landau theory

The theory of classical phase transitions is built around the existence of an *order parameter* which is identically zero in a disordered phase and takes on a finite value in an ordered phase. It is usually related to an obvious macroscopic feature in a physical system such as the magnetization near a ferromagnetic transition or the density of Cooper pairs near a superconducting transition. A phase transition can occur between the ordered and disordered phases (where disorder here refers to a phase without long range order, not to be confused with quenched randomness or defects) by tuning the temperature of the system. The nature of the phase transition, either continuous (second order) or discontinuous (first order) is related to the continuity of the order parameter across the critical point. One of the most common phase transitions which occurs in nature, the melting of ice to form water is first order, as the two phases coexist at the critical point and a latent heat is released. We will be primarily concerned with the theory of continuous phase transitions, which do not have phase mixing and exhibit fluctuations of the order parameter at the critical point with both diverging length and time scales. Standard sources which include much more detail on these and other points include Refs. [52] and [53].

Landau theory assumes that the free energy of the system F is analytic in a spatially uniform order parameter m and can be written as a power series expansion

$$F = hm + rm^2 + vm^3 + um^4 + \cdots \tag{1.56}$$

where all constants h, r, v and u are unknown, but usually some of their values can be set to zero by symmetry. For example if the system we are attempting to describe with F is invariant under the transformation $m \to -m$ then we would necessarily require that $h = v = 0$ and we will consider this case here. It is also assumed that the leading order temperature dependence is contained within $r = r_0(T - T_c)$ where T_c is the critical temperature at which the phase transition occurs. In the absence of the linear or cubic terms, the free energy can be trivially minimized with respect to variations of the order parameter and it is clearly seen that for $T > T_c$ or $r > 0$ the minimum will occur for m identically zero. For $T < T_c$, $r < 0$ and a non-zero solution appears with $m = \sqrt{-r/2u}$.

If we identify m as the magnetization of a ferromagnetic Ising model, then as the critical point is approached from the ordered phase $m \sim |r|^\beta$ where $\beta = 1/2$ is a mean field critical exponent, with similar exponents existing for other macroscopic observables. Thus Landau theory provides an experimentally verifiable prediction for the onset of order in *any* system invariant under the change of sign of its order parameter as the temperature is reduced. This is an example of the concept of *universality*, where macroscopic critical behavior is independent of any of the microscopic details of a given system. Universality is indeed observed in experiments, but it is not as strong as the hyper-universality of Landau theory would predict. In reality, different systems can be grouped into various universality classes which depend on both the dimension of space d and the number of components (or symmetry) N of the order parameter.

The main flaw in Landau theory is that it does not allow for any fluctuations of the order parameter about its mean field value. It is known that lower dimensions or more order parameter components tend to produce larger fluctuations, and such systems are poorly described by Landau theory. This observation leads naturally to the concept of an *upper critical dimension* d_{UCD} above which fluctuations can be neglected and the simple Landau theory provides the correct leading order physical description of critical behavior. On the other end of the spectrum lies the *lower critical dimension* d_{LCD} where fluctuations are so strong that they completely destroy the possibility of any ordered phase, and no finite phase transition can exist. If the dimension of the system of interest lies between the lower and upper critical dimension than a phase transition will exist, but it will exhibit non-mean field critical behavior.

$d_{\mathrm{UCD}} = 4$ for all values of N, while $d_{\mathrm{LCD}} = 1$ for $N = 1$ and $d_{\mathrm{LCD}} = 2$ for $N > 1$. A more subtle phase transition exists in the special marginal case of $d = 2$ and $N = 2$ known as the Kosterlitz-Thouless (KT) transition.

1.5.2 The scaling hypothesis

The failings of Landau theory can be overcome below the upper critical dimension by generalizing the spatially independent order parameter m to a coarse grained field $\phi(\boldsymbol{x})$ which should not be thought of as a microscopic variable, but rather as an average of some quantity over a region of space. With this generalization, the simple free energy in Eq. (1.56) now takes the form of the classical O(N) model, a functional in d dimensions where

$$\mathcal{F}[\phi_a] = \int d^d x \left\{ |\boldsymbol{\nabla}\phi_a(\boldsymbol{x})|^2 + r\phi_a^2(\boldsymbol{x}) + \frac{u}{4!}[\phi_a^2(\boldsymbol{x})]^2 - h_a\phi_a(\boldsymbol{x}) \right\} \tag{1.57}$$

and $a = 1, \ldots, N$ will allow us to consider any order parameter symmetry and we use the usual short form notation

$$\phi_a^2(\boldsymbol{x}) \equiv \phi_1^2(\boldsymbol{x}) + \cdots + \phi_N^2(\boldsymbol{x}). \tag{1.58}$$

There is an energy cost associated with spatial gradients of the order parameter, and we have added a field h_a conjugate to ϕ_a. The partition function is defined by the functional integral over $\phi_a(\boldsymbol{x})$

$$\mathcal{Z} = \int \mathcal{D}\phi_a \; \mathrm{e}^{-\mathcal{F}[\phi_a]/k_\mathrm{B}T}, \tag{1.59}$$

and the study of the free energy functional, $\mathcal{F}$ is referred to as the Ginzburg-Landau (GL) or Ginzburg-Landau-Wilson (GLW) theory. The field ϕ_a has been defined such that its average value with respect to $\mathcal{Z}$, $\langle\phi_a(\boldsymbol{x})\rangle$ is the Landau order parameter of the previous subsection

$$m \equiv \frac{1}{\mathcal{Z}} \int \mathcal{D}\phi_a \, \phi_a(\boldsymbol{x}) \, \mathrm{e}^{-\mathcal{F}[\phi_a]/k_\mathrm{B}T} \tag{1.60}$$

where in general for any observable $\mathcal{O}$

$$\langle\mathcal{O}\rangle = \frac{1}{\mathcal{Z}} \int \mathcal{D}\phi_a \, \mathcal{O} \, \mathrm{e}^{-\mathcal{F}[\phi_a]/k_\mathrm{B}T}. \tag{1.61}$$

The free energy functional in Eq. (1.57) was introduced in order to allow for the study of fluctuations of the order parameter. These are characterized by its correlation function (or propagator)

$$G(\boldsymbol{x}) = \langle\phi_a(\boldsymbol{x})\phi_a(0)\rangle \tag{1.62}$$

which is expected to decay exponentially with separation in the disordered phase

$$G(\boldsymbol{x}) \sim \mathrm{e}^{-|\boldsymbol{x}|/\xi} \tag{1.63}$$

defining the correlation length ξ. As the ordered phase is approached, correlations diverge as

$$\xi \sim |r - r_c|^{-\nu} \tag{1.64}$$

where r_c is the critical coupling signaling the onset of a phase transition and ν is defined as the correlation length critical exponent. The diverging correlation length has profound implications for critical phenomena, as it will be the *only* length scale affecting physical observables as the critical point is approached.

The existence of a single length scale is the crucial observation of the scaling hypothesis. Suppose we rescale all lengths in the system by a positive number b, but adjust all external parameters (temperature, magnetic field, etc) so that the correlation length retains its original value. We have just described a single iteration of the renormalization group (RG) procedure, and due to the sole dependence on ξ, all physical quantities must remain unchanged. To be precise, consider the free energy density f defined by

$$f = -\frac{k_{\mathrm{B}}T}{V} \ln \mathcal{Z} \tag{1.65}$$

where V is the volume. Performing the process described above for the Gaussian theory ($u = 0$) we find a homogeneity relation for the singular part of the free energy density

$$f_s(r, h) = b^{-d} f_s(\overline{r} b^{1/\nu}, \overline{h} b^{y_h}) \tag{1.66}$$

where y_h is another critical exponent and we have rescaled our coupling $\overline{r} = r/r_0$ and field $\overline{h} = h/h_0$ in order to make them dimensionless. In Eq. (1.66), b is a dimensionless scaling factor that we are free to choose, so let us pick $b = \overline{r}^{-\nu}$, and we have

$$f_s(r, h) = \overline{r}^{d\nu} \Phi_f \left(\frac{\overline{h}}{\overline{r}^{\nu y_h}} \right) \tag{1.67}$$

where Φ_f is a scaling function. Although the specific microscopic details of a given system are obfuscated in the scale factors r_0 and h_0, the functional form of Φ_f does not, it is *universal*. Similar relations can be derived for other observables by taking the appropriate derivatives of $f_s(r, h)$ leading to various universal critical exponents, and the scaling relations between them. The scaling laws can be rigorously derived within the framework of the renormalization group and all together lead to remarkable universal critical behavior due to the presence of a single diverging length scale, ξ.

1.5.3 Quantum statistical mechanics

The fundamental result of the existence of homogeneity relations is that the critical exponents that describe the properties of observables as the phase transition is reached are universal; they are the same for a wide variety of different types of phase transitions in different physical systems. They depend only on the *universality class*, a function of the dimension of space and the symmetry of the order parameter. All microscopic details are unimportant near the phase transition as the presence of a diverging length scale of fluctuations effectively averages over a larger and larger volume of the system.

Up until this point we have been able to completely neglect dynamics, or the time-dependence of physical observables, for the simple reason that in classical statistical mechanics the kinetic and potential parts of the Hamiltonian commute and we were able to study an effective classical field theory in terms a free energy functional $\mathcal{F}$. If we were instead to begin from a description of our system in terms of some N-particle Hamiltonian $\mathcal{H}(\boldsymbol{p}_i, \boldsymbol{q}_i)$, then the partition function would be written as an integral over all phase space variables $\{\boldsymbol{q}_i, \boldsymbol{p}_i\}$:

$$\begin{aligned}\mathcal{Z} &= \frac{1}{N!h^{Nd}} \int \prod_i d\boldsymbol{q}_i d\boldsymbol{p}_i \, \mathrm{e}^{-\beta\mathcal{H}(\boldsymbol{p}_i,\boldsymbol{q}_i)} \\ &= \frac{1}{N!h^{Nd}} \int \prod_i d\boldsymbol{p}_i \mathrm{e}^{-\beta\mathcal{H}_{\mathrm{kin}}(\boldsymbol{p}_i)} \int \prod_i d\boldsymbol{q}_i \mathrm{e}^{-\beta\mathcal{H}_{\mathrm{pot}}(\boldsymbol{q}_i)} \\ &= \mathcal{Z}_{\mathrm{kin}}\mathcal{Z}_{\mathrm{pot}},\end{aligned} \tag{1.68}$$

where $\beta = 1/k_{\mathrm{B}}T$ and h is Planck's constant. As the kinetic part simply consists of a product of simple Gaussian integrals it is singularity free, and it can be neglected, allowing us to study thermodynamic critical behavior using time independent theories, such as the GLW theory above. The situation is clearly not so simple in the quantum mechanical case where the kinetic and potential parts of the Hamiltonian do not commute. This is equivalent to the fact that when computing $\mathcal{Z}$ classically, we only need the Hamiltonian and not the equation of motion, but both factor into the quantum calculation. In other words, $\mathcal{H}$ alone does not fix the equation of motion, but we also need the Poisson brackets or commutation relations to determine the classical oscillation frequencies, ω, which when multiplied by $\hbar$ give the energy level spacings. As a result, the partition function does not factorize and we are left with the task of computing

$$\mathcal{Z} = \mathrm{Tr}\ \mathrm{e}^{-\beta\mathcal{H}}. \tag{1.69}$$

The expression for the quantum partition function can be very elegantly analyzed in the path-integral formulation of quantum mechanics due to Feynman with all the details provided in Ref. [54]. We first recall the usual time evolution operator of ordinary quantum mechanics

$$\mathcal{U}(t) = \mathrm{e}^{-i\mathcal{H}t/\hbar} \tag{1.70}$$

and note that it is equal to the expression we are tracing over in Eq. (1.69) if we evolve over imaginary instead of real time, i.e. $t = -i\beta\hbar$. Then writing the trace as a sum over states n

$$\mathcal{Z} = \sum_n \langle n|\mathcal{U}(-i\beta\hbar)|n\rangle \tag{1.71}$$

we observe that the partition function is just the sum of imaginary time transition amplitudes for the case where the system begins and returns to the same state $|n\rangle$ after an imaginary time $-i\beta\hbar$. We are thus led to one of the fundamental conclusions of quantum statistical mechanics:

Calculating the thermodynamics of a quantum system is equivalent to computing transition amplitudes for its evolution over an imaginary time interval set by the measurement temperature.

In the path integral formulation, the net transition amplitude between any two states of the system can be found by summing the individual amplitudes over all possible space-time trajectories which connect them. The key point is that although it is not possible to calculate the individual amplitudes over the full imaginary time interval, for an infinitesimal time interval they may be calculated in perturbation theory to any desired accuracy. We imagine breaking up the full time interval into M steps and can write

$$\begin{aligned}\mathcal{U}(-i\beta\hbar) &= \mathrm{e}^{-\beta\mathcal{H}} \\ &= \left(\mathrm{e}^{-\Delta\tau\mathcal{H}/\hbar}\right)^M \\ &= \left[\mathcal{U}(-i\Delta\tau)\right]^M \end{aligned} \tag{1.72}$$

where $\Delta\tau$ is taken to be a microscopic real time interval such that $\Delta\tau = \hbar\beta/M$ corresponding to the imaginary time interval $-i\Delta\tau$ with M a large integer. We proceed by inserting M complete sets of of intermediate states into our expression for the partition function Eq. (1.71)

$$\begin{aligned}\mathcal{Z} &= \sum_n \sum_{m_1} \langle n|\mathcal{U}(-i\Delta\tau)|m_1\rangle \left[\prod_{i=1}^{M-1} \sum_{m_{i+1}} \langle m_i|\mathcal{U}(-i\Delta\tau)|m_{i+1}\rangle\right] \langle m_M|\mathcal{U}(-i\Delta\tau)|n\rangle \\ &= \sum_{n,m_1,\ldots,m_M} \langle n|\mathrm{e}^{-\Delta\tau\mathcal{H}/\hbar}|m_1\rangle\langle m_1|\mathrm{e}^{-\Delta\tau\mathcal{H}/\hbar}|m_2\rangle \times \cdots \times \langle m_M|\mathrm{e}^{-\Delta\tau\mathcal{H}/\hbar}|n\rangle. \end{aligned} \tag{1.73}$$

This complicated looking expression has a rather straightforward physical interpretation, that of a classical partition function written as a sum over transfer matrices provided we think of our imaginary time direction as another spatial dimension. Thus, for a d dimensional quantum system at finite temperature, the expression in Eq. (1.73) appears to be a partition function for a *classical* system in $d+1$ dimensions, where the $+1^{th}$ dimension is not of infinite extent. This can be seen even more clearly if we take the limit $M \to \infty$ of $\mathcal{Z}$, $(\Delta\tau \to 0)$, then the sum over states can be converted into a functional integral in the usual way

$$\mathcal{Z} = \int \mathcal{D}\phi_a \, \mathrm{e}^{-\mathcal{S}[\phi_a]/\hbar} \tag{1.74}$$

and for the simple GLW theory presented above, the static free energy functional $\mathcal{F}$ can be promoted to the action

$$\mathcal{S}[\phi_a] = \int_0^{\hbar\beta} d\tau \int d^d x \left\{ \frac{1}{2}\left[[\partial_\tau \phi_a(\boldsymbol{x},\tau)]^2 + c|\boldsymbol{\nabla}\phi_a(\boldsymbol{x},\tau)|^2 + r\phi_a^2(\boldsymbol{x},\tau)\right] + \frac{u}{4!}[\phi_a^2(\boldsymbol{x},\tau)]^2 \right\} \tag{1.75}$$

where c is a velocity, r and u are coupling constants and the field $\phi_a(\boldsymbol{x}, \tau)$ is periodic in imaginary time τ with period $\hbar\beta$. We point out that in principle, one must distinguish the *bare* value of r which appears in the action with critical value r_c, and the renormalized or physical value which we will also sometimes call r which measures the true distance from the critical point. From this expression, the $d+1$ classical analogy is readily apparent. Furthermore, if $T \to 0$, then the upper bound on the time integral extends to infinity and we are left with a truly $d+1$ dimensional effective classical system.

The action $\mathcal{S}[\phi_\alpha]$ defines a continuum quantum field theory (CQFT) which, by altering the value of r at $T = 0$ can be tuned through a quantum phase transition between two phases, one with $\langle\phi_a\rangle = 0$ and the other with $\langle\phi_a\rangle \neq 0$. It turns out that every second order quantum phase transition will have such a description, with the interesting feature of it being defined on a somewhat peculiar slab geometry that is of infinite extent in d spatial dimensions, but has a finite "length" in the imaginary time direction given by

$$L_\tau = \hbar\beta = \frac{\hbar}{k_{\rm B}T}. \tag{1.76}$$

The quantum field theory shares many similarities to ordinary quantum mechanics with a unitary time evolution operator defined in a continuum limit, except that for the case of the field $\phi_a(\boldsymbol{x}, \tau)$, we have an infinite number of degrees of freedom per unit volume. The utility of such a description is that the concepts of universality introduced for the classical case carry over here. Only the essential qualitative features of the microscopic Hamiltonian, like the order parameter symmetry or dimension of space survive the continuum limit.

Our analysis of classical phase transitions completely relied on the existence of a single length scale ξ which diverged as the transition was approached according to $\xi \sim |r - r_c|^{-\nu}$ where $\nu = 1/2$ in the mean field or Gaussian theory. In the presence of a dynamic order parameter, causality requires the introduction of a diverging time scale, the correlation time ξ_τ. This follows directly from the observation that the time it takes to propagate information across a distance equal to the correlation length should increase as we approach the critical point. In $\mathcal{S}[\phi_a]$, space and imaginary time entered the action in the same way (the space and time derivative were raised to the same power), but this will not always be the case, and in fact, it will not be true for the superconductor-metal quantum phase transition considered in this thesis. Thus, we allow for an asymptotic relationship between space and time

$$\xi_\tau \sim \xi^z \tag{1.77}$$

which defines the *dynamic critical exponent* z. As mentioned, $z = 1$ for the CQFT in Eq. (1.75) but $z = 2$ for the SMT that will be described by Eq. (2.1).

Before addressing the specific details of quantum phase transitions at both zero and finite temperatures, we close this section by reiterating the statement of the quantum-classical mapping [48]:

> *The imaginary time correlations of a d dimensional quantum system at temperature T are related to the correlations of a d+1 dimensional classical system with a finite extent, $L_\tau = \hbar/k_\mathrm{B}T$ in one dimension.*

Or, in the language of statistical mechanics:

> *One can always reinterpret the imaginary time functional integral of a d dimensional quantum field theory as the finite temperature Gibbs ensemble of a $d+1$ dimensional classical field theory.*

The presence of a diverging time scale (Eq. (1.77)) implies that the frequency associated with critical fluctuations ω_c vanishes at the transition and a quantum system will behave classically provided that $\hbar\omega \ll k_\mathrm{B}T$; the critical fluctuations are classical. One is inevitably lead to the conclusion that the asymptotic critical behavior of any phase transition which occurs at a strictly non-zero value of temperature will be entirely classical.

1.5.4 Quantum critical phenomena

The power of the quantum-classical mapping is substantial, and based on the concluding sentence of the last chapter one might even wonder whether quantum mechanics plays any role whatsoever. The answers to this question ranges from subtle: the very existence of an order parameter may depend on quantum mechanics, to complex: analytic continuation of results to real time may be an ill posed problem, to banal: the corresponding $d+1$ dimensional classical models are either unphysical or have not been previously studied.

If we move sufficiently close to the critical point at finite temperature, quantum fluctuations must become important at the microscopic scale, but they will still not contribute at the large distances that dominate critical behavior. It is thus only exactly at $T = 0$, directly at the quantum phase transition, that the critical fluctuations must be treated quantum mechanically.

The quantum critical point ($T = 0$)

At zero temperature, the quantum phase transition occurs at the point where the characteristic energy scale of fluctuations above the ground state disappear as $r \to r_c$. If Δ is used to represent the energy of these fluctuations away from criticality then they vanish as

$$\Delta \sim |r - r_c|^{z\nu}. \tag{1.78}$$

The presence of a finite gap indicates that any autocorrelation function should decay exponentially to zero at long times. To see this, consider the Heisenberg representation of an operator $\mathcal{O}$ in imaginary time

$$\mathcal{O}(\tau) = \mathrm{e}^{\mathcal{H}\tau/\hbar}\mathcal{O}\mathrm{e}^{-\mathcal{H}\tau/\hbar}. \tag{1.79}$$

Its autocorrelation function is given by

$$\begin{aligned} G_{\mathcal{O}}(\tau) &= \langle 0|\mathcal{O}(\tau)\mathcal{O}(0)|0\rangle \\ &= \sum_n \mathrm{e}^{-(\epsilon_n-\epsilon_0)\tau/\hbar}\,|\langle 0|\mathcal{O}|n\rangle|^2 \end{aligned} \tag{1.80}$$

where we have inserted a complete set of states in the second line with $\mathcal{H}|n\rangle = \epsilon_n|n\rangle$. As $\tau \to \infty$, only the $n = 1$ term with $\Delta = \epsilon_1 - \epsilon_0$ contributes significantly to the sum and we have

$$\begin{aligned} G_{\mathcal{O}}(\tau) &\sim \mathrm{e}^{-\Delta\,\tau/\hbar} \\ &\sim \mathrm{e}^{-\tau/\xi_\tau} \end{aligned} \tag{1.81}$$

where we have used Eq. (1.78) and $\Delta\,\tau$ is the product of the gap Δ and the imaginary time τ, not be confused with the small time interval used previously. The autocorrelation function is thus an exponentially decaying function of imaginary time, with a characteristic time scale equal to the inverse energy gap; this confirms our assertion that all critical systems are gapless.

Away from the critical point, but with $|r - r_c| \ll 1$, we have argued that there must be only two large, but not yet infinite length scales that determine the critical behavior. In analogy with our homogeneity relation for the free energy density in Eq. (1.66) an operator $\mathcal{O}$ representing a general physical observable should obey the dynamic scaling form

$$\mathcal{O}(\boldsymbol{k}, \omega, r) = \xi^{\dim[\mathcal{O}]}\Phi_{\mathcal{O}}\left(k\xi, \omega\xi_\tau\right) \tag{1.82}$$

where $k \equiv |\boldsymbol{k}|$, $\dim[\mathcal{O}]$ is the scaling dimension of the operator $\mathcal{O}$ and $\Phi_{\mathcal{O}}$ is a scaling function. The scaling dimension of a given quantity defines how it behaves under the renormalization group transformation. It is simply the power to which the dimensionless length rescaling factor b introduced earlier must raised in order to obtain the proper scaling transformation. We point out that the tuning parameter r does not explicitly appear on the right hand side of Eq. (1.82) except through the dependence of the correlation length and the correlation time on the distance from the critical point.

Directly at the critical point when $r = 0$, both $\xi \to \infty$ and $\xi_\tau \to \infty$ and thus the scaling form in Eq. (1.82) is no longer meaningful. At the scale invariant critical point, the only possible length scale corresponds to the inverse wavevector at which the system is being probed, which immediately sets the characteristic frequency at $\omega \sim k^z$. Our scaling form can now be written in a simplified form

$$\mathcal{O}(k, \omega, 0) = k^{-\dim[\mathcal{O}]}\widetilde{\Phi}_{\mathcal{O}}\left(\frac{\omega}{ck^z}\right) \tag{1.83}$$

where c is a constant with engineering dimensions that depend on the value of z but scaling dimension 0.

At a classical phase transition driven by thermal fluctuations a unique ground state is selected in the ordered phase as $T \to 0$. At a quantum phase transition, fluctuations are driven by the Heisenberg uncertainty principle and persist at all length and time scales even at zero temperature. These fluctuations have a single characteristic frequency, given by k^z and thus all collective modes have become overdamped and the system is in a incoherent diffusive regime.

The proceeding discussion has focused on the properties of the zero temperature quantum critical point. Any real experiment has access to only finite temperatures, and in order to move beyond the purely theoretical, and strive towards the practical, we must extend the theory to $T > 0$. In this region of the phase diagram there will be a fascinating and complex reciprocity between quantum and thermal fluctuations. In forming an understanding of their contributions to critical phenomena, the quantum-classical mapping will once again come to our aid.

1.5.5 Finite temperature crossovers

We have already learned that turning on a finite temperature has the effect of placing our $d+1$ dimensional quantum field theory on a slab which is infinite in the d spatial dimensions but of finite length

$$L_\tau = \frac{\hbar}{k_{\rm B} T} \tag{1.84}$$

in the imaginary time direction. The leading order effects of temperature can therefore be deduced by appealing to the well established ideas of finite size scaling [55]. Before delving into the details, it is useful to think broadly about the two possible outcomes that may result from introducing any finite boundary conditions into our previously infinite system.

(i) The transition can be completely destroyed, with only the $T = 0$ quantum phase transition remaining. This is the case for an array of one dimensional Josephson junctions which have a continuous quantum degree of freedom equal to the phase of the superconducting order parameter. The quantum-classical mapping tells us that at finite temperature, this theory maps onto an effective classical O(2) model on an infinite strip of width $c\hbar\beta$ where c is a velocity. This system is clearly below its lower critical dimension and no ordered phase exists at $T > 0$.

(ii) The transition persists at $T > 0$, but changes to a different universality class. The quantum O(2) model in two dimensions has an effective classical theory at $T = 0$ corresponding to a three dimensional XY model. At finite temperatures the system is marginal and the transition is of the Kosterlitz-Thouless type mentioned previously.

The effects of temperature appear to be rather drastic, they either destroy the transition, or completely change its universality class. It turns out that if we are close enough to the quantum phase transition, the crossover physics is completely controlled by the quantum critical point itself. This is akin to saying that we can continuously tune the system away from criticality not by changing some parameter, but by smoothly reducing its dimensionality. If such a process can be done continually, then there must be a temperature scale at which for a given value of the tuning parameter r, the correlation time ξ_τ approaches L_τ and the system realizes for the first time that it is not at zero temperature and must therefore *crossover* to finite temperature behavior. Suppose we are at low temperatures and far from the critical point in the quantum disordered phase. The characteristic frequencies will obey $\hbar\omega \gg k_{\rm B}T$ and the system is quantum mechanical in nature. On the other hand, suppose $|r - r_c| \ll 1$ but the temperature is large, the correlation length will also be sizeable and $\xi_\tau = \xi^z$, therefore $\hbar\omega \ll k_{\rm B}T$ and the critical behavior is effectively classical. The phenomena of quantum-classical crossover is schematically shown in Fig. 1.10. The existence of the crossover frequency $k_{\rm B}T/\hbar$ leads to a physical crossover thermal length scale $L_\tau^{1/z}$, which spatial fluctuations associated with quantum fluctuations cannot exceed. Using the quantitative theory of finite size scaling, and again appealing to our previous homogeneity relations we arrive at the finite temperature generalization of the scaling relation in Eq. (1.82)

$$\mathcal{O}(\boldsymbol{k}, \omega, r, T) = \left(\frac{\hbar}{k_{\rm B}T}\right)^{\dim[\mathcal{O}]/z} \Phi\left(\frac{\hbar k^z}{k_{\rm B}T}, \frac{\hbar\omega}{k_{\rm B}T}, \frac{\hbar|r - r_c|^{\nu z}}{k_{\rm B}T}\right), \tag{1.85}$$

where we have written the arguments of the scaling function in terms of T and $|r-r_c|$, parameters equivalent to ξ and L_τ. The most important feature of this expression is that temperature alone sets the length scale one must measure the wavevector against, the time scale to measure the frequency against and the relative distance from the critical point. Directly at the critical coupling $r = r_c$, there is only *one* energy scale equal to $k_{\rm B}T$.

The singular quantity of import is the ratio of the finite size in the time direction to the $T = 0$ temporal correlation length in that dimension. At zero temperature, the quantum critical point is gapless and we have quantum fluctuations at all energies and length scales. Moving to finite temperature introduces a new dominant energy scale to the problem and modes with $\omega > k_{\rm B}T/\hbar$ will be unaffected, while those with $\omega < k_{\rm B}T/\hbar$ will become occupied with many quanta leading to classical behavior. In other words, the existence of a finite temperature scale cuts off coherent quantum fluctuations in the infrared.

The presence of such coherence effects leads to the natural introduction of a dephasing time, τ_ϕ which has no classical analog and is the time scale over which the many-body wavefunction retains the memory of its phase. Any local measurement with an inverse frequency longer than τ_ϕ will display quantum interference effects.

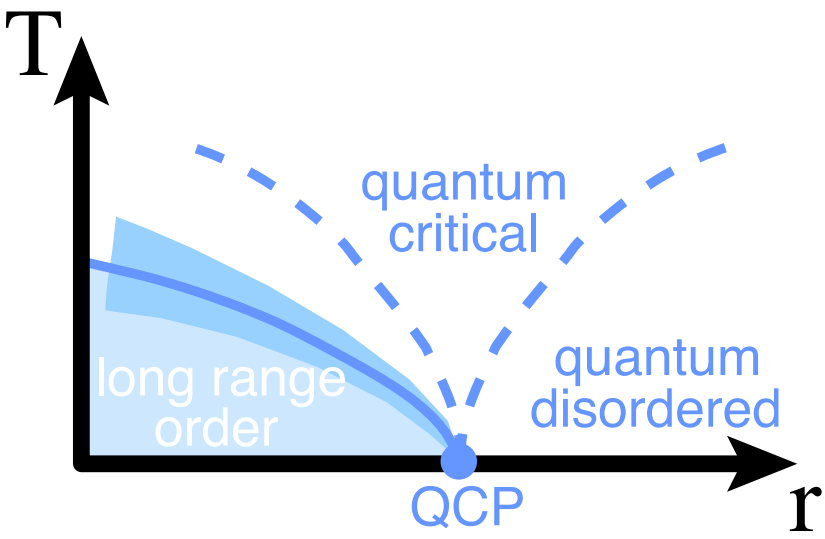

Figure 1.10: A schematic phase diagram corresponding to case (ii) in the text where a phase transition persists at $T > 0$. At zero temperature, a long range ordered state (lighter shaded region) is separated from a quantum disordered state by a quantum critical point (QCP) where the energy gap vanishes and all length and time scales diverge. The solid line at finite temperature corresponds to a continuous phase transition driven by thermal fluctuations with the darker shaded region indicating the portion of the phase diagram where the theory of classical critical behavior can be applied. The dashed lines are finite temperature crossovers, below which the temperature is smaller than the excitation gap and the system must be studied quantum mechanically. Above the dashed lines in the quantum critical regime, the correlation time is much longer than the time scale set by the temperature $\hbar T$ and the system is effectively classical.

The goal of the study of quantum phase transitions is to understand not only the zero temperature quantum critical behavior but also the effects it has on finite temperature dynamical quantities, usually response functions, that can be probed by experimentalists. The response functions can include spectral densities from angle resolved photoemission spectroscopy (ARPES) experiments, inelastic neutron scattering (NS) cross sections or relaxation rates measured with nuclear magnetic resonance (NMR) or muon spin rotation (μSR) techniques. The continuum quantum field theories introduced in this chapter are defined in imaginary time, and in order to obtain access to measurable quantities, they need to be analytically continued to real time. As mentioned previously, this can be a highly non-trivial process and any approximations made in imaginary time will usually lead to unreliable and even completely unphysical results in real time. The operation of expanding in some control parameter and analytical continuation do not in general commute and the problem becomes worse as the time scale of interest increases. Long time scales are associated with the

small probe frequencies we are most interested in, and thus in the finite temperature low frequency regime, we cannot appeal to the quantum-classical mapping and use existing analytical results from the theory of classical critical phenomena to provide any useful insights into dynamical processes.

Another problem that we will run into in the next section is the fundamental difference between the role of disorder in quantum and classical systems. Quenched disorder will in general have short range spatial correlations. However, in a quantum system, the frozen nature of any randomness means that it has infinite range correlations in imaginary time. Upon performing the quantum-classical mapping, the disorder profile of the resulting $d+1$ dimensional classical system will be highly irregular and an entirely new type of physics can sometimes emerge, that of infinite randomness and activated scaling.

In condensed matter physics, we will often be concerned with d dimensional CQFTs whose corresponding effective classical theory in $d+1$ spatial dimensions is close to the upper critical dimension. These strongly fluctuating theories are relevant to many systems of interest including the high temperature superconductors and low dimensional nanomaterials. Their study can lead to the calculation of various universal numbers which fully characterize their long wavelength and low frequency critical behavior which can be measured in real experiments.

1.6 Disordered critical phenomena

The real world is dirty, and pure systems without disorder rarely exist outside of idealized and sanguine theories. Disorder can appear in various forms in condensed matter including point defects, like vacancies or impurity atoms in crystals, or more extended forms such as dislocations or grain boundaries. In Section 1.5 the important concepts of continuous phase transitions and universality were introduced and this is a natural point to ponder the question of how quenched (or frozen in) disorder might change our conclusions. If a clean system exhibits a phase transition, three questions naturally arise upon the inclusion of disorder.

(i) Will the phase transition remain sharp, or will it be smeared out as different regions of the sample order independently?

(ii) If there is a sharp phase transition, will the critical behavior change quantitatively causing the universality class to be altered, or even qualitatively where the wonted power-law scaling of observables may no longer apply.

(iii) Can disorder have far reaching effects away from the phase transition that drastically alter the ordered and disordered phase?

In the absence of translational invariance, there are almost no exact solutions and few analytical approaches that can address these questions. The study of disordered

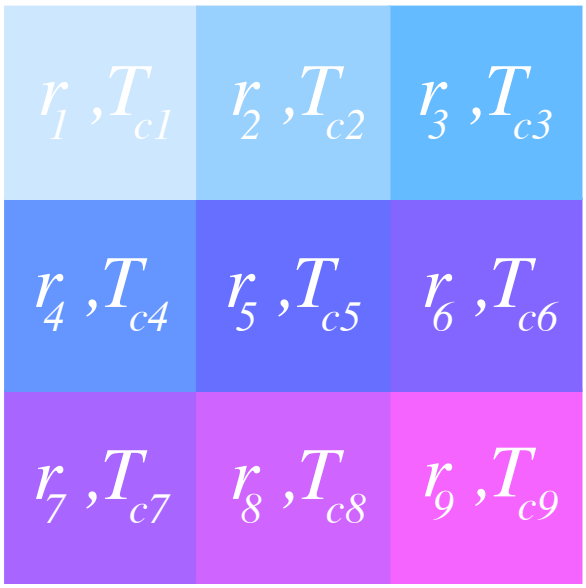

Figure 1.11: The simple random-T_c model which assumes that the predominant effects of disorder break the system up into a number of independent regions with their own *local* value of coupling constants and the critical temperature.

systems is a massive field and there are many excellent introductory reviews of the methods and results that are currently understood; two very approachable sources are Refs. [56] and [57]. In this thesis we provide a somewhat brief introduction to this deep and fascinating subject, beginning with a simple rule for the existence of a phase transition, then moving on to a study of spin glasses and the replica trick. Finally we conclude with a discussion of the effects of rare regions and strong disorder.

1.6.1 The Harris criterion

Let us consider the simplest case of impurities or defects leading to spatial variations in some coupling strength $r = r_0(T - T_c)$ without any modification of the bulk phases connected by the transition; the tendency towards the ordered phase is now a function of position. This case, shown schematically in Fig. 1.11 and sometimes referred to as the random-T_c or random-mass model, was used by Harris [58] to derive a remarkably simple and astonishingly sweeping result. He used this picture to construct a test for the perturbative stability of a clean critical point against the introduction of weak disorder. If disorder leads to the fragmentation of the system into blocks of volume ξ^d with effective critical temperature T_{ci} found by averaging $r + \delta r(x)$ within block i (Fig. 1.11), where r is the positive and renormalized distance from criticality, then a sharp phase transition can only occur if the standard deviation Δr of the local critical temperatures from block to block is smaller than the global

distance from the critical point r. For disorder with short range correlations (the blocks only interact at their boundaries) the central limit theory yields $\Delta r \sim \xi^{-d/2}$ and assuming that $\xi \sim r^{-\nu}$ we have

$$\Delta r \sim r^{d\nu/2}. \tag{1.86}$$

Thus for a transition to occur we must satisfy the *Harris criterion*: $\Delta r < r$ or

$$d\nu > 2. \tag{1.87}$$

This criterion can be used to classify critical points based on the behavior of the average disorder strength as the length scale under consideration is increased.

(i) The Harris criterion $d\nu > 2$ is satisfied and the strength of disorder decreases under coarse graining with the system becoming asymptotically homogeneous at long length scales. An example of this case, where all macroscopic variables are self-averaging is the three dimensional classical Heisenberg model with $\nu = 0.698$ [59].

(ii) Under renormalization, the relative disorder strength increases to some finite value and the system remains inhomogeneous. The critical point still exhibits conventional scaling behavior but the critical exponents are modified such that their new values satisfy the Harris criterion. The width of the probability distribution for observables is no longer zero and they are consequently not self averaging. The three dimensional Ising model belongs to this case where $\nu = 0.627$ [60] in the clean system and shifts to $\nu = 0.684$ [61] in the presence of disorder.

(iii) Finally, the relative magnitude of the randomness continues to increase without limit upon coarse graining with a fixed point characterized by an infinite disorder strength. At this fixed point, the scaling is qualitatively modified taking on a highly asymmetric exponential form and all probability distributions become extremely broad, diverging with system size. Physical observables are no longer self-averaging but have averages dominated by rare events. Manifestations of such behavior occur in the McCoy-Wu model (Fig.1.12) [62, 63] and the quantum random transverse field Ising model [64, 65].

Not surprisingly, most early work on disordered systems focused on cases (i) or (ii) where the average effects of disorder fluctuations on large length scales are small. Before returning to the very interesting case (iii), let us first briefly mention for completeness one of the most important weak disorder approaches which is suitable even when the ordered phase is of a fundamentally different structure than its clean counterpart.

1.6.2 Spin Glasses

A pedagogical review of classical disordered systems can be found in Refs. [66, 67], but it will be convenient to introduce some of their physical properties in terms of a particular model consisting of Ising spins coupled randomly to all other spins; the Sherrington-Kirkpatrick (SK) model [68]. It is described by the Hamiltonian

$$\mathcal{H} = -\frac{1}{2}\sum_{i,j} J_{ij}\sigma_i\sigma_j \tag{1.88}$$

where the exchange constants are randomly distributed according to

$$P(J_{ij}) = \frac{1}{\sqrt{2\pi J^2}}\exp\left(\frac{J_{ij}^2}{2J^2}\right) \tag{1.89}$$

and it is the spread in the signs of the interaction parameters J_{ij} that provides frustration and can lead to *glassy* behavior. It is assumed that the variance of the coupling distribution is not too large and such systems are referred to as "spin glasses". The presence of disorder leads to an extraordinarily rough free energy landscape with many nearly degenerate minima separated by large barriers, and one can imagine three possible scenarios.

(i) The energy barriers separating the different minima are finite. The system can thus explore its phase space and will be paramagnetic ($\langle\sigma_i\rangle = 0$) although with possibly slow dynamics.

(ii) A certain state could have a much lower free energy than all other states, and at low enough temperatures the system would freeze into this state. However, due to the presence of disorder, $\langle\sigma_i\rangle$ will still fluctuate from site-to-site and the total magnetization

$$m = \frac{1}{N}\sum_i \sigma_i \tag{1.90}$$

will be identically zero.

(iii) At low temperatures there exists a large number of states in which the system could be frozen into, separated by infinite energy barriers in the thermodynamic limit.

Focusing on the third case, below some critical temperature, T_c, a phase transition of ergodicity breaking takes place and the energy landscape is divided into many valleys separated by large (possibly infinite) energy barriers. At $T = T_c - \delta T$, each valley will be characterized by a non-zero value of $\langle\sigma_i\rangle_{(\alpha)}$ at each site where $\langle\cdots\rangle_{(\alpha)}$ refers to a thermal average limited to valley α. In the presence of broken ergodicity, only such

restricted expectation values make sense and the order parameter which characterizes freezing in each valley is

$$q = \frac{1}{N}\left[\sum_i \langle\sigma_i\rangle_{(\alpha)}\right]^2 \tag{1.91}$$

where q is independent of the valley in the thermodynamic limit ($N \to \infty$) and goes to zero as $T \to T_c$ from below. The key point is that any further decrease in the temperature leads to new ergodicity breaking phase transitions; each valley breaks into smaller ones, separated by infinite energy barriers. This is a continuous process below T_c and within each infinite minimum, there may still be many finite valleys so the spectrum of energy barriers goes smoothly to infinity. This hierarchical structure of minima is known as the ultrametricity of the spin glass state [69].

In Eq. (1.88), each spin can interact with every other spin and there is no concept of space or a lattice; the SK model effectively lives in infinite dimensions. It is this mean field or maximally coupled behavior that allows for a solution and it can be studied using a clever way of rewriting the partition function known as the *replica trick*. For suitably weak disorder and at large length scales the free energy should be a self-averaging quantity, and we are thus only interested in the logarithm of the partition function averaged over disorder. We exploit a crafty way of writing the natural logarithm,

$$\ln \mathcal{Z} = \lim_{n\to 0} \frac{\mathcal{Z}^n - 1}{n} \tag{1.92}$$

and say that we have *replicated* the partition function n times, and $\mathcal{Z}^n$ can now be straightforwardly averaged over the distribution of disorder, with translational invariance reappearing at the expense of generating additional interactions between replicas. The replica method and replica field theory has formed the basis for a large amount of the work done on random systems. Without serious consideration, it might appear that the expectation values of physical observables should not depend on a replica index, this is known as the replica symmetric solution . However, this solution often leads to unphysical results (such as negative entropy) and we are ineluctably lead to consider more and more complicated methods of breaking replica symmetry. The physical origin of replica symmetry breaking may lay hidden in the limit $n \to 0$ required by Eq. (1.92) which does not necessarily commute with the thermodynamic limit of infinite system size formally required for the existence of a phase transition. In addition, within replica field theory, many approaches are perturbative, and rely on the presence of only weak disorder. It is now becoming increasingly clear that for even moderately strong randomness, an important role is played by rare but large disorder fluctuations and the atypical spatial regions where they occur.

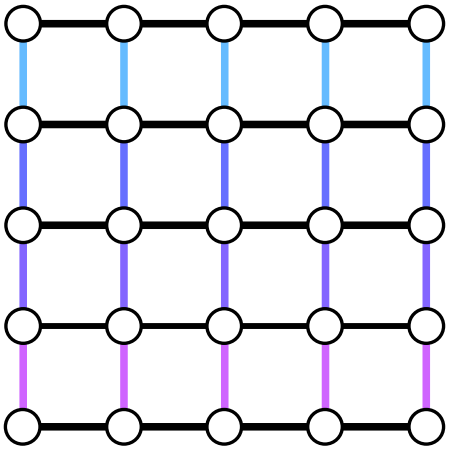

Figure 1.12: The McCoy-Wu model [62, 63] where each circle represents an Ising spin and although all horizontal bonds are equal, the vertical bonds are different in each row.

1.6.3 Rare region effects

The appearance of rare regions contributing to thermodynamic behavior was first noticed in the McCoy-Wu model [62, 63], a two dimensional Ising model with long range disorder correlations in one dimension pictured schematically in Fig. 1.12. The physics can be more easily understood in a diluted classical Ising ferromagnet, as depicted in Fig. 1.13. In the presence of dilution, the critical temperature T_{c0} of the clean system, is reduced to T_c but in an infinitely large system there will always exist arbitrarily large portions of the sample with volume V_{RR} without any impurities (as seen in the highlighted portion of Fig. 1.13) with probability

$$P(V_{\mathrm{RR}}) \sim \mathrm{e}^{-pV_{\mathrm{RR}}} \tag{1.93}$$

where p is the impurity concentration. For all temperatures $T_c < T < T_{c0}$, these areas will exhibit local magnetic order even though the bulk is paramagnetic. Griffiths showed that these *rare regions* (RR) can lead to a singularity in the free energy, over an entire region of parameter space close to the transition now known as the *Griffiths phase* [70]. The type of singularity depends strongly on various details and in classical systems with short range disorder, the singularity is only essential leading to very weak thermodynamic Griffiths effects. Inside the Griffiths phase, the long time dynamics is completely dominated by rare regions leading to a spin-spin autocorrelation function which decays as a power-law in time for the diluted ferromagnet considered here.

At a quantum phase transition, the rare regions become infinitely extended in the imaginary time direction (Fig. 1.14) precipitating even more sluggish fluctuations. The slow dynamics of rare regions can have a considerable effect, and in the presence of completely static order, can even lead to the complete destruction of the phase

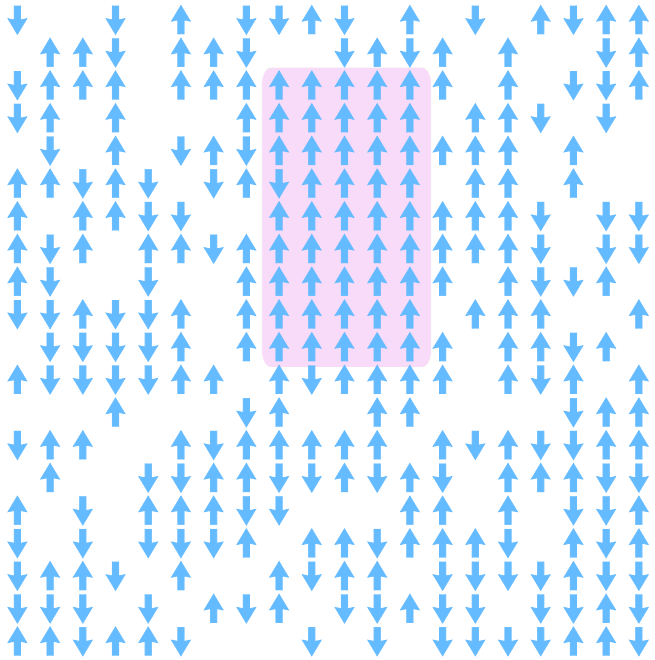

Figure 1.13: A diluted ferromagnet in the paramagnetic phase where the highlighted area shows a region in the sample devoid of impurities which is strongly ordered and can lead to a singularity in the free energy.

transition. The importance of RR physics in a given system depends on the relationship between the contribution of a single region to macroscopic observables and its size. We can characterize this behavior by considering a single isolated rare region with linear size L_{RR} that is locally in the ordered phase, that is, the local average bare coupling r defined along the lines of the random-mass model (Fig. 1.11) is negative. There are three distinct possibilities depending on the effective dimensionality, d_{RR} of the rare region, where d_{RR} is the sum of both the temporal and spatial dimensions of the droplet.

(i) If $d_{\mathrm{RR}} < d_{\mathrm{LCD}}$, where d_{LCD} is the lower critical dimension, the rare region cannot order independently of the rest of the system and its local coupling will be renormalized to a positive value $\widetilde{r} > 0$. The leading contributions to all thermodynamic variables are controlled by at most a power of $\widetilde{r}$ which cannot overcome the exponential scarcity of a RR. An example is found in any classical systems with point defects where $d_{\mathrm{RR}} = 0$; the rare regions are finite in dimension, and all their effects are subleading at the critical point.

(ii) If $d_{\mathrm{RR}} = d_{\mathrm{LCD}}$, the rare region cannot undergo a phase transition by itself, and although the renormalized coupling $\widetilde{r}$ is positive, it decreases exponentially quickly to zero with the volume of the region. The contribution to observables

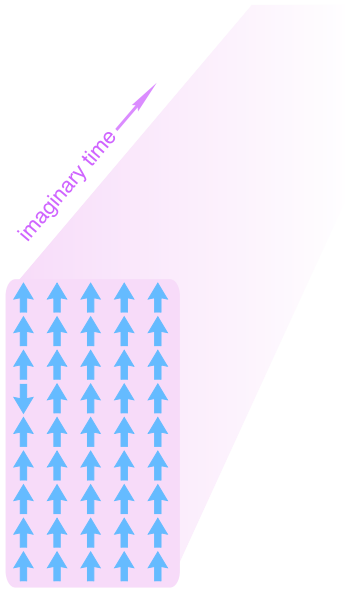

Figure 1.14: The strongly ordered rare region from Fig. 1.13 extended a "length" $L_\tau = \hbar\beta$ in imaginary time, $L_\tau \to \infty$ at the quantum phase transition.

thus increases exponentially with size, exactly compensating for their exponentially suppressed probability in Eq. (1.93). The result is that the critical point is dominated by rare regions, leading to exotic non-power law activated scaling. Examples include the McCoy-Wu model shown in Fig. 1.12 where the defects are extended linear objects and $d_{\rm RR} = 1$, the lower critical dimension of the Ising model. The same is true for the quantum random transverse field Ising model which has rare regions with spatial dimension zero, but temporal dimension one at zero temperature.

(iii) If $d_{\rm RR} > d_{\rm LCD}$, the rare region can autonomously order, the renormalized coupling is negative and all dynamics freeze out as a static order parameter develops. The global phase transition is destroyed by smearing due to different parts of the system ordering at different values of $\widetilde{r}$. Classical three dimensional Ising models with planar defects exhibit such behavior as $d_{\rm RR} = 2$ and $d_{\rm LCD} = 1$ [71, 72] as well as one dimensional quantum Ising models with suitably strong damping [73, 74].

Very little analytical progress was made towards understanding the quantitative effects of rare regions until D.S. Fisher's [64, 65] ingenious solution of the quantum random transverse field model using the strong disorder renormalization group procedure of Ma, Dasgupta and Hu [75]. The details of his derivation are beyond the scope of this introductory chapter and are saved until Section 5.1.

We have argued that disorder can have profound implications for critical phenom-

ena ranging from small quantitative changes arbitrarily close to criticality, all the way to causing exotic non-power law activated dynamic scaling or the complete destruction of the phase transition. This section has attempted to provide an overview of this phenomenology with special focus on the effects of rare regions characterized by the relationship between their size and the lower critical dimension. The connection will be revisited in Chapter 5 when we find compelling evidence for an infinite randomness fixed point and activated scaling at the superconductor-metal quantum phase transition.

1.7 Organization

This rest of this thesis is composed of four chapters providing details on methods and results and a final concluding chapter.

We begin by introducing a particular continuum quantum field theory for the superconductor-metal quantum phase transition in nanowires in terms of a Cooper pair order parameter and discuss a number of its general properties through a scaling analysis. The relationship between its coupling constants and microscopic quantities is discussed with specific details provided on their values in the clean and dirty limit. In the approximation where the number of components of the order parameter is large, we perform a detailed study of the electrical and thermal transport properties of ultra-narrow wires throughout the phase diagram. We next discuss a systematic expansion that can be performed for a finite number of order parameter components and find fluctuation corrections to various results near criticality. Finally we introduce quenched disorder into our theory and find evidence for infinite randomness and activated scaling. We conclude with some general observations on the diverse types of physics on display at the superconductor-metal transition and discuss some promising avenues for future research.

Chapter 2

Dissipative Theory of the Superconductor-Metal Transition

This chapter will focus on a possible model for the quantum phase transition between a superconductor and a metal (a SMT). The physical system of interest, as studied in numerous recent experiments [35, 45, 38, 76, 77, 44, 78, 39, 37] and introduced in Chapter 1, is a quasi-one dimensional nanowire, of length L with a large number of transverse conduction channels, $N_\perp$. This guarantees that surface effects will not be particularly destructive, and that the electronic localization length $\xi_{\rm loc}$, given by $\xi_{\rm loc} = N_\perp \ell$ is much larger than the mean free path ℓ.

From the Cooper instability in BCS theory we know that the existence of a non-trivial quantum critical point in a metal implies a finite electron interaction strength. Naively the existence of interactions would seem to preclude the possibility of any quantum phase transition between a superconductor and a metal because the ordered phase will exist at all strictly non-zero temperatures for arbitrarily weak paring (see Eq. (1.21)). Moreover, if the temperature is driven to zero in a pure BCS superconductor pair fluctuations will be completely eliminated [79]. The solution arrives in the form of pair-breaking interactions, or any perturbation that is odd under time reversal, which act differently on the spin and momentum reversed constituents of a Cooper pair. The presence of these interactions effectively cuts of the logarithmic singularity in the pair susceptibility and sets a critical value for the strength of the pair potential before superconductivity can develop. Therefore, our proposed SMT must live in the pair-breaking universality class.

As discussed in the introduction, the mean-field theory for the SMT goes back to the early work [41] of Abrikosov and Gor'kov (AG). In one of the preliminary discussions of a quantum phase transition, they showed that a large enough concentration of magnetic impurities could induce a SMT at $T = 0$. It has since been shown that such a theory applies in a large variety of situations with *pair-breaking* perturbations: anisotropic superconductors with non-magnetic impurities [80, 81, 82], lower-dimensional superconductors with magnetic fields oriented in a direction parallel to

the Cooper pair motion [83, 84], and s-wave superconductors with inhomogeneity in the strength of the attractive BCS interaction [43]. Indeed, it is expected that pair-breaking is present in any experimentally realizable SMT at $T = 0$. In the nanowire experiments, explicit evidence for pair-breaking magnetic moments on the wire surface was presented recently by Rogachev *et al.* [37] and in Section 1.4.2 we described an avenue by which they could lead to the destruction of superconductivity as the radius of the wire is reduced.

Fluctuations about the AG theory have been considered [85, 86, 87, 83, 84] in the metallic state, and lead to the well-known Aslamazov-Larkin (AL), Maki-Thompson (MT) and Density of States (DoS) corrections to the conductivity. The form of these corrections is usually introduced in terms of the structure of their diagrammatic representation within the finite temperature disordered electron perturbation theory but they all have the same physical origin: in the presence of strong pair-breaking, the normal metal still experiences pairing fluctuations near the Fermi surface as a result of its proximity to the superconducting state. Specifically, the AL effect comes from the direct charge transfer from fluctuating Cooper pairs, the MT correction results from coherent Andreev scattering off the fluctuating pairs and the Density of States (DoS) correction is due to the reduction of the normal electron density of states near the Fermi surface accounting for the paired electrons [88]. At the SMT, field-theoretic analyses [89, 90] show that the AG theory, along with the AL, MT and DoS corrections, is inadequate in spatial dimension $d \leq 2$, and additional repulsive self-interactions among Cooper pairs have to be included. Here, d defines the dimensionality of the Cooper pair motion. The confining dimension, or radius of the wire, R, is larger than the inverse Fermi wavevector, but smaller than the superconducting coherence length or Cooper pair size, ξ. This is the exact condition discussed in the introduction for the quasi-one dimensional limit. While the Cooper pairs are effectively one dimensional, any unpaired electrons have a three dimensional Fermi surface and thus strictly 1d Luttinger liquid physics do not apply.

In the remaining chapters of this thesis, we will examine the $d = 1$ SMT for both a clean and disordered wire in great detail. We will find that the transition is described by a strongly-coupled field theory of bosonic Cooper pairs, overdamped by their coupling to the fermionic quasiparticles (normal electrons).

As our goal is to understand the aforementioned experiments on ultra-thin metallic wires and we are interested in the fluctuation corrections to the thermal and electrical conductivity across the SMT as well as the nature of the crossovers from this universal quantum critical physics to previously studied regimes at low T about the superconducting and metallic phases. To frame the discussion in the duration of this chapter, the full crossover phase diagram is summarized in Fig. 2.1. The important features of the global pair-breaking phase diagram are as follows. On the metallic side of the transition, there is a crossover to a low T regime described by the theory [83] of AL+MT+DoS corrections in $d = 1$ (dashed line in Fig. 2.1). On the superconducting side, there is a regime of intermediate temperatures where the classical phase slip

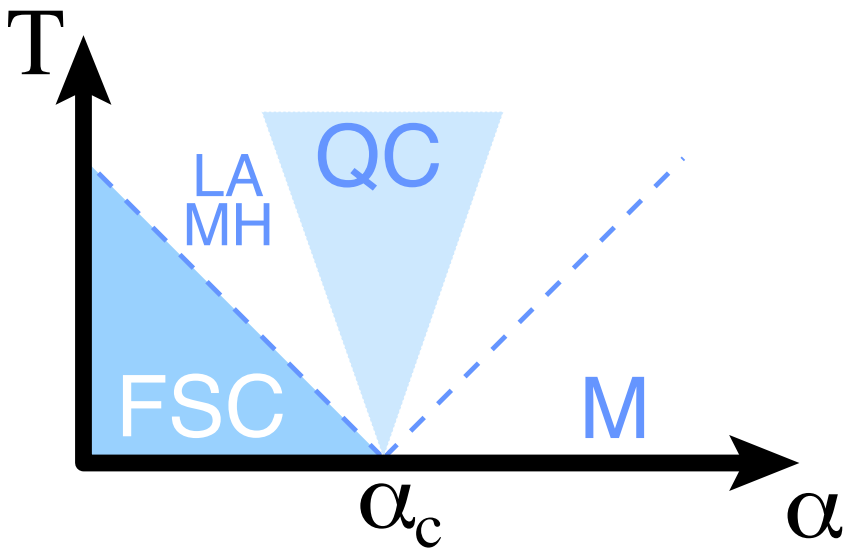

Figure 2.1: Crossover phase diagram of the superconductor-metal transition in a quasi-one dimensional superconductor. The *metal* (M) is described by the perturbative theory of Ref. [83]. The *quantum critical* (QC) region is described by our effective theory $\mathcal{S}_\alpha$ for temperatures above $T_{\rm dis}$ where the effects of disorder may be neglected. The Mooij-Schön mode is present everywhere, but couples strongly to superconducting fluctuations only in the *fluctuating superconductor* (FSC) regime, where it is described by Eq. (2.31); note that $\mathcal{S}_\alpha$ does *not* apply here. The dashed lines are crossover boundaries which occur at $T \sim |\alpha - \alpha_c|$ (from Eq. (2.11)) and the intermediate LAMH region should be described by the theory of thermally activated phase slips discussed in Chapter 1 with the possible modifications of Chapter 3.

theory of Langer, Ambegaokar, McCumber, and Halperin (LAMH) applies [19, 20], and eventually another crossover at still lower temperatures to a phase fluctuating regime whose description requires a non-linear σ-model of fermion pair fluctuations coupled to the superconducting order [91]. Intermediate between these regimes is the quantum criticality we describe here, in which phase and amplitude fluctuations must be treated on equal footing.

In the rest of this chapter, we present details of the dissipative theory which will be used as the starting point for all computations in this thesis. After a brief scaling analysis, the role of particle-hole symmetry and the Mooij-Schön [92] mode is discussed, as well as the relationship between the model parameters and the microscopic BCS theory. Finally, the effects of the Cooper pair self-interactions on universality throughout the quantum critical regime and the role of disorder are highlighted.

2.1 Dissipative model

The approach to the SMT taken here is akin to previously studied theories [93, 94, 95] of disordered superconducting films with unconventional pairing symmetry. Such films are assumed to be composed of a network of small Josephson coupled superconducting islands. The transition between the normal and superconducting state can be tuned by altering the distance between the grains; if the separation becomes large enough, quantum fluctuations can destroy superconducting order even at zero temperature. Physically, the transition occurs when the Josephson coupling becomes less than the Coulomb energy due to the transfer of a single Cooper pair between islands. These arguments can be made more rigorous by starting from microscopic BCS theory and deriving an effective model for the fluctuations of the Cooper pair order parameter. The order parameter is strongly overdamped by decay into quasiparticle excitations manifest as an interaction that is long range in imaginary time [80, 79, 83, 84, 43].

These ideas can be directly applied to the $d = 1$ quantum superconductor-metal transition in the pair-breaking universality class which is relevant for ultra-narrow quasi one-dimensional metallic wires. The physical ingredients include repulsive paired states and a lack of charge conservation of the condensate requiring the existence of a semi-infinite bath (the large number of transverse conduction channels) into which the former member electrons of a disassociated Cooper pair can flow into upon breaking. The final description will be in terms of a strongly-coupled field theory of bosonic Cooper pairs, overdamped by their coupling to the normal unpaired fermionic states of the metal.

It turns out that the fluctuation corrections to transport associated with the AL correction discussed above are naturally captured in this picture. These have [83, 84] a Cooper pair propagator $(\widetilde{D}k^2 + |\omega_n| + \alpha)^{-1}$ at wavevector k and imaginary bosonic Matsubara frequency $i\omega_n$ in the metal in both the clean and dirty limits. Here, the "mass" or pair-breaking frequency α measures the strength of the pair-breaking interaction which could come from a variety of sources as mentioned in the introduction. $\widetilde{D}$ is equal to the usual diffusion constant $\widetilde{D} = D = v_{\rm F}\ell/3$ ($v_{\rm F}$ is the Fermi velocity) in the dirty limit where the mean free path is much smaller than the superconducting coherence length ($\ell \ll \xi_0$). In the clean limit, where $\ell \gg \xi_0$, $\widetilde{D}$ will be in general some non-universal number that depends on the specific microscopic details (such as the lattice constant) of the system in question. This motivates the quantum critical theory of Ref. [89, 96] for a field $\Psi(x, \tau)$ which represents the local

Cooper pair operator

$$\begin{aligned}\mathcal{S}_\alpha = &\int_0^L dx \int_0^{1/T} d\tau \left[\widetilde{D}|\partial_x \Psi(x,\tau)|^2 + \alpha|\Psi(x,\tau)|^2 + \frac{u}{2}|\Psi(x,\tau)|^4\right] \\ &+ \; T\sum_{\omega_n}\int_0^L dx\, \gamma|\omega_n||\Psi(x,\omega_n)|^2,\end{aligned} \tag{2.1}$$

where we have used the temporal Fourier transform of $\Psi(x,\tau)$

$$\Psi(x,\omega_n) = \int_0^{1/T} dt \Psi(x,\tau) \mathrm{e}^{i\omega_n \tau}. \tag{2.2}$$

with $\omega_n = 2\pi n T$ to more compactly express the non-locality of the dissipative term in imaginary time and we will work in units where $\hbar = k_\mathrm{B} = 1$ for convenience. From this point forward, we will suppress the limits of integration for the sake of compactness unless their inclusion is required for clarity. The quartic coupling u must be positive to ensure stability, and describes the repulsion between Cooper pairs. The pairs are strongly overdamped, and the rate of their decay into the metallic bath is characterized by the coupling constant multiplying the $|\omega_n|$ term, γ, which is required to be positive by causality. It will be convenient to rescale the field Ψ such that the coefficient of the Landau damping term is equal to unity. In addition, we rescale all couplings according to

$$\Psi \to \frac{\Psi}{\sqrt{\gamma}}; \quad \widetilde{D} \to \gamma \widetilde{D}; \quad \alpha \to \gamma\alpha; \quad u \to \gamma^2 u. \tag{2.3}$$

This theory describes the vicinity of a superconductor-metal quantum critical point, corresponding to the (bare) value $z = 2$ for the dynamic critical exponent. A different description ($z \neq 2$) cannot be completely ruled out, but it would most likely require additional tuning parameters as well as the inclusion of unusual pairing phenomena like gapless superconductivity [79].

The transition is driven by altering the strength of the pair-breaking frequency α as was shown schematically in Fig. 2.1. As α is reduced, the quantum critical point, α_c is defined as the special value where the Cooper pair operator first acquires a non-zero expectation value, $\langle\Psi(x,\tau)\rangle_{\mathcal{S}_\alpha} \neq 0$. For $\alpha > \alpha_c$ there is normal metallic conduction, while for $\alpha < \alpha_c$ both thermal and quantum phase slips, included under the guise of amplitude fluctuations of Ψ destroy the superflow.

The field theory in Eq. (2.1) is identical in form to the Hertz-Millis-Moriya theory [47, 97, 98] describing the Fermi liquid to spin-density wave (SDW) transition, with the Cooper pair operator Ψ replaced by an $O(3)$ order parameter representing diffusive

paramagnons. In the neighborhood of this transition, k measures the magnitude of the deviation from the SDW ordering wave vector $\boldsymbol{K}$ and the dissipative $|\omega_n|$ term arises from the damping of order parameter fluctuations resulting from coupling to gapless fermionic excitations of the metal near points on the Fermi surface connected by $\boldsymbol{K}$. A more careful analysis leads to the realization that at $T = 0$ on the ordered (SDW) side of the transition, a gap appears in the fermion spectrum for small k. Thus, this description is only fully accurate at $T = 0$ on the disordered (metallic) side of the transition or at finite temperature in the quantum critical regime above the SDW state. The same logic applies to the role of phase fluctuations at low temperatures in the superconducting phase near the SMT. We will return to this point later with a thorough discussion of the Mooij-Schön normal mode, but for now we begin with a detailed scaling analysis of $\mathcal{S}_\alpha$.

2.2 Scaling analysis

Let us rewrite the rescaled version of Eq. (2.1) via Eq. (2.3) in d dimensions

$$\begin{aligned}\mathcal{S}_\alpha = &\int d^dx \int d\tau \left[\widetilde{D}|\partial_x \Psi(x,\tau)|^2 + \alpha|\Psi(x,\tau)|^2 + \frac{u}{2}|\Psi(x,\tau)|^4\right] \\ &+ \; T\sum_{\omega_n}\int d^dx\, |\omega_n||\Psi(x,\omega_n)|^2.\end{aligned} \tag{2.4}$$

The anisotropic relationship between space and time allows us to identify the dynamical critical exponent $z = 2$ implying that $\dim[\omega_n] = \dim[T] = z$ so simple power counting leads to

$$\dim[\Psi] = \frac{d}{2} \tag{2.5a}$$

$$\dim[\alpha] = 2 \tag{2.5b}$$

$$\dim[u] = 2 - d \tag{2.5c}$$

where $\dim[\cdots]$ is the scaling dimension introduced in Section 1.5.4. From the scaling dimension for u we can immediately identify the lower critical dimension of the SMT as $d = 2$. By definition, for $d > 2$ the quartic coupling is irrelevant, and all physical properties could be computed perturbatively in the (small) value of u, resulting in u-dependent non-universal results. $d = 2$ is marginal, and for the case considered here, $d = 1$, u is a relevant perturbation, and we will need to employ alternate methods. However, in the strong coupling regime ($u \to \infty$) we can expect results to be universal.

Pankov *et al.* [99] studied a theory similar to $\mathcal{S}_\alpha$ with Ψ replaced by an $O(N)$ field ϕ_a via the renormalization group (RG) in an $\epsilon = 2 - d$ expansion in one and two dimensions at zero temperature. The most important result obtained from their

RG analysis is that the damping term, $|\omega_n|$, generated from the long-range $1/\tau^2$ interaction between order parameter fluctuations does not require an independent renormalization, and thus the frequency dependence of the propagator only involves wavefunction renormalization. At $T = 0$ and $\alpha = \alpha_c$ in one dimension, they find a non-trivial fixed point and an analysis of the RG equations leads to an expression for the dynamical susceptibility at small frequencies and momenta

$$\begin{aligned}\chi(k,\omega) &= \int d\tau \int dx \langle \phi_a(x,\tau)\phi_a(0,0)\rangle \mathrm{e}^{-i(kx-\omega\tau)} \\ &= k^{-2+\eta}\widetilde{\Phi}_\chi\left(\frac{\omega}{ck^{2-\eta}}\right)\end{aligned} \tag{2.6}$$

where $\widetilde{\Phi}_\chi$ is a universal scaling function. This is simply Eq. (1.83) with the scaling dimension of the susceptibility $\dim[\chi] = 2 - \eta$. The constant c turns out to be universal

$$c = \frac{(N+2)[6\pi^2 \ln 2 - 11\zeta(3)]}{1728} \tag{2.7}$$

with $\zeta(x)$ the Riemann zeta function and N the number of real order parameter components.

These results carry through to the study of our effective action, Eq. (2.4) with the only modification being that c changes to a non-universal number due to the presence of $\widetilde{D}$. From Eq. (2.6) and Eq. (1.83), the modified dynamical critical exponent can be read off as

$$z = 2 - \eta \tag{2.8}$$

where η is the anomalous dimension; a result which holds to all orders due to the existence of only wavefunction renormalization [99, 100]. This scaling form can be generalized to finite temperatures (see Eq. (1.85) with $r = r_c$ and $\hbar = k_\mathrm{B} = 1$) where we expect

$$\chi(k,\omega_n,T) = \frac{1}{T}\Phi_\chi\left(\frac{\omega_n}{T}, \frac{c_1 k}{T^{1/z}}\right), \tag{2.9}$$

with Φ_χ another universal scaling function and c_1 a non-universal constant. Most interestingly, at $k = 0$ and $\omega = 0$ the value of the inverse susceptibility in the quantum critical region will be fixed by temperature alone,

$$\chi^{-1}(0,0) = \mathcal{C}_1 T \tag{2.10}$$

and the highly non-trivial universal constant $\mathcal{C}_1$ will be computed in a $1/N$ expansion in chapter 4.

Scaling functions for the most singular parts of the dc electrical σ and thermal κ conductivities can also be derived with a knowledge of their scaling dimensions alone. We know that in one dimension, the conductivity is equal to e^2/h times a length, and for $k = \omega_n = 0$ but finite temperature we have only one length scale available to

us, the *thermal length*, $L_\tau^{1/z}$. Similar considerations for the thermal conductivity in conjunction with Eq. (1.85) allow us to write

$$\sigma = \frac{e^2}{\hbar}\left(\frac{k_B T}{\hbar \widetilde{D}}\right)^{-1/z} \Phi_\sigma\left(\frac{[\hbar(\alpha-\alpha_c)]^\nu}{(k_B T)^{1/z}}\right) \tag{2.11}$$

and

$$\kappa = \frac{k_B^2 T}{\hbar}\left(\frac{k_B T}{\hbar \widetilde{D}}\right)^{-1/z} \Phi_\kappa\left(\frac{[\hbar(\alpha-\alpha_c)]^\nu}{(k_B T)^{1/z}}\right) \tag{2.12}$$

where $z = 2$ and $\nu = 1/2$ in the Gaussian limit and we have returned to real physical engineering units. If we include interactions but perform calculations in the large-N limit, z is unchanged, but $\nu = 1$ and one would need to replace

$$\frac{[\hbar(\alpha-\alpha_c)]^\nu}{(k_B T)^{1/z}} \to \frac{\hbar(\alpha-\alpha_c)}{(k_B T)^{2/z\nu}} \tag{2.13}$$

in the scaling functions. Upon comparing Eq. (2.11) with the microscopic result for the conductivity calculated within perturbation theory [83, 84] and reproduced in Eq. (3.4) we see that the the most divergent contribution at $T > 0$ but for $|\alpha - \alpha_c| \ll 1$, corresponding to the AL correction of the direct contribution of Cooper pairs to the metallic conductivity is included in our critical theory.

This section has unequivocally demonstrated the power and utility of scaling and universality, allowing us to derive scaling forms for the finite temperature dynamic order parameter susceptibility as well as the electrical and thermal conductivity with almost no effort in terms of the critical exponents ν, η and z. We now provide some previously determined analytical and numerical results for their values.

The anomalous dimension η and correlation exponent ν defined by $\xi \sim |\alpha - \alpha_c|^{-\nu}$, can be computed in the $\epsilon = 2 - d$ expansion [99, 89] and are found to be

$$\eta = \frac{(N+2)(12-\pi^2)}{4(N+8)^2}\epsilon^2 + O(\epsilon^3) \tag{2.14}$$

$$\nu = \frac{1}{2} + \frac{(N+2)}{4(N+8)}\epsilon + \frac{(N+2)[6N^2 + (228-7\pi^2)N + 792 - 38\pi^2]}{48(N+8)^3}\epsilon^2 + O(\epsilon^3). \tag{2.15}$$

These results are in agreement with Monte Carlo simulations [101] which found $z = 1.97(3)$, $z + \eta = 1.985(20)$ and $\nu = 0.689(6)$. The exponents ν and η can also be computed in the $1/N$ expansion and the results are detailed in chapter 4.

The main results of this section, and the analysis of Ref. [99] is that $\mathcal{S}_\alpha$ satisfies conventional hyperscaling relations at the $T = 0$ SMT in the absence of disorder. This implies that we can neglect any irrelevant operators, and transport should be

fully described by Eq. (2.4). Moreover, the most singular part of the dc conductivity of a given wire will be described by Eq. (2.11) which is independent of its length L. The is a consequence of the dominant physics in the quantum critical regime being controlled by low energy superconducting fluctuations with a characteristic length scale equal to the extent of the wire [89] itself.

2.3 Particle-hole asymmetry

In the scaling analysis of the previous section, we neglected an important detail; for $z = 2$, when the energy dependence of the electronic density of states near the Fermi level is included, a propagating term in the action can arise from the weak particle-hole asymmetry of the electronic spectrum

$$\mathcal{S}_\eta = \int dx \int d\tau \eta \, \Psi^*(x,\tau) \frac{\partial}{\partial \tau} \Psi(x,\tau). \tag{2.16}$$

The magnitude of particle-hole symmetry breaking, η is proportional to the energy derivative of the density of states at the Fermi energy, and we therefore expect its bare value to be small. This is supported by the fact that our quasi-one dimensional treatment of Cooper pairs coupled to a bath composed of three dimensional electrons, required the ratio of the pairing to Fermi energy to be small. In fact, a microscopic weak coupling derivation of Eq.(2.4) for a dirty two dimensional superconductor with d-Wave pairing symmetry [80] finds that the ratio of the dissipative to propagative terms is proportional to the dimensionless conductivity of the normal phase, $\eta \propto 1/\epsilon_{\rm F}\tau$ where τ is the scattering time in the self-consistent Born approximation. For a good metal, the product of the scattering time and Fermi energy is large, and thus $\eta \ll 1$. This is consistent with results at finite temperature for a weak-coupling short coherence length superconductor [102].

At tree level, η is marginal, and as just argued, we expect its bare value to be small. However, we can examine the renormalization group fate of $\mathcal{S}_\eta$ near the fixed point of $\mathcal{S}_\alpha$. The scaling dimension of η can be computed in a $d = 2 - \epsilon$ expansion for a massless ($\alpha = 0$) quantum critical theory through the conventional method of isolating any logarithmic singularities (or $1/\epsilon$ poles) in the Feynman diagrams corresponding to all possible insertions of the perturbing term, $i\eta\omega$. For the case considered here, there are two unique graphs

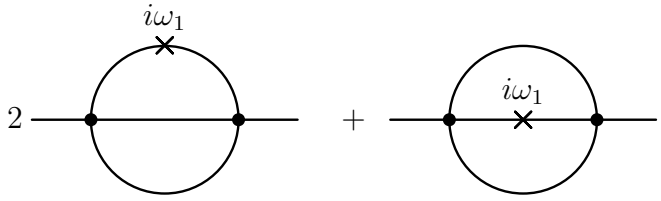

(2.17)

where a solid line is equal to the bare propagator $(k^2+|\omega|)^{-1}$, a dot represents the quartic interaction u and a cross is an insertion coming from Eq. (2.16).

If the external lines have frequency Ω and zero momentum, then the combination of these graphs leads to the integral

$$I(\Omega) = -i2\eta u^2 \int \frac{d\omega_1}{2\pi} \int \frac{d\omega_2}{2\pi} \int \frac{d^dk}{(2\pi)^d} \int \frac{d^dq}{(2\pi)^d} \times \frac{\omega_1}{(k^2+|\omega_1|)^2(q^2+|\omega_2|)[(k+q)^2+|\omega_1+\omega_2+\Omega|]}. \tag{2.18}$$

A simple power counting analysis of the integrand in $d = 2-\epsilon$ dimensions leads to the appearance of the predicted pole

$$I(\Omega) = i\Omega\eta \frac{A}{2\epsilon}, \tag{2.19}$$

where as usual, the flow equation for η is related to the residue A via

$$\frac{d\eta}{d\ell} = A\eta. \tag{2.20}$$

Doing the two momentum integrals by employing Feynman parameters we find

$$I(\Omega) = -i2\eta u^2 \frac{\Gamma(4-d)}{(4\pi)^d} \int_0^1 dx \int_0^1 dy \int \frac{d\omega_1}{2\pi} \int \frac{d\omega_2}{2\pi} \frac{(1-y)y^{1-d/2}}{[1-y(x^2-x+1)]^{d/2}} \times \frac{\omega_1}{[(1-y)|\omega_1| + y(1-x)|\omega_2| + xy|\omega_1+\omega_2+\Omega|]^{4-d}}. \tag{2.21}$$

where $\Gamma(x)$ is the gamma function. The double frequency integral, can be done by determining the sign of the various absolute values in the relevant seven regions of the $\omega_1 - \omega_2$ plane, leading to the following useful but complicated looking result

$$\begin{aligned} I_\omega(A,B,C,\sigma) &= \int \frac{d\omega_1}{2\pi} \int \frac{d\omega_2}{2\pi} \frac{\omega_1}{(A|\omega_1| + B|\omega_2| + C|\omega_1+\omega_2+\Omega|)^\sigma} \\ &= -\frac{ABC\Gamma(\sigma-3)\Omega^{3-\sigma}}{\pi^2\Gamma(\sigma)} \left\{ A^{3-\sigma} \left[\frac{2(2A^2-B^2-C^2)}{(A^2-B^2)^2(A^2-C^2)^2} \right.\right. \\ &\quad \left. - \frac{3-\sigma}{A^2(A^2-C^2)(A^2-B^2)} \right] - B^{3-\sigma} \left[\frac{2}{(B^2-C^2)(A^2-B^2)^2} \right] \\ &\quad \left. + C^{3-\sigma} \left[\frac{2}{(B^2-C^2)(A^2-C^2)^2} \right] \right\}. \end{aligned} \tag{2.22}$$

In $d = 2-\epsilon$ and $\sigma = 2+\epsilon$, I_ω has a pole at $\epsilon = 0$ with a residue that can be read off from

$$I_\omega(A,B,C,2+\epsilon) = -\frac{\Omega}{\pi^2} \left[\frac{BC(2A+B+C)}{(A+B)^2(A+C)^2(B+C)} \right] \frac{1}{\epsilon} + O(1). \tag{2.23}$$

Using Eq. (2.23) in Eq. (2.21) we find

$$I(\Omega) = \frac{i\Omega u^2}{8\pi^4\epsilon}\int_0^1 dx \int_0^1 dy \frac{xy(1-x)(1-y)(2-y)}{[1-y(x^2-x+1)][1-y+xy^2(1-x)]^2}$$
$$= \frac{i\Omega u^2\eta}{8\pi^4\epsilon}\left(\frac{\pi^2}{4}-2\right) \tag{2.24}$$

and comparing with Eq. (2.20) we can read off the flow equation

$$\frac{d\eta}{d\ell} = \frac{u^2}{16\pi^2}\left(1-\frac{8}{\pi^2}\right)\eta. \tag{2.25}$$

The fixed point value of u is given in Ref. [99] for the equivalent $z = 2$ $O(N)$ model with the change of notation $u_0 = 3u$. Equivalently it can be easily computed to one loop order as

$$u^* = \frac{2\pi^2}{5}\epsilon \tag{2.26}$$

leading to

$$\frac{d\eta}{d\ell} = \frac{\epsilon^2}{100}(\pi^2-8)\eta \tag{2.27}$$

or $\eta(\ell) \sim \mathrm{e}^{0.02\epsilon^2\ell}$ at RG scale ℓ. Thus we conclude that although η is relevant, its scaling dimension is extremely small. In conjunction with a bare value that we have argued should be small, we will neglect $\mathcal{S}_\eta$ in future calculations.

There is still one piece missing in our analysis of $\mathcal{S}_\alpha$ as alluded to in the previous section; the role of charge conservation (which $\mathcal{S}_\alpha$ breaks) and the associated normal modes.

2.4 Phase fluctuations

Models similar to Eq. (2.1), but lacking amplitude fluctuations (so called phase-only theories) have been previously applied to the physical situation considered here [32, 103, 104, 105, 106]. In these continuum theories, the destruction of superconductivity is due to the proliferation of quantum phase slips resulting in a normal phase which we maintain is *insulating* and not metallic at $T = 0$. Such theories may describe a quantum superconductor-insulator transition (SIT) which could be appropriate in short inhomogeneous wires. The superfluid's conductivity will be controlled by irrelevant phase-slip operators since the resulting $d = 1$ SIT in this description lives in the Kosterlitz-Thouless universality class [107].

From hydrodynamic arguments, we know that a one-dimensional metal or superconductor should support a gapless plasmon, or a Mooij-Schön normal mode [92], which disperses as $\omega \sim k\ln^{1/2}(1/(kR))$. Our discussion of this issue parallels that in

Refs. [108, 109] on the role of conservation laws in the critical fluctuations of quantum transitions in metallic systems for which the order parameter is overdamped (as is the case here). We couple Ψ to a fluctuating scalar potential A_τ with bare action

$$\mathcal{S}_A = \int \frac{dk}{2\pi} \int \frac{d\omega}{2\pi} \frac{|A_\tau(k,\omega)|^2}{4\ln(1/(kR))}. \tag{2.28}$$

However, the nature of the A_τ-Ψ coupling differs between the "quantum critical" and "fluctuating superconductor" regimes of Fig. 2.1. For the main results of this study, we need only the coupling in the quantum critical region, where the physics of the plasmon mode is unchanged from that in the "Metal" region of Fig. 2.1. After integrating out the fermions, we obtain the A_τ action

$$\mathcal{S}_\Pi = \int \frac{dk}{2\pi} \int \frac{d\omega}{2\pi} \frac{1}{2} \Pi(k,\omega) |A_\tau(k,\omega)|^2, \tag{2.29}$$

where Π is the irreducible density correlation function (the "polarizability") of the metal. For $\omega \gg k$, we have $\Pi(k,\omega) \sim k^2/\omega^2$, and then $\mathcal{S}_A + \mathcal{S}_\Pi$ has a pole at the plasmon frequency noted above. We also observe that the coupling between these A_τ fluctuations and Ψ is negligible: a slowly varying A_τ is a shift in the local chemical potential, and to the extent we can ignore the variation in the electronic density of states at these energy scales, the effective couplings in $\mathcal{S}_\alpha$ do not change with A_τ, and there is no $A_\tau - \Psi$ coupling. The existence of an $A_\tau - \Psi$ coupling non-analytic in frequency has been discussed by Ioffe and Millis [108]. However, they show by Ward identities, which also apply here, that these couplings do not contribute to the physical charge correlations. So, in the quantum critical region, $\mathcal{S}_\alpha$ and $\mathcal{S}_A + \mathcal{S}_\Pi$ are independent theories describing the pairing and charge fluctuations respectively.

As described in the previous section, the coupling constant which measures particle-hole asymmetry is formally, albeit weakly relevant (see Eq. (2.27)) and thus a small $A_\tau - \Psi$ coupling appears by making the τ-derivative in Eq. (2.16) Gauge covariant

$$\mathcal{S}_\eta = \int dx d\tau \left[\eta \, \Psi^* \left(\frac{\partial}{\partial \tau} - 2ei A_\tau \right) \Psi \right]. \tag{2.30}$$

However, the combination of the small scaling dimension and the small bare value of η implies that such particle-hole asymmetric effects, and the consequent coupling between pairing and charge fluctuations, can justifiably be ignored in theories hoping to describe realistic experiments.

We conclude by addressing the physics in the "Fluctuating superconductor" regime of Fig. 2.1 for $\alpha < \alpha_c$. Now coupling between the pairing and charge fluctuations is much stronger. When $T < (\alpha_c - \alpha)$ the action $\mathcal{S}_\alpha$ does *not* apply for the smallest frequencies. The reasons for this are again analogous to arguments made for the spin-density-wave ordering transition in metals, as discussed in Section 2.1 and Ref. [48].

For the latter case, it was argued that with the emergence of long-range spin density wave order, the low energy fermionic particle-hole excitations at the ordering wavevector were gapped out, and so the diffusive paramagnon action applied only for energies larger than this gap. At energies smaller than the gap, spin-waves with dispersion $\omega \sim k$ emerge. In the superconducting case, there is no true long-range order at any $T > 0$, but the order is disrupted primarily by 'renormalized classical' thermal fluctuations of the phase, ϕ of the complex Ψ field. We assume that there is a local pairing amplitude in the fermion spectrum, analogous to the spin-density wave order. The low energy effective action for ϕ obtained by integrating the fermions in the presence of a local pairing, is

$$\mathcal{S}_\phi = \int dx d\tau \left[K_1 (\partial_\tau \phi - 2eA_\tau)^2 + K_2 (\partial_x \phi)^2 \right] \tag{2.31}$$

where $K_{1,2}$ vanish as power of $(\alpha_c - \alpha)$ [109]. The strongly coupled pairing and charge fluctuations in the "Fluctuating superconductor" regime of Fig. 2.1 are described by $\mathcal{S}_A + \mathcal{S}_\phi$, and this theory contains the Mooij-Schön mode, which is the analog of the 'spin-wave' mode. We do *not* claim that $\mathcal{S}_A + \mathcal{S}_\phi$ can extended across quantum criticality into the normal phase, in contrast to other works [32] which consider vortex unbinding in such a theory.

The arguments presented in this section strive to justify the use of $\mathcal{S}_\alpha$ throughout the quantum critical regime, and we now make a slight aside to discuss the relationship between the parameters of the theory, α, γ, u and $\widetilde{D}$ to those of the microscopic BCS theory.

2.5 Connection to microscopic BCS theory

In order to motivate the experimental relevance of the effective action $\mathcal{S}_\alpha$, we would like to determine the microscopic values of the pair-breaking frequency α, the bare diffusion constant $\widetilde{D}$, dissipation strength γ and quartic coupling u in both the clean and dirty limits. We begin with the connection of the pair-breaking frequency to various experimentally relevant geometries, then move on to the relationship between our theory and a time dependent Ginzburg-Landau (TDGL) theory for a conventional superconductor.

2.5.1 Pair-breaking in quasi-one dimensional wires

As mentioned in the Section 1.4, one can consider pair-breaking perturbations coming from a variety of sources. The most theoretically appealing consists of magnetic impurities localized on the surface of a metallic wire leading to an inhomogeneous BCS coupling (Fig. 1.7). In this case, the microscopic value of α is not known exactly, but it can be related to the inverse of the spin-flip scatting time. However,

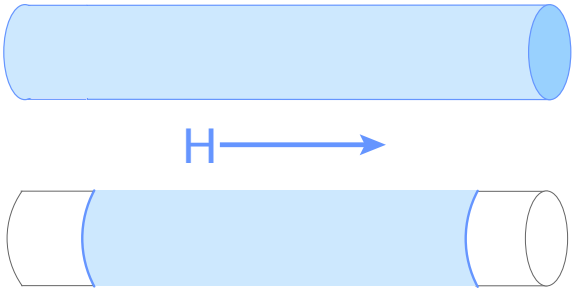

Figure 2.2: Two possible geometries discussed in the introduction, consisting of a metallic nanowire or a cylinder (formed by coating an insulating core) with a diameter on the order of the zero temperature BCS coherence length in a longitudinal magnetic field.

there are a number of well-defined experimental geometries where one can compute the actual value of α in terms of the physical properties of the system. Two such cases which are of interest here were previously introduced, along with some experimental manifestations. These include a narrow metallic wire or multiply connected metallic cylinder in a parallel magnetic field, schematically shown in Fig. 2.2.

In the dirty limit, Shah and Lopatin [84] have computed the precise form of α through the use of the Usadel equation formalism. They find that for a narrow diffusive wire with radius R smaller than both the superconducting coherence length and the magnetic penetration depth placed in a parallel magnetic field H,

$$\alpha_{\text{wire}} = \frac{D}{2}\left(\frac{eHR}{c}\right)^2 \tag{2.32}$$

where D is the diffusion constant and c the speed of light. Alternatively, for a multiply connected cylinder of inner radius R_1 and outer radius R_2 in a parallel magnetic field they find

$$\alpha_{\text{cyl}} = D\left\{\frac{eH}{4c}\left[\frac{eH}{c}(R_1^2+R_2^2)-4n\right]+n^2\frac{\ln(R_2/R_1)}{R_2^2-R_1^2}\right\}, \tag{2.33}$$

where n is the integer that minimizes the superfluid velocity for a given value the trapped flux. As mentioned in Chapter 1, the former geometry is relevant to the measurements of Rogachev *et al* on T_c suppression in MoGe nanowires [44] in a parallel magnetic field (Fig. 1.8), while the in-field phase diagram of ultra-thin Al and $Au_{0.7}In_{0.3}$ cylinders has been measured in Ref. [45] (Fig. 1.9).

2.5.2 Microscopic parameters in the clean and dirty limits

The microscopic values of $\widetilde{D}$,γ and u can be found through an analysis of the time dependent Ginzburg-Landau theory studied by Tucker and Halperin [110]. There, the

three dimensional equation of motion for the Cooper pair operator $\Psi(\boldsymbol{x},t)$ in real time is given by

$$\hbar\gamma\frac{\partial}{\partial t}\Psi(\boldsymbol{x},t) = -\left[a + b|\Psi(\boldsymbol{x},t)|^2 + \delta(-i\nabla)^2\right]\Psi(\boldsymbol{x},t). \tag{2.34}$$

Rescaling, to ensure that the coefficient of the time derivative term is unity (as we have done in Eq. (2.4), and performing an integral over the cross-sectional area of the wire to move to the quasi-one dimensional case of interest ($\Psi(x,y,z,t) \sim \Psi(x,t)$), we read off the value of the coupling constants to be

$$\widetilde{D} = \frac{\delta}{\hbar\gamma} \tag{2.35a}$$

$$u = \frac{b}{A\hbar^2\gamma^2} \tag{2.35b}$$

where A is the cross-sectional area of the wire. Appendix A of Ref. [110] gives the microscopic values of δ, b and γ as

$$\delta = \frac{\hbar^2}{2m}, \tag{2.36a}$$

$$b = \frac{\hbar^2}{2m\xi^2(0)}\frac{2}{N\chi(0.882\xi_0/l)}, \tag{2.36b}$$

$$\gamma = \frac{\pi\hbar^2}{16m\xi^2(0)k_BT_{c0}}. \tag{2.36c}$$

where $\xi(T)$ is the Ginzburg-Landau coherence length, ξ_0 the BCS coherence length, ℓ the mean free path and $\chi(\rho)$ the Gor'kov function defined by

$$\chi(\rho) = \sum_{n=0}^{\infty}\frac{1}{(2n+1)^2(2n+1+\rho)}\left[\sum_{n=0}^{\infty}\frac{1}{(2n+1)^3}\right]^{-1}. \tag{2.37}$$

The critical temperature and density of conduction electrons in the normal state are known to be

$$\frac{1}{k_BT_{c0}} = \frac{\xi_0}{0.18\hbar v_{\rm F}}; \tag{2.38a}$$

$$N = \frac{k_{\rm F}^3}{3\pi^2} \tag{2.38b}$$

respectively, while, the zero temperature coherence length and relevant Gor'kov function depend on whether we are in the clean or dirty limit

$$\xi(0) = \begin{cases} 0.74\xi_0 & ; \quad \xi_0 \ll \ell \\ 0.85\sqrt{\xi_0\ell} & ; \quad \xi_0 \gg \ell \end{cases}, \tag{2.39a}$$

$$\chi(0.882\xi_0/l) = \begin{cases} 1 & ; \quad \xi_0 \ll \ell \\ 1.33\ell/\xi_0 & ; \quad \xi_0 \gg \ell \end{cases}. \tag{2.39b}$$

We have now gathered all the required information to compute the actual microscopic values of our model parameters in the dirty ($\xi_0 \gg \ell$) and clean ($\xi_0 \ll \ell$) limits differentiated by the subscripts d for *dirty* and c for *clean*.

Dirty limit ($\xi_0 \gg \ell$)

Using the above relations, we find that for the dirty limit

$$\widetilde{D}_d = D = \frac{1}{3} v_{\mathrm{F}} \ell \tag{2.40a}$$

$$\gamma_d \simeq \frac{1.5}{k_{\mathrm{F}} \ell} \tag{2.40b}$$

$$u_d \simeq 2.9 \frac{v_F}{\hbar N_\perp} \tag{2.40c}$$

where the number of transverse conduction channels is assumed to be large, and is given by

$$N_\perp = \frac{2 k_{\mathrm{F}}^2 A}{3\pi}. \tag{2.41}$$

Clean limit ($\xi_0 \ll \ell$)

Similarly, in the clean limit

$$\widetilde{D}_c = \frac{1}{4} v_F \xi_0 \tag{2.42a}$$

$$\gamma_c \simeq \frac{2.0}{k_{\mathrm{F}} \xi_0} \tag{2.42b}$$

$$u_c = u_d \simeq 2.9 \frac{v_F}{\hbar N_\perp} \tag{2.42c}$$

where we note that the bare value of the quartic coupling is *identical* in both limits. The value of these parameters clearly depends on the particular normalization scheme chosen for the order parameter, but the final results for all physically measurable quantities, such as the conductivity, will obviously be normalization independent.

With these values computed, we may now discuss the role of Hartree corrections to our theory, that is, the temperature range where the quartic interaction u is strongly relevant and universal results may be expected.

2.6 Universality in the quantum critical regime

The microscopic theory of the superconductor-metal transition was considered in great detail by Shah and Lopatin [84] in a Gaussian theory of superconducting fluctuations that corresponds to the effective field theory presented here with u set

to zero. In Chapter 3 we will compare the transport properties computed from the effective action $\mathcal{S}_\alpha$ with Shah's results in the metallic regime where $\alpha \gg \alpha_c$ but armed with the microscopic values of our model parameters we can make a number of observations regarding the validity of the non-interacting theory in the strongly fluctuating quantum critical regime (which they refer to as the *classical regime*). The key point is their use of the mean-field temperature dependence of the superconductor-metal phase boundary $\alpha_c(T)$ computed from an expansion of Eq. (1.54) for $T \ll \alpha_c$ corresponding to the shaded "quantum critical" region of Fig. 2.1. They use rather unconventional notation to measure the deviation from criticality in terms of the finite temperature mean field phase boundary

$$\alpha_c(T) = \alpha_c - \frac{\pi\gamma k_{\rm B} T^2}{3\hbar T_{c0}}, \tag{2.43}$$

where $\gamma \approx 0.577$ is the Euler-Mascheroni constant and T_{c0} is the classical BCS transition temperature in the absence of pair-breaking. This somewhat strange notation (which we temporarily adopt) requires comment. The location of the quantum critical point is as usual defined as α_c at $T = 0$, but in Eq. (2.43) $\alpha_c(T)$ is the function which locates the value of the pair breaking frequency at which superconducting order is lost for a given temperature. It is the approximate functional inverse of the the solid line shown in Fig. 1.6 in the low temperature limit. To summarize, Shah and Lopatin are interested in large positive values of α (measured from the origin) far into the metallic phase and have chosen to define a coupling constant that measures the distance from classical criticality defined by the temperature dependent mean field phase boundary and *not* the distance from quantum criticality as we would normally do.

To successfully compare our two approaches we shift the definition of α accordingly and write

$$\begin{aligned}\mathcal{S}_\alpha = &\int dx \int d\tau \left[\widetilde{D} |\partial_x \Psi(x,\tau)|^2 + \frac{\pi\gamma k_{\rm B}}{3\hbar T_{c0}} T^2 |\Psi(x,\tau)|^2 + \frac{u}{2} |\Psi(x,\tau)|^4 \right] \\ &+ \frac{k_{\rm B} T}{\hbar} \sum_{\omega_n} \int dx \, |\omega_n| |\Psi(x,\omega_n)|^2,\end{aligned} \tag{2.44}$$

in this form, it is clear that the theory only goes critical at $T = 0$. We assume that $\widetilde{D}$ and u can take on the values computed in the previous section for the clean and dirty limits, but are primarily concerned with the role of the quartic coupling u, characterizing the strength of the Cooper pair self interaction. For $d = 1$, from Eq. (2.5c), this quantity has scaling dimension one and from Eq. (2.40c) it has engineering dimensions of inverse mass times inverse length or frequency squared times length over energy. We would like to identify the length scales or temperature ranges which define three distinct regions of the phase diagram near the critical coupling. These regions are defined by the conditions:

(I) The quartic coupling can be ignored and the Gaussian theory of Ref. [84] is correct.

(II) The quartic coupling is relevant, and Hartree corrections to the mass must be included leading to non-universal results.

(III) The quartic coupling is relevant, its bare value is large, and all results are universal.

Cases I and II can be distinguished by examining the lowest order correction to the perturbatively renormalized or Hartree corrected mass coming from Eq. (2.44) at one loop order

$$R = \frac{\pi\gamma k_{\rm B}T^2}{3\hbar T_{c0}} + \hbar u \int \frac{dk}{2\pi}\left(\frac{k_{\rm B}T}{\hbar}\sum_{\omega_n}\frac{1}{\widetilde{D}k^2 + |\omega_n| + \pi\gamma k_{\rm B}T^2/3\hbar T_{c0}} - \int\frac{d\omega}{2\pi}\frac{1}{\widetilde{D}k^2+|\omega|}\right) \tag{2.45}$$

where we have applied the usual shift to subtract off a zero temperature contribution so that our renormalized mass $R = 0$ at quantum criticality. The Hartree correction can be separated into two contributions, one coming from the integral, and one coming from the most dominant contribution to the sum, the $\omega_n = 0$ term. These are given by

$$\begin{aligned}\int\frac{d\omega}{2\pi}\int\frac{dk}{2\pi}\Big(\frac{1}{\widetilde{D}k^2 + |\omega_n| + \pi\gamma k_{\rm B}T^2/3\hbar T_{c0}} - \frac{1}{\widetilde{D}k^2+|\omega|}\Big) \\ = -\frac{1}{2\pi^2}\int dk \ln\left(1 + \frac{\pi\gamma k_{\rm B}T^2}{3\hbar\widetilde{D}k^2 T_{c0}}\right) \\ = -\frac{1}{\pi}\sqrt{\frac{\pi\gamma k_{\rm B}T^2}{3\hbar\widetilde{D}T_{c0}}}\end{aligned} \tag{2.46}$$

and

$$\begin{aligned}\frac{k_{\rm B}T}{\hbar}\int\frac{dk}{2\pi}\frac{1}{\widetilde{D}k^2+\pi\gamma T^2/3T_{c0}} &= \frac{k_{\rm B}T}{2\hbar}\sqrt{\frac{3\hbar T_{c0}}{\pi\gamma\widetilde{D}k_{\rm B}T^2}} \\ &= \frac{1}{2}\sqrt{\frac{3k_{\rm B}T_{c0}}{\pi\gamma\hbar\widetilde{D}}}\end{aligned} \tag{2.47}$$

respectively. Provided that $T < T_{c0}$, the second is the most dominant contribution, and thus the renormalized mass is significant when it is greater than the bare mass of Eq. (2.43),

$$\frac{\hbar u}{2}\sqrt{\frac{3k_{\rm B}T_{c0}}{\pi\gamma\hbar\widetilde{D}}} > \frac{\pi\gamma k_{\rm B}T^2}{3\hbar T_{c0}} \tag{2.48}$$

which defines the Hartree temperature

$$k_{\rm B}T_{\rm H} = \left(\frac{3\hbar k_{\rm B}T_{c0}}{\pi\gamma}\right)^{3/4}\left(\frac{u}{2\sqrt{\widetilde{D}}}\right)^{1/2}. \tag{2.49}$$

For temperatures above $T_{\rm H}$ one can ignore the presence of a repulsive interaction between the Cooper pairs, and the non-interacting results of Ref. [84] will be accurate.

The temperature below which all results scale to universal values can be obtained by considering the thermal length which follows naturally from the scaling analysis of Section 2.2, $L_T \sim L_\tau^{1/z} \sim T^{-1/z}$ or more precisely for $z = 2$

$$L_T = \sqrt{\frac{\hbar\widetilde{D}}{k_{\rm B}T}}. \tag{2.50}$$

The bare quartic coupling can be assumed to be large with respect to all other parameters and thus flow to infinite strength when the potential energy is greater than the kinetic energy, i.e.,

$$\frac{\hbar^2 u}{L_T} > \frac{\hbar\widetilde{D}}{L_T^2}. \tag{2.51}$$

This relation sets the temperature $T_{\rm u}$ below which one can safely take $u \to \infty$ and obtain universal results to be

$$k_{\rm B}T_{\rm U} = \frac{\hbar^3 u^2}{\widetilde{D}}. \tag{2.52}$$

We may now use the values of the microscopic parameters given above to evaluate the temperatures defined in Eqs. (2.49) and (2.52) which separate the regions I-II and II-III. As before, we will find different values in the clean and dirty limit.

Dirty Limit ($\xi_0 \gg \ell$)**:**

The Hartree temperature in the dirty limit can be found by substituting Eqs. (2.38a), (2.40a) and (2.40c) in Eq. (2.49)

$$T_{{\rm H},d} = 0.83\frac{\hbar v_{\rm F}}{(\xi_{\rm loc}N_\perp\xi_0^3)^{1/4}}, \tag{2.53}$$

where the single electron localization length is defined to be

$$\xi_{\rm loc} = N_\perp\ell. \tag{2.54}$$

This temperature can be converted into a length scale, which gives a lower bound on lengths over which one must explicitly include Hartree corrections

$$L_{{\rm H},d} = 0.63\xi_{\rm loc}^{1/4}(\ell\xi_0)^{3/8}. \tag{2.55}$$

The universal temperature scale is found from Eq. (2.52) to be

$$T_{\mathrm{U},d} = \frac{25}{N_\perp}\frac{\hbar v_\mathrm{F}}{\xi_\mathrm{loc}}, \tag{2.56}$$

corresponding to length scales longer than

$$L_{\mathrm{U},d} = 0.12\xi_\mathrm{loc}. \tag{2.57}$$

Clean Limit ($\xi_0 \ll \ell$)**:**

We can repeat the same analysis, now using Eqs. (2.42a) and (2.42c) for the clean limit. The Hartree temperature is given by

$$T_{\mathrm{H},c} = 0.96\frac{\hbar v_\mathrm{F}}{\sqrt{N_\perp}\xi_0} \tag{2.58}$$

with associated length scale

$$L_{\mathrm{H},c} = 0.51 N_\perp^{1/4}\xi_0. \tag{2.59}$$

For universal results we find

$$T_{\mathrm{U},c} = 33\frac{\hbar v_\mathrm{F}}{N_\perp^2\xi_0} \tag{2.60}$$

with

$$L_{\mathrm{U},c} = 0.090 N_\perp \xi_0. \tag{2.61}$$

The results are summarized in Table 2.1, but it is immediately clear that when in the clean limit, $L_T > L_{\mathrm{U},c}$ can be easily satisfied, whereas in the dirty limit $L_T > L_{\mathrm{U},d}$ would require lengths on the order of ℓ_loc, and thus weak localization effects not present in this analysis would have to be carefully considered.

2.7 The role of disorder

We conclude this chapter with a brief discussion on the region of the phase diagram in Fig. 2.1 where the effects of disorder, manifest as spatially dependent coefficients in $\mathcal{S}_\alpha$ can be safely neglected. This topic will be returned to in great detail in Chapter 5 but for now we can make a rough estimate of the temperature scale T_dis where disorder effects must be included by equating the thermal length with the localization length. This yields

$$L_T = \xi_\mathrm{loc} = N_\perp \ell, \tag{2.62}$$

and using Eq. (2.50) and Eq. (2.40a) we find

$$k_\mathrm{B}T_\mathrm{dis} = \frac{\hbar}{3N_\perp^2\tau_\mathrm{el}} \tag{2.63}$$

Gaussian	**non-Gaussian** **non-universal**	**non-Gaussian** **universal**
Dirty Limit ($\xi_0 \gg \ell$)		
$k_{\rm B}T > 0.83\frac{\hbar v_{\rm F}}{(\xi_{\rm loc}N_\perp\xi_0^3)^{1/4}}$	$\frac{25}{N_\perp}\frac{\hbar v_{\rm F}}{\xi_{\rm loc}} < k_{\rm B}T < 0.83\frac{\hbar v_{\rm F}}{(\xi_{\rm loc}N_\perp\xi_0^3)^{1/4}}$	$k_{\rm B}T < \frac{25}{N_\perp}\frac{\hbar v_{\rm F}}{\xi_{\rm loc}}$
$L < 0.63\xi_{\rm loc}^{1/4}(\ell\xi_0)^{3/8}$	$0.63\xi_{\rm loc}^{1/4}(\ell\xi_0)^{3/8} < L < 0.12\xi_{\rm loc}$	$L > 0.12\xi_{\rm loc}$
Clean Limit ($\xi_0 \ll \ell$)		
$k_{\rm B}T > 0.96\frac{\hbar v_{\rm F}}{\sqrt{N_\perp}\xi_0}$	$33\frac{\hbar v_{\rm F}}{N_\perp^2\xi_0} < k_{\rm B}T < 0.96\frac{\hbar v_{\rm F}}{\sqrt{N_\perp}\xi_0}$	$k_{\rm B}T < 33\frac{\hbar v_{\rm F}}{N_\perp^2\xi_0}$
$L < 0.51N_\perp^{1/4}\xi_0$	$0.51N_\perp^{1/4}\xi_0 < L < 0.090N_\perp\xi_0$	$L > 0.090N_\perp\xi_0$

Table 2.1: The temperature and length scales in the clean and dirty limits corresponding to the regions of applicability described in I-III for the effective action $\mathcal{S}_\alpha$.

where $\tau_{\rm el} = \ell/v_{\rm F}$ is the elastic scattering time. $T_{\rm dis}$ can therefore be made arbitrarily small by considering thicker or cleaner wires.

The analysis performed in this chapter has provided a firm foundation for the applicability of the effective action $\mathcal{S}_\alpha$ to the SMT in ultra-narrow wires. In the next chapter we compute transport results near this quantum phase transition in the limit where the number of complex components of Ψ is large.

Chapter 3

Thermoelectric Transport in the Large-N Limit

In this chapter, the effective dissipative action already discussed at length is considered with the generalization of the physical case of a 1-component complex field Ψ corresponding to the Cooper pair operator, to an N-component complex field Ψ_a with $a = 1, \ldots, N$. We will compute the thermal κ and electrical σ transport coefficients in the "LAMH", "quantum critical" and "metal" regimes described in Fig. 2.1 through the application of both analytical and numerical methods. It is always assumed, unless otherwise specified, that these fluctuation corrections are the most singular terms at finite temperature resulting from the direct contribution to transport due to Cooper pairs, (i.e. we suppress any subscripts on transport coefficients). It is understood, that in order to make contact with any real experiment, a subtraction of the normal state values would be required.

Before embarking on a detailed description of calculations for the large-N limit, we first discuss some previous approaches to transport both with and without pair-breaking perturbations. After computing both κ and σ in our theory, we will introduce the physical significance of their ratio, known as the Wiedemann-Franz law and compute its value which can be compared to the Lorenz number, its value for a normal metal.

3.1 Previous transport results

There are a number of tractable approaches to describing transport near the SMT and we will present the two most relevant to this work here. The first is the time-dependent Ginzburg-Landau theory of a low-dimensional BCS superconductor near its mean field transition temperature, and the second is a microscopic approach based on finite temperature disordered electron perturbation theory to lowest order, which applies in the low temperature metallic regime. The goal of this discussion will be to

highlight previous results as well as to frame our effective action as a useful tool for computing transport results in the quantum critical region and beyond.

3.1.1 LAMH theory

In Section 1 we have given a broad historical introduction to the study of the destruction of superconductivity by resistive fluctuations in quasi-one dimensional systems. Transport near the finite temperature phase boundary is controlled by thermally activated events, known as phase slips, which cause an unwinding of the phase of the superconducting order parameter by an integer multiple of 2π. The theory describing the size of the free energy barrier height ΔF and rate of phase slip events Ω was set down by Langer and Ambegaokar [19] and McCumber and Halperin [20] and is commonly known as the LAMH theory. When used in conjunction with the Josephson relation, we showed that the LAMH resistance of a wire is found to be [6]

$$R_{\rm LAMH} = R_q \frac{\hbar\Omega(T)}{k_{\rm B}T} {\rm e}^{-\Delta F(T)/k_{\rm B}T} \tag{3.1}$$

where $R_q = h/(2e)^2$ is the quantum of resistance and $\Omega(T)$ and $\Delta F(T)$ are given in Eqs. (1.35) and (1.29) respectively. This result can be applied to a nanowire of length L and normal resistance R_N to obtain the LAMH contribution to the conductivity [38]

$$\sigma_{\rm LAMH} = \frac{4e^2}{h} L \sqrt{\frac{R_N}{R_q}} \left(\frac{T\xi(0)}{T_c L}\right)^{3/2} \left(1-\frac{T}{T_c}\right)^{-9/4} \exp\left[0.83 \frac{T_c L}{T\xi(0)} \left(1-\frac{T}{T_c}\right)^{3/2}\right] \tag{3.2}$$

or

$$\sigma_{\rm LAMH} = L\ \frac{e^2}{h} \Phi_{\rm LAMH}\left(\frac{R_q}{R_N}, \frac{T}{T_c}, \frac{L}{\xi(0)}\right) \tag{3.3}$$

where $\Phi_{\rm LAMH}$ is a universal dimensionless function, T_c is the superconducting transition temperature and $\xi(0)$ is the zero temperature Ginzburg-Landau coherence length.

A multitude of experiments on superconducting nanowires [35, 45, 38, 76, 77, 44, 78, 39, 37] have confirmed the accuracy of the LAMH theory by fitting Eq. (3.2) to experimental transport measurements with T_c and $\xi(0)$ as free parameters with great success. We have already seen a set of excellent LAMH fits earlier for MoGe nanowires in Fig. 1.4. This description includes the effects of *only* thermally activated phase slips, and neglects the possibility of quantum phase slips at low temperatures [111, 112] where, if present, one would expect a deviation from the LAMH theory. There are some experimental indications that quantum phase slips (QPT) may indeed be present at the lowest temperatures [28, 29, 113] and we attempt to address some of these issues in Section 3.3 by presenting a version of the LAMH theory with parameters renormalized by quantum fluctuations.

3.1.2 Microscopic theory

Having discussed fluctuation corrections to transport near the ordered phase within LAMH theory, it will be useful to also place the results of this chapter for the metallic phase in the context of recent microscopic computations in BCS theory [83, 84]. These results are valid at low temperatures, with the pair-breaking parameter α larger than critical α_c of the SMT. They were obtained in the dirty limit ($\ell \ll \xi$), but we expect that the results computed here should apply in the quantum critical regime in the both the clean and dirty limits with some caveats (there are certainly distinctions in the "fluctuating superconductor" regime of Fig. 2.1). For the conductivity, these results are [83]

$$\sigma = \sigma_0 + \frac{e^2}{\hbar}\left(\frac{k_B T}{\hbar D}\right)^{-1/2}\left[\frac{\pi}{12\sqrt{2}}\left(\frac{k_B T}{\hbar(\alpha-\alpha_c)}\right)^{5/2}\right] + \frac{e^2}{\hbar}\left(\frac{k_B T}{\hbar D}\right)\left[c\frac{\hbar(\alpha-\alpha_c)}{k_B T}\right] \quad (3.4)$$

where σ_0 is a background metallic conductivity, c is a non-universal constant, D is the diffusion constant in the metal, and the remaining corrections from pairing fluctuations have been written in the form of a power of T times a factor within the square brackets which depends only upon the ratio $\hbar(\alpha-\alpha_c)/k_B T$. This way of writing the results allows us to deduce the importance of the fluctuations corrections, in the renormalization group sense, to the SMT. The first square bracket represents the usual Aslamazov-Larkin (AL) correction [85] and has a prefactor of a negative power of T, and so is a relevant perturbation; this is so even though this correction vanishes as $T \to 0$. The structure of this term is captured in our previously computed scaling function for the conductivity Eq. (2.11) and would require $\Phi_\sigma(x) \sim x^{-5}$, we will soon find that this is indeed the case. The second square bracket arises from the additional AL, Maki-Thompson (MT) [86, 87] and Density of States (DoS) corrections: the prefactor has no divergence as a power of T, and so this correction is formally irrelevant at the SMT. The complete second term has a finite limit as $T \to 0$, and so becomes larger than the formally relevant AL term at sufficiently low T in the metal. The second term is therefore identified as being *dangerously irrelevant* in critical phenomena parlance: it is important for the properties of the low T metallic region, but can be safely neglected in the shaded quantum critical region of Fig. 2.1.

3.2 Finite temperature dynamics

We are now ready to study the effective action of Eq. (2.1) generalized to the large-N limit

$$\begin{aligned}\mathcal{S}_\alpha = &\int dx \int d\tau \left[\widetilde{D}|\partial_x \Psi_a(x,\tau)|^2 + \alpha|\Psi_a(x,\tau)|^2 + \frac{u}{2}|\Psi_a(x,\tau)|^4\right] \\ &+ T\sum_{\omega_n}\int dx\, |\omega_n||\Psi_a(x,\omega_n)|^2,\end{aligned} \quad (3.5)$$

where we have used the short hand notation

$$|\Psi_a(x,\tau)|^2 \equiv |\Psi_1(x,\tau)|^2 + \cdots + |\Psi_N(x,\tau)|^2 \tag{3.6}$$

$$|\Psi_a(x,\tau)|^4 \equiv (|\Psi_1(x,\tau)|^2 + \cdots + |\Psi_N(x,\tau)|^2)^2 \tag{3.7}$$

for the sake of compactness. Such a procedure is required to address the fact that in $d = 1$ the quartic coefficient u is strongly relevant, and perturbative approaches are not possible.

Our goal will be the calculation of uniform electrical and thermal transport properties at zero frequency, the dc limit, while taking special care to ensure that $\omega \to 0$ while the temperature remains finite. We begin with a derivation of a quadratic action with an associated constraint which will be the starting point for many of the computations in this chapter. The universal properties of the SMT can be most easily accessed in the strong coupling regime, and focusing on only the quadratic and quartic terms in Eq. (3.5) we can write

$$\int dx \int d\tau \left[\alpha|\Psi_a(x,\tau)|^2 + \frac{u}{2}|\Psi_a(x,\tau)|^4\right] = \frac{\alpha^2}{2u}\int dx \int d\tau \left[\sqrt{\frac{u}{|\alpha|}}\Psi_a(x,\tau)|^2 - 1\right]^2 \tag{3.8}$$

where we have neglected a constant. A rescaling of the field $\Psi_a \to \sqrt{|\alpha|/u}\,\Psi_a$, leads to

$$\begin{aligned}\mathcal{S}_\alpha = \int dx \int d\tau \left\{\frac{\widetilde{D}|\alpha|}{u}|\partial_x\Psi_a(x,\tau)|^2 + \frac{\alpha^2}{2u}\left[|\Psi_a(x,\tau)|^2 - 1\right]^2\right\} \\ + \; T\sum_{\omega_n}\int dx\,\frac{|\alpha|}{u}|\omega_n||\Psi_a(x,\omega_n)|^2.\end{aligned} \tag{3.9}$$

Defining a new coupling constant

$$g = \frac{u}{\alpha} \tag{3.10}$$

we can send $u \to \infty$ while keeping the ratio of u to α fixed and arrive at a much simpler quadratic action

$$\mathcal{S}_g = \frac{1}{g}\int \frac{dk}{2\pi} T\sum_{\omega_n} |\Psi_a(k,\omega_n)|^2(\widetilde{D}k^2 + |\omega_n|). \tag{3.11}$$

along with the constraint $|\Psi_a(x,\tau)|^2 = 1$ where $\Psi_a(k,\omega_n)$ is the Fourier transform of $\Psi_a(x,\tau)$ defined by

$$\Psi_a(k,\omega_n) = \int dx \int d\tau \Psi_a(x,\tau)\mathrm{e}^{-i(kx-\omega_n\tau)}. \tag{3.12}$$

The parameter g now tunes us across the quantum critical point and the modified scaling dimensions at tree level are found to be

$$\dim[\Psi_a] = 0 \tag{3.13}$$

$$\dim[g] = -1. \tag{3.14}$$

3.2.1 Effective classical theory

The quantum partition function is given by

$$\mathcal{Z} = \int \mathcal{D}\Psi_a \mathcal{D}\Psi_a^* \; \delta(|\Psi_a|^2 - 1) \; \mathrm{e}^{-\mathcal{S}_g} \tag{3.15}$$

and our first approach will be to derive an effective classical model from $\mathcal{Z}$. This can be done in the large-N limit by first imposing the constraint $\Psi_a(x,\tau) = 1$ via a Lagrange multiplier μ

$$\prod_{a=1}^{N} \delta(|\Psi_a|^2 - 1) = \int \mathcal{D}\mu \; \exp\left[-\frac{i}{g}\int dx \int d\tau \mu(x,\tau)(|\Psi_a(x,\tau)|^2 - N)\right] \tag{3.16}$$

and then integrating out all non-zero Matsubara frequencies from $\mathcal{Z}$ over their Gaussian action. The resulting effective action has an overall factor of N, and as $N \to \infty$ we can perform the functional integral over μ by the method of steepest descents (the saddle point approximation) where we replace $r = i\mu$. This yields the classical partition function

$$\mathcal{Z}_c = \int \mathcal{D}\Psi_a \mathcal{D}\Psi_a^* \; \exp\left\{-\frac{N}{T}\int dx \left[\widetilde{D}|\partial_x \Psi_a(x)|^2 + V(|\Psi_a(x)|^2)\right]\right\} \tag{3.17}$$

where

$$\Psi_a(x) = \frac{T}{\sqrt{g}} \int_0^{1/T} d\tau \Psi_a(x,\tau) \tag{3.18}$$

is an imaginary time independent classical field governed by the sombrero shaped effective potential $V(z)$ ($z = |\Psi_a|^2$) given by

$$V(z) = zr(z) + T\sum_{\omega_n \neq 0} \int \frac{dk}{2\pi} \ln[\widetilde{D}k^2 + |\omega_n| + r(z)] - \frac{r(z)}{g}. \tag{3.19}$$

The function $r = i\mu$ is to be determined by solving the saddle point constraint equation $\partial V/\partial r = 0$,

$$z + T\sum_{\omega_n \neq 0} \int \frac{dk}{2\pi} \frac{1}{\widetilde{D}k^2 + |\omega_n| + r(z)} = \frac{1}{g}. \tag{3.20}$$

The scaling limit of equations (3.19) and (3.20) can be reached leading to a universal, cutoff-independent expression for $V(z)$. First consider Eq. (3.20) and note that the $T = 0$ quantum critical point is at $g = g_c$, where g_c is determined in the large-N limit by

$$\int \frac{d\omega}{2\pi} \int \frac{dk}{2\pi} \frac{1}{\widetilde{D}k^2 + |\omega|} = \frac{1}{g_c} \tag{3.21}$$

and we must include an ultra-violet (UV) cutoff for finiteness. Defining

$$\delta \equiv \sqrt{\widetilde{D}}\left(\frac{1}{g_c}-\frac{1}{g}\right), \tag{3.22}$$

we can use δ as our tuning parameter; the quantum critical point now resides at $\delta = 0$, $T = 0$. Subtracting Eq. (3.21) from (3.20) we obtain

$$\begin{aligned}\delta + z\sqrt{\widetilde{D}} &= \sqrt{\widetilde{D}}\int\frac{dk}{2\pi}\left[\int_{-\Lambda_\omega}^{\Lambda_\omega}\frac{d\omega}{2\pi}\frac{1}{\widetilde{D}k^2+|\omega|} - T\sum_{\omega_n\neq 0}^{|\omega_n|<\Lambda_\omega}\frac{1}{\widetilde{D}k^2+|\omega_n|+r(z)}\right]\\ &= \sqrt{\widetilde{D}}\int\frac{dk}{2\pi^2}\left[\ln\left(\frac{\Lambda_\omega+\widetilde{D}k^2}{\widetilde{D}k^2}\right) - \psi\left(1+\frac{\Lambda_\omega+\widetilde{D}k^2+r(z)}{2\pi T}\right)\right.\\ &\qquad \left. + \psi\left(1+\frac{\widetilde{D}k^2+r(z)}{2\pi T}\right)\right]\end{aligned} \tag{3.23}$$

where ψ is the digamma function. The limit $\Lambda_\omega \to \infty$ can now be safely be taken, and we find, after rescaling to a dimensionless momentum

$$\frac{\delta}{\sqrt{T}} + z\sqrt{\frac{\widetilde{D}}{T}} = \int\frac{dk}{2\pi^2}\left[\ln\left(\frac{2\pi}{k^2}\right) + \psi\left(1+\frac{k^2+r(z)/T}{2\pi}\right)\right]. \tag{3.24}$$

This is one of the most important results in the scaling limit, and determines $r(z)/T$ as a universal function of $\delta/\sqrt{T}$ and $z\sqrt{\widetilde{D}/T}$. A numerical solution of Eq. (3.24) is shown in Fig. 3.1, and we note that it has a minimum possible value of -2π due to the argument of the polygamma function. The effective potential $V = V(z, \delta, T)$ and renormalized mass $r = (z, \delta, T)$ are actually functions of three variables $z = |\Psi|^2$, δ and T. For the sake of brevity, we will usually just explicitly indicate their $z = |\Psi|^2$ dependence whenever possible.

Now consider the scaling limit of the effective potential in Eq. (3.19). Substituting the expression for $1/g$ in Eq. (3.20) into Eq. (3.19), and subtracting a constant which is independent of z, we obtain

$$\begin{aligned}V(z) &= T\sum_{\omega_n\neq 0}\int\frac{dk}{2\pi}\left[\ln\left(\frac{\widetilde{D}k^2+|\omega_n|+r(z)}{\widetilde{D}k^2+|\omega_n|}\right) - \frac{r(z)}{\widetilde{D}k^2+|\omega_n|+r(z)}\right]\\ &= \frac{T^{3/2}}{\sqrt{\widetilde{D}}}2\sum_{n=1}^{\infty}\int\frac{dk}{2\pi}\left[\ln\left(\frac{k^2+2\pi n+r(z)/T}{k^2+2\pi n}\right) - \frac{r(z)/T}{k^2+2\pi n+r(z)/T}\right]\\ &= \sqrt{\frac{2\pi}{\widetilde{D}}}T^{3/2}\sum_{n=1}^{\infty}\left[\frac{2n+r(z)/2\pi T}{\sqrt{n+r(z)/2\pi T}} - 2\sqrt{n}\right].\end{aligned} \tag{3.25}$$

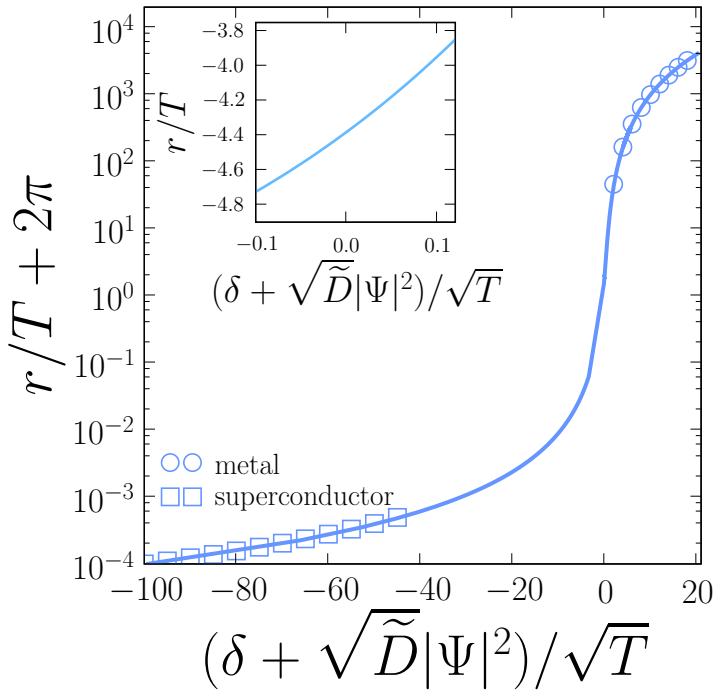

Figure 3.1: The numerical solution of the transcendental saddle point equation (3.24) which will be used in all computations of the effective classical potential $V(z)$. The symbols were calculated using the approximate solution to r/T found in the metallic (Eq. (3.33)) and superconducting (Eq. (3.41)) limits.

The structure of the effective classical potential indicates that it can be written in the scaling form

$$V(z,T,\delta) = \frac{T^{3/2}}{\sqrt{\widetilde{D}}}\Phi_V\left(\frac{\delta}{\sqrt{T}}, z\sqrt{\frac{\widetilde{D}}{T}}\right) \tag{3.26}$$

where Φ_V is a universal dimensionless function. By truncating the sum in Eq. (3.25) at some large, but finite value, the scaling function $\Phi_V(z)$ can be evaluated at fixed $\delta/\sqrt{T}$ as seen in Fig. 3.2. For $\delta/\sqrt{T} = z\sqrt{\widetilde{D}/T} = 0$ we find $r = -0.697278$ leading to $V(0) \simeq 1.5100$. For fixed $\delta/\sqrt{T}$, the effective potential is proportional to $|\Psi|^2$ as $|\Psi| \to 0$ and behaves like $|\Psi|^6$ for large $|\Psi|$. This behavior can be confirmed in the limiting cases corresponding to $\delta/\sqrt{T} \to \pm\infty$ where we will examine the effective potential as $T \to 0$.

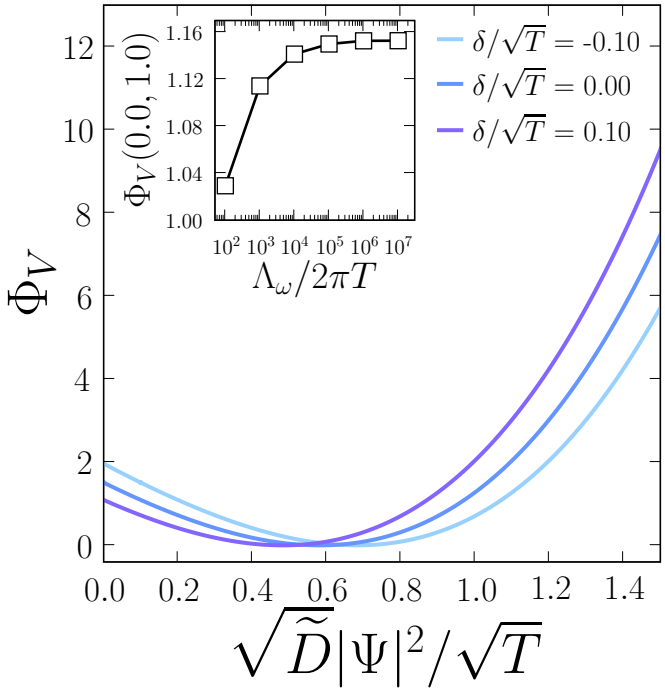

Figure 3.2: The scaling form of the effective potential calculated by including $N = 10^7$ terms in the frequency summation. The inset shows the convergence properties of the sum for fixed $\delta/\sqrt{T}$ and $z = |\Psi|^2$.

Metallic phase

Here we have $\delta/\sqrt{T} \to \infty$, which corresponds to setting $r(z) \to \infty$ in Eq. (3.24). In this limit, $\psi(y)$ is the digamma function with asymptotic expansion

$$\psi(1+y) = \ln y + \frac{1}{2y} - \sum_{n=1}^{\infty} \frac{\mathrm{B}_{2n}}{(2n)y^{2n}} \tag{3.27}$$

where B_{2n} are the even integer Bernoulli numbers. Let us rewrite the integral on the right hand side of Eq. (3.24) as

$$\mathcal{I}(z) = \int \frac{\mathrm{d}k}{2\pi^2} \left[\ln\left(\frac{2\pi}{k^2}\right) + \psi\left(\frac{k^2 + x(z)}{2\pi}\right) \right] \tag{3.28}$$

where we have defined

$$x(z) = 2\pi + \frac{r(z)}{T}. \tag{3.29}$$

Combining the logarithm in Eq. (3.24) with the logarithm in the expansion of the digamma function, we obtain the integral

$$\begin{aligned} I_0 &= \int_{-\infty}^{\infty} \frac{\mathrm{d}k}{2\pi^2} \ln\left(1+\frac{x}{k^2}\right) \\ &= \frac{\sqrt{x}}{\pi} \,. \end{aligned} \tag{3.30}$$

The expansion of the digamma function in inverse powers of $[x(z)+k^2]$ gives rise to integrals of the type

$$I_n = \int_{-\infty}^{\infty} \frac{\mathrm{d}k}{2\pi^2} \frac{(2\pi)^{2n}}{(k^2+x)^{2n}} \sim x^{-(2n-1/2)} \tag{3.31}$$

and we can write

$$\mathcal{I}(z) = \frac{\sqrt{x(z)}}{\pi} + \frac{1}{2\sqrt{x(z)}} - \frac{1}{\sqrt{2}\pi} \sum_{n=1}^{\infty} \frac{\mathrm{B}_{2n}}{2n} \frac{(2\pi)^{2n-1/2}\ \Gamma\left(2n-\frac{1}{2}\right)}{\Gamma(2n)} [x(z)]^{-(2n-1/2)}. \tag{3.32}$$

For large values of $x(z)$, the leading contribution to Eq. (3.28) is I_0. Indeed, one can find a solution of Eq. (3.24) for which $r(z)$ is large and it will be convenient to write

$$\begin{aligned} \sqrt{r(z)} &\simeq \pi\sqrt{T}\left(\frac{\delta}{\sqrt{T}} + z\sqrt{\frac{\widetilde{D}}{T}}\right) \quad \text{or} \\ r(z) &\simeq \pi^2\left(\delta + z\sqrt{\widetilde{D}}\right)^2 \,. \end{aligned} \tag{3.33}$$

This limiting case agrees very well with the exact result as see in Fig. 3.1.

For $r(z) \gg 1$ let us rewrite the effective potential in Eq. (3.25) in terms of a sum over Matsubara frequencies. Adding and subtracting the $n=0$ term we have

$$V(z) = -\frac{T}{\sqrt{\widetilde{D}}}\sqrt{r(z)} + \frac{T}{\sqrt{\widetilde{D}}} \sum_{n=0}^{\infty} \left(\frac{2\omega_n + r(z)}{\sqrt{\omega_n + r(z)}} - 2\sqrt{\omega_n}\right). \tag{3.34}$$

In the low temperature limit, the Matsubara summation can be converted into an integral

$$\begin{aligned} V(z) &\simeq -\frac{T}{\sqrt{\widetilde{D}}}\sqrt{r(z)} + \frac{1}{\sqrt{\widetilde{D}}} \int_0^{\infty} \frac{\mathrm{d}\omega}{2\pi} \left(\frac{2\omega + r(z)}{\sqrt{\omega + r(z)}} - 2\sqrt{\omega}\right) \\ &\simeq -\frac{T}{\sqrt{\widetilde{D}}}\sqrt{r(z)} + \frac{1}{3\pi\sqrt{\widetilde{D}}}[r(z)]^{3/2} \end{aligned} \tag{3.35}$$

which can be combined with Eq. (3.33) to give

$$V(z) \simeq \frac{T^{3/2}}{\sqrt{\widetilde{D}}} \left[-\pi \left(\frac{\delta}{\sqrt{T}} + z\sqrt{\frac{\widetilde{D}}{T}} \right) + \frac{\pi^2}{3} \left(\frac{\delta}{\sqrt{T}} + z\sqrt{\frac{\widetilde{D}}{T}} \right)^3 \right] \tag{3.36}$$

and as $T \to 0$ we find the temperature independent result

$$V(z) \sim \left(\delta + z\sqrt{\widetilde{D}} \right)^3 . \tag{3.37}$$

Superconducting phase

Here we have $\delta/\sqrt{T} \to -\infty$ and the analysis is less straightforward. If we now consider $x(z) \to 0$, the kernel of $\mathcal{I}(z)$ is well behaved for large k but tends to $-\infty$ as $k \to 0$. In order to extract the divergent behavior of $\mathcal{I}(z)$ in this limit, we consider the expansion of $\psi(y)$ for $y \ll 1$

$$\psi(y) = -\frac{1}{y} - \gamma + \sum_{n=2}^{\infty} (-1)^n \zeta(n) y^{n-1} \tag{3.38}$$

where γ is the Euler-Mascheroni constant and $\zeta(n)$ is the Riemann-Zeta function. The first term in this expression indicates that we can analyze the infrared singularity in $\mathcal{I}(z)$ by adding and subtracting the integral of $2\pi/(k^2 + x(z))$ to Eq. (3.28)

$$\mathcal{I}(z) = \int \frac{\mathrm{d}k}{2\pi^2} \left[\ln\left(\frac{2\pi}{k^2}\right) + \psi\left(\frac{k^2 + x(z)}{2\pi}\right) + \frac{2\pi}{k^2 + x(z)} - \frac{2\pi}{k^2 + x(z)} \right] . \tag{3.39}$$

The first three terms can be integrated numerically to give a finite constant $C_1(x)$ which only weakly depends on x for $x \ll 1$ and $C_1(0) = 0.5829571$. The last term can be integrated exactly and gives the singular form of $\mathcal{I}(z)$ as $x(z) \to 0$

$$\mathcal{I}(z) = -\frac{1}{\sqrt{x}} + C_1(x) \tag{3.40}$$

which when combined with Eq. (3.24) gives the limiting form of $r(z)$ when $\delta/\sqrt{T} \to -\infty$

$$\sqrt{\frac{\omega_1}{r(z) + \omega_1}} \simeq -\sqrt{2\pi} \left(\frac{\delta}{\sqrt{T}} + z\sqrt{\frac{\widetilde{D}}{T}} \right) \quad \text{or}$$

$$r(z) + \omega_1 \simeq T^2 \left(\delta + z\sqrt{\widetilde{D}} \right)^{-2} \tag{3.41}$$

where $\omega_1 = 2\pi T$ is the first Matsubara frequency and we find excellent agreement with the exact result in the correct limit (Fig. 3.1).

As $\delta/\sqrt{T} \to -\infty$ or $r(z) \to -\omega_1^+$ all terms in Eq. (3.25) are well behaved, *except* the $n = 1$ term. Let us extract this term and write

$$V(z) = \frac{T}{\sqrt{\widetilde{D}}} \left[\left(\frac{2\omega_1 + r(z)}{\sqrt{r(z) + \omega_1}} - 2\sqrt{\omega_1} \right) + \sum_{n=1}^{\infty} \left(\frac{2\omega_{n+1} + r(z)}{\sqrt{r(z) + \omega_{n+1}}} - 2\sqrt{\omega_{n+1}} \right) \right] \quad (3.42)$$

where we have shifted the sum by one. In the first term, we substitute Eq. (3.41) to investigate the divergence, while we set $r(z) + \omega_1 = 0$ in the second term

$$V(z) = \frac{T^{3/2}}{\sqrt{\widetilde{D}}} \left[-2\pi \left(\frac{\delta}{\sqrt{T}} + z\sqrt{\frac{\widetilde{D}}{T}} \right) - \left(\frac{\delta}{\sqrt{T}} + z\sqrt{\frac{\widetilde{D}}{T}} \right)^{-1} + \mathcal{C}_2 \right] \quad (3.43)$$

where $\mathcal{C}_2$ is a constant given by

$$\mathcal{C}_2 = \sqrt{2\pi} \left[\sum_{n=1}^{\infty} \left(\frac{2n+1}{\sqrt{n}} - 2\sqrt{n+1} \right) - 2 \right] = -3.66056590. \quad (3.44)$$

In the low temperature limit we can write

$$V(z) \sim -2\pi \left(\delta + z\sqrt{\widetilde{D}} \right) T \ . \quad (3.45)$$

It seems somewhat surprising that in the superconducting phase, the effective potential vanishes linearly with temperature, as $T \to 0$. However, at this point, we will endeavor to calculate transport only in the quantum critical regime where $\delta/\sqrt{T} \ll 1$ and can thus safely ignore the irregularity. We will return to the issue in Section 3.3 by investigating the low temperature ordered phase through a calculation of the Coleman-Weinberg effective potential at $T = 0$, as well as constructing an effective Ginzburg-Landau potential, near T_c.

3.2.2 Classical conductivity

In order to calculate the electrical conductivity via the Kubo formula [114], we reintroduce a *real* time dependence to our classical order parameter by approximating its low frequency dynamics by a Langevin equation [90].

$$\begin{aligned} \frac{\partial \Psi(x,t)}{\partial t} &= -\left[-\widetilde{D} \frac{\partial^2 \Psi(x,t)}{\partial x^2} + V'(|\Psi(x,t)|^2)\Psi(x,t) \right] + f(x,t) \\ &= -\left[-\widetilde{D} \frac{\partial^2 \Psi(x,t)}{\partial x^2} + r(|\Psi(x,t)|^2)\Psi(x,t) \right] + f(x,t) \end{aligned} \quad (3.46)$$

where f is a complex Gaussian correlated random noise obeying

$$\langle f(x,t)f^*(x',t')\rangle = 2T\delta(x-x')\delta(t-t') \tag{3.47}$$

and we have taken a derivative of Eq. (3.19) and used the saddle point equation (3.20) to obtain $V'(z) = r(z)$. This is simply the definition of Model A dynamics [115] and should capture the correct quantum critical dynamics whenever the renormalized mass r takes a value such that the $\omega_n \neq 0$ modes are sufficiently gapped.

The electrical current is defined to be

$$J = ie^*\widetilde{D}\left(\Psi^*\partial_x\Psi - \partial_x\Psi^*\Psi\right) \tag{3.48}$$

and thus the dc conductivity is given by

$$\sigma = \frac{1}{T}\int dx \int_0^\infty dt\langle J(x,t)J(0,0)\rangle \tag{3.49}$$

By dimensional analysis of the equation of motion and using the scaling form (3.26), we can deduce that the classical conductivity obeys the scaling form

$$\sigma = \frac{e^{*2}}{\hbar}\sqrt{\frac{\hbar\widetilde{D}}{k_{\rm B}T}}\Phi_\sigma\left(\frac{\delta}{\sqrt{\hbar k_{\rm B}T}}\right) \tag{3.50}$$

where we have inserted the dimensionally correct powers of $\hbar$ and $k_{\rm B}$ in the final result. This is simply Eq. (2.11) with the replacement given in Eq. (2.13) written in terms of our new measure of the distance from criticality δ.

The scaling function $\Phi_\sigma(x)$ is a smooth function of x through $x = 0$ and it can be determined by finding a numerical solution to the classical equations of motion (3.46) for a one-component complex field Ψ. This was done by employing both classical Monte Carlo simulations and a stochastic partial differential equation solver. We begin by fixing $\delta/\sqrt{T}$ at some small value, and discretize the Hamiltonian described by the classical partition function Eq. (3.17) to a unit spaced lattice of L sites. We are interested in equilibrium configurations of the order parameter field Ψ, and these can be obtained by Monte Carlo methods for a large number of initial conditions. These configurations are stored after a suitable number of Monte Carlo time steps (large enough to eliminate any possible autocorrelations) have been performed. The set of configurations are then used as the initial ($t = 0$) states of the stochastic equation of motion, Eq. (3.46). At each time step, we draw the noise function $f(x,t)$ from a suitable distribution and by using the second order stochastic Runge Kutta (or Heun) algorithm [116] the time dependence of $\Psi(x,t)$ can be determined. The current-current correlator in Eq. (3.49) is computed as an average over all temporal trajectories of Ψ and the dc conductivity can be found after integrating over all space

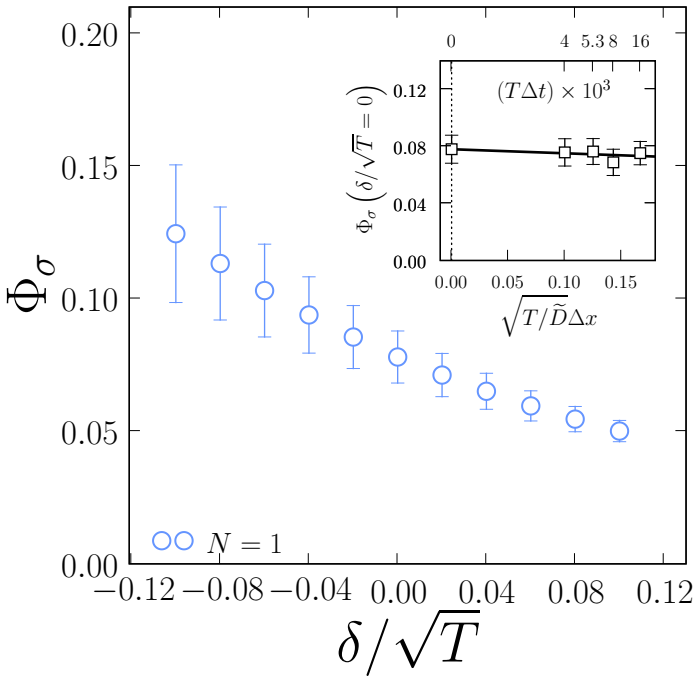

Figure 3.3: The dc conductivity scaling function Φ_σ near the quantum critical point calculated by brute force integrating the current-current correlator measured using the Langevin dynamics formalism for a one-component complex field ($N = 1$). The inset shows the spatial and temporal finite size scaling for a single data point corresponding to $\delta/\sqrt{T} = 0$.

and time. The results are necessarily dependent on the size of the spatial and temporal discretization and the final value for the scaling function Φ_σ must be finite size scaled in both space and time. The resulting value of Φ_σ directly above the quantum critical point, $\delta = 0$ $T > 0$ was found to be

$$\Phi_\sigma(0) = 0.07801 \pm 0.01. \tag{3.51}$$

This fully universal number is independent of any of the specific details of the particular quasi-one dimensional system under consideration. We have also computed the value of Φ_σ for a range of δ near the critical coupling as seen in Fig. 3.3. The semi-classical result for the physical one-component complex order parameter determined here should quite accurately reproduce the real electrical transport in the quantum critical regime, and we will use it to benchmark our $N = \infty$ results in Section 3.4.

3.3 The ordered phase

To address the physics of the ordered phase we again consider the action for an N component complex field $\Psi_a(x,\tau)$ with magnitude $|\Psi_a(x,\tau)| = 1$ but instead of treating the fluctuations semi-classically, we take a σ-model approach [117]. After enforcing the fixed magnitude constraint on Ψ_a with a Lagrange multiplier field $\mu(x,\tau)$, its action in the presence of a finite magnetic field h_a reads

$$\mathcal{S} = \frac{1}{g}\int dx \int d\tau \Big\{ \Psi_a^*(x,\tau)\left[-\widetilde{D}\partial_x^2 + |\partial_\tau| + i\mu(x,\tau)\right]\Psi_a(x,\tau) - i\mu(x,\tau) \\ - g\left[h_a\Psi_a^*(x,\tau) + h_a^*\Psi_a(x,\tau)\right]\Big\}. \tag{3.52}$$

where we have integrated the kinetic term by parts, and used the abuse of notation $|\partial_\tau|$ to infer the dissipative $|\omega_n|$ term in frequency space. To derive saddle point equations in the large-N limit, we explicitly break the $O(N)$ symmetry by choosing only one component of our conjugate field h_a to be non-zero in the N^{th} direction. Integrating over $N-1$ components of Ψ and keeping only one component σ (not to be confused with the conductivity and dropping the space and imaginary time dependence)

$$\begin{aligned}\mathcal{S}_{\text{eff}} &= \frac{N-1}{g}\int dx\int d\tau\left[\sigma^*\left(-\widetilde{D}\partial_x^2 + |\partial_\tau| + i\mu\right)\sigma - i\mu - g\left(h\sigma^* + h^*\sigma\right)\right] \\ &\quad + (N-1)\mathrm{Tr}\ln(-\widetilde{D}\partial_x^2 + |\partial_\tau| + i\mu) \\ &= (N-1)\int dx\int d\tau\left[\frac{1}{g}\sigma^*\left(-\widetilde{D}\partial_x^2 + |\partial_\tau|\right)\sigma + V\left(|\sigma|^2, i\mu\right) - \left(h\sigma^* + h^*\sigma\right)\right]\end{aligned} \tag{3.53}$$

where we have rescaled the coupling g by a factor of $N-1$. In the limit of large N, we can use the saddle point approximation, and defining $r = i\mu$, the effective potential is given by

$$V(|\sigma|^2, r) = \frac{r}{g}(|\sigma|^2 - 1) + T\sum_{\omega_n}\int\frac{dk}{2\pi}\ln(\widetilde{D}k^2 + |\omega_n| + r) \tag{3.54}$$

leading to the saddle point equations for r and σ

$$\sigma r = gh \tag{3.55a}$$

$$|\sigma|^2 = 1 - Tg\sum_{\omega_n}\int\frac{dk}{2\pi}\frac{1}{\widetilde{D}k^2 + |\omega_n| + r}. \tag{3.55b}$$

We note that an important distinction between Eq. (3.55a) and (3.55b) and the saddle point equation (3.20) derived in the last section is that here we integrate over

all Matsubara frequencies. In the absence of an external magnetic field at $T = 0$, the quantum critical point corresponds to the solution $\sigma = 0$, $s = 0$, and as before defines a critical coupling strength

$$\frac{1}{g_c} = \int \frac{d\omega}{2\pi} \int \frac{dk}{2\pi} \frac{1}{\widetilde{D}k^2 + |\omega|}. \tag{3.56}$$

It will also be convenient to use the notation of the previous section and parameterize the distance for this quantum critical point by introducing a parameter δ where

$$\delta \equiv \sqrt{\widetilde{D}} \left(\frac{1}{g_c} - \frac{1}{g} \right). \tag{3.57}$$

Using this definition, the solution to Eq. (3.55a) in zero magnetic field is given by $r = 0$ and thus from Eq.(3.55b) with $|\sigma|^2 = |\sigma_0|^2$ we have

$$|\sigma_0|^2 \equiv 1 - \frac{g}{g_c} = -\frac{g}{\sqrt{\widetilde{D}}}\delta \tag{3.58}$$

which is clearly only valid in the ordered phase characterized by $\delta < 0$. Using Eq. (3.58), Eq. (3.55b) can be rewritten as

$$|\sigma|^2 = |\sigma_0|^2 - g \int \frac{dk}{2\pi} \left[T \sum_{\omega_n} \frac{1}{\widetilde{D}k^2 + |\omega_n| + r} - \int \frac{d\omega}{2\pi} \frac{1}{\widetilde{D}k^2 + |\omega_n|} \right] \tag{3.59}$$

and by a method identical to the one used when integrating over all $\omega_n \neq 0$ we can write

$$|\sigma|^2 = -\frac{g}{\sqrt{\widetilde{D}}}\delta + g \int \frac{dk}{2\pi^2} \left[\psi \left(1 + \frac{\widetilde{D}k^2 + r}{2\pi T} \right) + \ln \left(\frac{2\pi T}{\widetilde{D}k^2} \right) - \frac{\pi T}{\widetilde{D}k^2 + r} \right], \tag{3.60}$$

where ψ is the digamma function. This expression can be inverted numerically to provide r as a function of $|\sigma|^2$ and δ. After this has been accomplished, Eqs. (3.54) and (3.55b) can be combined to give the finite temperature effective potential

$$V(|\sigma|^2, \delta) = T \sum_{\omega_n} \int \frac{dk}{2\pi} \left[\ln \left(1 + \frac{r(|\sigma|^2, \delta)}{\widetilde{D}k^2 + |\omega_n|} \right) - \frac{r(|\sigma|^2, \delta)}{\widetilde{D}k^2 + |\omega_n| + r(|\sigma|^2, \delta)} \right], \tag{3.61}$$

where we have subtracted off a term independent of r.

3.3.1 Zero temperature effective potential

At zero temperature we return to Eq. (3.59) and write the momentum and frequency integrals in an isotropic fashion. For finite magnetic field, both $|\sigma|^2$ and r are

nonzero, and dropping the explicit $|\sigma|^2$ and δ dependence of r

$$\begin{aligned} V(|\sigma|^2,\delta) &= \frac{4}{\sqrt{\widetilde{D}}}\int \frac{d^3p}{(2\pi)^3}\left[\ln\left(1+\frac{r}{p^2}\right)-\frac{r}{p^2+r}\right] \\ &= \frac{r^{3/2}}{3\pi\sqrt{\widetilde{D}}} \end{aligned} \tag{3.62}$$

where the saddle point equation (3.55b) can now be solved as

$$\begin{aligned} |\sigma|^2 &= |\sigma_0|^2 + \frac{4g}{\sqrt{\widetilde{D}}}\int \frac{d^3p}{(2\pi)^3}\frac{s}{p^2(p^2+r)} \\ &= |\sigma_0|^2 + \frac{g}{\pi\sqrt{\widetilde{D}}}\sqrt{s}\ , \end{aligned} \tag{3.63}$$

which indicates that a solution exists only for $|\sigma|^2 > |\sigma_0|^2$, requiring the presence of a non-zero conjugate field h. In the ordered phase, this equation cannot be solved for $|\sigma|^2 < |\sigma_0|^2$, and hence the effective potential defined below will not be valid in the weakly ordered regime.

The zero temperature Coleman-Weinberg effective action for a quantum field Ψ is defined to be [118]

$$\Gamma[\Psi_{cl}] = -S_{\text{eff}}[\Psi_{cl}] - \int dx \int d\tau\, (h^*\Psi_{cl} + h\Psi^*_{cl}) \tag{3.64}$$

such that it is the function whose minimum gives exactly $\Psi_{cl} = \langle\Psi\rangle$. To lowest order in perturbation theory it is simply the classical potential energy, but is modified by quantum corrections at higher order. Using Eqs. (3.53), (3.62) and (3.63), we obtain

$$\begin{aligned} V_{eff} = \frac{\Gamma(|\sigma|^2,\delta)}{\Omega(N-1)} &= \frac{\pi^2\widetilde{D}}{3g^3}\left(|\sigma|^2-|\sigma_0|^2\right)^3 \\ &= \frac{\pi^2}{3\sqrt{\widetilde{D}}}\left(\frac{\sqrt{\widetilde{D}}}{g}|\sigma|^2+\delta\right)^3 \end{aligned} \tag{3.65}$$

where Ω denotes the system volume in space-time. As noted above, this effective potential is only valid for $|\sigma|^2 > |\sigma_0|^2$, as it has a minima at $|\sigma|^2 = 0$ (for $\delta < 0$) and a point of inflection at $|\sigma|^2 = |\sigma_0|^2$.

In order to find a solution for $|\sigma|^2 < |\sigma_0|^2$, and to derive a Ginzburg-Landau effective potential for the description of any slow degrees of freedom, we should not integrate over all degrees of freedom, but only over those with a wavelength smaller than some cutoff Λ^{-1}. This is necessary due to the fact that when integrating over all Matsubara frequencies we are restricted to $r > 0$ and thus can never access $|\sigma|^2 < |\sigma_0|^2$. In Ref. [20] a similar viewpoint was expressed, and the cutoff was taken to be of

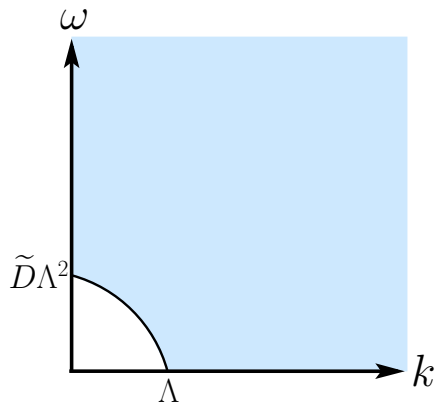

Figure 3.4: The shaded portion shows the region of integration after the implementation of a symmetric infrared cutoff in frequency and momentum.

the order of the zero temperature superconducting coherence length. We will follow this approach here, and the cutoff is implemented symmetrically in momentum and frequency space, consistent with dynamically critical exponent $z = 2$. A schematic diagram showing the shaded region of integration can be seen in Fig.3.4. We can now define a zero temperature effective potential, with $r < 0$ as

$$V_{eff} = \frac{r}{g}(|\sigma|^2 - |\sigma_0|^2) + \frac{4}{\sqrt{\widetilde{D}}} \int\limits_{\sqrt{\widetilde{D}}\Lambda}^{\infty} \frac{d^3p}{(2\pi)^3} \left[\ln\left(1 + \frac{r}{p^2}\right) - \frac{r}{p^2} \right]. \tag{3.66}$$

Differentiation with respect to r gives rise to the modified saddle point equation (for negative r)

$$|\sigma|^2 = |\sigma_0|^2 - \frac{2g}{\pi^2}\sqrt{\frac{|r|}{\widetilde{D}}} \int\limits_{\sqrt{\frac{\widetilde{D}}{|s|}}\Lambda}^{\infty} dp \frac{1}{p^2 - 1}, \tag{3.67}$$

where $|\sigma_0|^2$ is now modified from Eq. (3.58) as a result of our infrared cutoff

$$\begin{aligned} |\sigma_0|^2 &= 1 - \frac{g}{g_c} + \frac{1}{\pi^2} \int\limits_0^{\Lambda} dk \int\limits_0^{\widetilde{D}(\Lambda^2 - k^2)} \frac{d\omega}{\widetilde{D}k^2 - \omega} \\ &= -\frac{g\delta}{\sqrt{\widetilde{D}}} + \frac{2g\Lambda}{\pi^2}. \end{aligned} \tag{3.68}$$

In order to gain intuition about the relative size of the cutoff and the effective mass (Lagrange multiplier) r, we calculate the zero temperature superconducting coherence

length $\xi(0)$ as a function of r. It is determined as usual by the relation

$$\left.\frac{dV_{eff}}{d|\sigma|^2}\right|_{|\sigma|^2=0} = -\frac{\widetilde{D}}{g}\frac{1}{\xi^2(0)}. \tag{3.69}$$

By explicitly differentiating the effective potential Eq. (3.66) and using Eq. (3.67), we find

$$\left.\frac{dV_{eff}}{d|\sigma|^2}\right|_{|\sigma|^2=0} = \frac{1}{g}r(|\sigma|^2=0), \tag{3.70}$$

and combining the last two equations leads to the relation

$$\xi(0) = \sqrt{\frac{\widetilde{D}}{|r(|\sigma|^2=0)|}}. \tag{3.71}$$

Using this definition at $T=0$ and $|\sigma|^2=0$ we can now determine the coherence length $\xi(0)$ self-consistently from Eq. (3.67)

$$\begin{aligned}\xi(0) &= \frac{2g}{\pi^2|\sigma_0|^2}\int\limits_{\xi(0)\Lambda}^{\infty} dp\frac{1}{p^2-1} \\ &= \frac{g}{\pi^2|\sigma_0|^2}\ln\left(\frac{\xi(0)\Lambda+1}{\xi(0)\Lambda-1}\right) \\ &= \frac{\sqrt{\widetilde{D}}}{\pi^2|\delta|}\left[\ln\left(\frac{\Lambda\xi(0)+1}{\Lambda\xi(0)-1}\right)-2\Lambda\xi(0)\right],\end{aligned} \tag{3.72}$$

where we have used Eq. (3.68). Note that this equation has a solution for all choices of Λ such that $1<\xi(0)\Lambda\lesssim 6/5$ with $\xi(0)\to\infty$ logarithmically as $\Lambda\xi(0)\to 1$ and $\xi(0)\to 0$ as $\Lambda\xi(0)\to 6/5$. Let us parameterize $\Lambda\xi(0)=1+\epsilon$ where $\epsilon\ll 1$, and defining

$$f(\epsilon) = \frac{1}{\pi^2}\left[\ln\left(1+\frac{2}{\epsilon}\right)-2(1+\epsilon)\right] \tag{3.73}$$

the zero temperature coherence length is

$$\xi(0) = \frac{\sqrt{\widetilde{D}}}{|\delta|}f(\epsilon). \tag{3.74}$$

Due to the logarithmic divergence as $\epsilon\to 0$, one possible choice of $\epsilon\simeq 1.4\times 10^{-5}$ gives $f(\epsilon)\simeq 1$ leading to the simple relation $\xi(0)=\sqrt{\widetilde{D}}/|\delta|$ or $\Lambda\simeq|\delta|/\sqrt{\widetilde{D}}$. The proceeding arguments now allow us to express the effective potential (Eq. (3.66))

in terms of $|\sigma(r<0)|^2 < |\sigma_0|^2$ and δ. If we choose ϵ such that $f(\epsilon) = \pi^2$, i.e. $\xi(0) = \sqrt{\widetilde{D}}\pi^2/|\delta|$ then the saddle point equation (3.67) simplifies to

$$-\frac{\sqrt{\widetilde{D}}}{g}|\sigma|^2 + \left(1+\frac{2}{\pi^2}\right)|\delta| - \frac{2}{\pi^2}\sqrt{|r|}\text{arctanh}\left(\sqrt{\frac{|r|}{\delta^2}}\right) = 0 \tag{3.75}$$

which when solved for numerically for r can be substituted into Eq. (3.66) to give the effective potential

$$V_{eff} = \frac{1}{\sqrt{\widetilde{D}}}\left\{ r\left[\frac{\sqrt{\widetilde{D}}}{g}|\sigma|^2 + \left(1+\frac{2}{\pi^2}\right)\delta\right] + \frac{2}{3\pi^2}\left[-r\delta + \delta^3\ln\left(1+\frac{r}{\delta^2}\right)\right.\right.$$
$$\left.\left. + \sqrt{r^3}\ln\left(\frac{\delta+\sqrt{|r|}}{\delta-\sqrt{|r|}}\right)\right]\right\}. \tag{3.76}$$

This result, valid at $T=0$ and $|\sigma|^2 < |\sigma_0|^2$ can now be combined with Eq. (3.65) which is valid for $|\sigma|^2 > |\sigma_0|^2$ to obtain the effective potential everywhere at $T=0$ and $\delta < 0$ corresponding to the ordered or superconducting state, as seen in Fig. 3.5.

3.3.2 Construction of a Ginzburg-Landau potential

Having computed the form of the infrared momentum cutoff Λ self-consistently as a function of δ and investigating the form of the effective potential at zero temperature, we now move to finite temperatures and consider expanding around some critical temperature T_c for the ordered phase. We posit the usual form for the potential

$$V_{GL} = V_0 + \alpha_0(T-T_c)|\sigma|^2 + \frac{1}{2}\beta|\sigma|^4 + \cdots \tag{3.77}$$

and will endeavor to evaluate T_c, α_0 and β in terms of the parameters g, $\widetilde{D}$ and δ. The goal of such a procedure will be to derive an effective Ginzburg-Landau theory for the superconducting state near T_c with quantum renormalized coefficients. By multiplying this potential by the finite temperature Ginzburg-Landau coherence length $\xi(T)$, we will obtain an effective free energy from which the barrier height for a thermally activated phase slip can be determined directly from the LAMH theory.

Evaluation of the critical temperature T_c

We begin by considering the saddle point equation (Eq. (3.55b)) in the presence of our symmetric cutoff. A similar procedure that led to Eq. (3.60) can be used here,

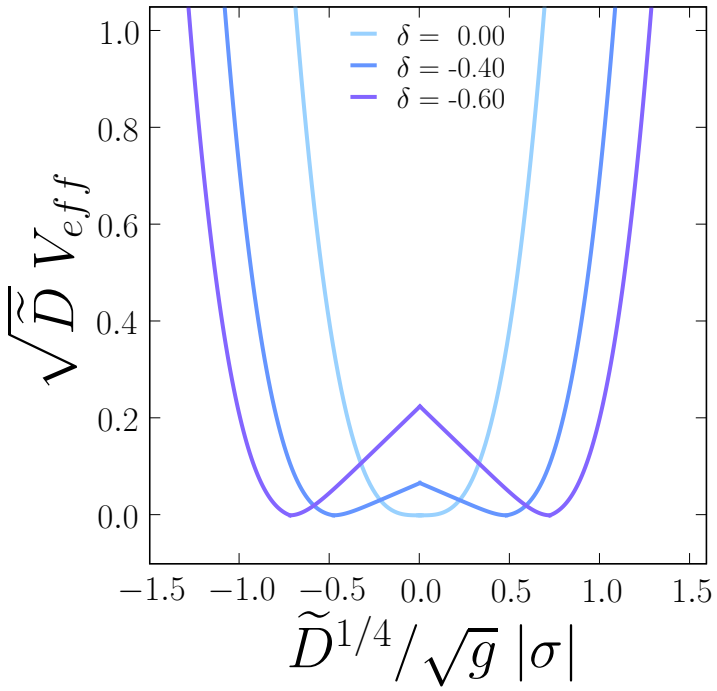

Figure 3.5: The effective quantum potential at $T = 0$ calculated via the Coleman-Weinberg procedure for $|\sigma|^2 > |\sigma_0|^2$ and through the self-consistent insertion of an infrared cutoff for $|\sigma|^2 < |\sigma_0|^2$ with $f(\epsilon) = \pi^2$.

giving

$$|\sigma|^2 = \frac{g|\delta|}{\sqrt{\widetilde{D}}} + \frac{g\Lambda}{\pi^2}\left[2 - \ln\left(\frac{\widetilde{D}\Lambda^2}{2\pi T}\right) + \psi\left(\frac{\widetilde{D}\Lambda^2 + r}{2\pi T}\right)\right] - \frac{g}{\pi^2}\int_{\Lambda}^{\infty} dk\left[\frac{\pi T}{\widetilde{D}k^2 + r} - \psi\left(1 + \frac{\widetilde{D}k^2 + r}{2\pi T}\right) + \ln\left(\frac{\widetilde{D}k^2}{2\pi T}\right)\right]. \tag{3.78}$$

Returning to Eq. (3.70) and noting that at $T = T_c$, $r(|\sigma|^2 = 0) = 0$, we can derive an equation for T_c from Eq. (3.78)

$$0 = \frac{|\delta|}{\sqrt{2\pi T_c}} + \frac{(1+\epsilon)}{\pi^2 f(\epsilon)}\frac{|\delta|}{\sqrt{2\pi T_c}}\left\{2 - \ln\left[\frac{(1+\epsilon)^2\delta^2}{2\pi T_c f^2(\epsilon)}\right] + \psi\left[\frac{(1+\epsilon)^2\delta^2}{2\pi T_c f^2(\epsilon)}\right]\right\} - \frac{1}{\pi^2}\int_{\frac{(1+\epsilon)|\delta|}{\sqrt{2\pi T_c} f(\epsilon)}}^{\infty} dk\left[\frac{1}{2k^2} - \psi(1+k^2) + \ln k^2\right], \tag{3.79}$$

where we have rescaled the momentum integral. Solving numerically using a secant method gives the result seen in Fig. 3.6. For a given cutoff, characterized by ϵ we find

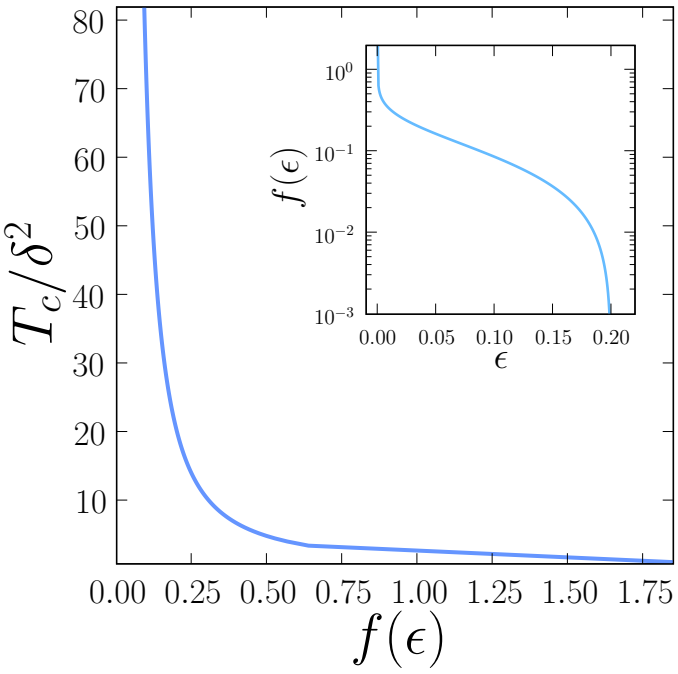

Figure 3.6: The rescaled critical temperature found from the solution of Eq. (3.79) as a function of $f(\epsilon)$ given in Eq. (3.73) which is shown in the inset.

that $T_c \propto \delta^2$ and more specifically

$$T_c = c_1(\epsilon)\delta^2 \tag{3.80}$$

where $c_1 \simeq 1.90$ for $f(\epsilon) = 1$. One could either fix ϵ at this value, or choose a value of ϵ using a plot like Fig. 3.6 that reproduced the relationship between T_c and δ measured in an experiment.

Evaluation of the quadratic coefficient α_0

In order to evaluate α_0 in Eq. (3.77) we again appeal to Eq. (3.70) and note that

$$\alpha_0(T - T_c) = \frac{1}{g} r(|\sigma|^2 = 0). \tag{3.81}$$

Near T_c we expect $r \ll 1$ and perform a double expansion of Eq. (3.78) in r and the reduced temperature $t = \frac{T-T_c}{T_c}$ leading to (after some considerable algebra)

$$\frac{r}{2\pi T_c}\left\{\frac{(1+\epsilon)}{\pi^2 f(\epsilon)}\frac{|\delta|}{\sqrt{2\pi T_c}}\psi^{(1)}\left[\frac{(1+\epsilon)^2\delta^2}{2\pi T_c f^2(\epsilon)}\right] + c_2(\epsilon)\right\} = \\ -t\left\{\frac{|\delta|}{2\sqrt{2\pi T_c}} + \frac{1}{\pi^2}\left[\frac{(1+\epsilon)|\delta|}{\sqrt{2\pi T_c} f(\epsilon)}\right]^3 \psi^{(1)}\left[\frac{(1+\epsilon)^2\delta^2}{2\pi T_c f^2(\epsilon)}\right] - \frac{\sqrt{2\pi T_c} f(\epsilon)}{4\pi^2|\delta|}\right\} \tag{3.82}$$

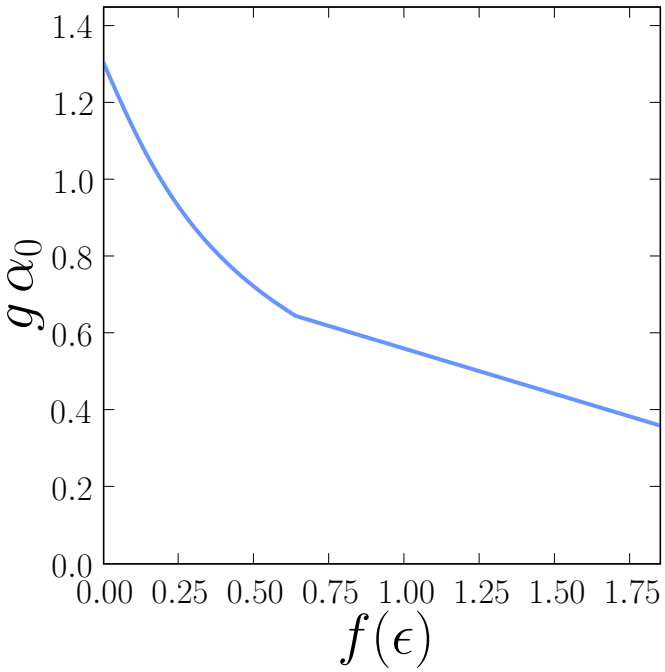

Figure 3.7: The rescaled quadratic coefficient $g\alpha_0$ found from Eq. (3.84) using the numerical solution to Eq. (3.79) as a function of $f(\epsilon)$ given in Eq. (3.73). $f(\epsilon)$ vs. ϵ can be seen in the inset of Fig. 3.6.

where we have kept only linear terms in r and t, $\psi^{(1)}(x)$ is the first polygamma function and

$$c_2(\epsilon) = \frac{1}{\pi^2} \int\limits_{\frac{(1+\epsilon)|\delta|}{\sqrt{2\pi T_c} f(\epsilon)}}^{\infty} dk \left[\frac{1}{2k^4} + \psi^{(1)}(1+k^2) \right]. \tag{3.83}$$

Comparing Eq. (3.82) with Eq. (3.81) we find

$$\alpha_0 = \frac{2\pi}{g} \frac{\frac{|\delta|}{2\sqrt{2\pi T_c}} + \frac{1}{\pi^2}\left[\frac{(1+\epsilon)|\delta|}{\sqrt{2\pi T_c} f(\epsilon)}\right]^3 \psi^{(1)}\left[\frac{(1+\epsilon)^2\delta^2}{2\pi T_c f^2(\epsilon)}\right] - \frac{\sqrt{2\pi T_c} f(\epsilon)}{4\pi^2|\delta|}}{\frac{(1+\epsilon)}{\pi^2 f(\epsilon)} \frac{|\delta|}{\sqrt{2\pi T_c}} \psi^{(1)}\left[\frac{(1+\epsilon)^2\delta^2}{2\pi T_c f^2(\epsilon)}\right] + c_2(\epsilon)} \tag{3.84}$$

which can be seen in Fig. 3.7, and upon choosing $f(\epsilon) = 1$ we find $c_2 \simeq 0.856$ and $\alpha_0 \simeq 0.509385/g$.

Evaluation of the quartic coefficient β

In order to determine the value of the quartic coefficient, we can examine Eqs. (3.70) and (3.77) at $T = T_c$ leading to

$$\beta \equiv \frac{d^2 V_{LG}}{d(|\sigma|^2)^2} = \frac{1}{g} \left. \frac{dr}{d|\sigma|^2} \right|_{T=T_c} . \tag{3.85}$$

Taking a derivative with respect to $|\sigma|^2$ of Eq. (3.78) we find

$$1 = \frac{g}{2\pi T_c} \left\{ \frac{\Lambda}{\pi^2} \psi^{(1)} \left(\frac{\widetilde{D}\Lambda^2}{2\pi T_c} \right) + \sqrt{\frac{2\pi T_c}{\widetilde{D}}} \frac{1}{\pi^2} \int\limits_{\sqrt{\frac{\widetilde{D}}{2\pi T_c}}\Lambda}^{\infty} dk \left[\frac{1}{2k^4} + \psi^{(1)}(1+k^2) \right] \right\} \left. \frac{dr}{d|\sigma|^2} \right|_{T=T_c} \tag{3.86}$$

and using our relation between Λ and $\xi(0)$, Eqs. (3.72) and (3.73) as well as Eq. (3.85), the quartic coefficient is given by

$$\beta = \frac{\sqrt{\widetilde{D}}}{g^2} |\delta| \left\{ \frac{(1+\epsilon)}{\pi^2 f(\epsilon)} \psi^{(1)} \left[\frac{(1+\epsilon)^2 \delta^2}{2\pi T_c f^2(\epsilon)} \right] + \frac{\sqrt{2\pi T_c} c_2(\epsilon)}{|\delta|} \right\}^{-1} . \tag{3.87}$$

where we have employed Eq. (3.83). The full expression is shown in Fig. 3.8, and for $f(\epsilon) = 1$ we find $\beta \simeq 0.495\sqrt{\widetilde{D}}|\delta|/g^2$.

We have now amassed all the required ingredients to construct the Ginzburg-Landau potential of Eq. (3.77) as seen in Fig. 3.9. We have presented the potential for $f(\epsilon) = \pi^2$ but as can be seen from Figs. 3.7 to 3.8, the $f(\epsilon)$ dependence of all coefficients is relatively weak for $f(\epsilon) > 1$. We find a relatively steep double well potential which unsurprisingly has both a barrier height and order parameter expectation value that depends on the value of δ.

3.3.3 Free energy barrier height and LAMH theory

Having derived a effective Ginzburg-Landau potential (which has engineering dimensions of energy divided by length) we may convert it into a free energy functional by multiplying by the finite temperature coherence length

$$\xi(T) = \xi(0) \left(1 - \frac{T}{T_c} \right)^{-1/2} . \tag{3.88}$$

This is due to the fact that the presence of phase slips below T_c necessarily reduce the phase coherence of the wire and we have $L/\xi(T)$ independent segments, that

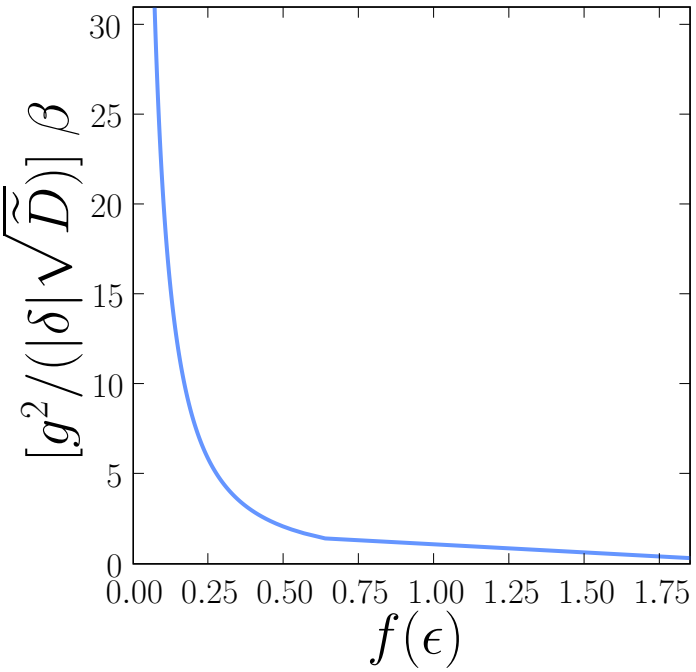

Figure 3.8: The rescaled quartic coefficient found from Eq. (3.87) using the numerical solution to Eq. (3.79) and Eq. (3.83), as function of $f(\epsilon)$ given in Eq. (3.73). $f(\epsilon)$ vs. ϵ can be seen in the inset of Fig. 3.6.

will be interact via Josephson coupling near the finite temperature transition. After discarding a constant we find the rather strange looking function

$$F_{GL} = \overline{\alpha}_0 \frac{\sqrt{\widetilde{D}} f(\epsilon)}{g\delta} \left(1 - \frac{T}{T_c}\right)^{1/2} |\sigma|^2 - \overline{\beta} \frac{\sqrt{T_c}\widetilde{D} f(\epsilon)}{2g^2\delta} \left(1 - \frac{T}{T_c}\right)^{-1/2} |\sigma|^4 \tag{3.89}$$

with a singular temperature dependence in the quartic term. We consider temperatures that place us in the LAMH region of the phase diagram displayed in Fig. 2.1 and so $1 - T/T_c \ll 1$, but that we are not too deep into the ordered phase. The rescaled distance from the critical point is negative ($\delta < 0$), and the dimensionless coefficients are

$$\overline{\alpha}_0 = g\alpha_0 \tag{3.90}$$

$$\overline{\beta} = \frac{g^2}{\sqrt{\widetilde{D}T_c}}\beta. \tag{3.91}$$

We now have a free energy barrier height with parameters that have been com-

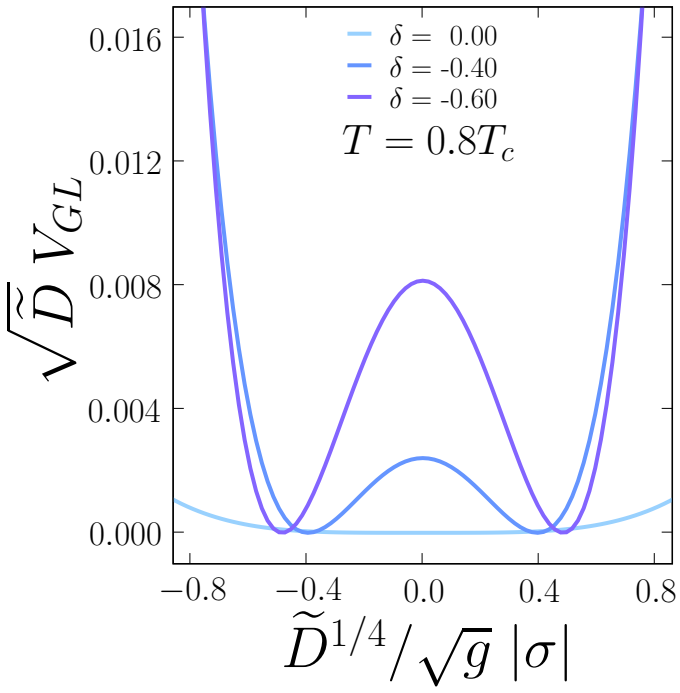

Figure 3.9: The Ginzburg-Landau potential of Eq. (3.77) for $\delta = 0.0, -0.4, -0.6$ using the values of T_c, α_0 and β found for $f(\epsilon) = \pi^2$ at $T = 0.8T_c$.

puted directly from the non-linear sigma model version of the full quantum theory,

$$\begin{aligned}
\Delta F &= -\frac{\alpha^2}{2\beta} \\
&= -\frac{\overline{\alpha}_0^2}{2\overline{\beta}} \frac{f(\epsilon) T_c^{3/2}}{\delta} \left(1 - \frac{T}{T_c}\right)^{3/2} \\
&= -T_c \frac{\sqrt{2\pi} f^3(\epsilon)}{4(1+\epsilon)^3} \left(\frac{\sqrt{T_c}}{\delta}\right)^3 \left(1 - \frac{T}{T_c}\right)^{3/2} \\
&\quad \times \frac{\left\{ \frac{\pi(1+\epsilon)}{f(\epsilon)} \frac{\delta^2}{T_c} + 4 \left[\frac{(1+\epsilon)\delta}{f(\epsilon)\sqrt{2\pi T_c}}\right]^4 \psi^{(1)}\left[\frac{(1+\epsilon)^2\delta^2}{f^2(\epsilon) 2\pi T_c}\right] - 1 \right\}^2}{c_2(\epsilon) - \frac{(1+\epsilon)\delta}{f(\epsilon)\sqrt{2\pi T_c}} \psi^{(1)}\left[\frac{(1+\epsilon)^2\delta^2}{f^2(\epsilon) 2\pi T_c}\right]}
\end{aligned} \tag{3.92}$$

which can be written in terms of a dimensionless scaling function of two unique scaling variables, the first expressing the classical and the second the quantum nature of the barrier height

$$\Delta F = T_c \Phi_{\Delta F}\left(\frac{T}{T_c}, \frac{\delta}{\sqrt{T_c}}\right). \tag{3.93}$$

ΔF can now be directly inserted into the LAMH theory in place of the phase slip

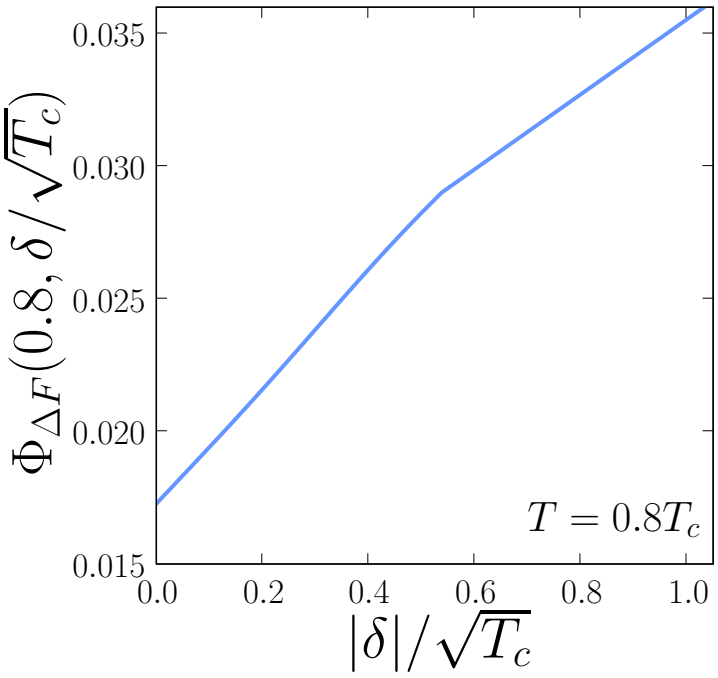

Figure 3.10: The dimensionless free energy barrier height corresponding to Eq. (3.89) as a function of a single scaling variable $\delta/\sqrt{T_c}$.

barrier height calculated by Langer and Ambegaokar, with the rest of the arguments leading to the LAMH resistance remaining unaffected.

Before this is done, we remark on the seemingly sneaky way in which we have written Eq. (3.93). The ability to write the barrier height as a cutoff independent scaling function with no explicit dependence on Λ or $f(\epsilon)$ is due to the fact that by fixing the dimensionless variable $\delta/\sqrt{T_c}$ a unique value of ϵ and thus $f(\epsilon)$ can be found from Eq (3.79). This is demonstrated in Fig. 3.10 where it appears that $\Phi_{\Delta F}$ is nearly a linear function of $\delta/\sqrt{T_c}$, with a slight kink for $T = 0.8T_c$. Therefore, using the same method as discussed in Section 3.1.1 we can write the quantum renormalized LAMH conductivity in terms of the scaling function $\Phi_{\Delta F}$ as

$$\sigma_{\mathrm{QRLAMH}} = 4\pi \frac{e^2}{h} \sqrt{\frac{\hbar D}{k_{\mathrm{B}} T_c}} \frac{f(\epsilon)}{c_1(\epsilon)\sqrt{\Phi_{\Delta F}(\delta/\sqrt{T_c})}} \left(\frac{T}{T_c}\right)^{3/2} \left(1 - \frac{T}{T_c}\right)^{-3/2} \times \exp\left[\Phi_{\Delta F}\left(\frac{\delta}{\sqrt{T_c}}\right)\frac{T_c}{T}\right]. \tag{3.94}$$

By the same argument given above for the cutoff independence of $\Phi_{\Delta F}$ and equating the thermal length with the wires length at T_c (which is suitable for the crossover

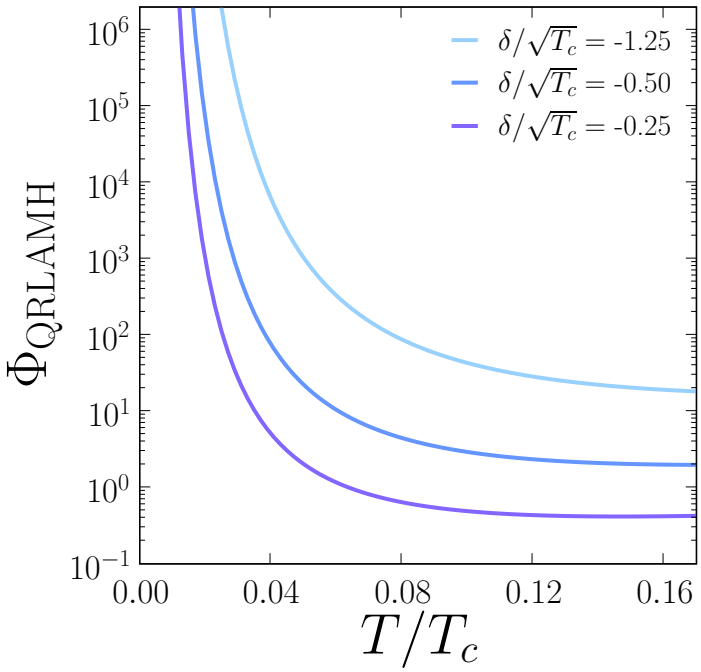

Figure 3.11: The quantum renormalized LAMH scaling function for the conductivity plotted as a function of the reduced temperature for three values of $\delta/\sqrt{T_c} = -1.25, -0.5, -0.25$.

behavior expected here at finite temperatures) we have

$$\sigma_{\mathrm{QRLAMH}} = L\,\frac{e^2}{h}\Phi_{\mathrm{QRLAMH}}\left(\frac{T}{T_c}, \frac{\delta}{\sqrt{T_c}}\right) \tag{3.95}$$

where Φ_{QRLAMH} is shown in Fig. 3.11. The arguments discussed in Section 2.5.1 provide a recipe to convert the parameter δ to the physical pair-breaking frequency α for a given experimental geometry. The suppression of the critical temperature as a result of an external magnetic field directed parallel to the wire has been observed in Ref. [44]. Thus, in principle, the relationship between δ and T_c could be determined experimentally from a fitting procedure, and the expression for the conductivity in Eq. (3.95) could be applied to the experimental transport results with one less fitting parameter than the form currently used in Eq. (3.3).

3.4 Large-N expansion

At low temperatures, away from the quantum critical point ($\sqrt{T} \ll \delta$), quantum fluctuations are large and we may now have finite Matsubara frequencies which lie

within the gap. Thus the classical model of Section 3.2.1 is not an adequate description of superconducting fluctuations. In this regime of the phase diagram we may however use the direct $1/N$ expansion on the full quantum theory. Starting with the effective action Eq. (3.5) and decoupling the quartic interaction with a Hubbard-Stratonovich field μ we arrive at the effective action

$$\mathcal{S} = \int dx \int d\tau \left[\widetilde{D} |\partial_x \Psi_a(x,\tau)|^2 + i\mu(x,\tau)|\Psi_a(x,\tau)|^2 + \frac{1}{2u}\mu^2(x,\tau) + i\frac{\alpha}{u}\mu(x,\tau) \right] + T\sum_{\omega_n} \int dx\, |\omega_n| |\Psi_a(x,\omega_n)|^2. \tag{3.96}$$

Integrating out Ψ_a over its now quadratic action, we as usual recognize an overall factor of N which allows us to perform the functional integral of the Hubbard-Stratonovich field μ in the saddle point approximation where we identify $R = i\mu$. In the universal limit we arrive at the new quadratic effective action

$$\mathcal{S}_R = \int \frac{dk}{2\pi} T \sum_{\omega_n} \Psi_a^*(k,\omega_n)(\widetilde{D}k^2 + |\omega_n| + R)\Psi_a(k,\omega_n), \tag{3.97}$$

where the 'mass' R is defined by the saddle point condition

$$\frac{1}{g} = \int \frac{dk}{2\pi} T \sum_{\omega_n} \frac{1}{\widetilde{D}k^2 + |\omega_n| + R}. \tag{3.98}$$

The evaluation of R is straightforward and follows our derivation of Eq (3.24)

$$\frac{\delta}{\sqrt{T}} = \int \frac{dk}{2\pi^2} \left[\ln\left(\frac{2\pi}{k^2}\right) + \psi\left(1 + \frac{k^2 + R/T}{2\pi}\right) - \frac{\pi}{k^2 + R/T} \right]. \tag{3.99}$$

In general, this expression must be inverted numerically to determine R/T as a function of $\delta/\sqrt{T}$ as is shown in Fig. 3.12. However, at the quantum critical point (QC, $\delta = 0$) and in the metallic (M,$\delta \to \infty$) and superconducting (SC, $\delta \to -\infty$) we can analyze Eq. (3.99) along the same lines as was done for Eq. (3.24) in Section 3.2.1. We write $R = T\Phi_R(\delta/\sqrt{T})$ and find the following results

$$\Phi_R(x) \simeq \begin{cases} 1/4x^2 & ; \quad x \to -\infty \\ 0.625 & ; \quad x \ll 1 \\ \pi^2 x^2 & ; \quad x \to \infty \end{cases}. \tag{3.100}$$

Understanding the behavior of the effective mass will be crucial in the following sections where we first define and then calculate the thermal and electrical transport coefficients in the zero frequency limit.

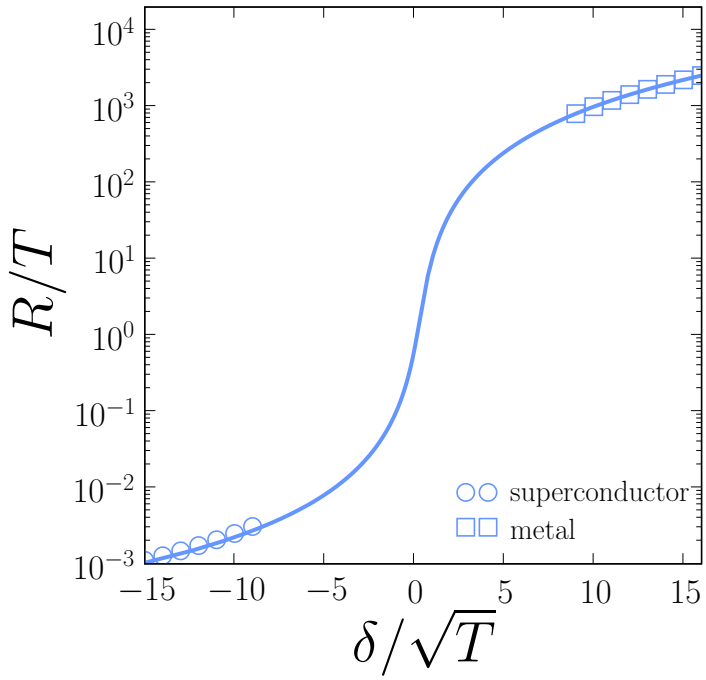

Figure 3.12: The renormalized mass R plotted as a function of the rescaled distance from criticality $\delta/\sqrt{T}$. The symbols refer to the analytic results of Eq. (3.100) in the metallic and superconducting limits.

3.4.1 Thermoelectric transport

The electrical (σ) and thermal (κ) conductivities and the Peltier coefficient (α) are defined in terms of the electrical $\boldsymbol{j}_0$ and thermal $\boldsymbol{j}_2$ current densities via the relation

$$\begin{pmatrix} \boldsymbol{j}_0 \\ \boldsymbol{j}_2 \end{pmatrix} = \begin{pmatrix} \sigma & \alpha \\ \alpha T & \tilde{\kappa} \end{pmatrix} \begin{pmatrix} \boldsymbol{E} \\ -\boldsymbol{\nabla} T \end{pmatrix}, \tag{3.101}$$

where $\boldsymbol{E}$ is an external electric field, $\boldsymbol{\nabla} T$ is an imposed temperature gradient and $\kappa/T = \tilde{\kappa}/T - \alpha^2/\sigma$. The current operators can also be defined in terms of the derivatives of our large-N action $\mathcal{S}_R$

$$j_0 = \frac{\partial \mathcal{S}_R}{\partial A_0} \tag{3.102a}$$

$$j_2 = \frac{\partial \mathcal{S}_R}{\partial A_2} \tag{3.102b}$$

where A_0 is the scalar electric potential and A_2 is the thermal vector potential, after we have made it gauge-covariant through the introduction of these two gauge fields [119] via the replacement

$$\partial_x \to \mathcal{D} \equiv \partial_x - ie^* A_0(x,\tau) - iA_2(x,\tau)(i\partial_\tau) \tag{3.103}$$

leading to

$$j_0 = ie^*\widetilde{D}\left[\psi^*\mathcal{D}\psi - \psi(\mathcal{D}\psi)^*\right] \tag{3.104}$$

$$j_2 = \widetilde{D}\left[\partial_\tau\psi(\mathcal{D}\psi)^* + \mathcal{D}\psi\partial_\tau\psi^*\right]. \tag{3.105}$$

where $e^* = 2e$ is the charge of a Cooper pair.

We now employ the quantum Kubo formula [114, 120], to obtain results for the thermoelectric conductivities at external frequency $i\omega_n$ (where we ignore the Peltier coefficient as its dc part will turn out to be identically zero)

$$\begin{aligned}\mathcal{G}_p(i\omega_n) &= -\frac{1}{\omega_n T^p}\frac{\partial}{\partial A_p}\left\langle\frac{\partial S}{\partial A_p}\right\rangle\Big|_{A_0=A_2=0} \\ &= -\frac{1}{\omega_n T^p}\left[\int_0^\beta d\tau\langle J_p(\tau)J_p(0)\rangle e^{i\omega_n\tau} - 2e^{*2-p}\widetilde{D}\int dx\left\langle\left|\partial_\tau^{p/2}\psi(x,0)\right|^2\right\rangle\right]\end{aligned} \tag{3.106}$$

where the currents are defined by

$$J_p(\tau) = ie^{*1-p/2}\widetilde{D}\int dx\left[\partial_\tau^{p/2}\psi^*(x,\tau)\partial_x\psi(x,\tau) - (-1)^{p/2}\partial_x\psi^*(x,\tau)\partial_\tau^{p/2}\psi(x,\tau)\right] \tag{3.107}$$

and $p = 0$ corresponds to the electrical conductivity while $p = 2$ defines the thermal conductivity, i.e. $\sigma(i\omega_n) = \mathcal{G}_0(i\omega_n)$ and $\kappa(i\omega_n)/T = \mathcal{G}_2(i\omega_n)$.

We express the conductivities in terms of a one-loop polarization function,

$$\mathcal{G}_p(i\omega_n) = -\frac{4\widetilde{D}^2 e^{*2-p}}{\omega_n T^p}\mathcal{K}_p(i\omega_n) \tag{3.108}$$

which contains both paramagnetic and diamagnetic contributions

$\mathcal{K}_p(i\omega_n) =$ 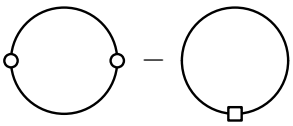

$$\begin{aligned}&= T\sum_{\epsilon_n}\int\frac{dk}{2\pi}k^2\left(\epsilon_n + \frac{\omega_n}{2}\right)^p\left[\frac{1}{(|\omega_n| + \widetilde{D}k^2 + R)(|\omega_n + \epsilon_n| + \widetilde{D}k^2 + R)}\right. \\ &\qquad\left. - \frac{1}{(|\omega_n| + \widetilde{D}k^2 + R)^2}\right],\end{aligned} \tag{3.109}$$

where a solid line represents the bare propagator $G_0(k,\omega_n) = (\widetilde{D}k^2 + |\omega_n| + R)^{-1}$, an open circle corresponds to a term linear in the potential A_p and an open square

to a term quadratic in A_p. We will employ the spectral representation for the bare propagator

$$\begin{aligned}\mathcal{A}(k,\omega) &= -2\mathrm{Im}\, G_0(k, i\omega_n \to \omega + i\eta) \\ &= -\frac{2\omega}{\omega^2 + (\widetilde{D}k^2 + R)^2}\end{aligned} \tag{3.110}$$

where a $|\omega_n|$ dependence along the imaginary frequency axis becomes $-i\omega$ just above the real frequency axis. The polarization function is then given by

$$\begin{aligned}\mathcal{K}_p(i\omega_n) = T\sum_{\epsilon_n}\int\frac{dk}{2\pi}k^2\int\frac{d\omega_1}{2\pi}\int\frac{d\omega_2}{2\pi}\left(\frac{\omega_1+\omega_2}{2}\right)^p \mathcal{A}(k,\omega_1)\mathcal{A}(k,\omega_2) \\ \times\left[\frac{1}{(i\epsilon_n-\omega_1)(i(\epsilon_n+\omega_n)-\omega_2)} - \frac{1}{(i\epsilon_n-\omega_1)(i\epsilon_n-\omega_2)}\right],\end{aligned} \tag{3.111}$$

where we have made the replacement $(\epsilon_n + \omega_n/2) \to (\omega_1+\omega_2)/2$, due to the temporal non-locality of j_2 [119, 121]. Performing the Matsubara sum, and analytically continuing to real frequencies yields

$$\begin{aligned}\mathcal{K}_p(\omega+i\epsilon) = \int\frac{dk}{2\pi}\int\frac{d\omega_1}{2\pi}\int\frac{d\omega_2}{2\pi}\left(\frac{\omega_1+\omega_2}{2}\right)^p \mathcal{A}(k,\omega_1)\mathcal{A}(k,\omega_2)k^2 \\ \times\ [n(\omega_1)-n(\omega_2)]\left(\frac{1}{\omega_2-\omega_1-\omega-i\eta} - \frac{1}{\omega_2-\omega_1}\right),\end{aligned} \tag{3.112}$$

where

$$n(\omega) = \frac{1}{\mathrm{e}^{\omega/T}-1} \tag{3.113}$$

is the Bose distribution function, and η is a positive infinitesimal. After checking that the delta-function contribution to $\mathrm{Re}\,\mathcal{G}_p(\omega)$ at zero frequency is proportional to the external frequency, i.e. it vanishes as $\omega \to 0$, we can combine Eqs. (3.108) and (3.112) to give the remaining regular part

$$\begin{aligned}\mathrm{Re}\,\mathcal{G}_p(\omega) = \frac{4\widetilde{D}^2 e^{*2-p}}{T^p}\int\frac{d\Omega}{\pi}\frac{[n(\Omega)-n(\Omega+\omega)]}{\omega}\left(\Omega+\frac{\omega}{2}\right)^p \\ \times\int\frac{dk}{2\pi}\frac{k^2\Omega(\Omega+\omega)}{[\Omega^2+(\widetilde{D}k^2+R)^2][(\Omega+\omega)^2+(\widetilde{D}k^2+R)^2]}.\end{aligned} \tag{3.114}$$

The classical limit of Eq. (3.114) corresponding to replacing $n(\omega) \simeq T/\omega$ is examined in Appendix A but here we directly perform the limit $\omega \to 0$ and obtain the quantum dc conductivities

$$\begin{aligned}\mathrm{Re}\,\mathcal{G}_p &= \frac{\widetilde{D}^2 {e^*}^{2-p}}{T^{p+1}}\int\frac{d\Omega}{\pi}\frac{\Omega^{2+p}}{\sinh^2(\Omega/2T)}\int\frac{dk}{2\pi}\frac{k^2}{[\Omega^2+(\widetilde{D}k^2+R)^2]^2} \\ &= \frac{\sqrt{2}e^{*2-p}\sqrt{\widetilde{D}}}{8T^{p+1}}\int\frac{d\Omega}{2\pi}\frac{\Omega^{2+p}}{\sinh^2(\Omega/2T)}\frac{1}{\sqrt{\Omega^2+R^2}\left(R+\sqrt{\Omega^2+R^2}\right)^{3/2}}.\end{aligned} \tag{3.115}$$

which is the major result of this section. From this expression it is immediately clear that the Peltier coefficient α (corresponding to $p = 1$) is identically zero by symmetry, and thus $\tilde{\kappa} = \kappa$.

In addition to the scaling function Φ_σ defined for the electrical conductivity in Eq. (3.50) and given by

$$\sigma = \frac{e^{*2}}{\hbar}\sqrt{\frac{\hbar\widetilde{D}}{k_{\rm B}T}}\Phi_\sigma\left(\frac{\delta}{\sqrt{\hbar k_{\rm B}T}}\right) \tag{3.116}$$

the thermal conductivity must obey a similar form

$$\frac{\kappa}{T} = \frac{k_{\rm B}^2}{\hbar}\sqrt{\frac{\hbar\widetilde{D}}{k_{\rm B}T}}\Phi_\kappa\left(\frac{\delta}{\sqrt{\hbar k_{\rm B}T}}\right), \tag{3.117}$$

where we have re-inserted the appropriate factors of $\hbar$ and $k_{\rm B}$ for clarity.

The $\delta/\sqrt{T}$ dependence of Φ_σ and Φ_κ can be found by numerically inverting Eq. (3.99), (Fig. 3.12) and the result is shown in Fig. 3.13. We can now compare the large-N result with the previously calculated value in Section 3.2.2 for $N = 1$. The quantitative agreement is not striking, but the two results have similar $\delta/\sqrt{T}$ dependence near $\delta = 0$ indicating that the correct physics are manifest even at $N = \infty$. The temperature dependence of the transport functions is found by fixing δ leading to the results displayed in Fig. 3.14 and 3.15. The singular correction to the electrical conductivity clearly shows behavior consistent with a quantum phase transition between a superconductor (diverging conductivity) and metal (finite or vanishing conductivity). Moreover, the inset shows that for a fixed value of δ which places us not too far into the metallic phase, as we lower the temperature a crossover can be seen from an increasing to decreasing conductivity. As mentioned in the introduction, experiments have seen evidence of such non-monotonic resistance in the metallic regime, and this strongly supports the crossover picture we have presented here.

We now attempt to quantify these crossovers by investigating the limiting forms of the two scaling functions Φ_σ and Φ_κ.

Limiting forms of σ an $\kappa/\mathbf{T}$

We can obtain analytical estimates for the electrical and thermal conductivity in three distinct limits using the results of Eq. (3.100). The first is deep in the superconducting (SC) regime where $\delta/\sqrt{T} \to -\infty$ or $R/T \to 0$. The next is at the quantum critical point (QC), where $\delta = 0$ or $R/T = 0.624798$ and the final regime is on the metallic side of the transition (M) where $\delta, R/T \to \infty$. For low temperatures,

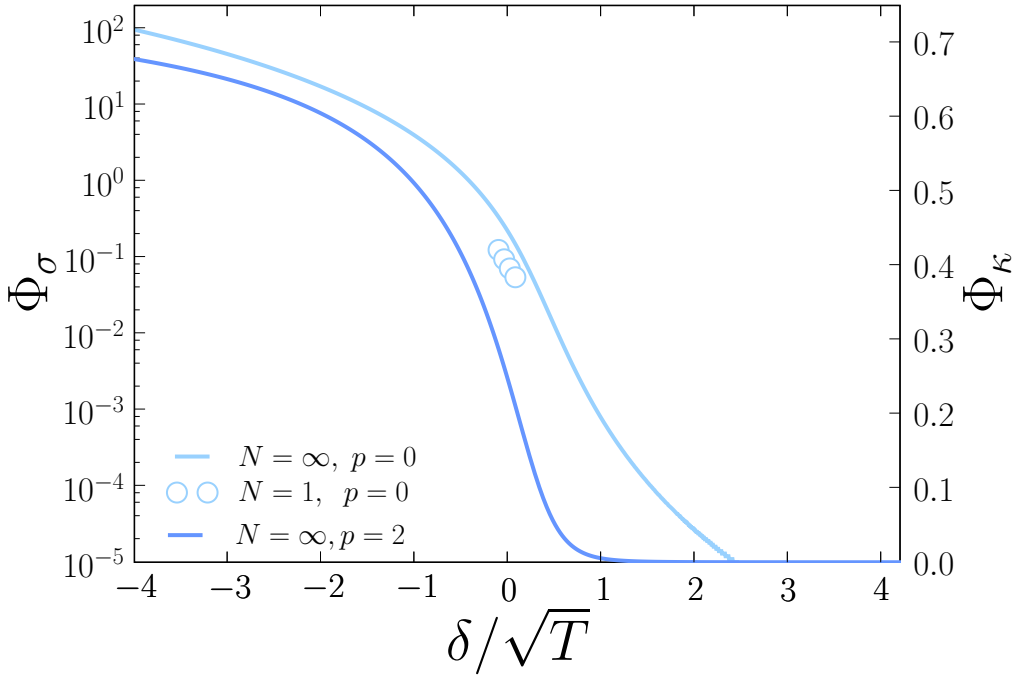

Figure 3.13: The solid lines show the $N = \infty$ universal scaling functions the electrical ($p = 0$, left axis) and thermal ($p = 2$, right axis) conductivity calculated by integration of Eq. (3.115). The symbols show the effective classical scaling function for the electrical conductivity calculated in the Langevin formalism in Section 3.2.2 and previously shown in Fig. 3.3 for a one component complex field.

we can evaluate Eq. (3.115) in these three limits leading to

$$\sigma = e^{*2}\sqrt{\frac{\widetilde{D}}{T}}\begin{cases} \frac{1}{8}\left(\frac{R}{T}\right)^{-3/2} & ; \quad SC \\ 0.217997\cdots & ; \quad QC \\ \frac{\pi}{12}\left(\frac{R}{T}\right)^{-5/2} & ; \quad M \end{cases} \tag{3.118}$$

$$\frac{\kappa}{T} = \sqrt{\frac{\widetilde{D}}{T}}\begin{cases} \frac{3}{4\sqrt{2\pi}}\zeta\left(\frac{3}{2}\right) & ; \quad SC \\ 0.24592\cdots & ; \quad QC \\ \frac{\pi^3}{15}\left(\frac{R}{T}\right)^{-5/2} & ; \quad M \end{cases} . \tag{3.119}$$

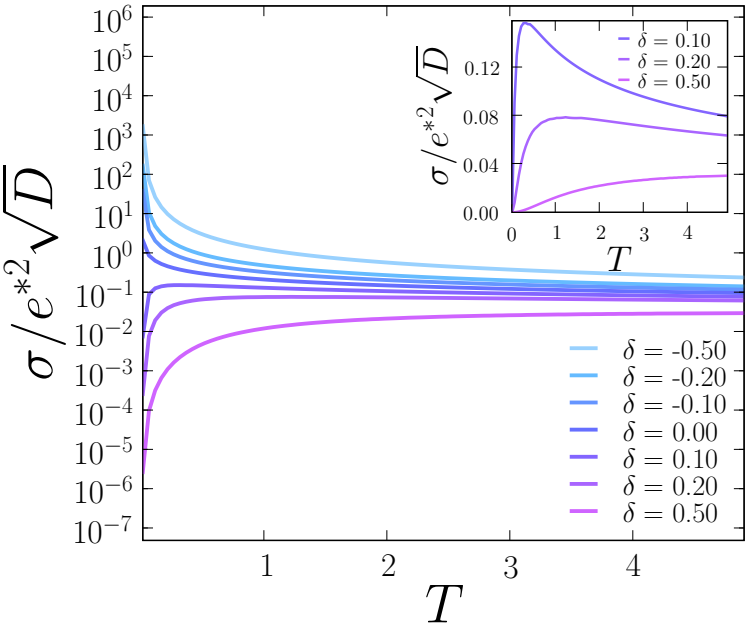

Figure 3.14: The temperature dependence of dc electrical conductivity at fixed values of δ. The inset shows non-monotonic behavior just above the quantum critical point defined by $\delta = 0$.

and using Eq. (3.100)

$$\Phi_\sigma(x) = \begin{cases} x^3 & ; \quad SC \\ 0.217997\cdots & ; \quad QC \\ (12\pi^4 x^5)^{-1} & ; \quad M \end{cases} \tag{3.120}$$

$$\Phi_\kappa(x) = \begin{cases} \frac{3}{4\sqrt{2\pi}}\zeta\left(\frac{3}{2}\right) & ; \quad SC \\ 0.24592\cdots & ; \quad QC \\ (15\pi^2 x^5)^{-1} & ; \quad M \end{cases} . \tag{3.121}$$

The temperature dependence of these results are summarized in Table 3.1. We have now derived the exact form of the temperature dependence describing the crossover behavior, with the conductivity increasing like $1/\sqrt{T}$ at high temperatures while the system is in the quantum critical regime of Fig. 2.1 and finally decreasing as T^2 after we have fully returned to metallic behavior. Although we are about to show that a microscopic theory reproduces the T^2 metallic conduction, the $1/\sqrt{T}$ dependence of the conductivity is not present in the simple Gaussian theory and an accurate determination of the full crossover phase diagram necessitates the inclusion of interactions between Cooper pairs.

We now comment on a shared regime of validity between our large-N theory and the disordered electron perturbation theory of Ref. [83]. A closer investigation of the

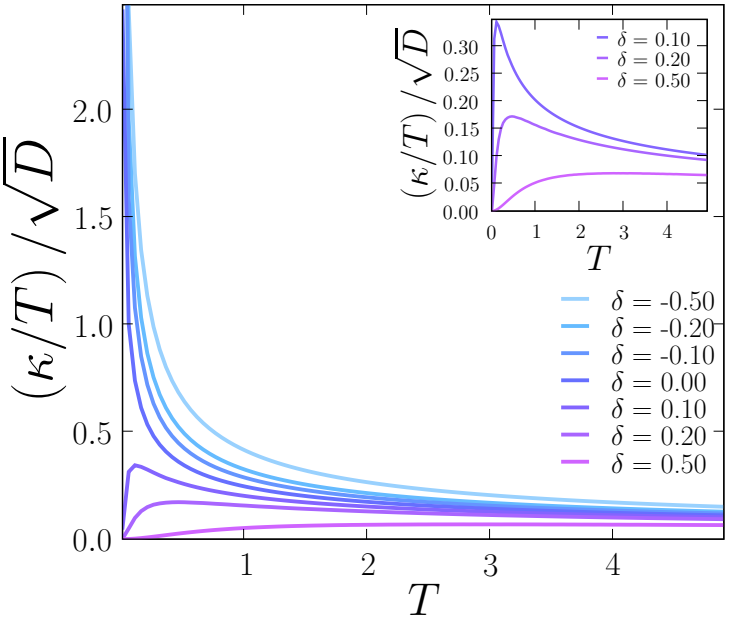

Figure 3.15: The temperature dependence of dc electrical conductivity at fixed values of δ. The inset shows non-monotonic behavior just above the quantum critical point defined by $\delta = 0$.

dc electrical conductivity in the metallic regime with careful attention to all prefactors yields

$$\sigma = \frac{e^{*2}}{\hbar} \frac{\pi \sqrt{\widetilde{D}} T^2}{12 R^{5/2}}. \tag{3.122}$$

We note that upon comparing the large-N propagator of Eq. (3.98) with Eq. (4) of Ref. [83] that *our* mass R is exactly double the mass α employed by Lopatin *et al.*, i.e. $R = 2[\alpha - \alpha_c(T)]$. Having made this identification, we may compare Eq. (3.122) above, with the finite temperature fluctuation correction to the normal state conductivity computed via diagrammatic perturbation theory (Eq. (8) in Ref. [83]), and find *exact* agreement. After a rather lengthy calculation it was confirmed that perfect correspondence is also found for the thermal conductivity in this limit [96]. The concurrence between the two theoretical approaches in this limit is a result of an approximation made in the diagrammatic calculation involving an infinite sum over a class of ladder diagrams which turns out to be equivalent to the large-N limit taken here.

	SC	**QC**	**M**
σ	$1/T^2$	$1/\sqrt{T}$	T^2
κ/T	$1/\sqrt{T}$	$1/\sqrt{T}$	T^2

Table 3.1: A summary of the temperature dependence of the electrical and thermal conductivity in the superconducting (SC), quantum critical (QC) and metallic (M) regimes.

3.5 Wiedemann-Franz ratio

The Wiedemann-Franz law relates the low temperature limit of the ratio

$$W \equiv \frac{\kappa}{\sigma T} \tag{3.123}$$

of the thermal and electrical conductivities of metals to the universal Lorenz number

$$l_0 = \frac{\pi^2}{3}\left(\frac{k_B}{e}\right)^2. \tag{3.124}$$

This remarkable relationship is independent of the strength of the interactions between the electrons, relates macroscopic transport properties to fundamental constants of nature, and depends only upon the Fermi statistics and charge of the elementary quasiparticle excitations of the metal. It has been experimentally verified to high precision in a wide range of metals [122], and realizes a sensitive macroscopic test of the quantum statistics of the charge carriers.

It is interesting to note the value of the Wiedemann-Franz ratio in some other important strongly interacting quantum systems. In superconductors, which have low energy bosonic quasiparticle excitations, σ is infinite for a range of $T > 0$, while κ is finite in the presence of impurities [123], and so $W = 0$. At quantum phase transitions described by relativistic field theories, such as the superfluid-insulator transition in the Bose Hubbard model, the low energy excitations are strongly coupled and quasiparticles are not well defined; in such theories the conservation of the relativistic stress-energy tensor implies that κ is infinite, and so $W = \infty$ [124]. In other words, any quantum critical point which exhibits Lorentz or Galilean invariance will have an infinite thermal conductivity since the boosted thermal distribution will never decay [90]. Li and Orignac [125] computed W in a disordered Luttinger liquid, and found deviations from L_0 leading to a non-zero universal value for W at the metal-insulator transition for spinless fermions. Finally Fazio *et al.* have computed the effects of plasmon scattering on the Lorenz number of thin wires coupled to reservoirs [126].

Upon examination of Table 3.1 it can immediately be seen that the Wiedemann-Franz ratio is temperature independent in both the quantum critical and metallic regimes. Remarkably, all important couplings between bosons and fermions scale to universal values, and consequently, by studying equations (3.118) and (3.119) we find the universal constant

$$W_{QC} = (0.28203\cdots)\left(\frac{k_B}{e}\right)^2 \tag{3.125}$$

in the quantum critical regime whereas in the metallic region of the phase diagram

$$W_M = \frac{\pi^2}{5}\left(\frac{k_B}{e}\right)^2. \tag{3.126}$$

Both of these corrections are smaller than the Lorenz number and thus it appears that the Cooper pairs tend to carry more charge than heat.

These results for the Wiedemann-Franz ratio conclude this chapter, but in the next chapter we will extend the theory presented here for $N = \infty$ to the first order in $1/N$. We will exploit the anomalous scaling dimension of the dynamical critical exponent z to find additional universal corrections to Eq. (3.125).

Chapter 4

$1/N$ Corrections to Transport

This chapter is quite heavy on calculational details and can be skipped by the casual reader. The main results include the derivation of a critical theory for a finite N component complex field Ψ_a governing the fluctuations of Cooper pairs near a superconductor-metal transition. This theory is used to systematically compute the $1/N$ corrections to critical exponents and the zero frequency transport coefficients calculated in the previous chapter at $N = \infty$ when the coupling parameter which drives the SMT attains its critical value. We will find (Eq. (4.86)) that although the individual values of the electrical and thermal conductivities are not universal, but depend explicitly on an ultra-violet cutoff, their Wiedemann-Franz ratio *is* a pure, temperature independent universal number proportional to $1/N$ that characterizes the most singular corrections to transport in the strongly fluctuating quantum critical regime

$$W = \left(0.282 + \frac{0.0376}{N}\right)\left(\frac{k_B}{e}\right)^2. \tag{4.1}$$

4.1 The critical theory

We begin by reintroducing the strong-coupling effective action of Eq. (3.11) for an N-component Cooper pair operator Ψ_a

$$\mathcal{S}_g = \frac{1}{g} T \sum_{\omega_n} \int \frac{dk}{2\pi} (k^2 + |\omega_n|) |\Psi_a(k, \omega_n)|^2 \tag{4.2}$$

where we have chosen to rescale distances by a factor of the square root of the effective diffusion constant $\widetilde{D}$ and must enforce the "hard spin" constraint $|\Psi(x,\tau)|^2 = 1$. Imposing the delta-function constraint via a Lagrange multiplier μ and performing a

rescaling of the field $\Psi_a \to \sqrt{g}\Psi_a$ we have the partition function

$$\mathcal{Z} = \int \mathcal{D}\Psi_a \mathcal{D}\Psi_a^* \mathcal{D}\mu \ \exp\left\{ - \int dx \int d\tau \left[\Psi_a^*(x,\tau) \left(-\partial_x^2 + |\partial_\tau| + i\mu(x,\tau) \right) \Psi_a(x,\tau) - \frac{N}{g} i\mu(x,\tau) \right] \right\}, \quad (4.3)$$

where we have again used the notation $|\partial_\tau|$ to infer $|\omega_n|$ after Fourier transforming. Integrating out the Ψ_a fields, we are left with

$$\mathcal{Z} = \int \mathcal{D}\mu \ \exp\left\{ -N \left[\mathrm{Tr} \ln \left(-\partial_x^2 + |\partial_\tau| + i\mu(x,\tau) \right) - \frac{i}{g} \int dx \int d\tau \mu(x,\tau) \right] \right\} \quad (4.4)$$

and as previously, for N large, we can approximate the functional integral over μ by its saddle point value defined to be $r = i\mu$ leading to

$$\frac{1}{g} = T \sum_{\omega_n} \int \frac{dk}{2\pi} \frac{1}{k^2 + |\omega_n| + r}. \quad (4.5)$$

This is an auspicious point to make a brief comment regarding the relationship between the notation introduced here and that of the previous chapter. Eq. (4.5) is identical to Eq. (3.98) with the replacement of $r \to R$. However, in this chapter, unless otherwise stated, we will be considering a critical theory (whether at zero or finite temperatures) with the coupling g equal to its critical value g_c which will be shifted from its $N = \infty$ value by a correction of order $1/N$. As a result, the effective mass r will be also corrected from its $N = \infty$ saddle point value. This will be made more explicit soon, but for now we simply indicate that $r = R + O(1/N)$ with R equal to its $N = \infty$ value defined by Eq. (3.98) with $g = g_c$.

Let us now look at fluctuations around the saddle point by defining $i\mu = r + i\lambda$, and after expanding to quadratic order in λ and noticing that with the help of Eq. (4.5) all linear terms cancel we have

$$\mathcal{Z} = \int \mathcal{D}\lambda \ \exp\left\{ -N \left[\mathrm{Tr} \ln(-\partial_x^2 + |\partial_\tau| + r) + \frac{1}{2} \sum_{\omega_n} \int \frac{dk}{2\pi} \lambda^2 \Pi_T(k, \omega_n, r) \right] \right\} \quad (4.6)$$

where

$$\Pi_T(k, \omega_n, r) = T \sum_{\epsilon_n} \int \frac{dq}{2\pi} \frac{1}{[(k+q)^2 + |\omega_n + \epsilon_n| + r](q^2 + |\epsilon_n| + r)} \quad (4.7)$$

can be thought of as the propagator for a λ field leading to $1/N$ fluctuations.

Upon examination of Eq. (4.6), we observe that we could have simply started from a partition function for our original field Ψ_a with an additional interaction term such

that its diagrammatic expansion is equivalent to that of Eq. (4.6), i.e.

$$\mathcal{Z} = \int \mathcal{D}\Psi_a \mathcal{D}\Psi_a^* \mathcal{D}\lambda \exp\left\{ -\int dx \int d\tau \left[\Psi_a^*(x,\tau)\left(-\partial_x^2 + |\partial_\tau| + r\right)\Psi_a(x,\tau) \right.\right. \\ \left.\left. + i\lambda(x,\tau)|\Psi_a(x,\tau)|^2 + \frac{N}{2}\int dx' \int d\tau' \lambda(x,\tau)\Pi_T(x-x',\tau-\tau',r)\lambda(x',\tau') \right] \right\} \tag{4.8}$$

leading to the effective action in momentum space

$$\mathcal{S}_r = T\sum_{\omega_n} \int \frac{dk}{2\pi} \left[(k^2 + |\omega_n| + r)|\Psi_a(k,\omega_n)|^2 + \frac{N}{2}|\lambda(k,\omega_n)|^2 \Pi_T(k,\omega_n,r) \right. \\ \left. + T\sum_{\epsilon_n} \int \frac{dq}{2\pi} \Psi_a^*(k,\omega_n)\Psi_a(q,\epsilon_n)\lambda(k-q,\omega_n-\epsilon_n) \right] \tag{4.9}$$

where we note that in order to avoid double-counting, the λ or fluctuation propagator Π_T cannot have a self-energy contribution of a single Ψ_a bubble (since it has already been included). Thus, performing a direct $1/N$ expansion from $\mathcal{Z}$ for $G(k,\omega_n) = \langle|\Psi_a(k,\omega_n)|^2\rangle$ [48] we have

$G(k,\omega_n) =$ 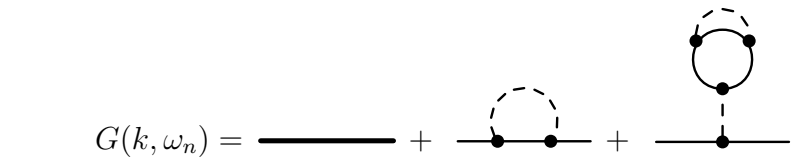 $+\cdots$ (4.10)

where a solid line is equal to $(k^2 + |\omega_n| + r)^{-1}$, a dashed line equal to Π_T/N and a solid dot represents the interaction vertex i. There is no tadpole graph as it is already included in the $1/N$ correction to the effective mass r. The third graph has two loops, but is only of order $1/N$ as we any closed Ψ_a loop gives a factor of N. Combining these graphs leads to

$$G^{-1}(k,\omega_n) = k^2 + |\omega_n| + r + \frac{1}{N}T\sum_{\epsilon_n}\int \frac{dq}{2\pi}\frac{1}{\Pi_T(q,\epsilon_n,r)}\frac{1}{((k+q)^2 + |\omega_n+\epsilon_n| + r)} \\ - \frac{1}{N}\frac{1}{\Pi_T(0,0,r)}T\sum_{\epsilon_n}\int\frac{dq}{2\pi}T\sum_{\nu_n}\int\frac{dp}{2\pi}\frac{1}{\Pi_T(q,\epsilon_n,r)} \\ \times \frac{1}{(p^2+|\nu_n|+r)^2[(p+q)^2+|\epsilon_n+\nu_n|+r]}. \tag{4.11}$$

4.1.1 Critical point at $T = 0$

Now let us determine the value of the critical coupling g_c to order $1/N$ at $T = 0$. At $T = 0$, the critical point is determined by the condition $G^{-1}(0,0) = 0$, $r = r_c$. So

keeping terms only up to order $1/N$

$$r_c = -\frac{1}{N}\int\frac{dk}{2\pi}\int\frac{d\omega}{2\pi}\frac{1}{\Pi_0(k,\omega,0)}\frac{1}{k^2+|\omega|} + \frac{1}{N}\frac{1}{\Pi_0(0,0,0)}\int\frac{dk}{2\pi}\int\frac{d\omega}{2\pi}\int\frac{dq}{2\pi}\int\frac{d\epsilon}{2\pi}\frac{1}{(k^2+|\omega|)^2[(k+q)^2+|\omega+\epsilon|]}\frac{1}{\Pi_0(q,\epsilon,0)} \tag{4.12}$$

where

$$\Pi_0(k,\omega,0) = \int\frac{dq}{2\pi}\int\frac{d\epsilon}{2\pi}\frac{1}{(q^2+|\epsilon|)[(k+q)^2+|\omega+\epsilon|]}$$
$$= \frac{1}{4\pi|k|}\left[2\arcsin\left(\frac{k^2-|\omega|}{k^2+|\omega|}\right)+\pi\right] \tag{4.13}$$
$$+ \frac{1}{4\pi\sqrt{k^2+2|\omega|}}\ln\left(\frac{2\sqrt{|\omega|}\sqrt{k^2+2|\omega|}+k^2+3|\omega|}{|2\sqrt{|\omega|}\sqrt{k^2+2|\omega|}-k^2-3|\omega||}\right) \tag{4.14}$$

with details given in Appendix B. Note that $\Pi_0(0,0,0)$ is infrared divergent, but this will shortly cancel out of observable quantities. Inserting the expansion for r_c in Eq. (4.5), we obtain

$$\frac{1}{g_c} = \int\frac{dk}{2\pi}\int\frac{d\omega}{2\pi}\frac{1}{k^2+|\omega|} + \frac{\Pi_0(0,0,0)}{N}\int\frac{dk}{2\pi}\int\frac{d\omega}{2\pi}\frac{1}{\Pi_0(k,\omega,0)}\frac{1}{k^2+|\omega|}$$
$$- \frac{1}{N}\int\frac{dk}{2\pi}\int\frac{d\omega}{2\pi}\int\frac{dq}{2\pi}\int\frac{d\epsilon}{2\pi}\frac{1}{(k^2+|\omega|)^2[(k+q)^2+|\omega+\epsilon|]}\frac{1}{\Pi_0(q,\epsilon,0)}$$
$$= \int\frac{dk}{2\pi}\int\frac{d\omega}{2\pi}\frac{1}{k^2+|\omega|} + \frac{1}{N}\int\frac{dk}{2\pi}\int\frac{d\omega}{2\pi}\int\frac{dq}{2\pi}\int\frac{d\epsilon}{2\pi}\frac{1}{\Pi_0(q,\epsilon,0)(k^2+|\omega|)^2}$$
$$\times\left[\frac{1}{q^2+|\epsilon|}-\frac{1}{(k+q)^2+|\omega+\epsilon|}\right] \tag{4.15}$$

which is free of infrared divergences.

4.1.2 Quantum critical propagator

Now let us move to $T>0$ at $g=g_c$ where we write $r = R+\widetilde{R}_1$ with $\widetilde{R}_1 \sim O(1/N)$. As mentioned previously, R is determined by setting $r=R$ in Eq. (4.5) when $g=g_c$ takes its $N=\infty$ value

$$T\sum_{\omega_n}\int\frac{dk}{2\pi}\frac{1}{k^2+|\omega_n|+R} = \int\frac{dk}{2\pi}\int\frac{d\omega}{2\pi}\frac{1}{k^2+|\omega|}. \tag{4.16}$$

We have seen this equation before in Eq. (3.98) with $g=g_c$ and can thus express it as Eq. (3.99) with $\delta=0$ giving an equation that can be inverted to uniquely determine

R/T,

$$0 = \int \frac{dk}{2\pi} \left[\frac{\pi T}{k^2 + R} - \psi \left(1 + \frac{k^2 + R}{2\pi T} \right) + \ln \left(\frac{k^2}{2\pi T} \right) \right] \tag{4.17}$$

where $\psi(x)$ is the polygamma function. Solving numerically we find

$$\frac{R}{T} \simeq 0.624798. \tag{4.18}$$

Now, returning to Eq. (4.5) we can write (to order $1/N$)

$$\begin{aligned} \frac{1}{g_c} &= T \sum_{\omega_n} \int \frac{dk}{2\pi} \frac{1}{k^2 + |\omega_n| + R + \widetilde{R}_1} \\ &= T \sum_{\omega_n} \int \frac{dk}{2\pi} \frac{1}{k^2 + |\omega_n| + R} - \Pi_T(0,0,R) \widetilde{R}_1 \end{aligned} \tag{4.19}$$

which can be compared with our expression for $1/g_c$ in Eq. (4.15) order by order to yield

$$\begin{aligned} \widetilde{R}_1 = -\frac{1}{N \Pi_T(0,0,R)} \int \frac{dk}{2\pi} \int \frac{d\omega}{2\pi} \int \frac{dq}{2\pi} \int \frac{d\epsilon}{2\pi} \frac{1}{(k^2 + |\omega|)^2} \frac{1}{\Pi_0(q,\epsilon,0)} \\ \times \left[\frac{1}{q^2 + |\epsilon|} - \frac{1}{(k+q)^2 + |\omega + \epsilon|} \right] \end{aligned} \tag{4.20}$$

and note that $\sqrt{T}\ \Pi_T(0,0,R)$ is a finite universal number given by (see Appendix B)

$$\sqrt{T}\ \Pi_T(0,0,R) = \frac{1}{4(2\pi)^{3/2}} \left[\zeta \left(\frac{3}{2}, \frac{R}{2\pi T} \right) + \zeta \left(\frac{3}{2}, \frac{R}{2\pi T} + 1 \right) \right], \tag{4.21}$$

where $\zeta(m,x)$ is the Hurwitz Zeta function.

Inserting everything in Eq. (4.11) we write

$$G^{-1}(k,\omega_n) = k^2 + |\omega_n| + R + R_1 + \Sigma(k,\omega_n) \tag{4.22}$$

where the self energy $\Sigma(k,\omega_n)$ is defined to be

$$\Sigma(k,\omega_n) = \frac{1}{N} T \sum_{\epsilon_n} \int \frac{dq}{2\pi} \frac{1}{\Pi_T(q,\epsilon_n,R)} \left[\frac{1}{(k+q)^2 + |\omega_n + \epsilon_n| + R} - \frac{1}{q^2 + |\epsilon_n| + R} \right] \tag{4.23}$$

such that $\Sigma(0,0) = 0$, and

$$\begin{aligned} R_1 = -\frac{1}{N \Pi_T(0,0,R)} \int \frac{dk}{2\pi} \int \frac{d\omega}{2\pi} \int \frac{dq}{2\pi} \int \frac{d\epsilon}{2\pi} \frac{1}{(k^2 + |\omega|)^2} \frac{1}{\Pi_0(q,\epsilon,0)} \\ \times \left[\frac{1}{q^2 + |\epsilon|} - \frac{1}{(k+q)^2 + |\omega + \epsilon|} \right] \\ - \frac{1}{\Pi_T(0,0,R)} T \sum_{\omega_n} \int \frac{dk}{2\pi} \frac{1}{(k^2 + |\omega_n| + R)^2} \Sigma(k,\omega_n). \end{aligned} \tag{4.24}$$

This is equivalent to Eq. (4.6) in Ref. [127]. It will be useful to interchange the orders of integration in both terms and write

$$R_1 = \frac{1}{N\Pi_T(0,0,R)}\left\{ -\int\frac{dq}{2\pi}\int\frac{d\epsilon}{2\pi}\frac{1}{\Pi_0(q,\epsilon,0)}\int\frac{dk}{2\pi}\int\frac{d\omega}{2\pi}\frac{1}{(k^2+|\omega|)^2} \right. \\ \times\left[\frac{1}{q^2+|\epsilon|}-\frac{1}{(k+q)^2+|\omega+\epsilon|}\right] \\ + T\sum_{\epsilon_n}\int\frac{dq}{2\pi}\frac{1}{\Pi_T(q,\epsilon,R)}T\sum_{\omega_n}\int\frac{dk}{2\pi}\frac{1}{(k^2+|\omega_n|+R)^2} \\ \left.\times\left[\frac{1}{(q^2+|\epsilon_n|+R)}-\frac{1}{(k+q)^2+|\omega_n+\epsilon_n|+R)}\right]\right\}. \quad (4.25)$$

Now, both the inner integral or sum over (k,ω) and (k,ω_n) is ultraviolet convergent, but the outer integral appears to be divergent. We carefully re-arrange the integral as follows (where we now explicitly indicate the integration bounds)

$$R_1 = \frac{1}{N\Pi_T(0,0,R)}\left\{ -\int_{-\Lambda^2}^{\Lambda^2}\frac{d\omega}{2\pi}\int_{-\Lambda}^{\Lambda}\frac{dk}{2\pi}\frac{1}{\Pi_0(k,\omega,0)} \right. \\ \times\int_{-\infty}^{\infty}\frac{dq}{2\pi}\int_{-\infty}^{\infty}\frac{d\epsilon}{2\pi}\frac{1}{(q^2+|\epsilon|)^2}\left[\frac{1}{k^2+|\omega|}-\frac{1}{(k+q)^2+|\omega+\epsilon|}\right] \\ \left.+T\sum_{|\omega_n|<\Lambda^2}\int_{-\Lambda}^{\Lambda}\frac{dk}{2\pi}\frac{1}{\Pi_T(k,\omega_n,R)}\left[\frac{\Pi_T(0,0,R)}{k^2+|\omega_n|+R}+\frac{1}{2}\frac{\partial\Pi_T(k,\omega_n,R)}{\partial R}\right]\right\}, \quad (4.26)$$

where Λ is an ultra-violet momentum cutoff. This expression can be evaluated numerically for a fixed Λ by rescaling the integration variables to be dimensionless such that

$$\frac{R_1}{T} = \frac{1}{N}\frac{8\sqrt{2}\pi^{3/2}}{\zeta(3/2,R/2\pi T)+\zeta(3/2,R/2\pi T+1)} \\ \times\left\{ -\int_{-\Lambda^2/T}^{\Lambda^2/T}\frac{d\omega}{2\pi}\int_{-\Lambda/\sqrt{T}}^{\Lambda/\sqrt{T}}\frac{dk}{2\pi}\frac{1}{\Pi_0(k,\omega,0)}\int_{-\infty}^{\infty}\frac{dq}{2\pi}\int_{-\infty}^{\infty}\frac{d\epsilon}{2\pi}\frac{1}{(q^2+|\epsilon|)^2} \right. \\ \times\left[\frac{1}{k^2+|\omega|}-\frac{1}{(k+q)^2+|\omega+\epsilon|}\right]+T\sum_{2\pi|n|<\Lambda^2/T}\int_{-\Lambda/\sqrt{T}}^{\Lambda/\sqrt{T}}\frac{dk}{2\pi}\frac{1}{\Pi_T(k,2\pi n,R/T)} \\ \left.\times\left[\frac{\zeta(3/2,R/2\pi T)+\zeta(3/2,R/2\pi T+1)}{(8\sqrt{2}\pi^{3/2})(k^2+2\pi|n|+R/T)}+\frac{1}{2}\frac{\partial\Pi_T(k,2\pi n,R/T)}{\partial(R/T)}\right]\right\}. \quad (4.27)$$

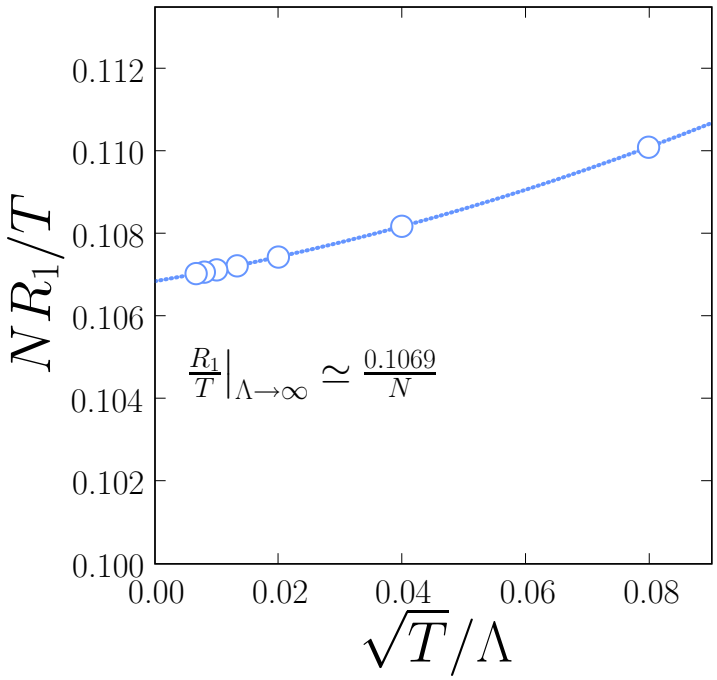

Figure 4.1: The behavior of Eq. (4.27) as the UV cutoff $\Lambda \to \infty$. When fit to a quadratic polynomial in $\sqrt{T}/\Lambda$ it converges to the value $R_1/T \simeq 0.1069/N$.

Using Eq. (4.18), we find that R_1/T converges to the universal finite value

$$\frac{R_1}{T} \simeq \frac{0.1069}{N} \tag{4.28}$$

as seen in in Fig. 4.1. Therefore, as described in Ref. [99] and Section 2.2 as a consequence of the scaling relation $z = 2 - \eta$ where η is the anomalous dimension of Ψ_a, the uniform static order parameter susceptibility

$$\chi = \int dx \int d\tau \langle \Psi_a^*(x,\tau)\Psi_a(0,0)\rangle \tag{4.29}$$

is determined by the value of $k_B T$ alone using Eqs. (4.18) and (4.22) as

$$\chi^{-1} = k_B T \left(0.6248 + \frac{0.107}{N}\right). \tag{4.30}$$

4.2 Critical exponents

With our quantum critical theory firmly established, we may now investigate any possible $1/N$ corrections to the large-N critical behavior characterized by exponents

$z = 2$ and $\nu = 1$. Such corrections can be obtained by exploiting the known scaling behavior of the susceptibility in conjunction with various hyperscaling relations. We begin by computing the anomalous dynamical scaling dimension η which corrects z at order $1/N$.

Evaluation of η

We know that the susceptibility should scale with momentum like $G^{-1}(k,0) = k^z$ where the bare dynamical critical exponent $z = 2$ will be corrected by the critical exponent η as $z = 2 - \eta$. Therefore, we can write

$$\begin{aligned} G^{-1}(k,0) &= k^{2-\eta} \\ &= k^2 \left(1 + \eta \ln \frac{\Lambda}{k}\right) \end{aligned} \tag{4.31}$$

where Λ is a large momentum cutoff. From Eq. (4.11) at $r = r_c$, $T = 0$ and $\omega = 0$ we have

$$G^{-1}(k,0) = k^2 + \frac{1}{N} \int \frac{dq}{2\pi} \int \frac{d\epsilon}{2\pi} \frac{1}{\Pi_0(q,\epsilon,0)} \left[\frac{1}{(k+q)^2 + |\omega + \epsilon|} - \frac{1}{q^2 + \epsilon} \right] \tag{4.32}$$

and thus we need only extract the log divergence in the above equation. Using Eq. (B.5) and rescaling such that all variables of integration are dimensionless we have

$$G^{-1}(k,0) = k^2 + \frac{k^2}{N} \int_{-\Lambda/k}^{\Lambda/k} \frac{dq}{2\pi} |q| \int_0^\infty \frac{d\epsilon}{\pi} \frac{1}{\Pi_0(1,\epsilon,0)} \left[\frac{1}{(1+1/q)^2 + \epsilon} - \frac{1}{1+\epsilon} \right]. \tag{4.33}$$

Expanding the integrand for large q and identifying the logarithmic prefactor leads to

$$\begin{aligned} \eta &= \frac{1}{\pi^2 N} \int_0^\infty d\epsilon \frac{3 - \epsilon}{\Pi_0(1,\epsilon,0)(\epsilon+1)^3} \\ &\simeq \frac{0.13106}{N}. \end{aligned} \tag{4.34}$$

Knowing the value of η will be particularly useful because it will fix the cutoff dependence of the quantum critical conductivity at order $1/N$, since $z = 2 - \eta$, and we expect $\sigma(T) \sim T^{-1/z}$. Thus, if $\sigma(T) = A/\sqrt{T}$ where A is a constant at $N = \infty$, then at order $1/N$ we should have $\sigma = (A/\sqrt{T})[1 + (\eta/2)\ln(\Lambda/\sqrt{T})]$.

Evaluation of ν

Calculating the $1/N$ correction to the correlation length exponent ν is unfortunately not so simple, but we begin by examining the behavior of the inverse susceptibility at $T = 0$ and $k = \omega = 0$ as one tunes the coupling constant g towards g_c

$$G^{-1}(0,0) \sim (g - g_c)^{\gamma} \tag{4.35}$$

which defines the susceptibility exponent γ. At $N = \infty$ we know $\gamma = 2$, and thus for finite N let us parameterize $\gamma = 2(1 - \alpha)$, which can be related to ν via the scaling relation $\gamma = (2 - \eta)\nu$. To this end, let us define r_g via

$$\begin{aligned} \frac{1}{g_c} - \frac{1}{g} &\equiv \int \frac{dk}{2\pi} \int \frac{d\omega}{2\pi} \left(\frac{1}{k^2 + |\omega|} - \frac{1}{k^2 + |\omega| + r_g} \right) \\ &= \frac{\sqrt{r_g}}{\pi}, \end{aligned} \tag{4.36}$$

where we have exploited the fact that

$$\sqrt{r_g} = \frac{1}{2\pi \Pi_0(0, 0, r_g)}. \tag{4.37}$$

Thus, from Eq. (4.36) we have $r_g \sim (g - g_c)^2$, and upon comparison with Eq. (4.35) we find

$$\begin{aligned} G^{-1}(0,0) &= (g - g_c)^{2(1-\alpha)} \\ &= r_g^{1-\alpha} \\ &= r_g \left(1 + \alpha \ln \frac{\Lambda^2}{r_g} \right). \end{aligned} \tag{4.38}$$

So again we can extract a critical exponent by determining the prefactor of a logarithmic divergence of G^{-1}. At this stage it will useful to quote the following two results (with details given in Appendix B)

$$\begin{aligned} \Pi_0(k, \omega, r) = \frac{1}{2\pi|k|} &\left[\operatorname{asin} \left(\frac{k^2 + |\omega|}{\sqrt{(k^2 + |\omega|)^2 + 4k^2 r}} \right) + \operatorname{asin} \left(\frac{k^2 - |\omega|}{\sqrt{(k^2 + |\omega|)^2 + 4k^2 r}} \right) \right] \\ + \frac{1}{4\pi\sqrt{k^2 + 2|\omega| + 4r}} &\left[\ln \left(\frac{2\sqrt{r + |\omega|}\sqrt{k^2 + 2|\omega| + 4r} + k^2 + 3|\omega| + 4r}{|2\sqrt{r + |\omega|}\sqrt{k^2 + 2|\omega| + 4r} - k^2 - 3|\omega| - 4r|} \right) \right. \\ &\left. - \ln \left(\frac{2\sqrt{r}\sqrt{k^2 + 2|\omega| + 4r} + k^2 + |\omega| + 4r}{|2\sqrt{r + |\omega|}\sqrt{k^2 + 2|\omega| + 4r} - k^2 - |\omega| - 4r|} \right) \right] \end{aligned} \tag{4.39}$$

and

$$\Pi_0'(k, \omega, r) \equiv \frac{\partial \Pi_0(k, \omega, r)}{\partial r} = -2 \int \frac{dq}{2\pi} \int \frac{d\epsilon}{2\pi} \frac{1}{(q^2 + |\epsilon| + r)^2 [(k + q)^2 + |\omega + \epsilon| + r]}. \tag{4.40}$$

Combining Eqs. (4.5) with (4.15) and (4.36) we can write

$$r = r_g - \frac{2\pi\sqrt{r_g}}{N}\int\frac{dk}{2\pi}\int\frac{d\omega}{2\pi}\int\frac{dq}{2\pi}\int\frac{d\epsilon}{2\pi}\frac{1}{(k^2+|\omega|)^2}\frac{1}{\Pi_0(q,\epsilon,0)} \times\left(\frac{1}{q^2+|\epsilon|}-\frac{1}{(k+q)^2+|\omega+\epsilon|}\right). \quad (4.41)$$

Now using Eq. (4.11) and (4.41), we have the result for the inverse susceptibility

$$\begin{aligned} G^{-1}(0,0) = r_g &+ \frac{1}{N}\int\frac{dk}{2\pi}\int\frac{d\omega}{2\pi}\frac{1}{\Pi_0(k,\omega,r_g)}\frac{1}{(k^2+|\omega|+r_g)} \\ &- \frac{1}{N}\frac{1}{\Pi_0(0,0,r_g)}\int\frac{dk}{2\pi}\int\frac{d\omega}{2\pi}\int\frac{dq}{2\pi}\int\frac{d\epsilon}{2\pi} \\ &\times\left\{\frac{1}{\Pi_0(q,\epsilon,r_g)}\frac{1}{(k^2+|\omega|+r_g)^2[(k+q)^2+|\omega+\epsilon|+r_g]}\right. \\ &\left.+\frac{1}{\Pi_0(q,\epsilon,0)}\frac{1}{(k^2+|\omega|)^2}\left[\frac{1}{q^2+|\epsilon|}-\frac{1}{(k+q)^2+|\omega+\epsilon|}\right]\right\} \quad (4.42) \end{aligned}$$

where we have been able to replace r with r_g in any term that is already of order $1/N$. A useful check is to note that $G^{-1}(0,0) = 0$ above for $r_g = 0$. Let us now write this result in the form

$$\begin{aligned} G^{-1}(0,0) = r_g + F(r_g) &- \frac{2\pi\sqrt{r_g}}{N}\int\frac{dk}{2\pi}\int\frac{d\omega}{2\pi}\int\frac{dq}{2\pi}\int\frac{d\epsilon}{2\pi}\frac{1}{\Pi_0(q,\epsilon,0)} \\ &\times\frac{1}{(k^2+|\omega|)^2}\left[\frac{1}{q^2+\epsilon}-\frac{1}{(k+q)^2+|\omega+\epsilon|}\right] \quad (4.43) \end{aligned}$$

where

$$F(r_g) = \frac{1}{N}\int\frac{dk}{2\pi}\int\frac{d\omega}{2\pi}\frac{1}{\Pi_0(k,\omega,r_g)}\left[\frac{1}{k^2+|\omega|+r_g}+\frac{\Pi_0'(k,\omega,r_g)}{2\Pi_0(0,0,r_g)}.\right] \quad (4.44)$$

The next step is to find the small r_g behavior of $F(r_g)$. For this, let us first examine the small r_g behavior of Π_0':

$$\begin{aligned} \Pi_0'(k,\omega,r_g) &= -2\int\frac{dq}{2\pi}\int\frac{d\epsilon}{2\pi}\frac{1}{(q^2+|\epsilon|+r_g)^2[(k+q)^2+|\omega+\epsilon|+r_g]} \\ &= -\frac{1}{\pi(k^2+|\omega|)\sqrt{r_g}}+C_1(k,\omega)+C_2(k,\omega)\sqrt{r_g}+\cdots \quad (4.45) \end{aligned}$$

where

$$\begin{aligned} C_1(k,\omega) &= 2\int\frac{dq}{2\pi}\int\frac{d\epsilon}{2\pi}\frac{1}{(q^2+|\epsilon|)^2}\left[\frac{1}{k^2+|\omega|}-\frac{1}{(k+q)^2+|\omega+\epsilon|}\right] \\ &\equiv \frac{1}{|k|^3}\Phi_1\left(\frac{|\omega|}{k^2}\right) \quad (4.46) \end{aligned}$$

with

$$\Phi_1\left(\frac{|\omega|}{k^2}\right) = \int \frac{dq}{2\pi}\int \frac{d\epsilon}{2\pi}\frac{1}{(q^2+|\epsilon|)^2}\left[\frac{1}{1+|\omega|/k^2} - \frac{1}{(1+q)^2+|\epsilon+\omega/k^2|}\right]. \quad (4.47)$$

and

$$\begin{aligned} C_2(k,\omega) &= -\lim_{r_g\to 0} 4\sqrt{r_g}\int\frac{dq}{2\pi}\int\frac{d\epsilon}{2\pi}\frac{d}{dr_g}\left[\frac{1}{(q^2+|\epsilon|+r_g)^2[(k+q)^2+|\omega+\epsilon|+r_g]}\right. \\ &\qquad - \frac{1}{(k^2+|\omega|)(q^2+|\epsilon|+r_g)^2} - \frac{1}{(q^2+|\epsilon|)^2[(k+q)^2+|\omega+\epsilon|]} \\ &\qquad \left. + \frac{1}{(q^2+|\epsilon|)^2(k^2+|\omega|)}\right] \\ &= \frac{3}{\pi(k^2+|\omega|)^2} + \frac{3k^2-|\omega|}{\pi(k^2+|\omega|)^3} \\ &\equiv \frac{1}{k^4}\Phi_2\left(\frac{|\omega|}{k^2}\right), \end{aligned} \quad (4.48)$$

with

$$\Phi_2\left(\frac{|\omega|}{k^2}\right) = \frac{2}{\pi}\frac{3+|\omega|/k^2}{(1+|\omega|/k^2)^3} \quad (4.49)$$

where we have used the fact that $|\epsilon| \ll \omega$ over the regime important for small r_g. From this expansion we can also determine the small r_g expansion of Π_0

$$\Pi_0(k,\omega,r_g) = \Pi_0(k,\omega,0) - \frac{2\sqrt{r_g}}{\pi(k^2+|\omega|)} + C_1(k,\omega)r_g + \frac{2C_2(k,\omega)}{3}r_g^{3/2} + \cdots \quad (4.50)$$

and finally that of $F(r_g)$

$$\begin{aligned} F(r_g) = \frac{\pi\sqrt{r_g}}{N}\int\frac{dk}{2\pi}\int\frac{d\omega}{2\pi}\frac{C_1(k,\omega)}{\Pi_0(k,\omega,0)} + \frac{r_g}{N}\int\frac{dk}{2\pi}\int\frac{d\omega}{2\pi}\left[\frac{2C_1(k,\omega)}{(k^2+|\omega|)\Pi_0^2(k,\omega,0)}\right. \\ \left. + \frac{\pi C_2(k,\omega)}{\Pi_0(k,\omega,0)} - \frac{1}{(k^2+|\omega|)^2\Pi_0(k,\omega,0)}\right]. \end{aligned} \quad (4.51)$$

Now, comparing this result with Eq. (4.38) and (4.43) the second term, which is linear in r_g defines α by

$$F(r_g) = \cdots + \alpha r_g \ln\left(\frac{\Lambda^2}{r_g}\right) + \cdots \quad (4.52)$$

where α is related to the critical exponents by $\gamma = 2(1-\alpha) = \nu(2-\eta)$. Using Eq. (B.5) to define

$$\Phi_0\left(\frac{|\omega|}{k^2}\right) = |k|\Pi_0(k,\omega,0) \quad (4.53)$$

and via Eqs. (4.46) and (4.48), α is given by

$$\begin{aligned}\alpha &= \frac{1}{2\pi^2 N}\int_0^\infty d\omega \left[\frac{2\Phi_1(\omega)}{(\omega+1)\Phi_0^2(\omega)} + \frac{\pi\Phi_2(\omega)}{\Phi_0(\omega)} - \frac{1}{(1+\omega)^2\Phi_0(\omega)}\right] \\ &\simeq \frac{0.455}{N}.\end{aligned} \tag{4.54}$$

The value of ν can be finally determined using Eq. (4.34) as

$$\begin{aligned}\nu &= 1 - \alpha + \frac{\eta}{2} \\ &\simeq 1 - \frac{0.389}{N}.\end{aligned} \tag{4.55}$$

The values found in this section for $z = 2 - \eta$ (Eq. (4.34)) and ν (Eq. (4.55)) corresponding to a N component complex field are fully consistent with previous calculations including an ϵ expansion near 2 dimensions [99, 89] (Eq. (2.14) and (2.15)) and via Monte Carlo simulations where $z = 1.97(3)$ and $\nu = 0.689(6)$ [101].

4.3 Quantum transport at finite N

We now we endeavor to compute the dc values of the thermal and electrical conductivity in a $1/N$ expansion in the quantum critical regime. Transport is again calculated via the Kubo formula, and the initial steps are identical to those presented in Section 3.4.1 for the derivation of Eq. (3.108). However, unlike the case where the number of components of our order parameter field was infinite, we now have the modified propagator of Eq. (4.22) and the single polarization bubble diagrams will be corrected by additional loops giving rise to corrections of order $1/N$.

It will turn out that although the individual values of the thermal (κ) and electrical (σ) conductivities are not by themselves universal to order $1/N$ their ratio is a universal number, solely as a result of the appearance of an anomalous dimension that alters the critical dynamic scaling.

4.3.1 Diagrammatic expansion

We refer the reader to Eq. (3.101) to Eq. (3.108) and begin by writing down the expression for the value of the transport coefficients ($p = 0$ for electrical conductivity and $p = 2$ for thermal conductivity) obtained from the Kubo formula in terms of a polarization function at external imaginary frequency $i\omega_n$

$$\mathcal{G}_p(i\omega_n) = -\frac{4e^{*2-p}}{\omega_n T^p}\mathcal{K}_p(i\omega_n). \tag{4.56}$$

Written in Fourier space it takes the form, where $\langle \cdots \rangle$ refers to an expectation value with respect to $\mathcal{S}_r$, Eq. (4.9).

$$\begin{aligned}\mathcal{K}_p(i\omega_n) = -\frac{T}{2}\sum_{\epsilon_n}\int \frac{dk}{2\pi}\,(\epsilon_n+\omega_n/2)^p\,\big[\langle|\psi(k,\epsilon_n)|^2\rangle \\ - k^2\langle\Psi_a^*(k,\epsilon_n)\Psi_a(k,\epsilon_n+\omega_n)\Psi_a^*(k,\epsilon_n+\omega_n)\Psi_a(k,\epsilon_n)\rangle\big]\,.\end{aligned} \tag{4.57}$$

As we are only interested in the dc thermal and electric transport, we will need to determine the imaginary part of $\mathcal{K}_p$, analytically continued to real frequencies. Our previous experience indicates that we need only focus on the *paramagnetic* contributions to Eq. (4.57) which correspond to the four-point correlation function above resulting from quadratic insertions of the scalar or thermal potentials A_j. The resulting paramagnetic polarization function has the diagrammatic expansion to order $1/N$ given by

$\mathcal{K}_p^{\rm para}(i\omega_n) =$ 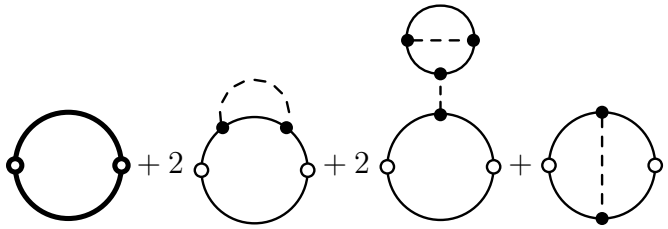 (4.58)

$=$ 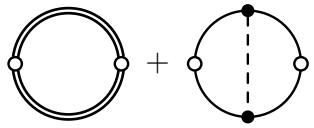 (4.59)

where

$$\text{——} = \frac{1}{k^2+|\epsilon_n|+r} \tag{4.60}$$

$$\text{——} = G_0(k,\epsilon_n) = \frac{1}{k^2+|\epsilon_n|+R} \tag{4.61}$$

$$\text{═══} = \frac{1}{k^2+|\epsilon_n|+R+R_1+\Sigma(k,\epsilon_n)}, \tag{4.62}$$

$r = R + \tilde{R}_1$ and an open circle indicates a factor of $k(\epsilon_n+\omega_n/2)^{p/2}$ where $p=0$ for electrical transport and $p=2$ for thermal transport. R_1 is the finite shift in the critical point to order $1/N$ given by Eq. (4.28) and the self-energy is defined in Eq. (4.23) such that $\Sigma(0,0)=0$. To identify the role of various $1/N$ corrections to

transport it will be useful to present the full integral form

$$\begin{aligned}\mathcal{K}_p^{\text{para}}(i\omega_n) = & T\sum_{\epsilon_n}\int\frac{dk}{2\pi}k^2(\epsilon_n+\omega_n/2)^p G_0(k,\epsilon_n)G_0(k,\epsilon_n+\omega_n) \\ & - 2R_1 T\sum_{\epsilon_n}\int\frac{dk}{2\pi}k^2(\epsilon_n+\omega_n/2)^p G_0^2(k,\epsilon_n)G_0(k,\epsilon_n+\omega_n) \\ & - 2T\sum_{\epsilon_n}\int\frac{dk}{2\pi}k^2(\epsilon_n+\omega_n/2)^p G_0^2(k,\epsilon_n)G_0(k,\epsilon_n+\omega_n)\Sigma(k,\epsilon_n) \\ & - \frac{2}{N}T^2\sum_{\epsilon_n,\Omega_n}\int\frac{dq}{2\pi}\int\frac{dk}{2\pi}\frac{k(k+q)(\epsilon_n+\omega_n/2)^{p/2}(\epsilon_n+\Omega_n+\omega_n/2)^{p/2}}{\Pi_T(q,\Omega_n,R)} \\ & \times G_0(k,\epsilon_n)G_0(k,\epsilon_n+\omega_n)G_0(k+q,\epsilon_n+\Omega_n)G_0(k+q,\epsilon_n+\Omega_n+\omega_n).\end{aligned} \tag{4.63}$$

The first term is just the paramagnetic contribution in the large-N polarization function previously defined in Eq. (3.109). The second term arises from the $1/N$ correction to the mass R, and the final two terms from the self-energy and vertex corrections respectively.

4.3.2 Frequency summations

We can perform the Matsubara sums by solving integrals in the complex plane with repeated use of the basic identity [128]

$$T\sum_{\epsilon_n}\mathcal{F}(i\epsilon_n) = \frac{1}{2}\int\frac{d\epsilon}{2\pi i}\coth\left(\frac{\epsilon}{2T}\right)[F(\epsilon+i\eta)-F(\epsilon-i\eta)] \tag{4.64}$$

where we note that if $F(i\epsilon_n)=\mathcal{F}(|\epsilon_n|)$ then after analytic continuation $F(\epsilon\pm i\eta)=\mathcal{F}(\mp i\epsilon)$. The full details on the derivation of various summation formulae used in this section are given in an Appendix C. The general approach will be as follows: use the relevant summation formula to obtain an expression for each term in Eq. (4.63) analytically continued to real frequencies. Since we are only interested in dc transport, an examination of Eq. (4.56) tells us that we will require the imaginary part of the term that is linear in the external frequency, ω. Thus by Taylor expanding our analytically continued result, we can extract the relevant transport coefficients. We will examine each term separately.

Large-N result

For the first term in Eq. (4.63) we could just as easily perform the Matsubara sum using the spectral representation of the bare Green function, which was done in

Section 3.4.1 and led to Eq. (3.115). This will allow us to test and benchmark our contour integration approach. We need to evaluate:

$$\begin{aligned} I_{2,p}(i\omega_n) &= T\sum_{\epsilon_n} \frac{(\epsilon_n+\omega_n/2)^p}{(k^2+R+|\epsilon_n|)(k^2+R+|\epsilon_n+\omega_n|)} \\ &\equiv T\sum_{\epsilon_n} \mathcal{F}_{2,p}(i\epsilon_n, i(\epsilon_n+\omega_n)) \end{aligned} \tag{4.65}$$

where we have suppressed the momentum dependence of $\mathcal{F}_{2,p}$ for compactness. Using Eq. (C.3) we find

$$\lim_{\omega\to 0}\frac{\mathrm{Im}\, I_{2,p}(\omega+i\eta)}{\omega} = \frac{1}{2T}\int\frac{d\epsilon}{2\pi}\frac{\epsilon^{2+p}}{\sinh^2(\epsilon/2T)}\frac{1}{[(k^2+R)^2+\epsilon^2]^2}, \tag{4.66}$$

which does indeed agree with our previous result, Eq. (3.115). Substituting into Eq. (4.56) and defining

$$\mathcal{G}_p \equiv \lim_{\omega\to 0}\mathcal{G}_p(\omega+i\eta) \tag{4.67}$$

$$= \mathcal{G}_p^{N=\infty} + \mathcal{G}_p^{R_1} + \mathcal{G}_p^{\Sigma} + \mathcal{G}_p^{\Gamma} \tag{4.68}$$

where we have broken the total dc transport into a sum of four contributions coming from the four types of terms in Eq. (4.63). Because we have ignored the diamagnetic part of the polarization function, $\mathcal{K}_p^{\mathrm{para}}$ is purely imaginary and thus after analytic continuation $\mathcal{G}_p$ is a real number. The $N=\infty$ contribution is

$$\begin{aligned} \mathcal{G}_p^{N=\infty} &= \frac{4e^{*2-p}}{2T^{p+1}}\int\frac{d\epsilon}{2\pi}\frac{\epsilon^{2+p}}{\sinh^2(\epsilon/2T)}\int\frac{dk}{2\pi}\frac{k^2}{[(k^2+R)^2+\epsilon^2]^2} \\ &= \frac{\sqrt{2}}{8}\frac{e^{*2-p}}{T^{p+1}}\int\frac{d\epsilon}{2\pi}\frac{\epsilon^{2+p}}{\sinh^2(\epsilon/2T)}\frac{1}{\sqrt{R^2+\epsilon^2}(R+\sqrt{R^2+\epsilon^2})^{3/2}} \\ &= \frac{1}{\sqrt{T}}\begin{cases} 0.217997\cdots\, e^{*2} & ;\quad p=0 \\ 0.24592\cdots & ;\quad p=2 \end{cases}. \end{aligned} \tag{4.69}$$

R_1 correction

Due to the finite shift in the critical point, coming from $R_1 \sim O(1/N)$, we need to evaluate a correction of the form

$$\begin{aligned} \widetilde{I}_{2,p}(i\omega_n) &= T\sum_{\epsilon_n} \frac{(\epsilon_n+\omega_n/2)^p}{(k^2+R+|\epsilon_n|)^2(k^2+R+|\epsilon_n+\omega_n|)} \\ &\equiv T\sum_{\epsilon_n} \widetilde{\mathcal{F}}_{2,p}(i\epsilon_n, i(\epsilon_n+\omega_n)) \end{aligned} \tag{4.70}$$

however, upon examination of Eq. (4.65) it is clear that in the dc limit, this can be evaluated by taking a derivative of Eq. (4.69) with respect to R.

$$\begin{aligned}
\mathcal{G}_p^{R_1} &= -\frac{1}{2}\frac{\partial}{\partial R}\left[(-2R_1)\mathcal{G}_p^{N=\infty}\right] \\
&= -\frac{\sqrt{2}R_1}{16}\frac{e^{*2-p}}{T^{p+1}}\int\frac{d\epsilon}{2\pi}\frac{\epsilon^{2+p}}{\sinh^2(\epsilon/2T)}\frac{3\epsilon^2+5R(R+\sqrt{R^2+\epsilon^2})}{(R^2+\epsilon^2)^{3/2}(R+\sqrt{R^2+\epsilon^2})^{5/2}} \\
&= -\frac{1}{\sqrt{T}N}\begin{cases} 0.062251\cdots\ e^{*2} & ;\ \ p=0 \\ 0.026867\cdots & ;\ \ p=2 \end{cases}
\end{aligned} \tag{4.71}$$

where we have used the previously calculated values of $R/T = 0.6248$ and $R_1/T = 0.1069/N$. Eq. (4.18).

Self-energy correction

Examining the third term in Eq. (4.63) we now have to perform a dual Matsubara sum over a function with four separate frequency arguments

$$\begin{aligned}
I_{4,p}(i\omega_n) &= T\sum_{\epsilon_n}\frac{(\epsilon_n+\omega_n/2)^p}{(k^2+R+|\epsilon_n|)^2(k^2+R+|\epsilon_n+\omega_n|)}\Sigma(k,\epsilon_n) \\
&= T^2\sum_{\epsilon_n,\Omega_n}\frac{(\epsilon_n+\omega_n/2)^p}{(k^2+R+|\epsilon_n|)^2\Pi_T(q,\Omega_n,R)(k^2+R+|\epsilon_n+\omega_n|)} \\
&\qquad\times\left[\frac{1}{(k+q)^2+R+|\epsilon_n+\Omega_n|}-\frac{1}{q^2+R+|\Omega_n|}\right] \\
&= T^2\sum_{\epsilon_n,\Omega_n}\mathcal{F}_{4,p}(i\epsilon_n,i\Omega_n,i(\epsilon_n+\Omega_n),i(\epsilon_n+\omega_n)).
\end{aligned} \tag{4.72}$$

Using Eq. (C.8) we can write:

$$\begin{aligned}
\lim_{\omega\to 0}\frac{\mathrm{Im}\,I_{4,p}(\omega+i\eta)}{\omega} = \frac{1}{T}\int\frac{d\Omega}{2\pi}\int\frac{d\epsilon}{2\pi}\frac{i^p\epsilon^{2+p}(k^2+R)\mathrm{csch}^2\left(\frac{\epsilon}{2T}\right)\mathrm{Re}\left[\Pi_T(q,\Omega,R)\right]^{-1}}{[(k^2+R^2)^2+\epsilon^2]^3} \\
\times\left\{\frac{(\epsilon+\Omega)\coth\left(\frac{\epsilon+\Omega}{2T}\right)}{[(k+q)^2+R]^2+(\epsilon+\Omega)^2}-\frac{\Omega\coth\left(\frac{\Omega}{2T}\right)}{(q^2+R)^2+\Omega^2}\right\}
\end{aligned} \tag{4.73}$$

which leads to the self-energy corrections to the dc conductivities

$$\begin{aligned}
\mathcal{G}_p^{\Sigma} = -\frac{8e^{*2-p}i^p}{NT^{p+1}}\int\frac{dq}{2\pi}\int\frac{d\Omega}{2\pi}\int\frac{dk}{2\pi}\int\frac{d\epsilon}{2\pi}\frac{\epsilon^{2+p}k^2(k^2+R)\mathrm{csch}^2\left(\frac{\epsilon}{2T}\right)}{[(k^2+R^2)^2+\epsilon^2]^3} \\
\times\ \mathrm{Re}\left[\Pi_T(q,\Omega,R)\right]^{-1}\left\{\frac{(\epsilon+\Omega)\coth\left(\frac{\epsilon+\Omega}{2T}\right)}{[(k+q)^2+R]^2+(\epsilon+\Omega)^2}-\frac{\Omega\coth\left(\frac{\Omega}{2T}\right)}{(q^2+R)^2+\Omega^2}\right\}.
\end{aligned} \tag{4.74}$$

Vertex correction

The final term in Eq. (4.63) has five separate frequency arguments

$$\begin{aligned} I_{5,p}(i\omega_n) = T^2 \sum_{\epsilon_n,\Omega_n} & \frac{(\epsilon_n+\omega_n/2)^{p/2}(\epsilon_n+\Omega_n+\omega_n/2)^{p/2}}{(k^2+R+|\epsilon_n|)(k^2+R+|\epsilon_n+\omega_n|)[(k+q)^2+R+|\epsilon_n+\Omega_n|]} \\ & \times \frac{1}{[(k+q)^2+R+|\epsilon_n+\Omega_n+\omega_n|]\Pi_T(q,\Omega_n,R)} \\ = T^2 \sum_{\epsilon_n,\Omega_n} & \mathcal{F}_{5,p}(i\epsilon_n, i(\epsilon_n+\omega_n), i(\epsilon_n+\Omega_n), i(\epsilon_n+\Omega_n+\omega_n), i\Omega_n). \end{aligned} \tag{4.75}$$

Using Eq. (C.13) we can write:

$$\begin{aligned} & \lim_{\omega\to 0} \frac{\mathrm{Im}\, I_{5,p}(\omega+i\eta)}{\omega} = \\ & \frac{1}{2T}\int\frac{d\Omega}{2\pi}\int\frac{d\epsilon}{2\pi}\frac{i^p[\epsilon(\epsilon+\Omega)]^{1+p/2}\mathrm{csch}^2\left(\frac{\epsilon}{2T}\right)\mathrm{csch}^2\left(\frac{\epsilon+\Omega}{2T}\right)\mathrm{Re}\left[\Pi_T(q,\Omega,R)\right]^{-1}}{[(k^2+R^2)^2+\epsilon^2]^2\{[(k+q)^2+R]^2+(\epsilon+\Omega)^2\}^2} \\ & \times \left\{(k^2+R)(\epsilon+\Omega)\sinh\left(\frac{\epsilon}{T}\right)+[(k+q)^2+R]\epsilon\sinh\left(\frac{\epsilon+\Omega}{T}\right)\right\} \end{aligned} \tag{4.76}$$

giving the vertex contribution to the $\omega = 0$ transport coefficients

$$\begin{aligned} \mathcal{G}_p^\Gamma = -\frac{4e^{*2-p}i^p}{NT^{p+1}}\int\frac{dq}{2\pi}\int\frac{d\Omega}{2\pi}\int\frac{dk}{2\pi}\int\frac{d\epsilon}{2\pi}\frac{k(k+q)[\epsilon(\epsilon+\Omega)]^{1+p/2}}{[(k^2+R^2)^2+\epsilon^2]^2} & \\ \times \frac{\mathrm{csch}^2\left(\frac{\epsilon}{2T}\right)\mathrm{csch}^2\left(\frac{\epsilon+\Omega}{2T}\right)\mathrm{Re}\left[\Pi_T(q,\Omega,R)\right]^{-1}}{\{[(k+q)^2+R]^2+(\epsilon+\Omega)^2\}^2} & \\ \times \left\{(k^2+R)(\epsilon+\Omega)\sinh\left(\frac{\epsilon}{T}\right)+[(k+q)^2+R]\epsilon\sinh\left(\frac{\epsilon+\Omega}{T}\right)\right\}. & \end{aligned} \tag{4.77}$$

4.3.3 Numerical evaluation

The $1/N$ corrections to thermoelectric transport coming from the self-energy and vertex corrections are written in Eqs. (4.74) and (4.77) as two *four* dimensional integrals that cannot be evaluated analytically. Before we attempt to compute them numerically, we first present a simple argument concerning their expected ultra-violet behavior. From scaling we understand

$$\mathcal{G}_p \sim \frac{1}{T^{1/z}} \tag{4.78}$$

where in Section 4.2 we found that $z = 2-\eta$ with $\eta \sim O(1/N)$. Thus we can write

$$\begin{aligned} \mathcal{G}_p &\sim \frac{1}{T^{1/(2-\eta)}} \\ &= \mathcal{G}_p^{N=\infty}\left(1+\frac{C_p}{N}+\frac{\eta}{2}\ln\frac{\Lambda}{\sqrt{T}}\right) \end{aligned} \tag{4.79}$$

where C_p are universal constants and Λ is a non-universal ultra violet cutoff. Immediately we see that to order $1/N$, the ratio of the thermal to electrical conductivity divided by temperature — the Wiedemann-Franz ratio — will be independent of any cutoff as $\Lambda \to \infty$:

$$\begin{aligned} W &\equiv \frac{\mathcal{G}_2}{\mathcal{G}_0} \\ &= \frac{\mathcal{G}_2^{N=\infty}}{\mathcal{G}_0^{N=\infty}} \left[1 + \frac{C_2 - C_0}{N} + O\left(\frac{\sqrt{T}}{\Lambda}\right) \right]. \end{aligned} \tag{4.80}$$

This is an important equation that guarantees the universality of our final result, and will allow us to test the accuracy of our numerical integration procedure.

We begin by combining the expressions for the self-energy and vertex corrections such that $\mathrm{Re}\left[\Pi_T(q,\Omega,R)\right]^{-1}$ (the most costly function to compute, as described in Appendix B) is in the outermost integral.

$$\begin{aligned} \mathcal{G}_p^{\Sigma} + \mathcal{G}_p^{\Gamma} = -\frac{4e^{*2-p}i^p}{NT^{p+1}} \int \frac{dq}{2\pi} \int \frac{d\epsilon}{2\pi} \mathrm{Re}\left[\frac{1}{\Pi_T(q,\Omega,R)}\right] \\ \times \int \frac{dk}{2\pi} \int \frac{d\omega}{2\pi} \left[Y_p^{\Sigma}(k,\epsilon,q,\Omega) + Y_p^{\Gamma}(k,\epsilon,q,\Omega) \right] \end{aligned} \tag{4.81}$$

where

$$\begin{aligned} Y_p^{\Sigma}(k,\epsilon,q,\Omega) = \frac{2k^2(k^2+R)\epsilon^{2+p}\mathrm{csch}^2\left(\frac{\epsilon}{2T}\right)}{[(k^2+R)^2+\epsilon^2]^3} \\ \times \left\{ \frac{(\epsilon+\Omega)\coth\left(\frac{\epsilon+\Omega}{2T}\right)}{[(k+q)^2+R]^2+(\epsilon+\Omega)^2} - \frac{\Omega\coth\left(\frac{\Omega}{2T}\right)}{(q^2+R)^2+\Omega^2} \right\} \end{aligned} \tag{4.82a}$$

$$\begin{aligned} Y_p^{\Gamma}(k,\epsilon,q,\Omega) = \frac{k(k+q)[\epsilon(\epsilon+\Omega)]^{1+p/2}\mathrm{csch}^2\left(\frac{\epsilon+\Omega}{2T}\right)\mathrm{csch}^2\left(\frac{\epsilon}{2T}\right)}{[(k^2+R)^2+\epsilon^2]^2\{[(k+q)^2+R]^2+(\epsilon+\Omega)^2\}^2} \\ \times \left\{ (k^2+R)(\epsilon+\Omega)\sinh\left(\frac{\epsilon}{T}\right) + [(k+q)^2+R]\epsilon\sinh\left(\frac{\epsilon+\Omega}{T}\right) \right\}. \end{aligned} \tag{4.82b}$$

We will first test for the correct divergent behavior described above by evaluating the inner Ω, k and ϵ-integrals. Defining

$$\widetilde{\mathcal{D}}_p(q) = -\frac{4}{T^{p+1}} \int \frac{d\Omega}{2\pi} \mathrm{Re}\left[\frac{1}{\Pi_T(q,\Omega,R)}\right] \int \frac{dk}{2\pi} \int \frac{d\omega}{2\pi} \left[Y_p^{\Sigma}(k,\epsilon,q,\Omega) + Y_p^{\Gamma}(k,\epsilon,q,\Omega) \right] \tag{4.83}$$

we can examine the large-q behavior of $\widetilde{\mathcal{D}}_p$ as seen in Fig. 4.2. The upper panel, corresponding to corrections to the electrical conductivity shows excellent agreement with the expected $1/q$ behavior for $q > 100$ while the lower panel, detailing corrections to thermal conductivity shows significantly slower convergence. This is due to

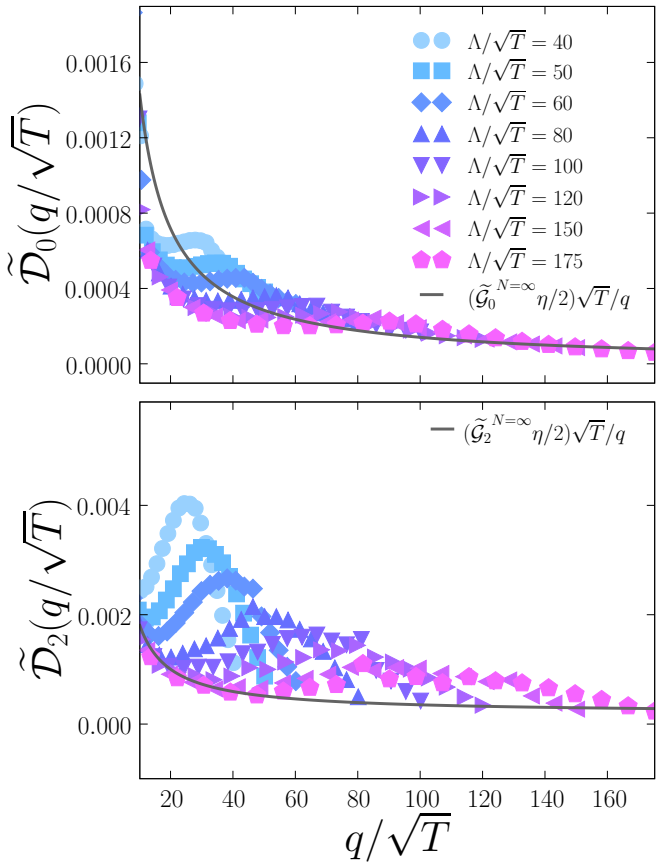

Figure 4.2: The large-q behavior of the outermost integrand in Eq. (4.81) defined by Eq. (4.83) for various values of an external cutoff Λ for $p = 0$ (top panel) and $p = 2$ (bottom panel). The solid lines are fits to the expected divergent form, $\widetilde{\mathcal{G}}_p^{N=\infty}\eta/2\log(\Lambda/\sqrt{T})$ where a tilde indicates that a quantity has been multiplied by a factor of $N\sqrt{T}/e^{*2-p}$ and both panels share the same legend.

two extra factors of frequency in the innermost ϵ-integral leading to a more poorly behaving numerical integrand for large q and ϵ.

Performing the outermost integral numerically using an adaptive routine we arrive at the final results shown in Fig. 4.3 where a tilde indicates that a quantity has been multiplied by a factor of $N\sqrt{T}/e^{*2-p}$. After fitting to the expected divergent form in Eq. (4.79), we find (as $\Lambda \to \infty$)

$$\mathcal{G}_0^{\Sigma} + \mathcal{G}_0^{\Gamma} = \frac{e^{*2}}{\sqrt{T}}\frac{0.118}{N} + \mathcal{G}_0^{N=\infty}\frac{\eta}{2}\ln\frac{\Lambda}{\sqrt{T}} \tag{4.84a}$$

$$\mathcal{G}_2^{\Sigma} + \mathcal{G}_2^{\Gamma} = \frac{1}{\sqrt{T}}\frac{0.151}{N} + \mathcal{G}_2^{N=\infty}\frac{\eta}{2}\ln\frac{\Lambda}{\sqrt{T}}, \tag{4.84b}$$

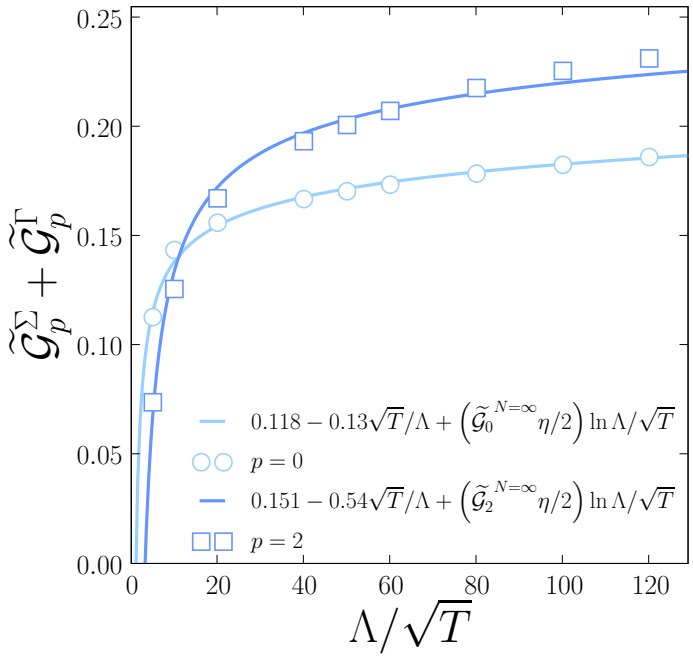

Figure 4.3: The $1/N$ corrections to thermoelectric transport coming from self-energy and vertex corrections ($p = 0$ for σ and $p = 2$ for κ/T) plotted as a function of a dimensionless external ultra violet momentum cutoff $\Lambda/\sqrt{T}$. The solid lines are fits to the expected divergent behavior, from which one can extract the non-divergent corrections as $\Lambda \to \infty$.

and combining with the previous results of Eq. (4.69) and (4.71) we have the dc thermoelectric transport coefficients to order $1/N$

$$\sigma = \frac{e^{*2}}{\sqrt{T}}\left(0.218 + \frac{0.0561}{N} + \frac{0.0142}{N}\ln\frac{\Lambda}{\sqrt{T}}\right) \tag{4.85a}$$

$$\frac{\kappa}{T} = \frac{1}{\sqrt{T}}\left(0.246 + \frac{0.124}{N} + \frac{0.0161}{N}\ln\frac{\Lambda}{\sqrt{T}}\right), \tag{4.85b}$$

which both explicitly depend on Λ as expected.

4.3.4 Wiedemann-Franz law in the quantum critical regime

We have evaluated the full fluctuation corrections to thermoelectric transport up to order $1/N$ (Eqs. (4.85a) and (4.85b)) coming from the direct contributions of Cooper pairs due to the proximate superconducting state. Initially dismayed by their cutoff dependence, we now recall the previous argument that led to Eq. (4.80). We found from scaling that the required $T^{-1/z}$ temperature dependence of κ/T and σ

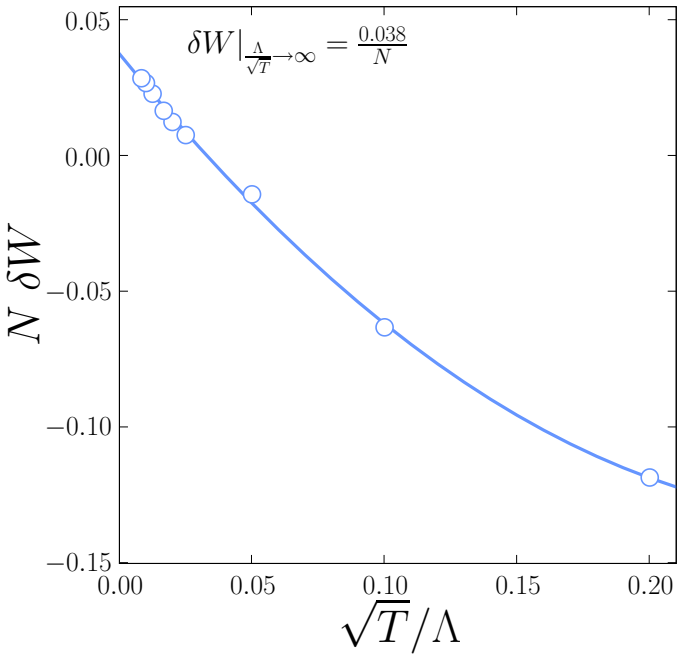

Figure 4.4: The $1/N$ corrections to the Wiedemann-Franz ratio plotted as a function of the inverse external rescaled ultra violet momentum cutoff. The solid line is a fit to a second order polynomial and the individual divergences of the electrical and thermal conductivity are canceled as $\Lambda/\sqrt{T} \to \infty$ giving the universal correction $\delta W = 0.0376/N$.

implied that when dividing them to form the Wiedemann-Franz (WF) ratio, all divergent Λ-dependence must exactly cancel. This exact cancellation is seen in Fig. (4.4) where we plot the total correction to the WF ratio, δW as a function of the inverse of the rescaled dimensionless cutoff. As $\Lambda \to \infty$, δW approaches a constant. Extracting the infinite cutoff result via a polynomial fit we find (after inserting the proper power of the Boltzmann constant)

$$W = \frac{\kappa}{\sigma T} = \left(0.282 + \frac{0.0376}{N}\right)\left(\frac{k_B}{e}\right)^2. \tag{4.86}$$

Therefore, the WF ratio is indeed obeyed, (i.e. is temperature independent) indicating the presence of only fully elastic scattering and is independent of any microscopic constants. The term proportional to $1/N$ is quite small, and for the physical case, $N = 1$ it corresponds to a correction on the order of ten percent.

Chapter 5

Infinite Randomness and Activated Scaling

The previous three chapters have dealt with the superconductor-metal quantum phase transition as described by a quantum field theory of fluctuating Cooper pairs coupled to an Ohmic bath of fermionic quasiparticles tuned by a pair-breaking interaction. Although the role of disorder was briefly discussed in Section 2.7 in terms of a temperature scale above which randomness could be neglected, and estimates for model parameters were given in both the clean and dirty limits, the issue has mostly been ignored. Moreover, the conditions summarized in Table 2.1 hinted at the possibility that there might be no *parametrically* large temperature range over which the self-interaction between Cooper pairs is large (a requisite condition for universal results) and weak localization corrections can be neglected. In fact, it was argued by de Gennes [15] that in the absence of suitably strong bulk or diffusive boundary scattering, (the clean limit) a superconducting quasi-one dimensional wire in a parallel magnetic field would be non-ergodic in the sense that time-reversal symmetry is spontaneously broken at long times. The physical implication of non-ergodicity is that the relative phase of the two members of a Cooper pair is not sufficiently randomized by the pair-breaking perturbation. The resulting modification of the pair susceptibility due the interaction which breaks time reversal symmetry cannot cut off the BCS logarithm, and there will always be a superconducting state down to zero temperature, where pair fluctuations completely cease.

In this chapter, we vigorously attack the problem of a *dirty* quasi-one dimensional superconductor at zero temperature in the presence of pair-breaking with great zeal. We will find that not only is disorder a relevant perturbation near the SMT, but the fixed point is of a quite exotic infinite randomness flavor. The details of the critical point are investigated using large scale numerical simulations and the rather surprising conclusion is that the transition is in the same universality class as the onset of ferromagnetism in the quantum random transverse field Ising model (RTFIM) — a model with discrete symmetry and no dissipation.

We begin with a brief reminder of the physics of infinite randomness and introduce the strong disorder renormalization group with special focus on the recent and subdolous calculations of Hoyos *et al.* [129]. We next define a discretized version of the continuum action studied in Chapters 2 to 4 in the presence of quenched disorder, and discuss how it can be replaced by an effective quadratic theory in the large-N limit. The quadratic theory has a concomitant constraint that is solved via a computational algorithm we refer to as the *solve-join-patch* or SJP procedure that is presented in detail. Finally, we provide both static and dynamic evidence for infinite randomness and dynamically activated scaling at the SMT through an analysis of equal time correlation functions, gap statistics and dynamic susceptibilities.

5.1 Strong disorder renormalization group

The role played by quenched randomness in quantum systems is of considerable interest as disorder correlations are of infinite range in the imaginary time direction. The quantum-classical mapping discussed in Section 1.6 provides little insight here, as disorder fluctuations can be strongly renormalized by quantum effects and except for a few carefully constructed artificial models, long range disorder correlations rarely appear in previously studied classical systems. Naively, it might appear that long range disorder correlations reduce the influence of randomness. However, it turns out that the opposite is actually true since it is *more difficult to integrate out an extended fluctuation than a local one*. As such, the inclusion of randomness in the vicinity of a quantum phase transition can lead to unusual and non-trivial modifications of the clean critical phenomena [57].

In Chapter 1 the modification of critical behavior in the presence of disorder was introduced in the context of the Harris criterion. It was concluded that three outcomes were possible; disorder is irrelevant and the clean critical behavior is unchanged, disorder is relevant, but there are only quantitative changes to critical exponents, and finally, disorder is relevant and its strength flows to infinity under renormalization leading to qualitative differences at the critical point and the emergence of non-power law activated scaling. The qualitative change in critical behavior is due to the role of rare regions, or spurious disorder configurations in the disordered system which are exponentially rare in their volume. Such regions are manifestly non-perturbative degrees of freedom and are not accounted for in conventional approximate approaches. As a result, a number of erroneous conclusions were made and it was not until Ma, Dasgupta and Hu [75] applied the strong disorder renormalization group (SDRG) procedure to the random antiferromagnetic spin chain that the physics of rare regions was fully understood.

The standard momentum shell renormalization group procedure assumes the presence of translational symmetry and is ill suited for disordered systems. The SDRG is essentially an RG in energy space, and since its introduction, it has been success-

fully applied to random quantum spin chains [64, 65, 130, 131, 132], ladders [133], random walks [134] and many non-equilibrium systems [135, 136] (for an exhaustive review see Ref. [137]). The main idea is as follows, at each energy scale, the strongest coupling in the system is determined, and the ground state of the corresponding part of the Hamiltonian is found *exactly*. The coupling of this part of the system to the remaining part is treated perturbatively. The excited states of the strongest coupling piece are neglected and a new effective Hamiltonian is derived with a reduced number of degrees of freedom. This basic step is repeated until some low energy scale is reached.

The SDRG procedure was applied with great success to the RTFIM in one dimension by D.S. Fisher [64, 65] where he calculated many results exactly and we will introduce its mechanics in this context here. The transverse field Ising model is one of the simplest Hamiltonians that is known to undergo a quantum phase transition as the strength of the transverse field is increased. In the presence of both random couplings and fields it is described by the Hamiltonian

$$\mathcal{H} = -\sum_i J_i \sigma_i^z \sigma_{i+1}^z - \sum_i h_i \, \sigma_i^x \tag{5.1}$$

where the $\{\sigma_i^\alpha\}$ are Pauli matrices and the interaction constants J_i and fields h_i are independent random variables drawn from some random distributions. As the model is one dimensional, a gauge transformation can be performed to make all the J_i and h_i positive excluding any possible frustration or the glassy physics that it can incur.

Beginning from this Hamiltonian, the SDRG procedure proceeds as follows. We first determine the maximum coupling in the system defined by $\Omega = \max_i(h_i, J_i)$. Suppose it is the random field at site k, $\Omega = h_k$, the part of the Hamiltonian containing this term is $\mathcal{H}_\Omega = -h_k \sigma_k^x$ which has ground state $|\rightarrow_k\rangle$ and excited state $|\leftarrow_k\rangle$ separated by a gap equal to h_k. The ground state of σ_k is mostly unaffected by a longitudinal field (it will make little contribution to the magnetic susceptibility) and it can thus be decimated out of the chain. The coupling of the spin σ_k to its neighbors, $-J_1\sigma_1^z\sigma_2^z - J_2\sigma_2^z\sigma_3^z$ are then treated in second order perturbation theory which results in a renormalized coupling

$$\widetilde{J} = \frac{J_k J_{k+1}}{h_k}. \tag{5.2}$$

The result is a new chain with one less spin and all couplings less than Ω. On the other hand, suppose the strongest coupling was a bond, $\Omega = J_k$, then the two spins connected by J_k can flip coherently in a longitudinal field, i.e. the unperturbed piece of the Hamiltonian $-J_k\sigma_k^z\sigma_{k+1}^z$ has two degenerate ground states $|\uparrow_k\uparrow_{k+1}\rangle$ and $|\downarrow_k\downarrow_{k+1}\rangle$. These two spins act as an effective composite spin and the fields h_k and h_{k+1} act on it in a perturbative manner described by a renormalized field

$$\widetilde{h} = \frac{h_k h_{k+1}}{J_k} \tag{5.3}$$

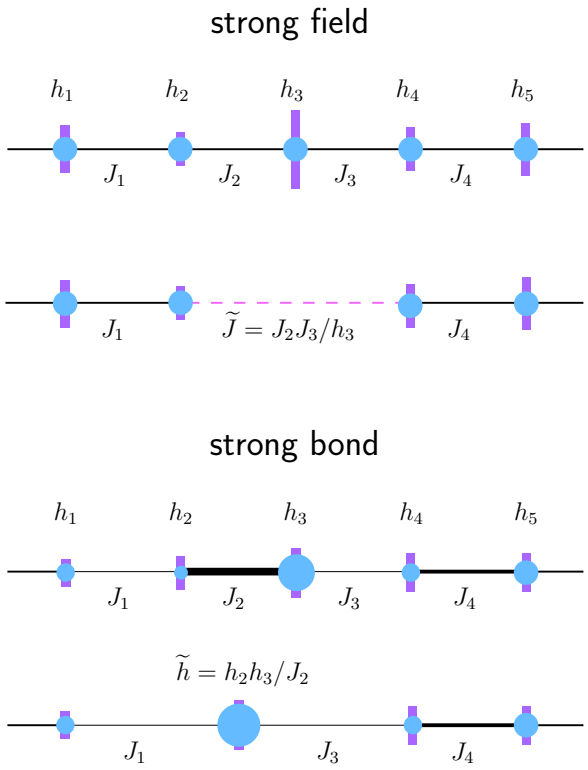

Figure 5.1: A schematic representation of a single strong disorder renormalization group step as described in the text for the special case of $k = 2$. In the presence of a strong field, a spin is decimated and the adjacent spins are connected by a renormalized bond. If a strong bond is present, two neighboring spins are merged and experience a renormalized field.

where we have thrown out the antiparallel states and the effective magnetic moment of the new spin cluster is given by

$$\widetilde{\mu} = \mu_k + \mu_{k+1}. \tag{5.4}$$

Again we have a new spin chain with one less degree of freedom and all couplings smaller than Ω. In summary, at each RG step, if the strongest coupling is a field, the corresponding cluster is annihilated and when it is a bond, the two clusters it connects are joined. This procedure is explained schematically in Fig. 5.1. In the paramagnetic phase annihilation dominates as $\Omega \to 0$ and no large clusters are formed, whereas in the ordered ferromagnetic phase, aggregation dominates as $\Omega \to 0$ and at $\Omega = 0$ an infinite cluster is formed. In this language, the quantum critical point is defined to be the point where the first infinite cluster appears.

The multiplicative structure of the recursion relations in Eq. (5.2) and (5.3) is crucial as it leads to the exponential relationship between lengths and energy scales;

at each step of the RG, clusters or bonds are added (see Eq. (5.4)) while their couplings are multiplied. RG flow equations can be written which describe how the probability distributions for $\ln J_i$ and $\ln h_i$ change as the energy is reduced. At the fixed point, these distributions become identical and the solution of the single RG equation leads to a striking conclusion: lengths and energies are not related in a simple power law manner, but scale according to

$$L^{\psi} \sim \ln \frac{\Omega_0}{\Omega} \tag{5.5}$$

$$\mu \sim \ln^{\phi} \frac{\Omega_0}{\Omega} \tag{5.6}$$

where Ω_0 is a reference energy scale. These expressions are starkly different from the usual power law relations between lengths and energies at conventional critical points ($\Omega \sim L^{-z}$) and the exponential relationship between space and has led to the term *activated dynamical scaling* to describe this behavior.

In addition to this novel scaling, Fisher [65] found that at the critical point defined by $\overline{\ln J_i} = \overline{\ln h_i}$ (where an overline indicates a disorder average), the probability distributions broaden without limit as the energy scale Ω is reduced. The fact that these distributions become infinitely broad is an a posteriori justification of the SDRG procedure since the recursion relations become asymptotically exactly in this limit. Any fixed point with RG equations that yield infinitely wide probability distributions for couplings constants is thus known as an *infinite randomness fixed point*.

Before discussing the specific critical properties found for the RTFIM, let us make some general comments on the physics of infinite randomness. In the disordered phase, there will be some length scale, say ξ, at which the RG procedure described above changes qualitatively. For lengths larger than ξ, all fields are larger than all exchange constants and upon further iteration, only fields will be decimated out of the chain leading to longer and weaker bonds, but no new clusters will be formed. The length ξ must therefore be related to the physical correlation length which diverges with the magnitude of the distance from criticality δ as

$$\xi \sim \delta^{-\nu} \tag{5.7}$$

which defines the correlation length exponent ν. A similar argument can be made in the ordered phase where excitations only exist up to a length scale defined by ξ. At distances longer than ξ, most exchange interactions are larger than any fields and upon further RG iterations all clusters are joined, leading to an infinite cluster for $\Omega = 0$.

The critical exponents ψ, ϕ and ν from Eqs. (5.5) to (5.7) completely determine the properties of the infinite randomness fixed point, and for the RTFIM due to the infinitely wide probability distributions, their values are known exactly to be $\nu = 2$ for average correlations (satisfying the Harris criterion $d\nu \geq 2$ in one dimension), $\psi = 1/2$

for tunneling between clusters and $\phi = (1+\sqrt{5})/2$ characterizing the moment of a cluster.

Activated scaling is also referred to as highly anisotropic scaling and can lead to extremely slow dynamics in the paramagnetic phase as highly ordered rare regions fluctuate sedately. This can have important consequences for correlation functions since their probability distributions will also become very broad with spins located in the same well-ordered cluster giving contributions to averages of order one. One must therefore make a distinction between the usual definition of an *average* observable $\overline{\mathcal{O}}(x)$ and a *typical* observable $\mathcal{O}_{\text{typ}}(x)$ defined by the re-exponentiated average of a logarithm:

$$\overline{\mathcal{O}}(x) = \int P(x)\mathcal{O}(x) \tag{5.8a}$$

$$\mathcal{O}_{\text{typ}}(x) = \exp\left[\int P(x)\ln\mathcal{O}(x)\right] \tag{5.8b}$$

where $P(x)$ is the probability distribution for the random variable x. The distinction between average and typical quantities is a hallmark of infinite randomness critical points and can persist well into the Griffiths region discussed in Section 1.6.

Defining the spin-spin correlation function as

$$C(x) = \left\langle \sigma_i^z \sigma_{i+x}^z \right\rangle \tag{5.9}$$

Fisher found that at the critical point ($\delta = 0$)

$$\overline{C}(x) \sim \frac{1}{x^{2(d-\phi\psi)}} \tag{5.10a}$$

$$C_{\text{typ}} \sim \mathrm{e}^{-x^{\psi}} \tag{5.10b}$$

whereas in the paramagnetic region where $\delta > 0$

$$\overline{C}(x) \sim \frac{\exp\left[-(x/\xi) - (27\pi^2/4)^{1/3}(x/\xi)^{1/3}\right]}{(x/\xi)^{5/6}} \tag{5.11a}$$

$$C_{\text{typ}} \sim \mathrm{e}^{-x/\widetilde{\xi}} \tag{5.11b}$$

with $\widetilde{\xi}$ defined to be the length scale which describes typical correlations with modified divergence

$$\widetilde{\xi} \sim \delta^{-\widetilde{\nu}} \tag{5.12}$$

and $\widetilde{\nu} = 1$.

A natural questions arises regarding how far the SDRG and the results found for the RTFIM can be generalized to other systems with different symmetries, dimensionality and interactions. In higher dimensions the aggregation/decimation procedure

highlighted in Fig. 5.1 does not lead to analytic recursion relations as the topology of the lattice is changed with each iteration. Motronich *et al.* [138] implemented a numerical version of the SDRG for the two dimensional Ising model in a random transverse field and find evidence for the flow to strong disorder with modified critical exponents $\nu \approx 1.1$, $\psi \approx 0.42$ and $\phi \approx 2.5$. Generalizing the Ising symmetry to a Potts model, Senthil and Majumdar [139] found that any random quantum system with a continuous quantum phase transition at which a discrete symmetry of a non-conserved order parameter is broken will have the same critical behavior as the RTFIM; its properties are hyper-universal. Strong disorder physics can even overcome frustration, as at an infinite randomness critical point, the coupling distribution becomes so broad that in any loop, the frustrated interaction can be neglected. Infinite randomness for Ising symmetry does not survive, however, in the presence of a relaxation mechanism such as the coupling to bath degrees of freedom [73, 74]. The tunneling between large ordered droplets is completely suppressed and the transition is destroyed by smearing. This behavior can be understood in terms of the localization transition in a dissipative two state system [140].

For disordered $O(N)$ models with continuous symmetry order parameters it appears that in $d > 1$, any infinite randomness fixed point is unstable and flows to a finite disorder fixed point with conventional power-law scaling. Systems with *both* continuous symmetry and dissipation — the case studied in this thesis — are only just starting to be understood, and will be the focus of the remaining part of this chapter. Such systems were first studied in the context of itinerant electron systems whose excitations are damped by coupling between magnetic modes and the gapless particle-hole excitations of the metal. Without any damping, the order parameter of a rare region slowly fluctuates and can give rise to quantum Griffiths effects. As mentioned above, the presence of dissipation retards dynamics, and can lead to the complete destruction of the phase transition by smearing [141, 142].

The particular case of $d = 1$ and Ohmic dissipation $z = 2$, corresponding to our overdamped Cooper pair model with disorder, was recently studied via the SDRG by Hoyos *et al.* [129]. They found evidence that the SMT is described by a strong disorder fixed point exhibiting activated dynamic scaling where the logarithm of characteristic frequencies of Ψ fluctuations grows as a power of their characteristic length scale. They argued further that the strong disorder fixed point is in the same universality class as the one describing the onset of ferromagnetism in the quantum random transverse field Ising model in one spatial dimension described in detail above.

Note that this is a non-trivial result, as the RTFIM contains *no dissipation*, and possesses a *discrete symmetry*. The remainder of this chapter presents numerical results which provide compelling evidence for the applicability of their strong randomness RG predictions.

5.2 Lattice theory

We begin with a generalized version of the field theory $\mathcal{S}_\alpha$ in Eq. (2.1) at zero temperature which describes the fluctuations of a coarse-grained N-component superconducting order parameter Ψ_a in $1+1$ dimensions

$$\begin{aligned}\mathcal{S}_\alpha = &\int dx \int d\tau \left[D(x)|\partial_x \Psi_a(x,\tau)|^2 + \alpha(x)|\Psi_a(x,\tau)|^2 + \frac{u(x)}{2}|\Psi_a(x,\tau)|^4 \right] \\ &+ \int \frac{d\omega}{2\pi} \int dx\, \gamma(x)|\omega||\Psi_a(x,\omega)|^2.\end{aligned} \tag{5.13}$$

Quenched disorder has entered the theory through the spatial dependence of all coupling constants, $D(x)$, $\alpha(x)$, $\gamma(x)$ and $u(x)$. We have dropped the tilde on the coupling constant D as in the dirty limit, it can be identified with the real electron diffusion constant $D = v_{\rm F}\ell/3$. Note that we have not yet performed any rescalings to obtain a unit strength coupling in front of the dissipative $|\omega|$ term, allowing for the possibility of a spatially dependent Ohmic bath.

In our previous studies of this action, we have taken the limit $u \to \infty$ at the outset to rapidly approach the strong coupling limit, which facilitated the calculation of universal results. In this chapter we will take a slightly different approach, where u is large with respect to other energy scales, but is still finite, and some results will take a slightly different form. The loss of translational invariance due to the presence of disorder inexorably necessitates a numerical approach to fluctuations of the Ψ_a field. We first briefly describe the disorder free theory at finite u before introducing the finite disordered chain that will be our focus for the duration of this chapter.

5.2.1 Infinite clean chain

To ground ourselves, we will first discretize the action on an infinite lattice in the clean limit with a space and time rescaled such that $D(x) = 1$, $\alpha(x) = \alpha$, $\gamma(x) = \gamma = 1$ and $u(x) = u$

$$\begin{aligned}\mathcal{S} = \sum_{j=1}^{\infty} \int d\tau \left[|\Psi_{a,j}(\tau) - \Psi_{a,j+1}(\tau)|^2 + \alpha|\Psi_{a,j}(\tau)|^2 + \frac{u}{2}|\Psi_{a,j}(\tau)|^4 \right] \\ + \int \frac{d\omega}{2\pi} \sum_{j=1}^{\infty} |\omega||\Psi_{a,j}(\omega)|^2\end{aligned} \tag{5.14}$$

where $\Psi_{a,j}(\tau)$ is the a^{th} component of the order parameter at lattice site j and imaginary time τ and

$$\Psi_{a,j}(\omega) = \int d\tau \Psi_{a,j}(\tau) \mathrm{e}^{i\omega\tau} \tag{5.15}$$

is the Fourier transform of $\Psi_{a,j}(\tau)$. In the large-N limit, the methods introduced in Chapter 3 can be straightforwardly generalized to the finite u case in order to derive the effective quadratic action (now suppressing the a subscript on all fields)

$$\mathcal{S}_{0,c} = \sum_j \int d\tau \left[D|\Psi_j(\tau) - \Psi_{j+1}(\tau)|^2 + r|\Psi_j(\tau)|^2 \right] + \int \frac{d\omega}{2\pi} \sum_j |\omega||\Psi_j(\omega)|^2. \quad (5.16)$$

The renormalized distance from criticality, r must be found from the self-consistency (saddle point) condition

$$\begin{aligned} r &= \alpha + u \left\langle |\Psi_j(\tau)|^2 \right\rangle_{\mathcal{S}_{0,c}} \\ &= \alpha + u \int_{-\pi}^{\pi} \frac{dk}{2\pi} \int_0^{\Lambda_\omega} \frac{d\omega}{\pi} \frac{1}{r + \omega + 2(1 - \cos k)}, \end{aligned} \quad (5.17)$$

and as usual, we have absorbed a factor of N into a redefinition of the quartic coupling, introduced a large frequency cutoff Λ_ω and set the lattice constant to unity. The quantum critical point is found by choosing $\alpha = \alpha_c$ so that $r = 0$ and hence taking the cutoff $\Lambda_\omega = \pi^2$ we find

$$\alpha_c = -u \int_{-\pi}^{\pi} \frac{dk}{2\pi} \int_0^{\pi^2} \frac{d\omega}{\pi} \frac{1}{\omega + 2(1 - \cos k)} \quad (5.18)$$

$$= -\frac{2u}{\pi} \text{asinh}\left(\frac{\pi}{2}\right) \quad (5.19)$$

and for $u = 1$, $\alpha_c \simeq -0.785$. It will be useful to keep the clean value of α_c in mind when we discuss the disordered theory as it provides an upper bound.

5.2.2 Finite disordered chain

Motivated by the calculations of Hoyos *et al.* [129] we desire to confirm their proposition that in the presence of Ohmic dissipation, quantum fluctuations strongly renormalize the effects of disorder, leading to a quantum phase transition between a superconductor and metal governed by an infinite randomness fixed point with the associated dynamically activated scaling.

As mentioned above, quenched disorder can be introduced into a L-site lattice discretization of the our continuum overdamped Cooper pair model $\mathcal{S}_\alpha$ at $T = 0$

$$\begin{aligned} \mathcal{S} = \int d\tau \Bigg\{ &\sum_{j=1}^{L-1} D_j |\Psi_j(\tau) - \Psi_{j+1}(\tau)|^2 + \sum_{j=1}^{L} \left[\alpha_j |\Psi_j(\tau)|^2 + \frac{u_j}{2} |\Psi_j(\tau)|^4 \right] \\ &+ c_l |\Psi_1(\tau)|^2 + c_r |\Psi_L(\tau)|^2 \Bigg\} + \int \frac{d\omega}{2\pi} \sum_{j=1}^{L} \gamma_j |\omega| |\Psi_j(\omega)|^2, \end{aligned} \quad (5.20)$$

where all couplings are random functions of j and we have introduced fixed but random boundary conditions c_l and c_r, similar to those employed in Ref. [89] to describe the effects of leads on the conductance of ultra-narrow finite length metallic wires. The quartic coefficients u_j must all be positive to ensure stability and repulsion between Cooper pairs. The dissipation into the metallic bath as represented by γ_j, is also required to be positive by causality. Finally, we can choose a gauge such that $D_j > 0$. A more careful analysis and suitable rescalings [110] allow us to reduce the randomness to only the spatial dependence of D_j and α_j while setting $u_j = u$ and $\gamma_j = 1$. Disorder in these two couplings alone is sufficient to generate disorder in γ_j under renormalization.

The random diffusion constant D_j is taken to be uniformly distributed on $(0, 1]$

$$P(D_j) = \begin{cases} 1 & ; \quad 0 < D_j \leq 1 \\ 0 & ; \quad \text{otherwise} \end{cases} \tag{5.21}$$

such that its mean $\overline{D} = 1/2$ while α_j is assumed to be Gaussian distributed with mean $\overline{\alpha}$ and standard deviation $\sqrt{\overline{\alpha^2} - \overline{\alpha}^2} = 1/2$ in units of γ^2

$$P(\alpha_j) = \sqrt{\frac{2}{\pi}} \mathrm{e}^{-2(\alpha_j - \overline{\alpha})^2}. \tag{5.22}$$

At zero temperature, the SMT can be tuned by reducing the mean of the α_j distribution, $\overline{\alpha}$, while keeping its variance constant.

Equivalently, we could have also chosen to work in a lattice model of fluctuating phases with $\Psi_j(\tau) = e^{i\theta_j(\tau)}$ of unit magnitude [89, 93]; this should have the same properties as $\mathcal{S}$, but our analysis proceeds more conveniently by also allowing for magnitude fluctuations.

While $\mathcal{S}$ is a suitable model for describing the influence of disorder on the fluctuating Cooper pair states, we also have to consider the effect of randomness on the single electron states. We have estimated such effects in the framework of weak-coupling BCS theory: at criticality, we find that on a scale parametrically smaller than the single electron localization length, the gain in condensation energy can offset the cost in elastic energy when order parameter fluctuations take advantage of randomness in the α_j. This justifies our focus on the influence of disorder in a purely bosonic overdamped Cooper pair theory (see Ref. [43]).

The RG analysis [129] was carried out in a model with an N-component order parameter and it was found that flows had only an irrelevant dependence on the value of N [143]. Thus the exact critical properties can be obtained by studying the model in the large-N limit. As above, this is equivalent to approximating $\mathcal{S}$ by the Gaussian

action

$$\mathcal{S}_0 = \int \frac{d\omega}{2\pi} \Bigg[\sum_{j=1}^{L-1} D_j |\Psi_j(\omega) - \Psi_{j+1}(\omega)|^2 + \sum_{j=1}^{L} (r_j + |\omega|) |\Psi_j(\omega)|^2 + c_l |\Psi_1(\omega)|^2 + c_r |\Psi_L(\omega)|^2 \Bigg]$$
$$= \sum_{j=1}^{L} \int \frac{d\omega}{2\pi} \Psi_j^*(\omega) \left(\mathsf{M}_{ij} + |\omega| \delta_{ij} \right) \Psi_j(\omega) \tag{5.23}$$

where the frequency independent coupling matrix is given by

$$\mathsf{M}_{ij} = \begin{cases} D_1 + c_l + r_1 & ; \quad i = j = 1 \\ D_{L-1} + c_r + r_L & ; \quad i = j = L \\ (D_i + D_{i-1} + r_i)\delta_{i,j} - D_j \delta_{i,j+1} - D_i \delta_{i,j-1} & ; \quad \text{otherwise} \end{cases} \tag{5.24}$$

with each r_j determined self-consistently by solving the *now* site dependent saddle point equation

$$r_j = \alpha_j + \left\langle |\Psi_j(\tau)|^2 \right\rangle_{\mathcal{S}_0}, \tag{5.25}$$

and we have set $u = 1$ to reach a strong coupling regime. In this simplified form, the average equal time on-site order parameter susceptibility in Eq. (5.25) is given by

$$\left\langle |\Psi_j(\tau)|^2 \right\rangle_{\mathcal{S}_0} = \int \frac{d\omega}{2\pi} \left[\, |\omega| \mathbb{1} + \mathsf{M} \, \right]^{-1}_{jj} \tag{5.26}$$

where $\mathbb{1}$ is the $L \times L$ identity matrix.

From Eq. (5.24), it is clear that M is a real, symmetric tridiagonal matrix (due to the fixed boundary conditions chosen), and it will convenient to find its spectral decomposition in terms of the eigenvector V_{ij} and accompanying diagonal eigenvalue $\mathsf{E}_{ij} = \lambda_j \delta_{ij}$ matrices defined by

$$\sum_{j=1}^{L} \mathsf{M}_{ij} \mathsf{V}_{jk} = \mathsf{V}_{ik} \lambda_k \tag{5.27}$$

where V is orthogonal. This decomposition can be used to write inverses involving M like the one in Eq. (5.26) as

$$\left[\, |\omega| \mathbb{1} + \mathsf{M} \, \right]^{-1}_{ij} = \sum_{k=1}^{L} \frac{\mathsf{V}_{ik} \mathsf{V}_{kj}}{|\omega| + \lambda_k} \tag{5.28}$$

and thus the saddle point equation is given by

$$Q_i \equiv \frac{1}{\pi} \sum_{j=1}^{L} (\mathsf{V}_{ij})^2 \ln \left(1 + \frac{\pi^2}{\lambda_j} \right) + \alpha_j - r_j = 0 \tag{5.29}$$

where we sum over the i^{th} component of each eigenvector and have introduced an ultra violet cutoff $\Lambda_\omega = \pi^2$ for convergence of the frequency integral. It will be convenient to introduce the analytical form of the Hessian matrix at the saddle point given by

$$\frac{\partial Q_i}{\partial r_j} = -\delta_{i,j} - \frac{u}{\pi} \sum_{k,\ell=1}^{L} \mathsf{V}_{ik}\mathsf{V}_{jk}\mathsf{V}_{i\ell}\mathsf{V}_{j\ell} \frac{\ln \lambda_k - \ln \lambda_\ell}{\lambda_k - \lambda_\ell}. \tag{5.30}$$

By the use of the spectral decomposition of M we have eliminated the need to compute its inverse and are left with the task of diagonalizing a tri-diagonal matrix which can be accomplished using a standard QL algorithm which scales linearly with the number of sites L.

5.3 The solve-join-patch algorithm

Solving the innocuous looking Eq. (5.29) for a large number of disorder realizations and large system sizes was the primary time-consuming numerical step in obtaining the results of this chapter. Similar numerical large-N methods have been used previously for disordered systems with conventional (power law) dynamic scaling [144, 145] but the presence of activated scaling leads to sluggish dynamics and the necessity to properly include spurious disorder configurations that, although exponentially rare, can make large contributions to thermodynamic properties. The full numerical solution corresponding to the set $\{r_j\}$ for a given realization of disorder, system size L and mean random pair-breaking $\overline{\alpha}$ can be obtained by an iterative process using a modified version of Powell's hybrid method [146, 147]. The computational effort is drastically reduced by having access to the analytic form of the Hessian matrix given in Eq. (5.30). This approach works quite well for large $\overline{\alpha}$ or small system sizes, but as we draw nearer the critical point, characterized by the crossover condition that the correlation length $\xi \sim L$, the direct iterative solution of Eq. (5.25) quickly becomes computationally prohibitive. This is a result of the fact that the eigenmodes of $\mathcal{S}_0$ begin to delocalize and have a characteristic energy scale that is exponentially small in the distance from criticality, requiring that the solutions r_j be computed with exponentially increasing precision.

This obstacle was overcome through the development and implementation of an iterative *solve-join-patch* (SJP) procedure in the spirit of real space renormalization. It takes advantage of the presence of only short range nearest neighbor interactions in the effective action Eq. (5.23). The SJP algorithm which can be applied to very large systems near criticality is shown schematically in Fig. 5.2. Algorithmically, it is defined by the following steps.

1. Generate a realization of disorder for a system composed of $L = n\ell$ sites, labeled by $i = j\ell + k$ where $0 \leq j \leq n-1$, $1 \leq k \leq \ell$ and n is an even integer.

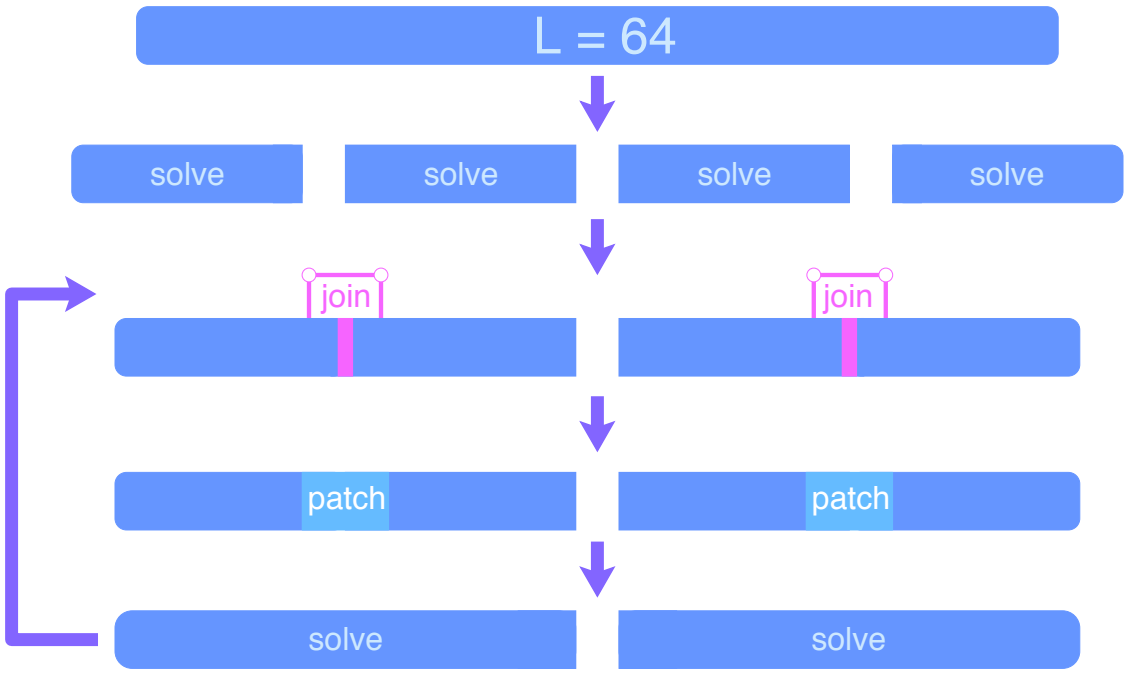

Figure 5.2: A schematic outline of one iteration of the solve-join-patch procedure for the specific case of $L = 64$ with $n = 4$ and $\ell = 16$.

2. Break the large system into n subsystems of size ℓ and iteratively solve Eq. (5.29) for each subsystem via Powell's method described above, with the modification that for *interior* systems ($0 < j < n - 1$), the fixed boundary conditions previously Determined by the random numbers c_l and c_r are replaced by $c_l = J_{j\ell}$ and $c_r = J_{j\ell+\ell+1}$. The result is n sets of ℓ r_i's which solve the individual subsystem self-consistency equations, (5.29).

3. Join the now solved n subsystems into $n/2$ larger subsystems of length 2ℓ. Not surprisingly, Eq. (5.29) for the new enlarged subsystem will be poorly satisfied near the interfaces where the neighboring values of r_i are poorly matched. This can be addressed through a patching procedure where one considers a small mini-system composed of only six sites, centered at the joint.

4. For each subsystem whose *left* half is labeled by j construct the mini-system composed of the sites $i = j\ell + \ell - 2, \ldots, j\ell + \ell + 3$. Set $c_l = J_{j\ell+\ell-3}$ and $c_r = J_{j\ell+\ell+4}$ and iteratively solve for the six new values $\{r'_i\}$. With these new values included, each subsystem of length 2ℓ is now quite close to satisfying $Q_i = 0$ and can be quickly solved using the set of initial conditions $\{r_{j\ell+1}, \ldots, r_{j\ell+\ell-3}, r'_{j\ell+\ell-2}, \ldots, r'_{j\ell+\ell+3}, r_{j\ell+\ell+4}, \ldots, r_{j\ell+2\ell}\}$ producing a solution set $\{r_i\}$.

5. Redefine $\ell \to 2\ell$, $n \to n/2$.

6. Iteratively repeat the SJP procedure outlined in steps $3 \to 5$ until a self-consistent solution is found to $Q_i = 0$ for the full system composed of L sites ($n = 1$, $\ell = L$).

Although the SJP method works quite well, we are still limited by the requirement of performing a full diagonalization of larger and larger matrices and have considered up to 3000 realizations of disorder for the four system sizes, $L = 16, 32, 64, 128$. The thermodynamic limit is approximated by finite size scaling where appropriate.

5.4 Evidence for infinite randomness

Fisher's remarkable solution of the RTFIM [64, 65] includes asymptotically exact results for the exponents and correlation functions at the infinite randomness fixed point, and many directly translate to the RG calculations by Hoyos *et al.* [129] for the dissipative model considered here. In particular, one expects activated dynamic scaling with $\ln(1/\Omega) \sim L^{\psi}$ where Ω is a characteristic energy scale and $\psi = 1/2$ is a tunneling exponent. This reflects the fact that at an infinite randomness fixed point, the dynamical critical exponent z is formally infinite. The RG approach defines a real space decimation procedure that either creates or destroys *clusters* or *bonds* as the energy scale is reduced. The typical moment of a surviving cluster scales like $\mu \sim \ln^{\phi}(1/\Omega)$ at criticality, where $\phi = (1+\sqrt{5})/2 \simeq 1.62$ is the golden mean. Average correlations are described by a correlation length which diverges as $\xi \sim |\delta|^{-\nu}$ with $\nu = 2$ and δ a measure of the distance from criticality. From Ref. [129], δ is expected to be proportional to $\overline{\ln(r_i/r_c)}$ where r_c is some critical value. Our numerical study reveals that close to criticality this quantity is linearly related to the detuning of the average $\overline{\alpha}$ from its quantum critical value, $\overline{\alpha}_c$, (which has yet to be determined) and it further demonstrates that correlations among the r_i due to their self-consistency does not affect the strong randomness RG flow.

The remainder of this chapter will present a numerical confirmation of the results of Ref. [129] by providing arguments for the presence of dynamically activated scaling at the quantum SMT, characterized by exponents ν, ψ and ϕ taking on their RTFIM values. The evidence comes from an analysis of equal time correlations, energy gap statistics and dynamic susceptibilities in the weakly disordered quantum Griffiths phase [70].

5.4.1 Equal time correlation functions

We begin by studying the disorder averaged equal-time correlation function

$$\overline{C}(x) = \overline{\langle \Psi_x^*(\tau)\Psi_0(\tau)\rangle}_{\mathcal{S}_0}, \tag{5.31}$$

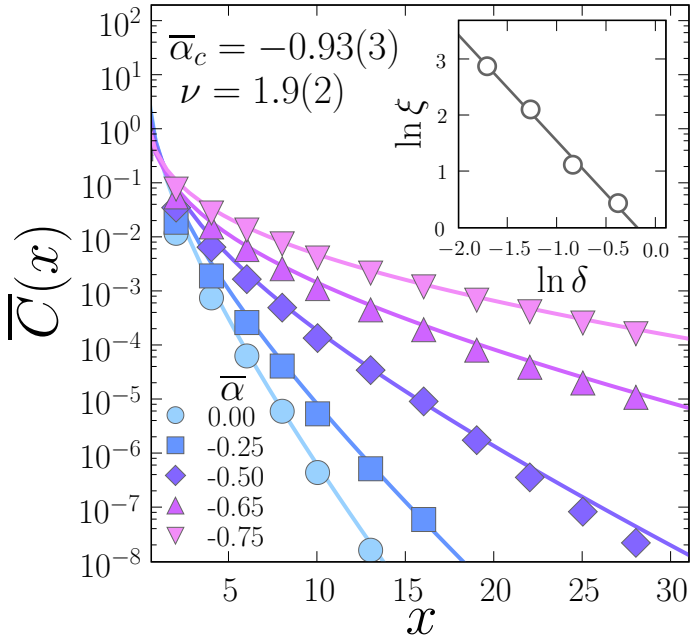

Figure 5.3: The equal-time disorder averaged correlation functions for $L = 64$ and five values of the mean of the α_j distribution, $\overline{\alpha}$. The solid lines are fits to the asymptotic form described in Eq. (5.32) via ξ and an overall scale parameter. The inset shows the result of a fit to the power law form of the finite size scaled correlation length leading to an estimate for the location of the critical point $\overline{\alpha}_c = -0.93(3)$ and the correlation length exponent $\nu = 1.9(2)$.

(where x is now a site index) which can be computed from the quadratic effective action $\mathcal{S}_0$ once the full set of solutions $\{r_j\}$ has been obtained, and an overline indicates an average over realizations of disorder. In the disordered phase, where $\delta \equiv \overline{\alpha} - \overline{\alpha}_c > 0$ the asymptotic form of $\overline{C}(x)$ for the RTFIM has been predicted to describe both exponential as well as stretched exponential decay in addition to power law behavior [65]

$$\overline{C}(x) \sim \frac{\exp\left[-(x/\xi) - (27\pi^2/4)^{1/3}(x/\xi)^{1/3}\right]}{(x/\xi)^{5/6}}. \tag{5.32}$$

If we use this expression to define the correlation length ξ, we can perform fits for each value of L and various $\overline{\alpha}$ to extract $\xi(L, \overline{\alpha})$ as is seen in Fig. 5.3 for $L = 64$. We find remarkable agreement (solid lines) with Eq. (5.32) over six orders of magnitude for all system sizes considered.

As mentioned above, the length scale which describes average correlations is expected to diverge like $\xi \sim |\delta|^{-\nu}$ as the critical point is approached. We have employed this result to perform a log-log fit to the finite size scaled correlation length (data extrapolated to $L \to \infty$) as a function of δ, as is shown in the inset of Fig. 5.3. The

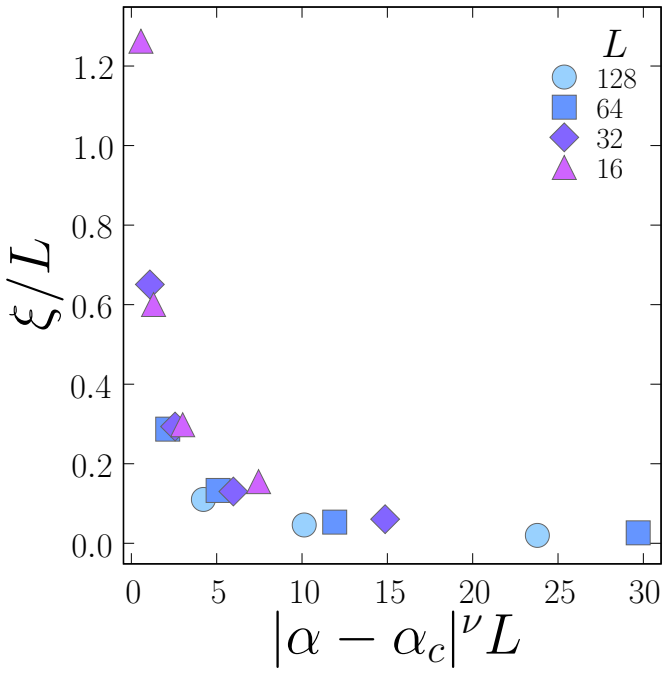

Figure 5.4: Data collapse of the finite size data for the correlation length using $\overline{\alpha}_c = -0.93$ and $\nu = 1.9$ highlighting the consistency of the finite size scaling and fitting procedures.

value of $\overline{\alpha}_c$ was found from the mean of the critical α_j distribution which minimized the least square error of power law fits involving $\delta = \overline{\alpha} - \overline{\alpha}_c$. This leads to a value of $\overline{\alpha}_c = -0.93(3)$ for the critical point and $\nu = 1.9(2)$ for the correlation length exponent with the number in brackets indicating the uncertainty in the last digit computed from the fitting procedure. The obtained value of ν is in accord with the value of 2 predicted for the RTFIM. The correlation length could also have been defined via the exponential tail of $\overline{C}(x)$ at large separations which yields compatible values for both $\overline{\alpha}_c$ and ν. The accuracy of the finite size scaling and fitting results was confirmed through the observation of good data collapse when plotting $\xi(L,\delta)L^{-1}$ against $\delta^{\nu}\ L$ [52] as seen in Fig. 5.4.

5.4.2 Energy gap statistics

For each realization of disorder and each value of $\overline{\alpha}$ we define the gap $\Omega(L)$ to be the smallest excitation energy in the system, which in general corresponds to the most delocalized mode of $\mathcal{S}_0$. Rare disorder configurations cause clusters to behave as if they were much more critical than the global value of δ would suggest. These clusters dominate the critical modes and exhibit abnormally small gaps that make

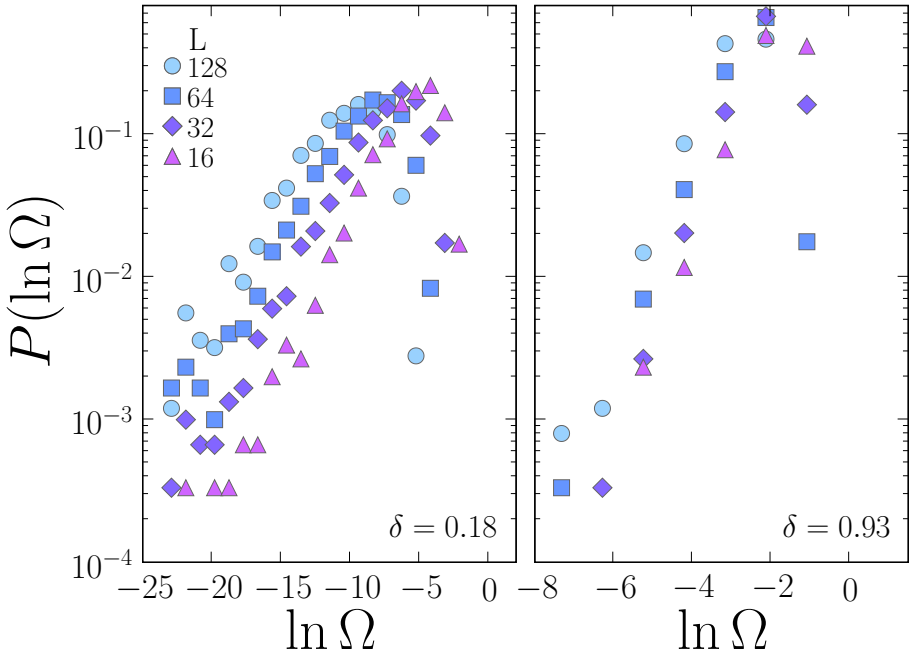

Figure 5.5: The system size dependent probability distribution (over all realizations of disorder) for the logarithm of the gap (minimum eigenvalue) for $\overline{\alpha}$ close to criticality (left panel) and far from criticality (right panel) where $\delta = \overline{\alpha} - \overline{\alpha_c}$ with $\overline{\alpha}_c = -0.93$.

large contributions to disorder averages of $\ln\Omega$, leading to the highly anisotropic scaling relationship between space and time that is the hallmark of strong disorder fixed points. We have performed a direct analysis of the probability distribution for the logarithm of the energy gap with the result shown in Fig. 5.5. We observe that when the mean of the α_j distribution is close to its critical value (left panel) the gap distribution gets broader with increasing system size, characteristic of having more "space" in the sample where a strongly ordered (rare) region can form. Far from criticality (right panel) the histograms look very similar for different system sizes and are just horizontally shifted from one another. This is consistent with the idea that well into the disordered phase the excitations leading to a small gap are well localized and have a probability proportional to L. The drastic change in qualitative behavior between $\delta = 0.18$ and $\delta = 0.93$, with the width of the small δ distribution strongly depending on system size, provides cogent evidence for $z = \infty$ at the critical point. A similar analysis for the RTFIM was carried out by Young and Rieger [148] where they found identical results. In addition we find that $\ln\Omega$, as the minimal excitation energy, is naturally characterized by extreme value statistics and has a Gumbel probability distribution

$$P(x) = \frac{1}{\beta}\exp\left[\left(\frac{x-\mu}{\beta}\right) - \exp\left(\frac{x-\mu}{\beta}\right)\right] \tag{5.33}$$

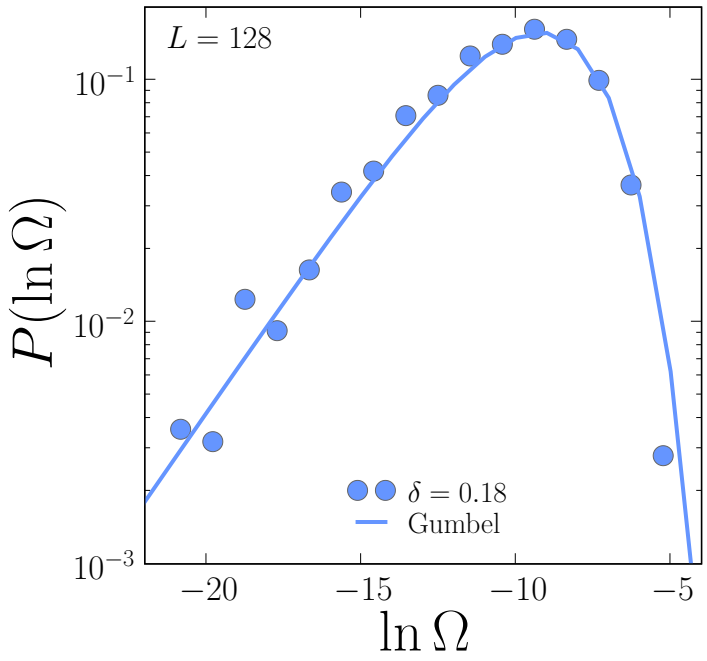

Figure 5.6: A fit of the probability distribution of the minimum excitation energy for system size $L = 128$ and $\delta = 0.18$ (symbols) to a Gumbel distribution with location $\mu \simeq -9.2$ and scale $\beta \simeq 2.3$ (solid line). The Gumbel form is not unexpected as the logarithm of the gap for each realization of disorder is an extremal value.

with location μ and scale β. A Gumbel fit for $L = 128$ and $\delta = 0.18$ is shown in Fig. 5.6.

If activated dynamic scaling is indeed present, the disorder averaged value of the logarithm of the gap should scale like

$$|\overline{\ln \Omega}| \sim \xi^{\psi} \sim \delta^{-\nu\psi} \tag{5.34}$$

where we have used the scaling form of the correlation length. Such divergent behavior for the finite size scaled value of $|\overline{\ln \Omega}|$ is demonstrated in Fig. 5.7. The possibility of conventional scaling was considered but ultimately excluded through the examination of the maximum likelihood estimator for a wide range of power law fits. Using the previously determined values of $\overline{\alpha}_c$ and ν, the tunneling exponent can be extracted from a log-log linear fit of the average logarithmic spectrum as shown in the inset of Fig. 5.7, producing $\psi = 0.53(6)$ which is consistent with the RTFIM prediction of $1/2$. A final consistency check is to investigate data collapse for the probability distribution of the rescaled logarithmic energy scale $\delta^{\nu\psi} \ln \Omega$ near criticality as detailed in Fig. 5.8.

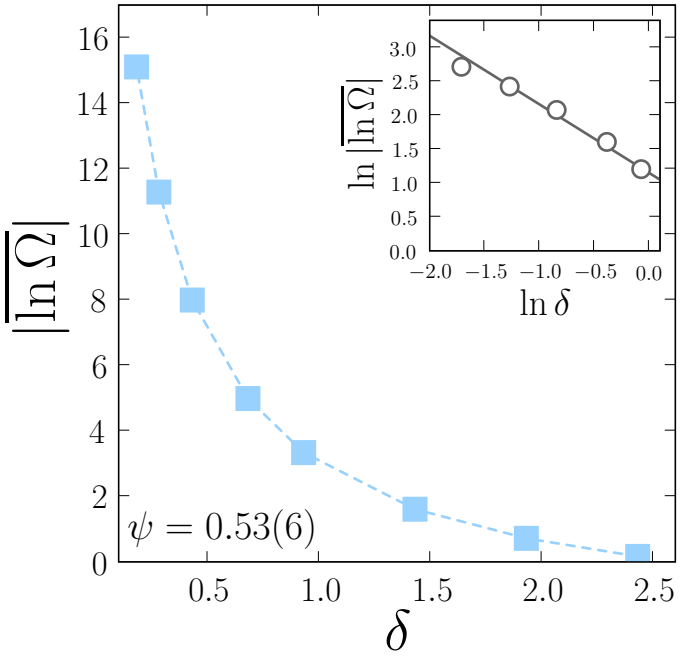

Figure 5.7: The finite size scaled value of the disorder averaged logarithm of the minimum excitation energy plotted against the distance from the critical point δ. We observe divergence consistent with the scaling form $\overline{|\ln \Omega|} \sim \delta^{-\nu\psi}$ and using the value of $\overline{\alpha}_c$ and ν found above we determine $\psi = 0.53(6)$ from a log-log linear fit (inset).

5.4.3 Dynamical Susceptibility

To confirm full agreement with the universality class of the RTFIM, we must finally determine the value of the exponent ϕ which controls the average moment, $\mu \sim |\ln \omega|^{\phi}$, of a cluster fluctuating with frequency ω. This can be accomplished by investigating the imaginary part of the disorder averaged dynamical order parameter susceptibilities after they have been analytically continued to real frequencies. We are interested in the average ($k = 0$) and local susceptibilities defined by

$$\mathrm{Im}\ \overline{\chi}(\omega) = \frac{1}{L}\sum_{x} \mathrm{Im}\ \overline{\langle \Psi_x^*(i\omega)\Psi_0(i\omega)\rangle}_{\mathcal{S}_0}\Big|_{i\omega\to\omega+i\epsilon} \tag{5.35a}$$

$$\mathrm{Im}\ \overline{\chi_{\mathrm{loc}}}(\omega) = \mathrm{Im}\ \overline{\langle \Psi_0^*(i\omega)\Psi_0(i\omega)\rangle}_{\mathcal{S}_0}\Big|_{i\omega\to\omega+i\epsilon} \tag{5.35b}$$

respectively, where $\langle\cdots\rangle_{\mathcal{S}_0}$ indicates an average with respect to the large-N action in Eq. (5.23) and $x = |i-j|$ is the separation between two sites. Note that ω is now a real frequency, and we point out that our facile access to such dynamical quantities is one of the perquisites of the numerical approach we have taken. All frequencies are measured with respect to an ultra-violet cutoff Λ_ω which is required for convergence when computing the set of solutions to Eq. (5.25).

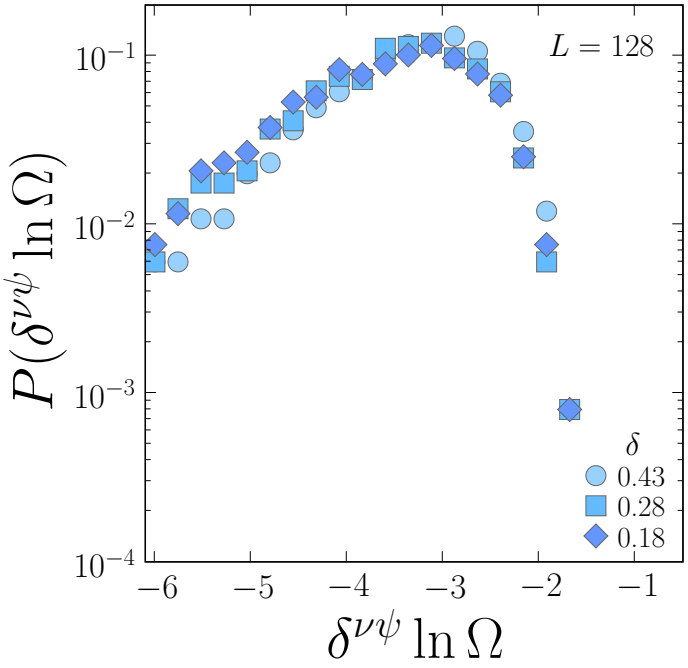

Figure 5.8: The rescaled probability distribution for the natural logarithm of the smallest excitation energy for $L = 128$ and $\delta = 0.18, 0.23, 0.43$ which exhibits data collapse consistent with activated scaling for the values $\overline{\alpha}_c = -0.93$, $\nu = 1.9$ and $\psi = 0.53$ discussed in the text.

The spectral decomposition of the coupling matrix M introduced in Section 5.2.2 can be used here to derive explicit results for the average and local susceptibility, whose forms will be useful in determining scaling relations. For a single realization of disorder, Eq. (5.28) leads to an expression for the dynamic order parameter susceptibility between two sites i and j at imaginary frequency $i\omega$

$$\begin{aligned} \chi_{ij}(i\omega) &= \langle \Psi_i^*(i\omega)\Psi_j(i\omega)\rangle_{\mathcal{S}_0} \\ &= [\,|\omega|\mathbb{1} + \mathsf{M}\,]^{-1}_{ij} \\ &= \sum_{k=1}^{L} \frac{\mathsf{V}_{ik}\mathsf{V}_{kj}}{|\omega| + \lambda_k} \end{aligned} \tag{5.36}$$

where λ_k is an eigenvalue corresponding to the k^{th} column of the eigenvector matrix V. The local susceptibility is an average over all sites of the response to a local "field"

at each site

$$\begin{aligned}\chi_{\rm loc}(i\omega) &= \frac{1}{L}\sum_{i=1}^{L}\chi_{ii}(i\omega)\\ &= \frac{1}{L}\sum_{i,j=1}^{L}\frac{(\mathsf{V}_{ij})^2}{|\omega|+\lambda_j}\\ &= \frac{1}{L}\sum_{i=1}^{L}\frac{1}{|\omega|+\lambda_i}\end{aligned} \tag{5.37}$$

where we have used the orthogonality of V. Analytically continuing to real frequencies $i\omega \to \omega + i\eta$ and taking the imaginary part of both sides

$$\mathrm{Im}\,\chi_{\rm loc}(\omega) = \frac{1}{L}\sum_{i=1}^{L}\frac{\omega}{\omega^2+\lambda_i^2} \tag{5.38}$$

where we immediately observe that $\mathrm{Im}\,\chi_{\rm loc} \sim \omega^{-1}$ for $\omega \gg \Omega$ and $\mathrm{Im}\,\chi_{\rm loc} \sim \omega$ for $\omega \ll \Omega$, with the gap $\Omega = \min_i\{\lambda_i\}$.

Identical arguments lead to an expression for the average susceptibility defined as the $k = 0$ component of the spatial Fourier transform of $\chi_{ij}(i\omega)$

$$\mathrm{Im}\,\chi(\omega) = \frac{1}{L^2}\sum_{i,j,k=1}^{L}\frac{\omega \mathsf{V}_{ik}\mathsf{V}_{jk}}{\omega^2+\lambda_j^2} \tag{5.39}$$

which should have the same leading frequency dependence as $\mathrm{Im}\,\chi_{\rm loc}$ except the expressions will be modified by a term $\sum_{ij}\mathsf{V}_{ik}\mathsf{V}_{jk}$ which is directly related to the magnitude of local order (the cluster moment).

Appendix D provides a detailed derivation of the scaling forms for the dynamical susceptibilities in the quantum Griffiths region, and from Eq. (D.16a) and Eq. (D.16b)

$$\mathrm{Im}\,\chi_{\rm loc}(\omega) \sim \frac{\delta^{1/\psi-\phi\nu\delta}\left(\delta^{\nu\psi}\,|\ln\omega\,|\right)^{\delta/\psi}}{\omega^{1-\delta/\psi}}. \tag{5.40}$$

$$\mathrm{Im}\,\chi(\omega) \sim \frac{\delta^{1/\psi-\phi\nu\psi(1+\delta/\psi)}\left(\delta^{\nu\psi}\,|\ln\omega\,|\right)^{1-\delta/\psi}}{\omega^{1-\delta/\psi}}. \tag{5.41}$$

The disorder averaged dynamical susceptibilities are plotted for $\delta > 0$ in Figs. 5.9 and 5.10 for $L = 128$ with insets that show data collapse confirming the predicted scaling behavior of Eqs. (5.40) and (5.41). The leading order frequency dependence of both susceptibilities can be understood as follows: for $\omega \gtrsim \Lambda_\omega = \pi^2$ we find a trivial $1/\omega$ behavior, independent of δ. However, as argued above, the non-trivial frequency dependence of the susceptibility can be understood in terms of the relative

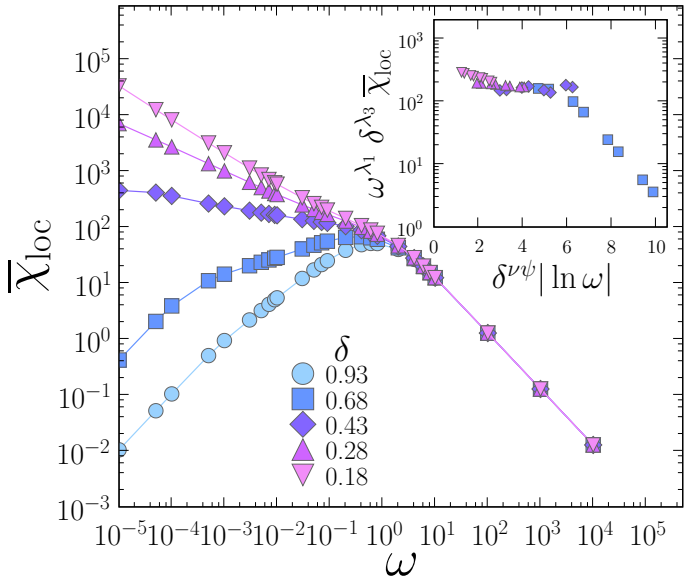

Figure 5.9: The disorder averaged local dynamical susceptibility for five values of δ in the quantum Griffiths phase with $L = 128$. The inset shows data collapse compatible with Eq. (5.40) where $\lambda_1 = 1 - \delta/\psi$ and $\lambda_3 = \phi\nu\delta - 1/\psi$.

size of ω when compared to the energy of the most critical mode, labeled by Ω. For $\omega \ll \Lambda_\omega$ and $\delta \sim 1$ we are far from criticality and all modes are well localized. The probe frequency is the smallest energy scale in the system and the susceptibility is linear in ω. When $\delta \ll 1$, vanishingly low energy modes may appear as a consequence of strongly ordered rare regions; the susceptibility is now inversely proportional to probe frequency.

Physically, one can argue that the average cluster moment will be given by the ratio of the average to local susceptibility due to the extra sum over sites implicit in in Eq. (5.35a). This is proven in Appendix D, and we define

$$\mathcal{R}(\omega) = \frac{\mathrm{Im}\overline{\chi}(\omega)}{\mathrm{Im}\overline{\chi_{\rm loc}}(\omega)} \sim |\ln\omega|^{\phi}\ \Phi_{\mathcal{R}}\left(\delta^{\nu\psi}|\ln\omega|\right) , \tag{5.42}$$

where the scaling function $\Phi_{\mathcal{R}}$ approaches a constant when the dimensionless variable $\delta^{\nu\psi}|\ln\omega| \ll 1$. In the quantum disordered phase with $\delta^{\nu\psi}|\ln\omega| \gg 1$, a scaling analysis (Appendix D) predicts $\Phi_{\mathcal{R}}(x) \sim x^{1-\phi}$ and hence

$$\mathcal{R} \sim \delta^{\nu\psi(1-\phi)}|\ln\omega|. \tag{5.43}$$

In order to determine the value of ϕ, it is useful to consider a rescaled value of the susceptibility ratio

$$\widetilde{\mathcal{R}}(\delta) = \frac{\mathcal{R}(\omega)}{\delta^{\nu\psi}|\ln\omega|} \tag{5.44}$$

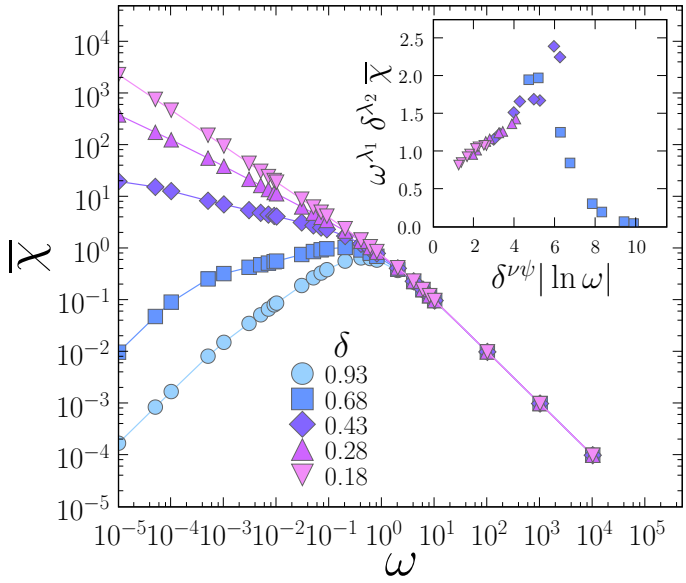

Figure 5.10: The disorder averaged average dynamical susceptibility for five values of δ in the quantum Griffiths phase with $L = 128$. The inset shows data collapse compatible with Eq. (5.41) where $\lambda_1 = 1 - \delta/\psi$ and $\lambda_2 = \phi\nu\psi(1 + \delta/\psi) - 1/\psi$.

which should be frequency independent according to the predicted scaling form for $\mathcal{R}(\omega)$ as $\omega \to 0$. We plot the finite size scaled susceptibility ratio in Fig. 5.11 for the three smallest values of δ, and find confirmation of its linear $|\ln\omega|$ dependence. The inset of Fig. 5.11 confirms the frequency independence of $\widetilde{\mathcal{R}}$ and by determining the best linear fit of $\ln\widetilde{\mathcal{R}}$ to $\ln\delta$ for $\omega \leq 10^{-3}$ with $\nu\psi = 1.0(1)$, we find a cluster exponent $\phi = 1.6(2)$ which is very close to the predicted RTFIM value of $(1+\sqrt{5})/2$.

5.4.4 Summary

The results of the previous section, as highlighted in Figs. 5.3, 5.7 and 5.11, provide compelling evidence for the applicability of the real space RG analysis of Hoyos *et al.*, and further reproduces a number of results of [65] to unexpected accuracy. This confirms that the considered model for overdamped repulsive Cooperon fluctuations in the presence of quenched disorder near a SMT exhibits dynamically activated scaling and is controlled by an infinite randomness fixed point in the same universality class as the RTFIM with the schematic phase diagram shown in Fig. 5.12. As summarized in Table 5.1, the transition is characterized by the numerically computed critical exponents $(\nu, \psi, \phi) \simeq (1.9, 0.53, 1.6)$ which are entirely consistent with those of the one dimensional random quantum Ising model in a transverse field $(2, 1/2, (1+\sqrt{5})/2)$.

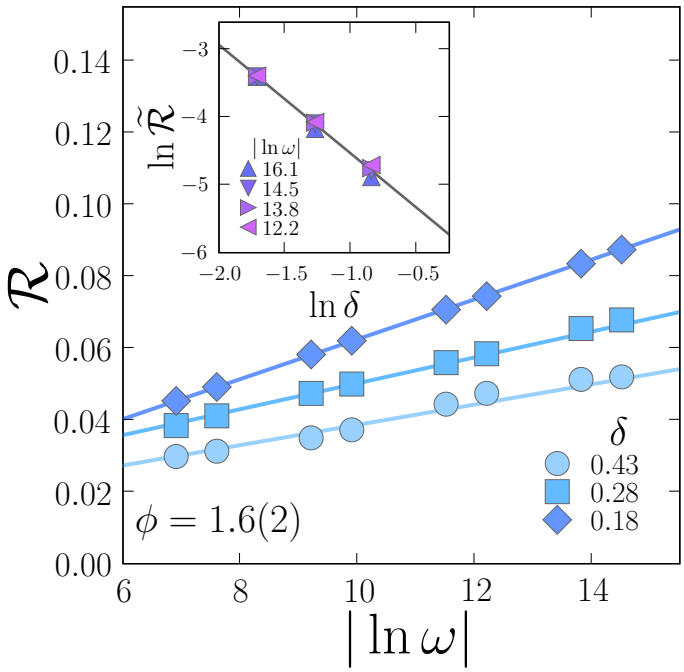

Figure 5.11: The real frequency dependence of the finite size scaled value of the disorder averaged susceptibility ratio defined in Eq. (5.42) for three values of $\delta = \overline{\alpha} - \overline{\alpha}_c$. We observe the predicted $|\ln\omega|$ behavior. After a suitable rescaling described in the text we find that $\widetilde{R}$ does not depend on frequency as $\omega \to 0$ (inset), and a log-log linear fit gives the value of the cluster exponent to be $\phi = 1.6(2)$.

	ν	ψ	ϕ
RTFIM	2	1/2	$(1+\sqrt{5})/2$
Ohmic Cooperon Theory	1.9(2)	0.53(6)	1.6(2)

Table 5.1: A summary and comparison of the critical exponents describing the correlation length (ν), tunneling (ψ) and cluster moment (ϕ) for the onset of ferromagnetism in the quantum random transverse field Ising model (RTFIM) where their values are asymptotically exact, and the zero temperature quantum phase transition between a superconductor and a metal in a dissipative theory of Cooperon fluctuations coupled to an Ohmic bath which have been calculated numerically.

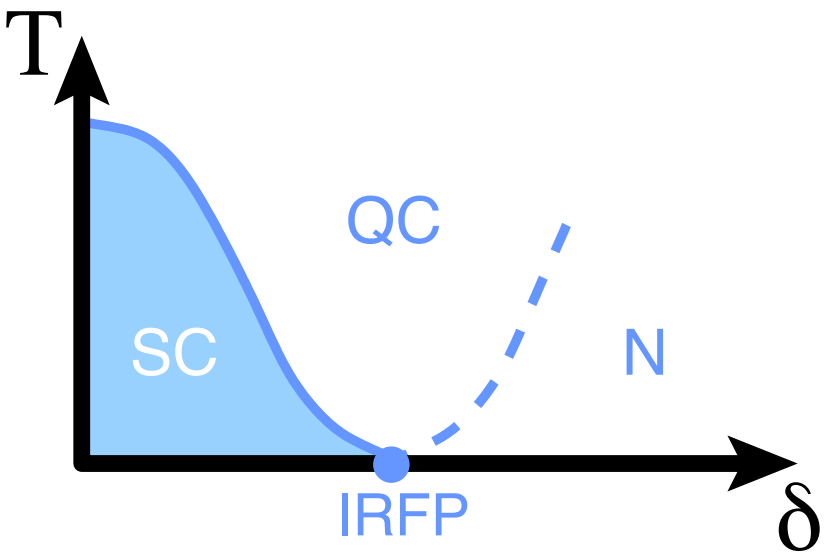

Figure 5.12: A schematic phase diagram for the transition between a superconducting (SC) and normal (N) state connected by an infinite randomness fixed point (IRFP). The shape of the finite temperature phase boundary was predicted to be $T_c \sim \exp(-\mathcal{C}|\delta|^{\nu\psi})$ in Ref. [129] where $\mathcal{C}$ is a constant.

Chapter 6

Conclusions

This thesis has been concerned with a topic that could be mistakingly confused with one of limited scope, the pair-breaking quantum phase transition between a superconductor and a metal in an ultra-narrow wire as modeled by a continuum quantum field theory. Instead, we have discovered a remarkably rich phase diagram full of interesting phases and crossovers, and even the presence of infinite randomness and exotic non-power law activated scaling relations between space and time in the presence of disorder.

Experimental motivations exist in the form of transport experiments on metallic nanowires, formed through molecular templating by sputtering material on top of a long rigid "bridge" or "backbone" molecule lying over a trench [35]. In this way, wires with diameters of less than 10 nm can be fabricated; a giant step towards reaching the quantum limit. In an applied current and at fixed temperatures, below the bulk superconducting transition temperature for the wires composite material, a given wire can display either metallic or superconducting behavior depending on its radius, with the general trend that thinner wires are less superconducting. In addition, for a particular wire which does exhibit electrical transport without resistance, superconductivity can be destroyed by turning on a suitably strong magnetic field oriented along its parallel axis. In both of these cases, it is some non-thermal parameter which tunes between the superconducting and normal metallic state at zero temperature providing an excellent manifestation of a quantum phase transition.

The description of the transition that we have adopted in this thesis is in terms of a critical theory of strongly repulsive, fluctuating Cooper pairs, written in terms of a complex order parameter overdamped by its coupling to a bath of unpaired fermions resulting from the presence of some type of pair-breaking interaction. The existence of the bath, imagined as a large number of unpaired electrons residing in the transverse conduction channels of the wire, leads to a long range interaction in imaginary time providing Ohmic dissipation in the form of a non-analytic $|\omega_n|$ term in the effective action. The presence of such an anisotropic relationship between space and time in the presence of a continuous symmetry order parameter fixes the dynamical critical

exponent at $z = 2$, and the resulting upper critical dimension is $d_{\rm UCD} = 2$.

The thinness of these wires provided us with a useful theoretical framework in the form of the quasi-one dimensional limit, where the radius of the wire R is on the order of, or much smaller than the superconducting coherence length ξ_0 at low temperatures. The length scale ξ_0 measures the average separation between the electrons in a Cooper pair, and as $R < \xi_0$ they begin to *feel* the boundary. If the wire is sufficiently long, the paired states can be described in terms of a quantum field theory in one space and one imaginary time dimension. In $1 + 1$ dimensions, we found ourselves below $d_{\rm UCD}$, with the repulsive self-interactions between Cooper pairs being strongly relevant. As a result, any perturbative or mean field approaches were unable to provide a complete and accurate picture of the physical phenomena.

By employing a large number of field theoretic and numerical techniques in conjunction with a careful scaling analysis, we have determined the behavior of the zero frequency (dc) conductivity as a function of temperature and the pair-breaking parameter which drives the transition. Our first experimentally testable result is a complete crossover phase diagram for the quantum superconductor-metal transition (SMT). We predict that upon fixing the source of pair-breaking (either magnetic field or wire radius) at a value near criticality, as function of decreasing temperature, the conductivity should first increase as $1/\sqrt{T}$ due to the influence of the quantum critical point, then change to decreasing as T^2 once the low temperature metallic phase has been reached. There is already qualitative evidence for transport in this regime that is non-monotonic in temperature.

The second prediction is that in the quantum critical regime at finite temperatures, defined by a pair-breaking strength that is close to the one that would destroy order at zero temperatures, the ratio of dc thermal (κ) to electrical (σ) conductivity (the Wiedemann-Franz ratio) should be linear in temperature, with a proportionality constant that is corrected from the Lorenz number for a normal metal. We have computed the exact value of this correction in a systematic expansion in the inverse number of complex order parameter components N and found

$$W \equiv \frac{\kappa}{\sigma T} = \left(0.282 + \frac{0.0376}{N}\right)\left(\frac{k_B}{e}\right)^2 . \tag{6.1}$$

Conversations with experimentalists have been initiated on the feasibility of performing thermal transport experiments on nanowires and we are hopeful that such measurements will be made in the foreseeable future.

Further avenues for theoretical progress still remain in these systems, including a full understanding of the low temperature ordered phase which has not been attempted here. Such a description would require proper inclusion of the pairing interaction as well as Coulomb repulsion, leading to a plasmon mode describing the strongly fluctuating phase of the superconducting order parameter.

Possible real time approaches like Keldysh or even the density matrix renormalization group (DMRG) might also offer directions of attack. In particular, it would

be of considerable interest to determine the best method for simulating an Ohmic bath in DMRG by approximating the formally infinite number of degrees of freedom that would exist at each spatial location.

The role of randomness in the nanowire transport experiments is still an open question, as it can be difficult to obtain an accurate picture of how much disorder is present in the real ultra-narrow wires beyond estimates inferred from their normal state resistance. There is some evidence that the surface of the wires may be home to localized magnetic impurities but beyond that little is known. The theoretical inclusion of disorder is straightforward in principle, and can be done by allowing any coupling constants to have an explicit spatial dependence.

Spurred on by some compelling strong disorder RG results, we have simulated a large number of finite length disordered wires ranging from 16 to 128 "sites". At zero temperature, we analyzed both equal time and dynamic correlation functions and found a phase transition between a superconductor and metal described by an infinite randomness fixed point. The physics near such a critical point has some unusual and fascinating properties due to the contribution of rare regions, including highly anisotropic scaling relations between space and time (activated scaling) and a measurable difference between the average and typical values of macroscopic observables. An even more interesting property of this transition is that it is fully described by three critical exponents, $\nu \simeq 1.9$ which determines the diverging length scale describing average equal time order parameter correlations, $\psi \simeq 0.53$ a tunneling exponent which relates the logarithm of the characteristic frequency of fluctuations to their wavevector and $\phi \simeq 1.6$ which fixes how the magnitude of a critical mode describing local order scales with the logarithm of its characteristic frequency. These exponents are in full agreement with $\nu = 2$, $\psi = 1/2$ and $\phi = (1 + \sqrt{5})/2$ which are known to exactly describe the infinite randomness fixed point which characterizes the onset of ferromagnetic order in a one dimensional quantum Ising model in a random transverse field [64]. We find that our $1 + 1$ dimensional description of the quantum SMT in terms of a $z = 2$ theory of overdamped Cooperon fluctuations not only exhibits infinite randomness, but is also in the same universality class as the random transverse field Ising model (RTFIM).

This appears to be a highly non-trivial result, as the RTFIM has discrete symmetry and no dissipation, to be contrasted with at least $O(2)$ symmetry and strong damping for the model considered in this thesis. It can be understood in the context of the effective dimensionality of the strongly ordered rare regions in our theory in relation to their lower critical dimension. For the pair-breaking quantum SMT with disorder at zero temperature, the rare regions are well-ordered droplets that have an infinite extent in the imaginary time direction with a long range $1/\tau^2$ coupling (which gives $|\omega|$ in frequency space). It is known that a one dimensional classical $O(N)$ model with long range $1/x^2$ interactions in space has a lower critical dimension $d_{\mathrm{LCD}} = 1$ [149]. The quantum-classical mapping tells us that our rare regions can be effectively described in this manner and we expect them to be marginal. The strong damping in

the form of an Ohmic bath leads to this marginality and the resultant flow to infinite randomness, as the dynamics of the largest ordered regions become extremely slow as the energy scale is reduced producing Griffiths singularities in the disordered phase. The correspondence to the Ising model can be framed in terms of its hyper-universality and the rough picture that a region of the wire possesses a kind of effective discrete symmetry in that it either has phase coherence or it does not.

The resulting infinite randomness fixed point of the superconductor-metal transition could have profound and novel implications. Many future research directions are immediately clear, with the most obvious being a study of transport at zero temperature via the Kubo formula. Although a type of ac spin transport has already been computed for some one dimensional spin models possessing infinite randomness critical points [150], no *real* electron transport calculations have ever been performed in the presence of activated scaling. The formalism presented here can also be straightforwardly generalized to finite temperatures and one could even study the temperature dependence of the conductivity in the presence of strong disorder physics. The physical description would be in terms of weak-links, where for small currents, a suitably disordered region of a wire could completely destroy electrical transport below some temperature scale. An understanding of this behavior could lead to better agreement between theory and experiment, and even spur new measurements in the nanowire systems.

The method can also be extended to higher dimensions, setting our sights on the ambitious problem of the superconductor-metal transition in amorphous two dimensional films. This problem has a long history with basic questions and controversy surrounding the correct model and mechanisms still unresolved. Recent progress has been made within a droplet picture of superconducting islands that are coupled to a metallic bath described by the $z = 2$ theory, with the addition of a long range Josephson coupling between the islands [151]. Our numerical methods could be easily generalized to this case with with the benefits of being able to treat the marginal repulsion between Cooper pairs self-consistently.

There is also a possibility of wider applicability of our disordered $z = 2$ theory beyond the SMT to other systems, including the onset of spin density wave order in itinerant magnets like CeCuAu where experimentalists have some systematic control over the number of impurities. In the cleanest systems, there are indications of metallic Hertz-like behavior, and one could try to study the crossovers that would naturally arise upon entering the strong disorder regime.

A muted but resolute undercurrent of this thesis is that the adage of having to "resort to numerics", often uttered by theorists and experimentalists alike, is both antiquated and banal. The analytical results of this work were completely dependent on modern numerical methods. We used multi-scale adaptive mesh techniques to cancel subtle divergences in high dimensional integrals in the $1/N$ expansion, and both classical Monte Carlo and high order spatial and temporal finite differencing methods to solve a stochastic equation of motion in the Langevin formalism leading

to strong support for the accuracy $N = \infty$ limit. Our large scale numerics for disordered systems were both motivated and informed by the principles of universality and scaling, as well as calculations done within the strong disorder renormalization group formalism. In fact, an analysis of the numerical data that ultimately lead to the determination of the tunelling exponent ϕ resulted in the location and eventual correction of a previously published analytical scaling result [129]. The label "numericist" is no longer appropriate, and our aspirations towards the observation, manipulation and understanding of matter at the truly atomic scale will surely require the successful unification and not divergence of many analytical and numerical methods.

Appendix A

Classical transport

The classical limit of Eq. (3.114) is obtained by approximating $n(\Omega) \simeq T/\Omega$. This leads to

$$\mathrm{Re}\left[G_{p,cl}(\omega)\right] = \frac{4\widetilde{D}^2 e^{*2-p}}{T^{p-1}} \int \frac{dk}{2\pi} k^2 \int \frac{d\Omega}{\pi} \frac{\Omega^p}{[(\Omega-\omega/2)^2 + (\widetilde{D}k^2+R)^2]} \times \frac{1}{[(\Omega-\omega/2)^2 + (\widetilde{D}k^2+R)^2]}, \tag{A.1}$$

and thus the classical conductivity at frequency ω , corresponding to $p = 0$ above is

$$\mathrm{Re}\left[\sigma_{cl}(\omega)\right] = 8\widetilde{D}^2 e^{*2} T \int \frac{dk}{2\pi} \frac{k^2}{(\widetilde{D}k^2+R)[\omega^2 + 4(\widetilde{D}k^2+R)^2]} \tag{A.2}$$

and in the dc limit

$$\sigma_{cl} = \frac{e^{*2}}{\hbar} \frac{\sqrt{\hbar\widetilde{D}} k_{\mathrm{B}} T}{8} \left(\frac{\hbar}{R}\right)^{3/2}. \tag{A.3}$$

Note that Eq. (3.100) tells us that in the metallic phase, $R \sim \delta^2$ and thus $\sigma_{\mathrm{cl}} \sim T$ at low temperatures. This clearly incorrect result for the temperature dependence indicates a breakdown of the classical theory in this regime where quantum fluctuations are important. Keeping this fact in mind, we press on and calculate the ac conductivity which is better analyzed in the time domain, and using Eqs. (3.49) and

(3.50) we obtain

$$\begin{aligned}\int dx\langle J(x,t)J(0,0)\rangle &= T\int_{-\infty}^{\infty}\frac{d\omega}{2\pi}2\mathrm{Re}[\sigma_{\mathrm{cl}}(\omega)]e^{i\omega t}\\ &= \frac{4e^{*2}T^2}{\hbar}\int\frac{dk}{2\pi}\frac{D^2k^2e^{-2(\widetilde{D}k^2+R)|t|}}{(\widetilde{D}k^2+R)^2}\\ &= \frac{e^{*2}\widetilde{D}^{1/2}T^2}{\hbar R^{1/2}}\left[(4R|t|+1)\mathrm{erfc}\left(\sqrt{2R|t|}\right)-\sqrt{\frac{8R|t|}{\pi}}e^{-2R|t|}\right].\end{aligned} \tag{A.4}$$

The expression in the square brackets has the value 1 at $t = 0$, decays exponentially for large t, and its integral over t is $1/(8R)$ which agrees with Eq. (A.3).

Although we argued above that the classical result is unphysical in the metallic regime, we can still use the full frequency dependence of the classical conductivity to benchmark the numerical procedure that was used to compute effective classical transport in the quantum critical regime (Section 3.2.2). This is done by taking R to be the mass of a Gaussian theory for a N-component classical complex field

$$S_{\mathrm{free}} = \int dx\left[\widetilde{D}|\partial_x\Psi_a(x)| + R|\Psi_a(x)|^2\right] \tag{A.5}$$

where we know that the $N = 1$ and $N = \infty$ results are identical. We assume simple relaxational dynamics in real time, and can brute force solve the stochastic partial differential equation

$$\frac{\partial\Psi(x,t)}{\partial t} = \widetilde{D}\frac{\partial^2\Psi(x,t)}{\partial x^2} - R\Psi(x,t) + f(x,t) \tag{A.6}$$

where f is a complex Gaussian correlated random noise obeying

$$\langle f(x,t)f^*(x',t')\rangle = 2T\delta(x-x')\delta(t-t') \tag{A.7}$$

for the time dependence of the one component complex field $\Psi(x,t)$. By averaging over all space-time trajectories of the current operator, we obtain the classical conductivity from Eq (3.49). This result can then be compared with the analytic result of Eq. (A.4) as seen in Fig. (A.1). All error bars are smaller then symbol sizes and the excellent agreement, in principle indicates the accuracy of our effective classical results where the field is no longer free, but fluctuates in the presence of the effective classical potential Eq. 3.25.

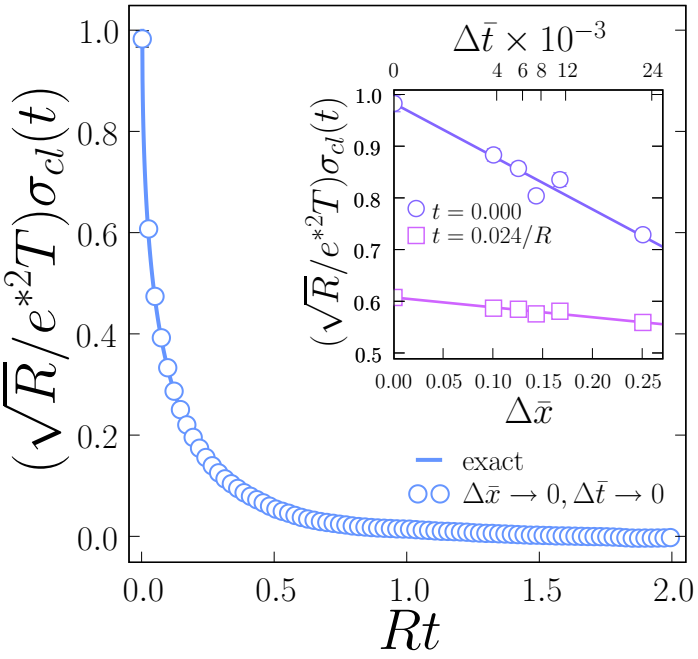

Figure A.1: The time dependence of the classical conductivity in the continuum limit obtained by finite size scaling the numerical solutions of the Langevin equation after averaging over 50 initial conditions in units where $\hbar = \widetilde{D} = k_{\mathrm{B}} = 1$. The solid line is the exact result from the Gaussian model as described in Eq. (A.4). The inset shows the only two time values which had any appreciable finite size dependency. Note the nonlinear relationship between $\Delta\bar{x} = \sqrt{R}\Delta x$ and $\Delta\bar{t} = R\Delta t$.

Appendix B

The Fluctuation Propagator

In this appendix, we will provide details on various results related to the evaluation of the fluctuation propagator at both zero and finite temperatures.

B.1 $T = 0$

At zero temperature, and coupling g the fluctuation propagator is given by

$$\Pi_0(k,\omega,r) = \int \frac{dq}{2\pi} \int \frac{d\epsilon}{2\pi} \frac{1}{(q^2+|\epsilon|+r)[(k+q)^2+|\omega+\epsilon|+r]}. \tag{B.1}$$

The momentum and frequency integrals can be done by employing Feynman parameters to yield

$$\begin{aligned}
\Pi_0(k,\omega,r) &= \frac{1}{2\pi} \int_0^1 dx \frac{1}{2x-1} \left(\frac{x}{\sqrt{(k^2-|\omega|)x - k^2x^2 + |\omega|}} + \frac{x-1}{\sqrt{(k^2+|\omega|)x - k^2x^2}} \right) \\
&= \frac{1}{2\pi|k|} \left[\text{asin}\left(\frac{k^2+|\omega|}{\sqrt{(k^2+|\omega|)^2+4k^2r}} \right) + \text{asin}\left(\frac{k^2-|\omega|}{\sqrt{(k^2+|\omega|)^2+4k^2r}} \right) \right] \\
&\quad + \frac{1}{2\pi\sqrt{k^2+2|\omega|+4r}} \left\{ \text{Re}\left[\text{atanh}\left(\frac{k^2+3|\omega|+4r}{2\sqrt{k^2+2|\omega|+4r}\sqrt{r+|\omega|}} \right) \right] \right. \\
&\quad \left. - \text{Re}\left[\text{atanh}\left(\frac{k^2+|\omega|+4r}{2\sqrt{k^2+2|\omega|+4r}\sqrt{r}} \right) \right] \right\}.
\end{aligned} \tag{B.2}$$

Using the relation

$$\text{Re}\left[\text{atanh}(z)\right] = \frac{1}{2} \ln \left| \frac{1+z}{1-z} \right| \tag{B.3}$$

we can write

$$\Pi_0(k,\omega,r) = \frac{1}{2\pi|k|}\left[\text{asin}\left(\frac{k^2+|\omega|}{\sqrt{(k^2+|\omega|)^2+4k^2r}}\right)+\text{asin}\left(\frac{k^2-|\omega|}{\sqrt{(k^2+|\omega|)^2+4k^2r}}\right)\right] + \frac{1}{4\pi\sqrt{k^2+2|\omega|+4r}}\left[\ln\left(\frac{2\sqrt{r+|\omega|}\sqrt{k^2+2|\omega|+4r}+k^2+3|\omega|+4r}{|2\sqrt{r+|\omega|}\sqrt{k^2+2|\omega|+4r}-k^2-3|\omega|-4r|}\right) - \ln\left(\frac{2\sqrt{r}\sqrt{k^2+2|\omega|+4r}+k^2+|\omega|+4r}{|2\sqrt{r+|\omega|}\sqrt{k^2+2|\omega|+4r}-k^2-|\omega|-4r|}\right)\right] \quad \text{(B.4)}$$

and at the critical coupling where $r=0$ this simplifies to

$$\Pi_0(k,\omega,0) = \frac{1}{4\pi|k|}\left[2\text{asin}\left(\frac{k^2-|\omega|}{k^2+|\omega|}\right)+\pi\right] + \frac{1}{4\pi\sqrt{k^2+2|\omega|}}\ln\left(\frac{2\sqrt{|\omega|}\sqrt{k^2+2|\omega|}+k^2+3|\omega|}{|2\sqrt{|\omega|}\sqrt{k^2+2|\omega|}-k^2-3|\omega||}\right). \quad \text{(B.5)}$$

B.2 $T > 0$

A key step required for the evaluation of the shift in the critical point coming from $1/N$ corrections (Eq. (4.27)) and the thermoelectric transport coefficients (Eq. (4.81)) is the fast and accurate computation of $\Pi_T(k,\omega_n,R)$ as well as the real and imaginary parts of its analytically continued value just above the real axis where $i\omega_n \to \omega + i\eta$.

B.2.1 Numerical evaluation

Starting from Eq. (4.7) and performing the momentum integral we have

$$\begin{aligned}\Pi_T(k,\omega_n,R) &= T\sum_{\epsilon_n}\int\frac{dq}{2\pi}\frac{1}{[(k+q)^2+|\omega_n+\epsilon_n|+R](q^2+|\epsilon_n|+r)}\\ &= T\sum_{\epsilon_n}\frac{\sqrt{|\epsilon_n|+R}+\sqrt{|\epsilon_n+\omega_n|+R}}{2\sqrt{(|\epsilon_n|+R)(|\epsilon_n+\omega_n|+R)}}\\ &\quad\times\frac{1}{k^2+(\sqrt{|\epsilon_n|+R}+\sqrt{|\epsilon_n+\omega_n|+R})^2}.\end{aligned} \quad \text{(B.6)}$$

Let us first find the value of the finite temperature fluctuation propagator at $k = \omega_n = 0$. Starting form Eq. (B.6) above we can derive a simple result

$$\begin{aligned}\Pi_T(0,0,R) &= \frac{1}{8\sqrt{2}\pi^{3/2}\sqrt{T}}\sum_{n=-\infty}^{\infty}\frac{1}{(|n|+R/2\pi T)^{3/2}}\\ &= \frac{1}{8\sqrt{2}\pi^{3/2}\sqrt{T}}\left[\zeta\left(\frac{3}{2},\frac{R}{2\pi T}\right)+\zeta\left(\frac{3}{2},\frac{R}{2\pi T}+1\right)\right],\end{aligned} \quad \text{(B.7)}$$

where $\zeta(a,x)$ is the Hurwitz zeta function. In order to evaluate the sum in Eq. (B.6) at finite frequencies and wavevectors, we explicitly sum the terms up to some large value of $|\epsilon_n| < 2\pi L$ where $2\pi L \gg |\omega_n|$. For the remaining terms, we perform a series expansion of the summand in powers of $1/|\epsilon_n|$ and then use the asymptotic series

$$\begin{aligned}\sum_{n=L}^{\infty}\frac{1}{n^s} &= \frac{L^{-s+1}}{\Gamma(s)}\int_0^{\infty}\frac{y^{s-2}e^{-y}dy}{1-e^{-s/L}} \\ &= L^{-s+1}\left[\frac{1}{s-1}+\frac{1}{2L}+\frac{s}{12L^2}-\frac{\Gamma(s+3)}{720\Gamma(s)L^4}+\frac{\Gamma(s+5)}{30240\Gamma(s)L^6}\right. \\ &\qquad \left.-\frac{\Gamma(s+7)}{1209600\Gamma(s)L^8}+\frac{\Gamma(s+9)}{47900160\Gamma(s)L^{10}}+\ldots\right]. \qquad \text{(B.8)}\end{aligned}$$

As discussed in Ref. [127], we must use the value of R given in Eq. (4.18) for the resulting $\Pi_T(k,\omega_n,R)$ to be well behaved at large k and ω_n.

B.2.2 $\mathrm{Re}\left[\Pi_T(q,\Omega,R)\right]^{-1}$

Here we provide details on the use of the summation formulas described in Appendix C to evaluate the real and imaginary parts of the fluctuation propagator analytically continued to real frequencies. Again, we start from

$$\Pi_T(q,\Omega_n,R) = T\sum_{\epsilon_n}\int\frac{dk}{2\pi}\frac{1}{(k^2+R+|\epsilon_n|)[(k+q)^2+R+|\epsilon_n+\Omega_n|]} \qquad \text{(B.9)}$$

and need to analytically continue to real frequencies $i\Omega_n \to \Omega + i\eta$. Thus, using Eq. (C.3) we perform the Matsubara summation to give

$$\begin{aligned}\Pi_T(q,\Omega+i\eta,R) = \frac{1}{2}\int\frac{dk}{2\pi}\int\frac{d\epsilon}{2\pi}\Bigg\{ &\coth\left(\frac{\epsilon}{2T}\right)\Big[F_\Pi(q,k,\epsilon+i\eta,\epsilon+\Omega+i\eta) \\ &- F_\Pi(q,k,\epsilon-i\eta,\epsilon+\Omega+i\eta)\Big] \\ &+ \coth\left(\frac{\epsilon+\Omega}{2T}\right)\Big[F_\Pi(q,k,\epsilon-i\eta,\epsilon+\Omega+i\eta) \\ &- F_\Pi(q,k,\epsilon-i\eta,\epsilon+\Omega-i\eta)\Big]\Bigg\} \qquad \text{(B.10)}\end{aligned}$$

where

$$F_\Pi(q,k,\epsilon\pm i\eta,\nu\pm i\eta) = \frac{1}{(k^2+R\mp i\epsilon)[(k+q)^2+R\mp i\nu]}. \qquad \text{(B.11)}$$

Considering each of the four terms in Eq. (B.10) separately, we will have to perform an integral of the form

$$I_{\Pi}(q,a,b) = \int \frac{dk}{2\pi} \frac{1}{(k^2+a)[(k+q)^2+b]} = \frac{1}{2}\left(\frac{1}{\sqrt{a}}+\frac{1}{\sqrt{b}}\right)\frac{1}{q^2+(\sqrt{a}+\sqrt{b})^2} \quad \text{(B.12)}$$

which was evaluated using Feynman parameters and in the particular case considered here $\mathrm{Re}\, a = \mathrm{Re}\, b = R > 0$.

We will use the fact that

$$\frac{1}{\sqrt{a \mp ib}} = \frac{1}{\sqrt{2}\sqrt{a^2+b^2}}\left(\sqrt{\sqrt{a^2+b^2}+a} \pm i\ \mathrm{sgn}(b)\sqrt{\sqrt{a^2+b^2}-a}\right) \quad \text{(B.13)}$$

and

$$\mathrm{Re}\,\frac{1}{q^2+(\sqrt{a-i\zeta_b b}+\sqrt{a-i\zeta_c c})^2} = \frac{1}{\Delta(q,a,b,\zeta_b,c,\zeta_c)}\left[q^2+2a+\sqrt{(\sqrt{a^2+b^2}+a)(\sqrt{a^2+c^2}+a)}\right.$$
$$\left. -\ \zeta_b\zeta_c\ \mathrm{sgn}(b)\ \mathrm{sgn}(c)\sqrt{(\sqrt{a^2+b^2}-a)(\sqrt{a^2+c^2}-a)}\right] \quad \text{(B.14a)}$$

$$\mathrm{Im}\,\frac{1}{q^2+(\sqrt{a-i\zeta_b b}+\sqrt{a-i\zeta_c c})^2} = \frac{1}{\Delta(q,a,b,\zeta_b,c,\zeta_c)}\left[\zeta_b b+\zeta_c c+\zeta_c\ \mathrm{sgn}(c)\sqrt{(\sqrt{a^2+b^2}+a)(\sqrt{a^2+c^2}-a)}\right.$$
$$\left. +\ \zeta_b\ \mathrm{sgn}(b)\sqrt{(\sqrt{a^2+b^2}-a)(\sqrt{a^2+c^2}+a)}\right] \quad \text{(B.14b)}$$

where

$$\Delta(q,a,b,\zeta_b,c,\zeta_c) = \left[q^2+2a+\sqrt{(\sqrt{a^2+b^2}+a)(\sqrt{a^2+c^2}+a)}\right.$$
$$\left. -\ \zeta_b\zeta_c\ \mathrm{sgn}(b)\ \mathrm{sgn}(c)\sqrt{(\sqrt{a^2+b^2}-a)(\sqrt{a^2+c^2}-a)}\right]^2$$
$$+\ \left[\zeta_b b+\zeta_c c+\zeta_c\ \mathrm{sgn}(c)\sqrt{(\sqrt{a^2+b^2}+a)(\sqrt{a^2+c^2}-a)}\right.$$
$$\left. +\ \zeta_b\ \mathrm{sgn}(b)\sqrt{(\sqrt{a^2+b^2}-a)(\sqrt{a^2+c^2}+a)}\right]^2 \quad \text{(B.15)}$$

with $a, b, c \in \mathbb{R}$ and $\zeta_{b,c} = \pm 1$.

Therefore, using Eq. (B.12) to Eq. (B.15) we can write the real and imaginary parts of the analytically continued fluctuation propagator as (suppressing all R dependence)

$$\begin{aligned}\operatorname{Re}\Pi_T(q,\Omega\pm i\eta) = \frac{1}{2}\int\frac{d\epsilon}{2\pi}\Bigg\{ &\coth\left(\frac{\epsilon}{2T}\right)\operatorname{Im} f_\Pi(q,\epsilon+i\eta,\epsilon+\Omega+i\eta)\\ &- \coth\left(\frac{\epsilon+\Omega}{2T}\right)\operatorname{Im} f_\Pi(q,\epsilon-i\eta,\epsilon+\Omega-i\eta)\\ &+\left[\coth\left(\frac{\epsilon+\Omega}{2T}\right)-\coth\left(\frac{\epsilon}{2T}\right)\right]\operatorname{Im} f_\Pi(q,\epsilon-i\eta,\epsilon+\Omega+i\eta)\Bigg\}\end{aligned} \tag{B.16a}$$

$$\begin{aligned}\operatorname{Im}\Pi_T(q,\Omega\pm i\eta) = \mp\frac{1}{2}\int\frac{d\epsilon}{2\pi}\Bigg\{ &\coth\left(\frac{\epsilon}{2T}\right)\operatorname{Re} f_\Pi(q,\epsilon+i\eta,\epsilon+\Omega+i\eta)\\ &- \coth\left(\frac{\epsilon+\Omega}{2T}\right)\operatorname{Re} f_\Pi(q,\epsilon-i\eta,\epsilon+\Omega-i\eta)\\ &+\left[\coth\left(\frac{\epsilon+\Omega}{2T}\right)-\coth\left(\frac{\epsilon}{2T}\right)\right]\operatorname{Re} f_\Pi(q,\epsilon-i\eta,\epsilon+\Omega+i\eta)\Bigg\}\end{aligned} \tag{B.16b}$$

with

$$\begin{aligned}&\operatorname{Re} f_\Pi(q,\epsilon+i\zeta_\epsilon\eta,\nu+i\zeta_\nu\eta) =\\ &\quad\frac{1}{2\sqrt{2}\Delta(q,R,\epsilon,\zeta_\epsilon,\nu,\zeta_\nu)}\Bigg\{\left(\frac{\sqrt{\sqrt{R^2+\epsilon^2}+R}}{\sqrt{R^2+\epsilon^2}}+\frac{\sqrt{\sqrt{R^2+\nu^2}+R}}{\sqrt{R^2+\nu^2}}\right)\\ &\qquad\times\Bigg[q^2+2R+\sqrt{(\sqrt{R^2+\epsilon^2}+R)(\sqrt{R^2+\nu^2}+R)}\\ &\qquad\quad-\zeta_\epsilon\zeta_\nu\operatorname{sgn}(\epsilon)\operatorname{sgn}(\nu)\sqrt{(\sqrt{R^2+\epsilon^2}-R)(\sqrt{R^2+\nu^2}-R)}\Bigg]\\ &\qquad-\left(\zeta_\epsilon\operatorname{sgn}(\epsilon)\frac{\sqrt{\sqrt{R^2+\epsilon^2}-R}}{\sqrt{R^2+\epsilon^2}}+\zeta_\nu\operatorname{sgn}(\nu)\frac{\sqrt{\sqrt{R^2+\nu^2}-R}}{\sqrt{R^2+\nu^2}}\right)\\ &\qquad\times\Bigg[\zeta_\epsilon\epsilon+\zeta_\nu\nu+\zeta_\nu\operatorname{sgn}(\nu)\sqrt{(\sqrt{R^2+\epsilon^2}+R)(\sqrt{R^2+\nu^2}-R)}\\ &\qquad\qquad+\zeta_\epsilon\operatorname{sgn}(\epsilon)\sqrt{(\sqrt{R^2+\epsilon^2}-R)(\sqrt{R^2+\nu^2}+R)}\Bigg]\Bigg\}\end{aligned} \tag{B.17a}$$

and

$$\begin{aligned}
&\operatorname{Im} f_{\Pi}(q, \epsilon + i\zeta_\epsilon \eta, \nu + i\zeta_\nu \eta) = \\
&\frac{1}{2\sqrt{2}\Delta(q, R, \epsilon, \zeta_\epsilon, \nu, \zeta_\nu)} \Bigg\{ \left(\zeta_\epsilon \operatorname{sgn}(\epsilon) \frac{\sqrt{\sqrt{R^2+\epsilon^2} - R}}{\sqrt{R^2+\epsilon^2}} + \zeta_\nu \operatorname{sgn}(\nu) \frac{\sqrt{\sqrt{R^2+\nu^2} - R}}{\sqrt{R^2+\nu^2}} \right) \\
&\qquad \times \Bigg[q^2 + 2R + \sqrt{(\sqrt{R^2+\epsilon^2} + R)(\sqrt{R^2+\nu^2} + R)} \\
&\qquad - \zeta_\epsilon \zeta_\nu \operatorname{sgn}(\epsilon) \operatorname{sgn}(\nu) \sqrt{(\sqrt{R^2+\epsilon^2} - R)(\sqrt{R^2+\nu^2} - R)} \Bigg] \\
&\qquad + \left(\frac{\sqrt{\sqrt{R^2+\epsilon^2} + R}}{\sqrt{R^2+\epsilon^2}} + \frac{\sqrt{\sqrt{R^2+\nu^2} + R}}{\sqrt{R^2+\nu^2}} \right) \\
&\qquad \times \Bigg[\zeta_\epsilon \epsilon + \zeta_\nu \nu + \zeta_\nu \operatorname{sgn}(\nu) \sqrt{(\sqrt{R^2+\epsilon^2} + R)(\sqrt{R^2+\nu^2} - R)} \\
&\qquad + \zeta_\epsilon \operatorname{sgn}(\epsilon) \sqrt{(\sqrt{R^2+\epsilon^2} - R)(\sqrt{R^2+\nu^2} + R)} \Bigg] \Bigg\}, \quad \text{(B.17b)}
\end{aligned}$$

where $\zeta_{\epsilon,\nu} = \pm 1$. Such a formulation allows us to compute both the real and imaginary parts of Π_T without having to resort to a Kramers-Kronig relation, leading to

$$\operatorname{Re}\left[\frac{1}{\Pi_T(q, \Omega, R)}\right] = \frac{\operatorname{Re}\Pi_T(q, \Omega, R)}{[\operatorname{Re}\Pi_T(q, \Omega, R)]^2 + [\operatorname{Im}\Pi_T(q, \Omega, R)]^2}. \quad \text{(B.18)}$$

Appendix C

Details on the Evaluation of Matsubara Sums

We begin with the basic identity [128]

$$T\sum_{\epsilon_n}\mathcal{F}(i\epsilon_n)=\frac{1}{2}\int\limits_{-\infty}^{\infty}\frac{d\epsilon}{2\pi i}\coth\left(\frac{\epsilon}{2T}\right)\left[F(\epsilon+i\eta)-F(\epsilon-i\eta)\right], \tag{C.1}$$

noting that if $F(i\epsilon_n)=\mathcal{F}(|\epsilon_n|)$, then after analytic continuation $F(\epsilon\pm i\eta)=\mathcal{F}(\mp i\epsilon)$. By a similar application of contour integration we obtain

$$\begin{aligned}I_2(i\omega_n)&=T\sum_{\epsilon_n}\mathcal{F}(i\epsilon_n,i(\epsilon_n+\omega_n))\\&=\frac{1}{2}\int\limits_{-\infty}^{\infty}\frac{d\epsilon}{2\pi i}\coth\left(\frac{\epsilon}{2T}\right)\Big[F(\epsilon+i\eta,\epsilon+i\omega_n)-F(\epsilon-i\eta,\epsilon+i\omega_n)\\&\qquad+\;F(\epsilon-i\omega_n,\epsilon+i\eta)-F(\epsilon-i\omega_n,\epsilon-i\eta)\Big]\end{aligned} \tag{C.2}$$

and so

$$\begin{aligned}I_2(\omega+i\eta)&=\int\limits_{-\infty}^{\infty}\frac{d\epsilon}{2\pi i}\Bigg\{\coth\left(\frac{\epsilon}{2T}\right)\Big[F(\epsilon+i\eta,\epsilon+\omega+i\eta)-F(\epsilon-i\eta,\epsilon+\omega+i\eta)\Big]\\&\qquad+\;\coth\left(\frac{\epsilon+\omega}{2T}\right)\Big[F(\epsilon-i\eta,\epsilon+\omega+i\eta)-F(\epsilon-i\eta,\epsilon+\omega-i\eta)\Big]\Bigg\}\\&=\int\limits_{-\infty}^{\infty}\frac{d\epsilon}{2\pi i}\Bigg\{\coth\left(\frac{\epsilon}{2T}\right)\Big[F(++)-F(-+)\Big]\\&\qquad+\;\coth\left(\frac{\epsilon+\omega}{2T}\right)\Big[F(-+)-F(--)\Big]\Bigg\}\end{aligned} \tag{C.3}$$

where in the last expression we only denote the sign of the $i\eta$ term, because the frequency arguments remain the same in *all* terms:

$$F(\pm\pm) \equiv F(\epsilon \pm i\eta, \epsilon + \omega \pm i\eta). \tag{C.4}$$

Rearranging the terms to preserve the order of the frequency arguments will allow us to pull out common factors in the numerator and lead to many simplifications.

Any corrections coming from the presence of a finite self energy at order $1/N$ require that we perform a dual Matsubara summation over a function with four frequency arguments. Through a further generalization of the method of contour integration used to obtain Eq. (C.2 we find

$$\begin{aligned} I_4(i\omega_n) &= T^2 \sum_{\epsilon_n,\Omega_n} \mathcal{F}(i\epsilon_n, i\Omega_n, i(\epsilon_n+\Omega_n), i(\epsilon_n+\omega_n)) \\ &= T\sum_{\epsilon_n} \frac{1}{2}\int_{-\infty}^{\infty} \frac{d\Omega}{2\pi i} \coth\left(\frac{\Omega}{2T}\right) \Big[F(i\epsilon_n, \Omega+i\eta, \Omega+i\epsilon_n, i(\epsilon_n+\omega_n)) \\ &\qquad - F(i\epsilon_n, \Omega-i\eta, \Omega+i\epsilon_n, i(\epsilon_n+\omega_n)) \\ &\qquad + F(i\epsilon_n, \Omega-i\epsilon_n, \Omega+i\eta, i(\epsilon_n+\omega_n)) \\ &\qquad - F(i\epsilon_n, \Omega-i\epsilon_n, \Omega-i\eta, i(\epsilon_n+\omega_n)) \Big] \qquad \text{(C.5)} \\ &= \frac{1}{4}\int_{-\infty}^{\infty} \frac{d\Omega}{2\pi i} \coth\left(\frac{\Omega}{2T}\right) \int_{-\infty}^{\infty} \frac{d\epsilon}{2\pi i} \coth\left(\frac{\epsilon}{2T}\right) \\ &\qquad \times \Big[\Upsilon_4^+(\epsilon, \Omega, i\omega_n; i\eta) - \Upsilon_4^-(\epsilon, \Omega, i\omega_n; i\eta) \Big] \qquad \text{(C.6)} \end{aligned}$$

where

$$\begin{aligned} \Upsilon_4^+(\epsilon, \Omega, i\omega_n; i\eta) &= F(\epsilon+i\eta, \Omega+i\eta, \Omega+\epsilon+i\eta, \epsilon+i\omega_n) \\ &+ F(\epsilon+i\eta, \Omega-\epsilon-i\eta, \Omega+i\eta, \epsilon+i\omega_n) + F(\epsilon-i\eta, \Omega-i\eta, \Omega+\epsilon-i\eta, \epsilon+i\omega_n) \\ &+ F(\epsilon-i\eta, \Omega-\epsilon+i\eta, \Omega-i\eta, \epsilon+i\omega_n) + F(\epsilon-i\omega_n, \Omega+i\eta, \Omega+\epsilon-i\omega_n, \epsilon+i\eta) \\ &+ F(\epsilon-i\omega_n, \Omega-\epsilon+i\omega_n, \Omega+i\eta, \epsilon+i\eta) + F(\epsilon-i\omega_n, \Omega-i\eta, \Omega+\epsilon-i\omega_n, \epsilon-i\eta) \\ &+ F(\epsilon-i\omega_n, \Omega-\epsilon+i\omega_n, \Omega-i\eta, \epsilon-i\eta) \end{aligned} \tag{C.7}$$

and

$$\begin{aligned} \Upsilon_4^-(\epsilon, \Omega, i\omega_n; i\eta) &= F(\epsilon+i\eta, \Omega-i\eta, \Omega+\epsilon+i\eta, \epsilon+i\omega_n) \\ &+ F(\epsilon+i\eta, \Omega-\epsilon-i\eta, \Omega-i\eta, \epsilon+i\omega_n) + F(\epsilon-i\eta, \Omega+i\eta, \Omega+\epsilon-i\eta, \epsilon+i\omega_n) \\ &+ F(\epsilon-i\eta, \Omega-\epsilon+i\eta, \Omega+i\eta, \epsilon+i\omega_n) + F(\epsilon-i\omega_n, \Omega-i\eta, \Omega+\epsilon-i\omega_n, \epsilon+i\eta) \\ &+ F(\epsilon-i\omega_n, \Omega-\epsilon+i\omega_n, \Omega-i\eta, \epsilon+i\eta) + F(\epsilon-i\omega_n, \Omega+i\eta, \Omega+\epsilon-i\omega_n, \epsilon-i\eta) \\ &+ F(\epsilon-i\omega_n, \Omega-\epsilon+i\omega_n, \Omega+i\eta, \epsilon-i\eta) \end{aligned}$$

so that

$$
\begin{aligned}
I_4(\omega+i\eta) = \frac{1}{4}\int\limits_{-\infty}^{\infty}\frac{d\Omega}{2\pi i}\int\limits_{-\infty}^{\infty}\frac{d\epsilon}{2\pi i} \\
\times\ \Bigg\{ &\coth\left(\frac{\Omega}{2T}\right)\coth\left(\frac{\epsilon}{2T}\right)\Big[F(++{+}{+}) - F(+-{+}{+}) \\
&\qquad +\ F(---{+}) - F(-+-{+})\Big] \\
&+\ \coth\left(\frac{\Omega+\epsilon}{2T}\right)\coth\left(\frac{\epsilon}{2T}\right)\Big[F(+-{+}{+}) - F(+--{+}) \\
&\qquad +\ F(-+-{+}) - F(-++{+})\Big] \\
&+\ \coth\left(\frac{\Omega}{2T}\right)\coth\left(\frac{\epsilon+\omega}{2T}\right)\Big[F(-+-{+}) - F(---{+}) \\
&\qquad +\ F(----) - F(-+--)\Big] \\
&+\ \coth\left(\frac{\Omega+\epsilon}{2T}\right)\coth\left(\frac{\epsilon+\omega}{2T}\right)\Big[F(-++{+}) - F(-+-{+}) \\
&\qquad +\ F(-+--) - F(-++{-})\Big]\Bigg\}. \qquad \text{(C.8)}
\end{aligned}
$$

Multiple change of variable transformations have been performed to ensure that the function F in the terms above have the same arguments ϵ, Ω, $\epsilon+\Omega$, $\epsilon+\omega$, and thus only the signs of the $i\eta$ terms have been denoted,

$$F(\pm\pm\pm\pm) = F(\epsilon\pm i\eta, \Omega\pm i\eta, \epsilon+\Omega\pm i\eta, \epsilon+\omega\pm i\eta). \qquad \text{(C.9)}$$

Finally, the vertex corrections are similar in that we still need to perform a dual Matsubara sum, but now the frequency arguments are more complicated, and there

are five unique combinations

$$
\begin{aligned}
I_5(i\omega_n) &= T^2 \sum_{\epsilon_n,\Omega_n} \mathcal{F}(i\epsilon_n, i(\epsilon_n+\omega_n), i\Omega_n, i(\Omega_n+\omega_n), i(\Omega_n-\epsilon_n)) \\
&= T\sum_{\epsilon_n} \frac{1}{2}\int_{-\infty}^{\infty}\frac{d\Omega}{2\pi i}\coth\left(\frac{\Omega}{2T}\right) \\
&\quad\times\Big[F(i\epsilon_n, i(\epsilon_n+\omega_n), \Omega+i\eta, \Omega+i\omega_n, \Omega-i\epsilon_n) \\
&\quad- F(i\epsilon_n, i(\epsilon_n+\omega_n), \Omega-i\eta, \Omega+i\omega_n, \Omega-i\epsilon_n) \\
&\quad+ F(i\epsilon_n, i(\epsilon_n+\omega_n), \Omega-i\omega_n, \Omega+i\eta, \Omega-i\epsilon_n-i\omega_n) \\
&\quad- F(i\epsilon_n, i(\epsilon_n+\omega_n), \Omega-i\omega_n, \Omega-i\eta, \Omega-i\epsilon_n-i\omega_n) \\
&\quad+ F(i\epsilon_n, i(\epsilon_n+\omega_n), \Omega+i\epsilon_n, \Omega+i\omega_n+i\epsilon_n, \Omega+i\eta) \\
&\quad- F(i\epsilon_n, i(\epsilon_n+\omega_n), \Omega+i\epsilon_n, \Omega+i\omega_n+i\epsilon_n, \Omega-i\eta)\Big] \\
&= \frac{1}{4}\int_{-\infty}^{\infty}\frac{d\Omega}{2\pi i}\coth\left(\frac{\Omega}{2T}\right)\int_{-\infty}^{\infty}\frac{d\epsilon}{2\pi i}\coth\left(\frac{\epsilon}{2T}\right) \\
&\qquad\times\Big[\Upsilon_5^+(\epsilon,\Omega,i\omega_n;i\eta)-\Upsilon_5^-(\epsilon,\Omega,i\omega_n;i\eta)\Big]
\end{aligned}
\tag{C.10}
$$

where

$$
\begin{aligned}
\Upsilon_5^+(\epsilon,\Omega,i\omega_n;i\eta) &= F(\epsilon+i\eta, \epsilon+i\omega_n, \Omega+i\eta, \Omega+i\omega_n, \Omega-\epsilon-i\eta) \\
&\quad+ F(\epsilon+i\eta, \epsilon+i\omega_n, \Omega-i\omega_n, \Omega+i\eta, \Omega-\epsilon-i\omega_n) \\
&\quad+ F(\epsilon+i\eta, \epsilon+i\omega_n, \Omega+\epsilon+i\eta, \Omega+i\omega_n+\epsilon, \Omega+i\eta) \\
&\quad+ F(\epsilon-i\eta, \epsilon+i\omega_n, \Omega-i\eta, \Omega+i\omega_n, \Omega-\epsilon+i\eta) \\
&\quad+ F(\epsilon-i\eta, \epsilon+i\omega_n, \Omega-i\omega_n, \Omega-i\eta, \Omega-\epsilon-i\omega_n) \\
&\quad+ F(\epsilon-i\eta, \epsilon+i\omega_n, \Omega+\epsilon-i\eta, \Omega+i\omega_n+\epsilon, \Omega-i\eta) \\
&\quad+ F(\epsilon-i\omega_n, \epsilon+i\eta, \Omega+i\eta, \Omega+i\omega_n, \Omega-\epsilon+i\omega_n) \\
&\quad+ F(\epsilon-i\omega_n, \epsilon+i\eta, \Omega-i\omega_n, \Omega+i\eta, \Omega-\epsilon-i\eta) \\
&\quad+ F(\epsilon-i\omega_n, \epsilon+i\eta, \Omega+\epsilon-i\omega_n, \Omega+\epsilon+i\eta, \Omega+i\eta) \\
&\quad+ F(\epsilon-i\omega_n, \epsilon-i\eta, \Omega-i\eta, \Omega+i\omega_n, \Omega-\epsilon+i\omega_n) \\
&\quad+ F(\epsilon-i\omega_n, \epsilon-i\eta, \Omega-i\omega_n, \Omega-i\eta, \Omega-\epsilon+i\eta) \\
&\quad+ F(\epsilon-i\omega_n, \epsilon-i\eta, \Omega+\epsilon-i\omega_n, \Omega+\epsilon-i\eta, \Omega-i\eta)
\end{aligned}
\tag{C.11}
$$

and

$$\begin{aligned}\Upsilon_5^-(\epsilon,\Omega,i\omega_n;i\eta) = {} & F(\epsilon+i\eta,\epsilon+i\omega_n,\Omega-i\eta,\Omega+i\omega_n,\Omega-\epsilon-i\eta)\\ & +\ F(\epsilon+i\eta,\epsilon+i\omega_n,\Omega-i\omega_n,\Omega-i\eta,\Omega-\epsilon-i\omega_n)\\ & +\ F(\epsilon+i\eta,\epsilon+i\omega_n,\Omega+\epsilon+i\eta,\Omega+i\omega_n+\epsilon,\Omega-i\eta)\\ & +\ F(\epsilon-i\eta,\epsilon+i\omega_n,\Omega+i\eta,\Omega+i\omega_n,\Omega-\epsilon+i\eta)\\ & +\ F(\epsilon-i\eta,\epsilon+i\omega_n,\Omega-i\omega_n,\Omega+i\eta,\Omega-\epsilon-i\omega_n)\\ & +\ F(\epsilon-i\eta,\epsilon+i\omega_n,\Omega+\epsilon-i\eta,\Omega+i\omega_n+\epsilon,\Omega+i\eta)\\ & +\ F(\epsilon-i\omega_n,\epsilon+i\eta,\Omega-i\eta,\Omega+i\omega_n,\Omega-\epsilon+i\omega_n)\\ & +\ F(\epsilon-i\omega_n,\epsilon+i\eta,\Omega-i\omega_n,\Omega-i\eta,\Omega-\epsilon-i\eta)\\ & +\ F(\epsilon-i\omega_n,\epsilon+i\eta,\Omega+\epsilon-i\omega_n,\Omega+\epsilon+i\eta,\Omega-i\eta)\\ & +\ F(\epsilon-i\omega_n,\epsilon-i\eta,\Omega+i\eta,\Omega+i\omega_n,\Omega-\epsilon+i\omega_n)\\ & +\ F(\epsilon-i\omega_n,\epsilon-i\eta,\Omega-i\omega_n,\Omega+i\eta,\Omega-\epsilon+i\eta)\\ & +\ F(\epsilon-i\omega_n,\epsilon-i\eta,\Omega+\epsilon-i\omega_n,\Omega+\epsilon-i\eta,\Omega+i\eta). \qquad \text{(C.12)}\end{aligned}$$

Again performing multiple variable shifts yields a much simpler expression where the frequency arguments of each term are the same. Suppressing the frequency depen-

dence of $I_5 = I_5(\omega + i\eta)$ we have

$$
\begin{aligned}
I_5 = \frac{1}{4} \int_{-\infty}^{\infty} \frac{d\Omega}{2\pi i} \int_{-\infty}^{\infty} \frac{d\epsilon}{2\pi i} \\
\times \Bigg\{ & \coth\left(\frac{\Omega}{2T}\right) \coth\left(\frac{\epsilon}{2T}\right) \Big[F(+++++) - F(++++-) \\
& \qquad + F(-+-+-) - F(-+-++) \Big] \\
& + \coth\left(\frac{\Omega+\epsilon}{2T}\right) \coth\left(\frac{\epsilon}{2T}\right) \Big[F(++++-) - F(++-+-) \\
& \qquad + F(-+-++) - F(-++++) \Big] \\
& + \coth\left(\frac{\Omega+\epsilon+\omega}{2T}\right) \coth\left(\frac{\epsilon}{2T}\right) \Big[F(++-+-) - F(++---) \\
& \qquad + F(-+---) - F(-+-+-) \Big] \\
& + \coth\left(\frac{\Omega+\epsilon}{2T}\right) \coth\left(\frac{\epsilon+\omega}{2T}\right) \Big[F(-++++) - F(-+-++) \\
& \qquad + F(---++) - F(--+++) \Big] \\
& + \coth\left(\frac{\Omega+\epsilon+\omega}{2T}\right) \coth\left(\frac{\epsilon+\omega}{2T}\right) \Big[F(-+-+-) - F(-+---) \\
& \qquad + F(----+) + F(---++) \Big] \\
& + \coth\left(\frac{\Omega}{2T}\right) \coth\left(\frac{\epsilon+\omega}{2T}\right) \Big[F(-+-++) - F(-+-+-) \\
& \qquad + F(-----) + F(----+) \Big] \Bigg\}
\end{aligned}
\tag{C.13}
$$

where the arguments of F have been shifted to be ϵ, $\epsilon+\omega$, $\epsilon+\Omega$, $\epsilon+\Omega+\omega$, Ω,

$$
F(\pm,\pm,\pm,\pm,\pm) \equiv F(\epsilon \pm i\eta, \epsilon+\omega \pm i\eta, \epsilon+\Omega \pm i\eta, \epsilon+\Omega+\omega \pm i\eta, \Omega \pm i\eta). \tag{C.14}
$$

Appendix D

Susceptibility Scaling

In this appendix, we derive scaling forms for the average and local dynamical order parameter susceptibilities by appealing to the physical picture provided by the strong disorder renormalization group [129, 152]. In the presence of flow to infinite randomness, averages of physical quantities in the Griffiths phase will be dominated by rare regions that are strongly ordered. The susceptibility will feel a maximal contribution from the small number of clusters with abnormally small eigenvalues, thus we begin by considering the action of a single cluster at zero temperature characterized by order parameter Ψ

$$\mathcal{S}_{\text{clust}} = \int \frac{d\omega}{2\pi} \Psi^*(\omega)(r + \gamma_0|\omega|)\Psi(\omega) \tag{D.1}$$

where γ_0 measures the bare strength of the Ohmic dissipation. The renormalized distance from criticality, r, can be found by solving

$$\left\langle |\Psi(\tau)|^2 \right\rangle_{\mathcal{S}_{\text{clust}}} = 1. \tag{D.2}$$

Adding a source term and taking the suitable derivative we find

$$\chi^{\text{clust}}(i\omega) = \frac{1}{r + \gamma_0|\omega|} \tag{D.3}$$

or analytically continuing to real frequencies

$$\operatorname{Im} \chi^{\text{clust}}(\omega) = \frac{\gamma_0 \omega}{r^2 + \gamma_0^2 \omega^2}. \tag{D.4}$$

The above analysis neglects fluctuations within a cluster, and to compensate we define the average moment of a cluster fluctuating with frequency ω to be $\mu(\omega)$. Then from simple dimensional considerations, the renormalized single cluster contribution to the total susceptibility will be $\mu^2 \operatorname{Im} \chi^{\text{clust}}$ for the average susceptibility and

$\mu \operatorname{Im} \chi^{\text{clust}}$ for the local susceptibility:

$$\operatorname{Im} \chi^{\text{clust}}(\omega) \sim \frac{\mu^2 \gamma \omega}{r^2 + \gamma^2 \omega^2} \tag{D.5a}$$

$$\operatorname{Im} \chi^{\text{clust}}_{\text{loc}}(\omega) \sim \frac{\mu \gamma \omega}{r^2 + \gamma^2 \omega^2} \tag{D.5b}$$

where $\gamma = \mu\gamma_0$ has been renormalized due to the modified coupling between joined clusters and the bath (see for example Eq. (5.4) which describes how the moment renormalizes under cluster creation). In order to determine the total susceptibilities, the RG procedure is run down to an energy scale $\Omega = \gamma_0 \mu(\Omega)\omega$ where $\mu(\Omega)$ is the typical moment at frequency $\Omega/\hbar$ as a result of the narrow distribution of moments. The clusters that get eliminated while reducing the energy scale are strongly fluctuating and do not significantly contribute to the susceptibility. In fact, the only clusters that contribute will have $r \ll \Omega$ so we have

$$\operatorname{Im} \chi^{\text{clust}}(\omega) \sim \frac{\mu^2(\Omega)\gamma_0 \mu(\Omega)\omega}{\gamma_0^2 \mu^2(\Omega)\omega^2} = \frac{\mu(\Omega)}{\omega} \tag{D.6a}$$

$$\operatorname{Im} \chi^{\text{clust}}_{\text{loc}}(\omega) \sim \frac{\mu(\Omega)\gamma_0 \mu(\Omega)\omega}{\gamma_0^2 \mu^2(\Omega)\omega^2} = \frac{1}{\omega}. \tag{D.6b}$$

Now, performing a summation over all clusters in the sample which contribute at the energy scale Ω, we find that the total susceptibility is given by the results above, modified by a factor of $n(\Omega)$, the density of surviving clusters

$$\operatorname{Im} \chi(\omega) \sim \frac{\mu(\Omega) n(\Omega)}{\omega} \tag{D.7a}$$

$$\operatorname{Im} \chi_{\text{loc}}(\omega) \sim \frac{n(\Omega)}{\omega} \tag{D.7b}$$

which can be investigated for $\delta = 0$ at criticality and $\delta > 0$ in the disordered phase.

D.1 $\delta = 0$

Right at criticality, many results are known exactly from Fisher's solution of the RTFIM [64, 65] and specifically

$$n(\Omega) = |\ln \Omega|^{-1/\psi} \tag{D.8}$$

$$\mu(\Omega) = |\ln \Omega|^{\phi} \tag{D.9}$$

where $\psi = 1/2$ is the tunneling exponent and $\phi = (1 + \sqrt{5})/2$ is the cluster exponent for the RTFIM. When $\delta = 0$, we can set $\Omega \simeq \hbar\omega$ as corrections coming from $\mu(\Omega)$ are

beyond scaling. Substituting into Eqs. (D.7a) and (D.7b) we find

$$\operatorname{Im}\chi(\omega) \sim \frac{|\ln\omega|^{\phi-1/\psi}}{\omega} \tag{D.10a}$$

$$\operatorname{Im}\chi_{\mathrm{loc}}(\omega) \sim \frac{|\ln\omega|^{-1/\psi}}{\omega} \tag{D.10b}$$

and thus their ratio scales like the fluctuating cluster moment

$$\mathcal{R}(\omega) = \frac{\operatorname{Im}\chi(\omega)}{\operatorname{Im}\chi_{\mathrm{loc}}(\omega)} \sim |\ln\omega|^{\phi}. \tag{D.11}$$

This was the expected result, as physically argued in Section 5.4.3 or as can be seen from an examination of Eq. (D.7a) and (D.7b).

D.2 $\delta > 0$

In the quantum Griffiths phase we expect that $\delta^{\nu\psi}|\ln\omega| \gg 1$ where $\nu = 2$ is the correlation length exponent for the RTFIM, Eqs. (D.8) and (D.9) have the modified form [65, 153, 137]

$$n(\Omega) \sim \Omega^{\delta/\psi}\delta^{1/\psi} \tag{D.12}$$

$$\mu(\Omega) \sim \delta^{\nu\psi(1-\phi)}|\ln\Omega| \tag{D.13}$$

and now we must use the fact that $\Omega = \gamma_0\mu(\Omega)\omega$ which yields

$$n(\Omega) \sim \omega^{\delta/\psi}\delta^{1/\psi-\phi\nu\delta}\left(\delta^{\nu\psi}|\ln\omega|^{\delta/\psi}\right) \tag{D.14}$$

$$\mu(\Omega) \sim \delta^{-\nu\psi\phi}\left(\delta^{\nu\psi}|\ln\omega|\right). \tag{D.15}$$

Combining these results with Eq. (D.7a) and (D.7b) we find the scaling expressions in the Griffiths phase

$$\operatorname{Im}\chi(\omega) \sim \frac{\delta^{1/\psi-\phi\nu\psi(1+1/z)}\left(\delta^{\nu\psi}|\ln\omega|\right)^{1-1/z}}{\omega^{1-1/z}} \tag{D.16a}$$

$$\operatorname{Im}\chi_{\mathrm{loc}}(\omega) \sim \frac{\delta^{1/\psi-\phi\nu\delta}\left(\delta^{\nu\psi}|\ln\omega|\right)^{1/z}}{\omega^{1-1/z}} \tag{D.16b}$$

where we have identified $z \equiv \psi/\delta$ as an effective dynamic exponent. These scaling forms are confirmed in Figs. 5.9 and 5.10. Their ratio is given by

$$\mathcal{R}(\omega) = \frac{\operatorname{Im}\chi(\omega)}{\operatorname{Im}\chi_{\mathrm{loc}}(\omega)} \sim \delta^{-\phi\nu\psi}\left(\delta^{\nu\psi}|\ln\omega|\right) \tag{D.17}$$

and the existence of this scaling form was essential in our numerical computation of the exponent ϕ in Section 5.4.3.

References

[1] R. Feynman, *There is plenty of room at the bottom*, http://www.its.caltech.edu/ feynman/plenty.html, 1959.

[2] T. Newman, K. Williams, and R. Pease, J. Vac. Sci. Tech. B **5**, 88 (1987).

[3] C. Hirjibehedin, C. Lutz, and A. Heinrich, Science **312**, 1021 (2006).

[4] H. Onnes, Comm. Phys. Lab. Univ. Leiden **122**, 124 (1911).

[5] W. Meissner and R. Ochsenfeld, Naturwissenschaften **21**, 787 (1933).

[6] M. Tinkham, *Introduction to Superconductivity* (McGraw-Hill, New York, 1996).

[7] J. Bednorz and K. Müller, Z. Phys. B **64**, 189 (1986).

[8] P. Dai, B. Chakoumakos, G. Sun, K. Wong, Y. Xin, and D. Lu, Physica C **243**, 201 (1995).

[9] W. S. Corak, B. B. Goodman, C. B. Satterthwaite, and A. Wexler, Phys. Rev. **96**, 1442 (1954).

[10] L. N. Cooper, Phys. Rev. **104**, 1189 (1956).

[11] E. Maxwell, Phys. Rev. **78**, 477 (1950).

[12] C. A. Reynolds, B. Serin, W. H. Wright, and L. B. Nesbitt, Phys. Rev. **78**, 487 (1950).

[13] J. Bardeen, L. N. Cooper, and J. R. Schrieffer, Phys. Rev. **108**, 1175 (1957).

[14] N. Nagaosa, *Quantum Field Theory in Condensed Matter Physics* (Springer, Berlin, 1999).

[15] P. de Gennes, *Superconductivity of Metals and Alloys* (Perseus Books Group, New York, 1999).

[16] W. W. Webb and R. J. Warburton, Phys. Rev. Lett. **20**, 461 (1968).

[17] J. Bardeen, Rev. Mod. Phys. **34**, 667 (1962).

[18] W. A. Little, Phys. Rev. **156**, 396 (1967).

[19] J. S. Langer and V. Ambegaokar, Phys. Rev. **164**, 498 (1967).

[20] D. E. McCumber and B. I. Halperin, Phys. Rev. B **1**, 1054 (1970).

[21] N. D. Mermin and H. Wagner, Phys. Rev. Lett. **17**, 1133 (1966).

[22] P. C. Hohenberg, Phys. Rev. **158**, 383 (1967).

[23] R. Landauer, IBM J. Res. Dev. **44**, 251 (2000).

[24] L. Gor'kov, Soviet Phys. JETP **9**, 1364 (1959).

[25] B. Josephson, Phys. Lett. **1**, 251 (1962).

[26] D. E. McCumber, Phys. Rev. **172**, 427 (1968).

[27] A. Schmid, Phys. Rev. Lett. **51**, 1506 (1983).

[28] N. Giordano, Phys. Rev. Lett. **61**, 2137 (1988).

[29] N. Giordano, Physica B **203**, 460 (1994).

[30] A. O. Caldeira and A. J. Leggett, Phys. Rev. Lett. **46**, 211 (1981).

[31] J.-M. Duan, Phys. Rev. Lett. **74**, 5128 (1995).

[32] A. D. Zaikin, D. S. Golubev, A. van Otterlo, and G. T. Zimányi, Phys. Rev. Lett. **78**, 1552 (1997).

[33] A. Zaikin, D. Golubev, A. van Otterlo, and G. Zimanyi, Usp. Fiz. Nauk. **41**, 226 (1998).

[34] D. Golubev and A. Zaikin, Phys. Rev. B **64**, 14504 (2001).

[35] A. Bezryadin, C. Lau, and M. Tinkham, Nature **404**, 971 (2000).

[36] A. Bezryadin, NanoGallery, http://www.nanogallery.info, 2004.

[37] A. Rogachev, T.-C. Wei, D. Pekker, A. T. Bollinger, P. M. Goldbart, and A. Bezryadin, Phys. Rev. Lett. **97**, 137001 (2006).

[38] C. N. Lau, N. Markovic, M. Bockrath, A. Bezryadin, and M. Tinkham, Phys. Rev. Lett. **87**, 217003 (2001).

[39] F. Altomare, A. Chang, M. Melloch, Y. Hong, and C. Tu, Phys. Rev. Lett. **97**, 17001 (2006).

[40] A. Bollinger, R. Dinsmore, A. Rogachev, and A. Bezryadin, arXiv:0707.4532 (2008).

[41] A. Abrikosov and L. Gorkov, Sov. Phys. JETP **12**, 1243 (1961).

[42] P. Anderson, J. Phys. Chem. Solids **11**, 2 (1959).

[43] B. Spivak, A. Zyuzin, and M. Hruska, Phys. Rev. B **64**, 132502 (2001).

[44] A. Rogachev, A. T. Bollinger, and A. Bezryadin, Phys. Rev. Lett. **94**, 017004 (2005).

[45] Y. Liu, Y. Zadorozhny, M. Rosario, B. Rock, P. Carrigan, and H. Wang, Science **294**, 2332 (2001).

[46] W. A. Little and R. D. Parks, Phys. Rev. Lett. **9**, 9 (1962).

[47] J. A. Hertz, Phys. Rev. B **14**, 1165 (1976).

[48] S. Sachdev, *Quantum Phase Transitions* (Cambridge University Press, New York, 1999).

[49] T. Vojta, in *Computational Statistical Physics*, edited by K. Hoffmann and M. Schreiber (Springer, Berlin, 2002).

[50] T. Vojta, arXiv:0709.0964 (2007).

[51] S. L. Sondhi, S. M. Girvin, J. P. Carini, and D. Shahar, Rev. Mod. Phys. **69**, 315 (1997).

[52] N. Goldenfeld, *Lectures on Phase Transitions and the Renormalization Group* (Westview Press, New York, 1992).

[53] H. Stanley, *Introduction to Phase Transitions and Critical Phenomena* (Oxford University Press, New York, 1971).

[54] J. Negle and H. Orland, *Quantum Many-Particle Systems* (Addison-Wesley, New York, 1988).

[55] J. Cardy, *Scaling and renormalization in statistical physics* (Cambridge University Press, Cambridge, England, 1996).

[56] G. Grinstein, in *Fundamental Problems in Statitical Mechanics*, edited by E. Cohen (North Holland, Amsterdam, 1985), Vol. VI.

[57] T. Vojta, J. Phys. A: Math. Gen. **39**, R143 (2006).

[58] A. Harris, J. Phys. C **7**, 1671 (1974).

[59] C. Holm and W. Janke, Phys. Rev. B **48**, 936 (1993).

[60] A. M. Ferrenberg and D. P. Landau, Phys. Rev. B **44**, 5081 (1991).

[61] H. G. Ballesteros, L. A. Fernández, V. Martín-Mayor, A. Muñoz Sudupe, G. Parisi, and J. J. Ruiz-Lorenzo, Phys. Rev. B **58**, 2740 (1998).

[62] B. M. McCoy and T. T. Wu, Phys. Rev. Lett. **21**, 549 (1968).

[63] B. M. McCoy and T. T. Wu, Phys. Rev. **176**, 631 (1968).

[64] D. Fisher, Phys. Rev. Lett. **69**, 534 (1992).

[65] D. Fisher, Phys. Rev. B **51**, 6411 (1995).

[66] K. Binder and A. Young, Rev. Mod. Phys. **58**, 801 (1986).

[67] K. Fischer and J. Hertz, *Spin Glasses* (Cambridge University Press, Cambridge, England, 1991).

[68] D. Sherrington and S. Kirkpatrick, Phys. Rev. Lett. **35**, 1792 (1975).

[69] V. Dotsenko, *An Introduction to the Theory of Spin Glasses and Neural Networks* (World Scientific, New Jersey, 1994).

[70] R. Griffiths, Phys. Rev. Lett. **23**, 17 (1969).

[71] T. Vojta, J. Phys. A: Math. Gen. **36**, 10921 (2003).

[72] R. Sknepnek and T. Vojta, Phys. Rev. B **69**, 174410 (2004).

[73] G. Schehr and H. Rieger, Phys. Rev. Lett. **96**, 227201 (2006).

[74] J. Hoyos and T. Vojta, arXiv:0802.2303 (2008).

[75] S.-k. Ma, C. Dasgupta, and C.-k. Hu, Phys. Rev. Lett. **43**, 1434 (1979).

[76] A. Rogachev and A. Bezryadin, Appl. Phys. Lett. **83**, 512 (2003).

[77] G. Boogaard, A. Verbruggen, W. Belzig, and T. Klapwijk, Phys. Rev. B **69**, 220503 (2004).

[78] A. Bollinger, A. Rogachev, and A. Bezryadin, Europhys. Lett. **76**, 505 (2006).

[79] R. Ramazashvili and P. Coleman, Phys. Rev. Lett. **79**, 3752 (1997).

[80] I. F. Herbut, Phys. Rev. Lett. **85**, 1532 (2000).

[81] V. Galitski, Phys. Rev. B **77**, 100502 (2008).

[82] V. Galitski, Phys. Rev. Lett. **100**, 127001 (2008).

[83] A. V. Lopatin, N. Shah, and V. M. Vinokur, Phys. Rev. Lett. **94**, 037003 (2005).

[84] N. Shah and A. Lopatin, Phys. Rev. B **76**, 094511 (2007).

[85] L. Aslamazov and A. Larkin, Sov. Phys. Solid State **10**, 1104 (1968).

[86] K. Maki, Prog. Theor. Phys. **40**, 193 (1968).

[87] R. Thompson, Phys. Rev. B **1**, 327 (1970).

[88] B. Altshuler and A. Aronov, in *Electron–Electron Interactions in Disordered Systems*, edited by E. Efros and M. Pollak (North-Holland, Amsterdam, 1985).

[89] S. Sachdev, P. Werner, and M. Troyer, Phys. Rev. Lett. **92**, 237003 (2004).

[90] D. Podolsky, A. Vishwanath, J. Moore, and S. Sachdev, Phys. Rev. B **75**, 014520 (2007).

[91] D. A. Pesin and A. V. Andreev, Phys. Rev. Lett. **97**, 117001 (2006).

[92] J. E. Mooij and G. Schön, Phys. Rev. Lett. **55**, 114 (1985).

[93] M. V. Feigel'man and A. I. Larkin, Chem. Phys. **235**, 107 (1998).

[94] M. V. Feigel'man, A. I. Larkin, and M. A. Skvortsov, Phys. Rev. Lett. **86**, 1869 (2001).

[95] V. Galitski and A. Larkin, Phys. Rev. Lett. **87**, 87001 (2001).

[96] A. Del Maestro, B. Rosenow, N. Shah, and S. Sachdev, Phys. Rev. B **77**, 180501 (2008).

[97] A. J. Millis, Phys. Rev. B **48**, 7183 (1993).

[98] T. Moriya and A. Kawabata, J. Phys. Soc. Jpn. **34**, 639 (1973).

[99] S. Pankov, S. Florens, A. Georges, G. Kotliar, and S. Sachdev, Phys. Rev. B **69**, 054426 (2004).

[100] A. Gamba, M. Grilli, and C. Castellani, Nucl. Phys. B **556**, 463 (1999).

[101] P. Werner, M. Troyer, and S. Sachdev, J. Phys. Soc. Jpn. Supl. **74**, 67 (2005).

[102] S. Stintzing and W. Zwerger, Phys. Rev. B **56**, 9004 (1997).

[103] H. P. Büchler, V. B. Geshkenbein, and G. Blatter, Phys. Rev. Lett. **92**, 067007 (2004).

[104] G. Refael, E. Demler, Y. Oreg, and D. S. Fisher, Phys. Rev. B **75**, 014522 (2007).

[105] D. Meidan, Y. Oreg, and G. Refael, Phys. Rev. Lett. **98**, 187001 (2007).

[106] G. Refael, E. Demler, and Y. Oreg, arXiv:0803.2515 (2008).

[107] T. Giamarchi, Phys. Rev. B **46**, 342 (1992).

[108] L. B. Ioffe and A. J. Millis, Phys. Rev. B **51**, 16151 (1995).

[109] S. Sachdev, A. V. Chubukov, and A. Sokol, Phys. Rev. B **51**, 14874 (1995).

[110] J. Tucker and B. Halperin, Phys. Rev. B **3**, 3768 (1971).

[111] A. Van Run, J. Romijn, and J. Mooij, Jpn. J. Appl. Phys **26**, 1765 (1987).

[112] S. Saito and Y. Murayama, Phys. Lett. A **139**, 85 (1989).

[113] N. Shah, D. Pekker, and P. Goldbart, arXiv:0709.3971 (2007).

[114] G. Mahan, *Many-Particle Physics* (Plenum Publishing Corporation, Boston, 2000).

[115] P. Hohenberg and B. Halperin, Rev. Mod. Phys. **49**, 435 (1977).

[116] J. García-Ojalvo and J. Sancho, *Noise in Spatially Extended Systems* (Springer, New York, 1999).

[117] J. Zinn-Justin, *Quantum Field Theory and Critical Phenomena* (Oxford University Press, New York, 2002).

[118] M. Peskin and D. Schroeder, *An Introduction to Quantum Field Theory* (Perseus Books, New York, 1995).

[119] J. Moreno and P. Coleman, cond-mat/9603079 (1996).

[120] D. Fisher and P. Lee, Phys. Rev. B **23**, 6851 (1981).

[121] V. Ambegaokar and A. Griffin, Phys. Rev. **137**, 1151 (1965).

[122] F. Ronning, R. W. Hill, M. Sutherland, D. G. Hawthorn, M. A. Tanatar, J. Paglione, L. Taillefer, M. J. Graf, R. S. Perry, Y. Maeno, and A. P. Mackenzie, Phys. Rev. Lett. **97**, 067005 (2006).

[123] S. Vishveshwara and M. Fisher, Phys. Rev. B **64**, 174511 (2001).

[124] M. Vojta, Y. Zhang, and S. Sachdev, Int. J. Mod. Phys. B **14**, 3719 (2000); T. Senthil (unpublished).

[125] M. Li and E. Orignac, Europhys. Lett. **60**, 432 (2002).

[126] R. Fazio, F. Hekking, and D. Khmelnitskii, Phys. Rev. Lett. **80**, 5611 (1998).

[127] A. V. Chubukov, S. Sachdev, and J. Ye, Phys. Rev. B **49**, 11919 (1994).

[128] A. Abrikosov, L. Gorkov, and I. Dzyaloshinski, *Methods of Quantum Field Theory in Statistical Physics* (Prentice-Hall, New Jersey, 1963).

[129] J. Hoyos, C. Kotabage, and T. Vojta, Phys. Rev. Lett. **99**, 230601 (2007).

[130] D. S. Fisher, Phys. Rev. B **50**, 3799 (1994).

[131] C. Dasgupta and S.-k. Ma, Phys. Rev. B **22**, 1305 (1980).

[132] G. Refael, S. Kehrein, and D. S. Fisher, Phys. Rev. B **66**, 060402 (2002).

[133] J. A. Hoyos and E. Miranda, Phys. Rev. B **69**, 214411 (2004).

[134] D. S. Fisher, P. Le Doussal, and C. Monthus, Phys. Rev. Lett. **80**, 3539 (1998).

[135] J. Hooyberghs, F. Iglói, and C. Vanderzande, Phys. Rev. Lett. **90**, 100601 (2003).

[136] J. Hooyberghs, F. Iglói, and C. Vanderzande, Phys. Rev. E **69**, 066140 (2004).

[137] F. Iglói and C. Monthus, Phys. Rep. **412**, 277 (2005).

[138] O. Motrunich, S.-C. Mau, D. A. Huse, and D. S. Fisher, Phys. Rev. B **61**, 1160 (2000).

[139] T. Senthil and S. N. Majumdar, Phys. Rev. Lett. **76**, 3001 (1996).

[140] A. J. Leggett, S. Chakravarty, A. T. Dorsey, M. P. A. Fisher, A. Garg, and W. Zwerger, Rev. Mod. Phys. **59**, 1 (1987).

[141] A. J. Millis, D. K. Morr, and J. Schmalian, Phys. Rev. Lett. **87**, 167202 (2001).

[142] A. J. Millis, D. K. Morr, and J. Schmalian, Phys. Rev. B **66**, 174433 (2002).

[143] T. Senthil and S. Majumdar, Phys. Rev. Lett. **76**, 3001 (1996).

[144] Y. Tu and P. Weichman, Phys. Rev. Lett. **73**, 6 (1994).

[145] J. Hartman and P. Weichman, Phys. Rev. Lett. **74**, 4584 (1995).

[146] M. Powell, in *Numerical Methods for Nonlinear Algebraic Equations*, edited by P. Rabinowitz (Gordon and Breach, New York, 1970).

[147] J. Moré and M. Cosnard, ACM Trans. Math. Softw. **5**, 64 (1979).

[148] A. Young and H. Rieger, Phys. Rev. B **53**, 8486 (1996).

[149] T. Vojta and J. Schmalian, Phys. Rev. B **72**, 045438 (2005).

[150] O. Motrunich, K. Damle, and D. A. Huse, Phys. Rev. B **63**, 134424 (2001).

[151] B. Spivak, P. Oreto, and S. Kivelson, arXiv:0803.2902 (2008).

[152] T. Vojta, "private communication", 2008.

[153] F. Iglói, Phys. Rev. B **65**, 64416 (2002).